NBS SPECIAL PUBLICATION 607

U.S. DEPARTMENT OF COMMERCE / National Bureau of Standards

Refrigeration for Cryogenic Sensors and Electronic Systems

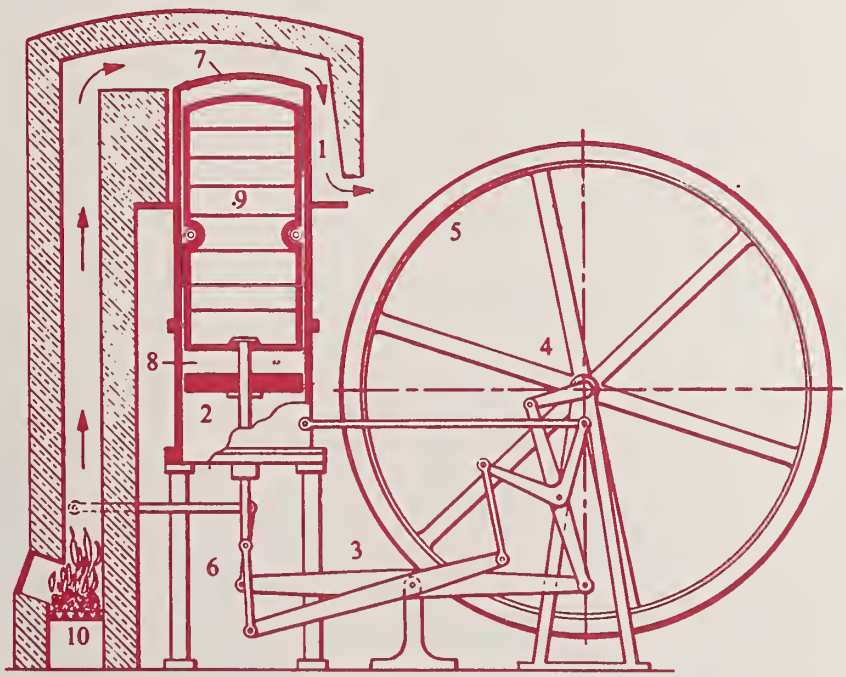

Sponsored by
International Institute of Refrigeration—Commission A 1/2
Office of Naval Research—Naval Research Laboratory
Cryogenic Engineering Conference
National Bureau of Standards

NATIONAL BUREAU OF STANDARDS

The National Bureau of Standards[1] was established by an act of Congress on March 3, 1901. The Bureau's overall goal is to strengthen and advance the Nation's science and technology and facilitate their effective application for public benefit. To this end, the Bureau conducts research and provides: (1) a basis for the Nation's physical measurement system, (2) scientific and technological services for industry and government, (3) a technical basis for equity in trade, and (4) technical services to promote public safety. The Bureau's technical work is performed by the National Measurement Laboratory, the National Engineering Laboratory, and the Institute for Computer Sciences and Technology.

THE NATIONAL MEASUREMENT LABORATORY provides the national system of physical and chemical and materials measurement; coordinates the system with measurement systems of other nations and furnishes essential services leading to accurate and uniform physical and chemical measurement throughout the Nation's scientific community, industry, and commerce; conducts materials research leading to improved methods of measurement, standards, and data on the properties of materials needed by industry, commerce, educational institutions, and Government; provides advisory and research services to other Government agencies; develops, produces, and distributes Standard Reference Materials; and provides calibration services. The Laboratory consists of the following centers:

Absolute Physical Quantities[2] — Radiation Research — Thermodynamics and Molecular Science — Analytical Chemistry — Materials Science.

THE NATIONAL ENGINEERING LABORATORY provides technology and technical services to the public and private sectors to address national needs and to solve national problems; conducts research in engineering and applied science in support of these efforts; builds and maintains competence in the necessary disciplines required to carry out this research and technical service; develops engineering data and measurement capabilities; provides engineering measurement traceability services; develops test methods and proposes engineering standards and code changes; develops and proposes new engineering practices; and develops and improves mechanisms to transfer results of its research to the ultimate user. The Laboratory consists of the following centers:

Applied Mathematics — Electronics and Electrical Engineering[2] — Mechanical Engineering and Process Technology[2] — Building Technology — Fire Research — Consumer Product Technology — Field Methods.

THE INSTITUTE FOR COMPUTER SCIENCES AND TECHNOLOGY conducts research and provides scientific and technical services to aid Federal agencies in the selection, acquisition, application, and use of computer technology to improve effectiveness and economy in Government operations in accordance with Public Law 89-306 (40 U.S.C. 759), relevant Executive Orders, and other directives; carries out this mission by managing the Federal Information Processing Standards Program, developing Federal ADP standards guidelines, and managing Federal participation in ADP voluntary standardization activities; provides scientific and technological advisory services and assistance to Federal agencies; and provides the technical foundation for computer-related policies of the Federal Government. The Institute consists of the following centers:

Programming Science and Technology — Computer Systems Engineering.

[1]Headquarters and Laboratories at Gaithersburg, MD, unless otherwise noted; mailing address Washington, DC 20234.
[2]Some divisions within the center are located at Boulder, CO 80303.

Refrigeration for Cryogenic Sensors and Electronic Systems

Proceedings of a Conference held at the
National Bureau of Standards,
Boulder, CO, October 6-7, 1980

Edited by:

J. E. Zimmerman, D. B. Sullivan, and S. E. McCarthy

Electromagnetic Technology Division
Center for Electronics and Electrical Engineering
National Engineering Laboratory
National Bureau of Standards
Boulder, CO 80303

Sponsored by:
International Institute of Refrigeration — Commission A 1/2
Office of Naval Research — Naval Research Laboratory
Cryogenic Engineering Conference
National Bureau of Standards

U.S. DEPARTMENT OF COMMERCE, Malcolm Baldrige, Secretary
NATIONAL BUREAU OF STANDARDS, Ernest Ambler, Director

Issued May 1981

Library of Congress Catalog Card Number: 81-600038

National Bureau of Standards Special Publication 607
Nat. Bur. Stand. (U.S.), Spec. Publ. 607, 223 pages (May 1981)
CODEN: XNBSAV

U.S. GOVERNMENT PRINTING OFFICE
WASHINGTON: 1981

For sale by the Superintendent of Documents, U.S. Government Printing Office, Washington, DC 20402
Price $6.50
(Add 25 percent for other than U.S. mailing)

ABSTRACT

This document contains the proceedings of a meeting of refrigeration specialists held at the National Bureau of Standards, Boulder, CO, on October 6 and 7, 1980. Participation included representatives of industry, government, and academia. The purpose of the meeting was to discuss progress in the development of refrigeration systems which have been specialized for use with cryogenic sensors and electronic systems. The meeting focused primarily on the temperature range below 20 K and cooling capacity below 10 W. The meeting was jointly sponsored by the International Institute of Refrigeration-Commission A 1/2, the Office of Naval Research, the Naval Research Laboratory, the Cryogenic Engineering Conference, and the National Bureau of Standards.

Key words: Cryocoolers; cryogenic sensors; helium; refrigeration; superconducting devices.

TABLE OF CONTENTS

INTRODUCTORY REMARKS AND SUMMARY

This document contains the proceedings of the second of two conferences held at the National Bureau of Standards Boulder Laboratories on the subject of closed-cycle cryocoolers for small superconducting devices and electronic systems.

The first conference, whose proceedings are available from the Superintendent of Documents, U. S. Government Printing Office, Washington, DC, as NBS Special Publication 508, entitled "Applications of Closed-Cycle Cryocoolers to Small Superconducting Devices", was a meeting of about 40 invited speakers and participants. Its purpose was to review the state-of-the-art of small cryocoolers for temperatures below about 20 K, and to describe the needs of various prospective users of cryocoolers for superconducting and other cryogenic instruments used in biomagnetism, geophysics, magnetic anomaly detection, superconducting computers, Josephson voltage standards, space applications, millimeter-wave and infrared detection, and laboratory measurements. Also presented at this meeting were some new ideas for very-low-power low-interference cryocoolers, Stirling and Joule-Thomson types, particularly suited to many of the listed applications. A subject of special interest was a review of progress on high-T_c superconductors, since the cost, complexity, and drive power of a cryocooler can be reduced considerably if the instrument can be operated at temperatures above 6 or 8 K rather than at 4 K or below. There are, of course, some applications where lower temperatures are required in any case.

In short, the purpose of the first conference was to define the problem. The present conference was organized quite differently. It was open to all interested participants, and most papers were contributed. Invited papers are those by Roubeau and by Nisenoff, the former being a rather free-ranging discussion of some unconventional approaches to cryogenic technology, and the latter a comprehensive review of recent developments in high-T_c superconducting devices and materials. The contributed papers are on refrigeration concepts, systems and components suited to the support of cryogenic sensors and electronic systems below 20 K. Techniques and components developed for higher temperatures that are applicable to low-temperature refrigeration are included.

In reviewing the progress that has been made during the last three years, it is apparent that the desired goals have not been achieved. Nevertheless, there have been some notable developments. Several funding agenices, in particular the Office of Naval Research and Wright-Patterson Air Force Base, are now supporting conceptual studies and developments of low-power cryocoolers for superconducting instruments, and a number of such projects are underway. As described in this report, a helium liquefier-cryocooler for a superconducting computer has been built and is being tested. Also in this report are papers demonstrating increasing interest and emphasis on gas refrigerators using resonant mechanical systems driven by linear reciprocating electric motors and supported by gas bearings or magnetic suspensions. These systems offer the potential of ultimate simplicity, freedom from contamination, long life, and (eventually) low cost. Although the operation of such systems may at first glance appear somewhat subtle, we might point out the obvious, namely that the mathematical description of a resonant reciprocating cryocooler is identical (except for non-linearities) in all essentials to that of coupled electrical resonant circuits with a sinusoidal driving force, a system as familiar as sunrise to most electronic engineers (Probably even the non-linearities are analogous to a considerable extent). Finally, a book by Prof. G. Walker, Stirling Machines, has just been published by Plenum Press, and a companion book, Cryocoolers, is in press. These books are a very comprehensive source of information and references on the whole technology.

Approximatley one-half (57) of the participants at this meeting returned a questionnaire, distributed during the meeting, with answers to three questions. To the question "Has the conference been worthwhile?", 56 said yes and 1 said somewhat. To "Should it be held again?", the answer was yes, unanimously. To "At what interval?" 11 said 1 year, 33 said 2 years, 12 said 3 years, and 1 said 4 years.

There were several useful comments and criticisms. One was to allow more lead time and to provide for distribution of reprints at the meeting. Some comments concerning more industry participation are well taken and we suggest that an earlier planning meeting by an organizing committee made up of an even mix of industry, university, and government representatives might lead in the right direction. One should note that both government and industry papers were withdrawn because they could not be cleared by their organizations (proprietary considerations will certainly constrain some industry participation). We believe that the conference will be more lively and useful if the mix of participants provides for discussion of both new concepts and well conceived and engineered systems.

There were several suggestions that the papers should have been better screened. This is an oft-raised criticism with every conference. It is clear that papers can be rejected for obvious technical flaws or for failure to fit into the basic limits of the conference. However, judgments concerning the quality of a contribution are very difficult to make and many conferences have opted to exercise such judgment only in the published conference proceedings. This is what we chose to do in 1980. The next organizing committee will have to face the question again.

To conclude, and quite apart from the question of the usefulness of this meeting or similar meetings, it might be useful to repeat again the growing conviction that the ultimate fate of superconducting and other cryogenic instruments will depend heavily on the development of reliable, compatible, low-cost cryocoolers like those envisioned by the aurhors of the following papers.

The Editors

Organizing Committee:
J. E. Zimmerman, National Bureau of Standards - Chairperson
E. A. Edelsack, Office of Naval Research
R. W. Guernsey, International Business Machines
W. Haskin, Air Force Flight Dynamics Laboratory
M. Nisenoff, Naval Research Laboratory
J. L. Olsen, Eidg. Technische Hochschule
A. Sherman, National Aeronautics & Space Administration
D. B. Sullivan, National Bureau of Standards
K. D. Timmerhaus, University of Colorado

Conference Secretary: S. E. McCarthy, National Bureau of Standards

A PREVIEW OF UNCONVENTIONAL SUGGESTED COOLING PROCESSES AND SOME PRACTICAL PROBLEMS RELATED TO SMALL REFRIGERATORS

Pierre M. Roubeau

DPh-G/PSRM - CEN Saclay
B.P. N°2 - 91190 Gif-sur-Yvette, France

This paper describes two non-conventional means of refrigeration, perhaps out of reach of practical realization, whose purpose is to shed light on some properties of gases and adsorbants having great potential applications. An account is given of a variation of the Stirling machine and finally a sketch is made of a crossed cycles method independent of the refrigeration process used.

This descriptive part is sandwiched by overall considerations on heat losses, mainly by the cryostat necks and in general by any structures for which the non-heat conducting properties could, in fact, be an important criterion of success for cryocoolers. Concerning minicoolers which make use of a circulating coolant, the need for a dry and tight compressor is equally emphasized and some solutions are suggested.

Key words: Adsorption; cryocoolers; cryostats; helium; refrigeration; Stirling cycle.

1. Foreword

In the following, the refrigeration process will be considered between essentially room and liquid helium temperatures. Transposition to another fluid and another temperature range would in general remain valid subject to proper numerical adjustments. .

2. No! to liquid helium

The straightforward means of cooling a system down to liquid helium temperature is, evidently... to immerse it in liquid helium.

But...

In the first place this is an expensive liquid. However, the purpose of the "cryocoolers", topic of this meeting is not only to save money, as it is well known that the scale factor is dramatic for small installations. At the refrigerator itself the negative calorie will always be cheaper the bigger the plant.

The problem is

1) most of the users are not nearby big liquefiers,
2) liquid helium is costly to transport,
3) its conservation is expensive and, even for relatively short durations, it is practically impossible to conserve in small quantities,
4) finally only very competent and conscientious personnel are able to handle it without prohibitive spillage ; and when, by chance, such people are available it is more advantageous to assign them to more productive tasks.

Evidently, other parameters come in balance, such as need of independence, weight, and volume considerations, available finance etc...

In every case the final conclusion has been :

use of liquid helium : excluded ⇒ cryocooler : mandatory.

3. Analysis of refrigeration needs

What is the objective of refrigeration ?

1) to keep a system at 4.2 K by compensating unavoidable losses $\dot{Q}_A$ due to various causes ; heat radiation, residual gas conduction in an insulating vacuum, conduction by supports.
2) to absorb a certain amount of heat $\dot{Q}_B$ produced in the 4.2 K region by the system during its normal operation.

In small installations, conduction by supports : usually the neck of the cryostat calls for a detailed analysis. When, as is frequently the case, $\dot{Q}_B = 0$, conduction in the structure of a cryocooler, well insulated from thermal radiation, turns out to be a very important element of the thermal loss.

Let us consider a cryostat with a neck, the cross-section S(x) of which changes in such a way as to keep a constant thermal gradient between 300 and 4.2 K (practically this section would depart only slightly from the average one. Hence the following can apply to a real cryostat). The heat flux down such a neck $\dot{Q} = k(T) \cdot S(x) \cdot dT/dx$ decreases essentially as k(T) i.e. more or less linearly with T and reaches a value 70 times smaller at 4.2 K where it is identical to $\dot{Q}_A$. A regularly decreasing heat flux means that some refrigeration has been provided all along the neck at each temperature level.

Without being exactly proportional, the input power requirements and the structural complexity of a cryocooler are strongly correlated to the minimum work required by a Carnot cycle work between room temperature and a) 4.2 K concerning $\dot{Q}_A$,
b) temperatures distributed between 300 and 4.2 K at which $69/70^{th}$ of the heat flux entering through the neck at 300 K are absorbed. The work related to $\dot{Q}_A$ is then $W_A = \dot{Q}_A \cdot (300-4.2)/4.2 = 70.4\ \dot{Q}_A$ while that related to the neck $W_N = \dot{Q}_A (1/4.2) \int_{4.2}^{300} (1/T)(300-T)dT = 234.5\ \dot{Q}_A = 3.33\ W_A$.

Thus, the total required power for the refrigeration of an ideal cryostat reduced to a neck, is more than four times that which is necessary to absorb the residual heat flow which reaches the 4.2 K level.

In practice cryostat necks display neither a perfectly constant thermal gradient, nor an exactly linear thermal conductivity. This ratio of 4 is nevertheless a good order of magnitude at least as a lower limit for real cryostats.

One can wonder why this considerable requirement of refrigerating power is sometimes unnoticed. There are two reasons : 1) real cryostats are not reduced to necks and the above ratios 70 and 4 have to be reduced by $\dot{Q}_A$ total / $\dot{Q}_A$ neck and if some extra power is dissipated at 4.2 K by : $(\dot{Q}_A+\dot{Q}_B)/\dot{Q}_A$. 2) finally and more importantly it happens that when one makes use of liquid helium, the latter, in excess of its heat of vaporization : 80 j/mole at 4.2 K, has a specific heat practically constant and equal to the perfect gas value : 21 J/mole.K between 4.2 and 300 K, and is thus capable of a total heat absorption of precisely 70 times the heat of vaporization of liquid helium at 4.2 K. The refrigeration power provided "free of charge" by the vapor between 4.2 and 300 K is therefore sufficient to absorb nearly all the heat 70 $\dot{Q}_A$ entering through the neck except for $\dot{Q}_A$ which is precisely the source which generates these vapours.

Practically, taking account of the unavoidable losses of other origin, the neck "costs" nothing in most of the cryostats which use liquid helium. In cryocoolers the neck will be resuscitated, then the choice of the refrigeration process should be made preferably among those offering several cooling levels and even, if possible, a refrigerating power distributed

throughout the whole temperature span between 300 and 4.2 K. We will come back later onto the neck problem after having proposed a number of non-conventional refrigeration processes the practical realization of which does not seem easy in the actual state of the technique and in the author's imagination. These processes will perhaps be vitiated by trivial error or by a fundamental flaw but it is hoped that these exposition will help to stimulate thinking along certain channels which are the present time seem insufficiently explored.

4. C_p against C_v

The simplest and most immediate way of cooling which is actually the least feasible, technically speaking, consists of a counter-flow heat exchanger in which a gas cooled at constant volume is subsequently warmed at constant pressure : figure 1. The gain is $C_p - C_v = R = 8.3$ J/mole.K for a perfect gas. The exchanged heat between 300 and 4.2 K is :

at constant volume, under an initial pressure of e.g. 3 bars :	3600 J/mole
at constant pressure under 3 bars :	6000 J/mole
under a constant, low pressure (e.g. $p < 0.1$ bar) :	5970 J/mole

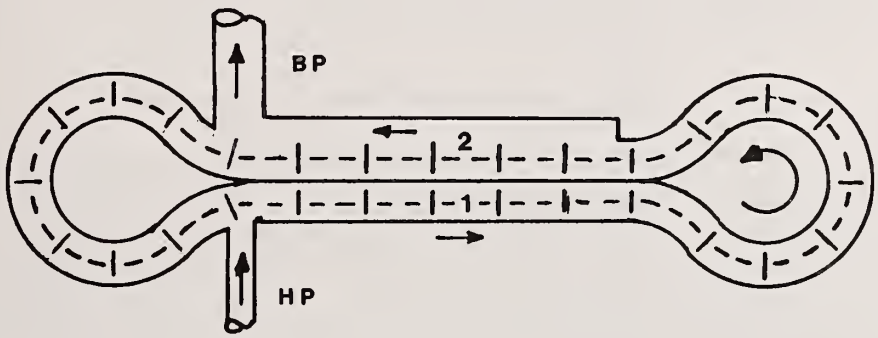

Figure 1 : *Refrigerator "C_p vs. C_v". In (1) the gas cools at constant volume, and in (2) it warms at constant pressure.*

Thus one can see that in a system operating between these pressures a cooling effect will be observed as soon as the efficiency attains : (6000-5970)/(5970-3600) = 1.27 % of the theoretical maximum.

Practically any leak or gas friction transfers a part of the gas flux to a Joule-Thomson cycle which is thermally neutral for a perfect gas and only slightly detrimental for helium (above 50 K).

Although this process has no immediate prospect one can anticipate some technological advances which would bring it nearer to a practical application :

1) availability of materials with a ratio $\frac{\text{E (elastic limit)}}{\text{C (specific heat)}}$ sufficiently high, at room temperature,

2) the discovery of rubber-like products preserving their elastic properties at low temperature,

3) the operation of a system in which the cooling takes place in a two dimensional space where one can realize constant "volumes" without walls (the surface of a sphere is an example),

4) the introduction of the gas at room temperature under a very high pressure into a matrix from which it could escape only as a superfluid below 2.17 K,

5) if... (any suggestion to fill this 5^{th} paragraph would be welcome).

We will make some supplementary remarks on this process. We will first calculate its refriger-

ation efficiency in the case of a perfect gas. It we take the optimum case, in which the pressure at the end of the cooling is equal to the constant pressure at which the warming occurs, one has the elementary compression work at constant temperature T_1(300 K) $dW = -P\,dV = RT_1 \frac{dP}{P}$ (for one mole). On the other hand, the cooling effect $dQ = (C_p - C_v)dT = R\,dT = RT \frac{dP}{P}$ from which the differential efficiency in the interval $\frac{dP}{P}$ (i.e. $\frac{dT}{T}$) is $n = \frac{dQ}{dW} = \frac{T}{T_1}$. The average efficiency $\frac{Q}{W} = \frac{R(T_1-T_2)}{RT_1 \mathrm{Log} T_1/T_2} = (1 - \frac{T_2}{T_1})/\mathrm{Log}\, T_1/T_2$ can be compared to the Carnot efficiency $n = T_2/(T_1-T_2)$. As an example for T_1 = 300 K, T_2 = 4.2 K: n = 0.014; and on a purely theoretical ground the cycle "C_p vs. C_v" becomes more advantageous than the simple stage Carnot refrigerating machine if both of the following assumptions are simultaneously realized :

1) $T_2 < T_1/2.5$ e.g. $T_2 < 120$ K

2) one needs distributed cooling between T_1 and T_2 and the Carnot machine envisaged delivers cooling at only one temperature: T_2

The "C_p vs. C_v" machine has two other peculiarities, when using a perfect gas : a) it provides no cooling at T_2. The necessary cooling will have to be delivered by a process founded on a different cycle.b) it does not "know" if it should produce cold or heat; it needs to be started in a refrigeration mode otherwise some parasitic heat source will start it in a warming mode and it will probably finally transform work into heat with an efficiency 1, and this is certainly not a remarkable performance.

5. The gas cocktail adsorption refrigerator

In this system a mixture of gases with different boiling temperatures is introduced under pressure into a column containing a moving adsorbant ribbon with which it moves parallel while being progressively adsorbed onto the coldest point where the saturation of the adsorbant is completed by the most volatile gas. The adsorbing ribbon is then led into a return channel under low pressure where the gases desorb successively at temperatures lower than those at which they have been adsorbed. Thus one produces : 1) a transportation of the heat of adsorption (practically independent of the temperature) from the lower to the higher temperature while creating a large ΔT favourable to thermal exchanges. 2) a counter-flow cooling of the adsorbed gas of specific heat $\simeq$ R by the desorbed low pressure gas of specific heat = C_p = 5/2 R.

The net effect for a gas mixture is hardly calculable due to the number of parameters but it is probably very important.

This cycle is akin to a multistage refrigerator using several refrigerating fluids with distributed boiling temperatures in which:

1) all fluids are incorporated in the same gas flux and use one compressor.

2) two bridges have been established between 50 and 25 K and between 14 and 5 K where mother nature has not yet produced any body in the liquid state.

What should be underlined is that only a relatively low adsorbant speed is necessary in order to realize a noteworthy gas flux. As an example, a flow of 1 cm^3 of activated charcoal per second displaces an amount of adsorbed gas of the order of 0.01 mole per second (at saturation).

The heat of adsorption is a function of the degree of saturation of the adsorber. It varies between a maximum (adsorbant degassed) and the heat of vaporization (adsorbant saturated). Table 1 gives approximate values of these heats relative to activated charcoal.[1]

The curves of figure 3 give, for instance, the cooling effect in joules/mole.K in the following application : adsorbant = activated charcoal, gas = He4, high pressure = 1 bar, low pressure = 1 millibar. The computation has been made using the formulas [1] : $L = 8600 - 2920 \log_{10}(V + 112)$ J/Mole and $\log_{10}P = [153 \log_{10}(V + 112) - 450].(1/T-.016) + 1.9 + \log_{10}V$, with P in Torr, V in $cm^3_{RTP}/gram$ of adsorbant, T in K.
(RTP = room conditions : 300 K, 1 bar, 1 Mole $\simeq$ 24500 cm^3).

Gas	Heat of adsorption on activated charcoal		Heat of vaporization (sublimation)
	maximum	average	
He	2500	1000	80
H_2	10000	4000	800
N_2	15000	10000	5600
CO_2	?	?	(18400)

Table 1 : *Approximate values of the heats of adsorption on activated charcoal (in Joule/mole).*

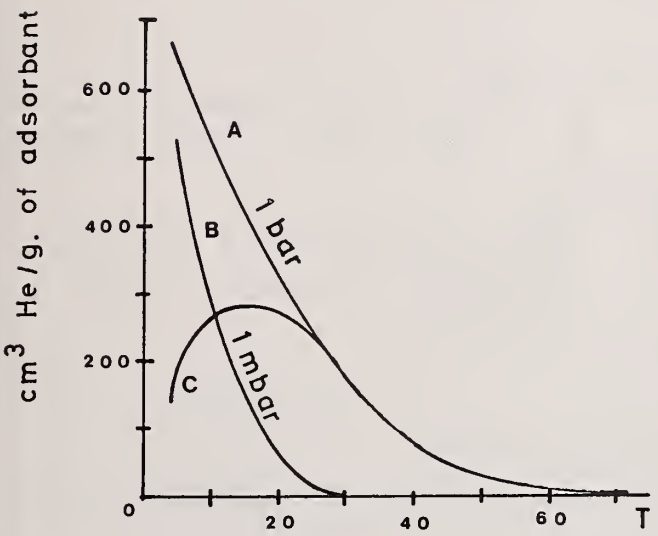

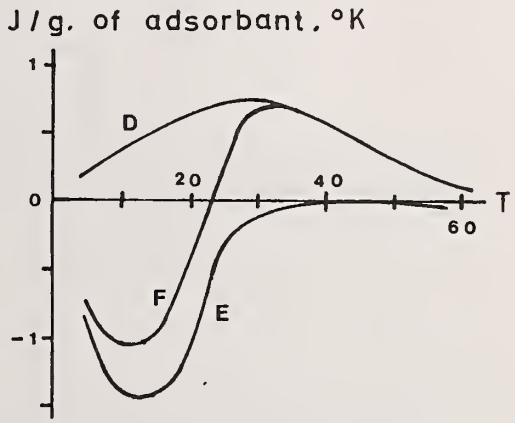

Figure 2 : *Amount adsorbed as a function of temperature.*
curve A : *P = 1 bar*
- B : *P = 1 millibar*
- C : *difference between A and B*

Figure 3 : *Differential heat of adsorption*
curve D : *P = 1 bar*
- E : *P = 1 millibar*
- F : *global effect = D-E*

The curves A and B in figure 2 give the amount adsorbed as a function of T under pressures of 1 bar and 1 millibar. Curves D and E of fig. 3 give the heats of adsorption (desorption) per gram of adsorbant and degree K under the same pressures. Curve F, which is the difference between D and E, gives the global effect. Finally, curve H (fig. 4) gives the net effect corrected with the specific heat difference times the difference of the amounts adsorbed : $((A-B)(\Delta V/24500)(5/2R-R))$. Besides this cooling effect which extends from 4.2 to 24 K one has the available heat of desorption at 4.2 K of 660-520 = 140 cm^3/g. of adsorbant, which will be calculated from the integral curve Q(V) given in figure 5 :
Q(660)-Q(520) = 27.5 - 25.8 = 1.7 J/g. of adsorbant which means 63 J/mole circulated.

Thus, the desorbing helium provides cooling essentially in the first zone 5K-14K where no liquid is available. Hydrogen will provide the bridge between 25 and 50 K and, above the latter temperature a number of gases exist for going up to room temperature.

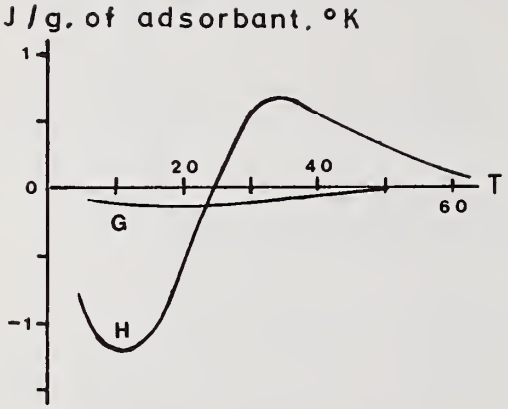

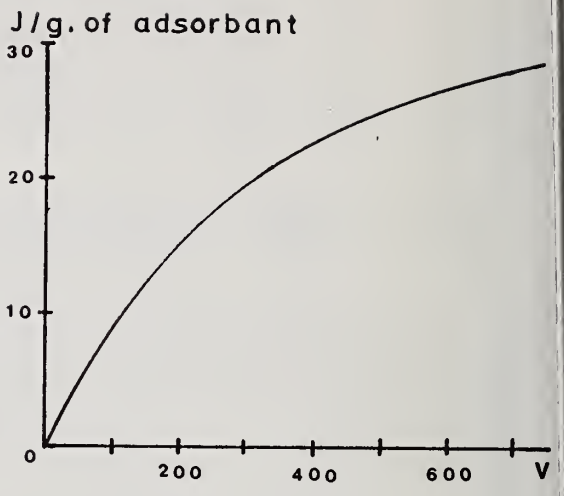

Figure 4 : corrected global thermal effect
curve G : correction due to the difference in specific heat $C_{p_3} - C_{v_2}$
curve H : corrected global effect = F+G

Figure 5 : Integral heat of adsorption $Q(V) = \int L(V)\, dV$.
(V in cm^3 RTP of helium for 1 gram of adsorbant).

6. The Bi-Stirling refrigerator

The machines which operate following a Stirling cycle, the Philips machine for instance, suffer contradictory requirements,

1) the pistons along which there is a thermal gradient have to move rapidly and offer an important clearance for minimizing the thermal exchanges between parts which periodically face each other when at different temperatures,

2) regenerators and heat exchangers must present temperature differences and pressure drops as small as possible and this demands a small gas speed,

3) at very low temperatures the specific heat of metals used in regenerators : copper, lead... becomes very small and lead to important volumes hence to important dead spaces.

In conclusion, the Stirling machine which is capable of reaching its full efficiency if compressions, expansions and exchanges are isothermal, even with arbitrary dead spaces (reversible cycles), suffers an efficiency decrease when the dead space increase coincides with the thermal gradients in the working space of the pistons.

The proposed variant consists of 1) replacing the pistons with bellows operated slowly which a) suppresses the shuttle effect and, b) allows isothermal compressions, expansions and thermal exchanges. The dead space of the bellows reduces to a certain point the specific power of refrigeration but has no effect on the thermodynamic efficiency, 2) replacing part or all of the regenerator by a heat exchanger between two machines which are 180° out of phase. One compressor with a manifold of valves assumes compressions and expansions. A separate system acts on the bellows to operate the gas transfers. Such a system is represented schematically in fig. 6.

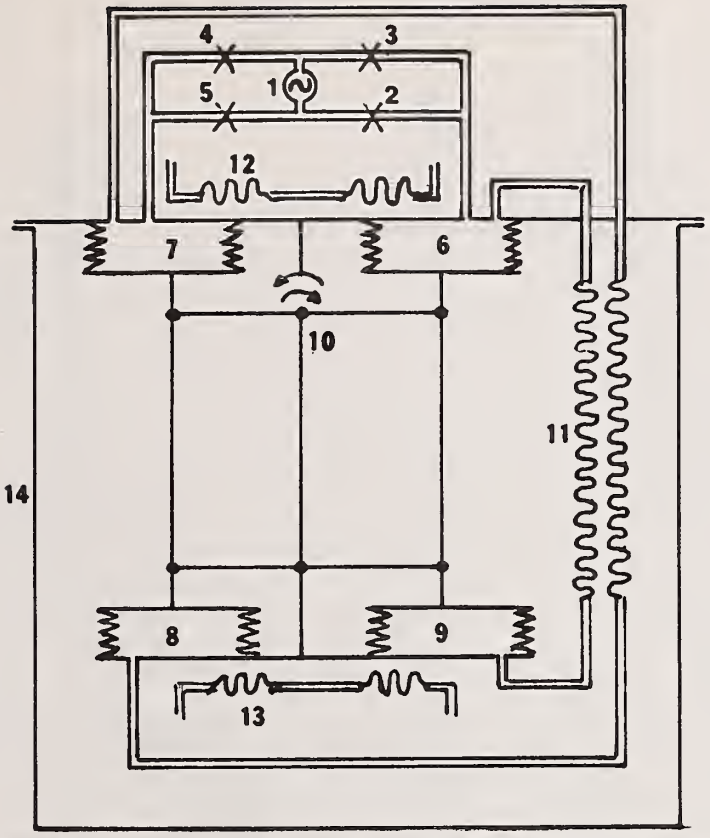

Figure 6. Schematic representation of the bi-Stirling refrigerator, in which the compressor-expander (1) and the valves (2, 3, 4, and 5) are operated in synchronism but 90° out of phase with the bellows (6, 7, 8, and 9) by the mechanical drive (10). The fluid undergoes a Stirling refrigeration cycle alternately in the left-hand set of bellows and in the right-hand set, with displacement through the counterflow heat exchanger (11). Heat is rejected at the warm (ambient) end through the heat-exchanger (12), and heat is absorbed at the cold end from the heat-exchanger (13). The outer shell (14) is the vacuum case.

7. The crossed cycles refrigerator

This proposed process combines a) an alternating flow of a caloric fluid in a fixed column of ideally zero specific heat, with b) a reversible local cycle external to each level of the column and operating at the same frequency with appropriate dephasing.

At each point of the column the external cycle induces a fluctuation of the temperature larger than the one of opposite sign, which would be due to the displacemnt of the fluid alone.

A molecule of this fluid follows the cycle represented in figure 7. The line AB would depict a cycle with zero dephasing. The elliptic curve suggests a real cycle obtained with a given dephasing. The arc NPR is related to the heating part of the external cycle, and the arc RQN to the absorption of heat by the latter.

The heat received by the fluid between x_P and x_m and given back to it between x_m and x_Q is represented in figure 8.

The overall result is an outgoing fluid at the warmer end at a temperature above room temperature and an outgoing fluid at the colder end at a temperature below T_2.

A practical realization would necessarily include a heat capacity effect related

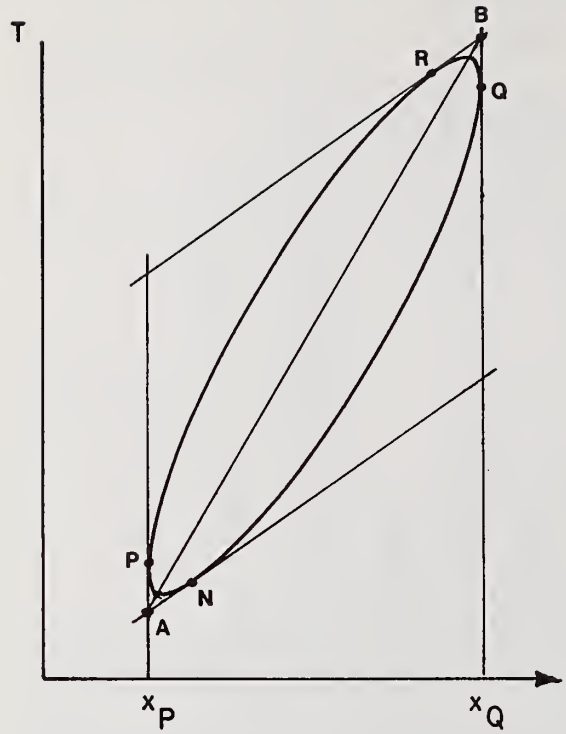

Figure 7 : thermal cycle of a molecule in the field.

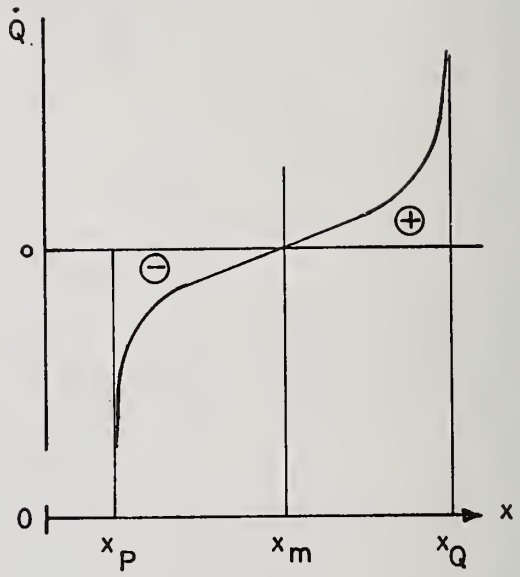

Figure 8 : heat exchanged in one cycle.

to the walls or to the local cycles, which will make this cycle more or less a relative of the Stirling cycle.

Figure 9a shows a conical piston compressor which, subject to an alternating displacement of small amplitude, cycles the pressure of a gas locally without displacing it. A separate system forces the fluid to oscillate from the warm end to the cold end and conversely.

Figure 9b shows a derived variant in which the displacement system has been omitted and replaced in its dephasing part by the pressure drop between cylindrical sliding parts. A net flow will occur if one chooses a displaced cold volume larger than the dead space at the volume warm end.

8. The necks of the cryostats

Cryocooler necks require special attention. In order to shed light on this problem let us consider, at first, the losses in a cryostat neck bathed by the vapours of an evaporated cryogenic liquid. These losses are represented in fig. 10 : $\dot{Q}_N$ represent the supplementary losses related to the neck as a function of the losses from other sources (normalization is made at unity for the value $\dot{Q}_N$ extrapolated for $\dot{Q}_N$ if $\dot{Q}_R \Rightarrow 0$). In most cases the thinnest neck would give a ratio $\dot{Q}_R/\dot{Q}_{N_o} >> 1$, but one can see that $\dot{Q}_N$ is practically zero for $\dot{Q}_R/\dot{Q}_{N_o} > 1.15$ and therefore one obtains a better mechanical sturdiness by increasing the neck thickness within the ratio $\dot{Q}_R/\dot{Q}_{N_o} > 1.5$ and ... one forgets the neck problem.

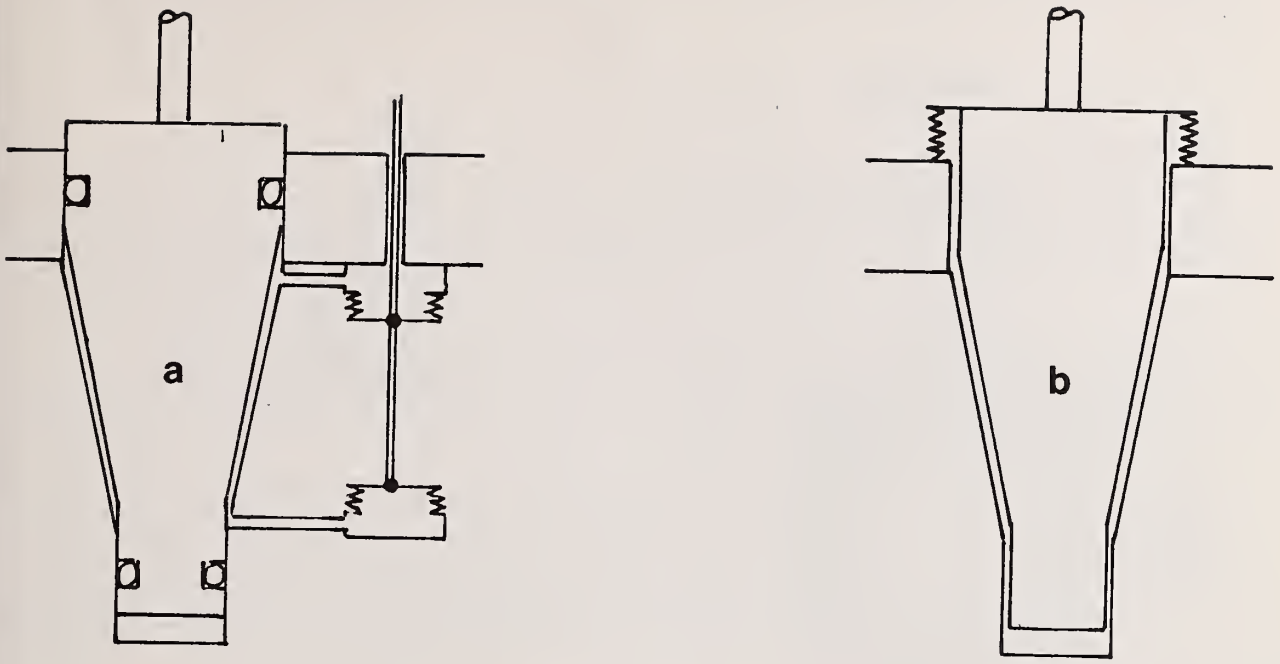

Figure 9 : *crossed cycles refrigerator with local adiabatic compression.*

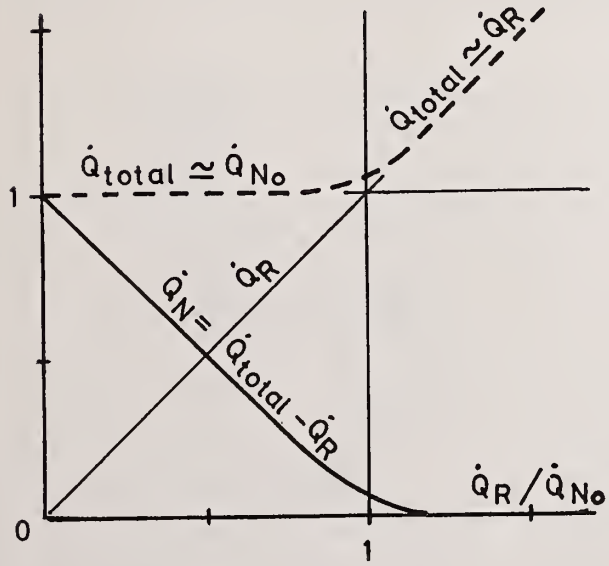

Figure 10 : *Losses in the necks compared to other sources of losses*

--------- $\dot{Q}_{total}/\dot{Q}_{N_o}$

———— $\dot{Q}_N/\dot{Q}_{N_o}$

In the case of cryocoolers one does not have this distributed source of refrigeration constituted by the vapours heat content. This would result in a heat loss due to the neck an order of magnitude higher which, in most cases, will overide the other heat loads. If one intends for example to dissipate at 4.2 K all the heat conducted along the neck from room temperature one will face a disastrous efficiency. Practically all proposed processes shall include an intermediate refrigeration level and it is more and more evident that those having the best performance will be 3 staged.

Let us take, for instance, the schematic cryostat of fig.11 which has 3 levels of refrigeration at temperatures arbitrarily fixed in geometrical progression i.e. below room

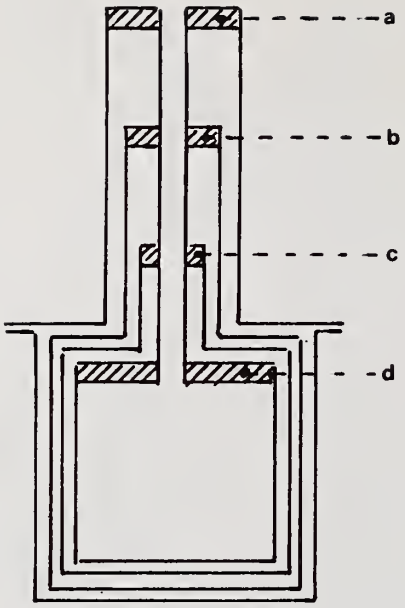

Figure 11 : *Typical cryostat*

a : warm end at 300 K
b : 1st stage at 72 K
c : 2nd stage at 17.4 K
d : 3rd stage at 4.2 K

temperature (300 K) : 72 K, 17.4 K and 4.2 K. The characteristics of this high performance cryostat and its calculated losses are given in table 2.

Characteristics:

useful volume : 2 liter

surface exposed to heat radiation : 1000 cm^2

emissivity : $\frac{\varepsilon_1+\varepsilon_2}{2} = 0.01$

neck: $l = 3 \times 10 = 30$ cm; e = 0.01 cm; Ø = 1.5 cm

Zone	$\dot{Q}$ Rad.	$\dot{Q}$ Neck	W.Carnot
300-72 K	500 mW	130 mW	2. watt
72-17.4 K	1.7 mW	13 mW	.040 watt
17.4-4.2 K	6. µW	800 µW	.003 watt

Table 2 : Typical cryostat characteristics.

The latter calls for two remarks : 1) The losses due to the neck between the lower stages are 10 times more important than the radiant heat between 72 K and 17.4 K and 100 times more important between 17.4 K and 4.2 K. This emphasizes the significance of progress in neck technology and generally in"supports-technology", that will be demanded by progress in other

related fields. 2) Every installation which will make use of liquid nitrogen for cooling of the first stage is, even with due regard to the scale factor, more than ten times smaller, ten times lighter,and finally ten times cheaper than a system starting from room temperature.

9. The need of contamination-free compressors

In every refrigerator which makes use of circulated helium, gas purification after compression, to free it from oil, water and other contaminants such as air or other gases is a burdensome task which often leads to the need of periodically stopping the system for clean-up. The use of dry and tight compressors would be a major improvement. But, even with many potential applications outside the field of cryogenics, it is surprising that a small contamination-free compressor, is not commercially available.

In fact we have used a two stage rubber diaphragm compressor with slightly modified heads for a year of uninterrupted service which worked between 0.2 and 3.5 bar abs. Only a very small contamination has been observed, probably due to diffusion of air through the diaphragm and the rilsan tubing which leads to monthly warmup and purging of impurities.

Two types of small compressors which should give satisfying results are represented in figures 12 and 13 . In the first one a very thin metallic bellows compressed by a liquid properly degassed, compressed itself by another bellows by means of a mechanical device, offers the advantages of 1) permitting an isothermal compression; 2) being insensitive to thermal expansion of the liquid and hence requires neither pump nor value for the liquid body and 3) capable of tolerating important depressions on the low pressure side.

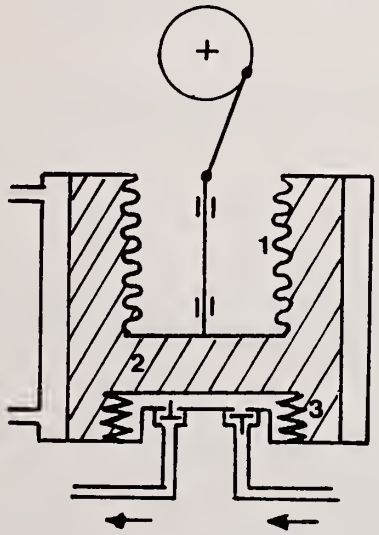

Figure 12 : *Bellows compressor*
1. *mechanical bellows*
2. *liquid*
3. *thin bellows*

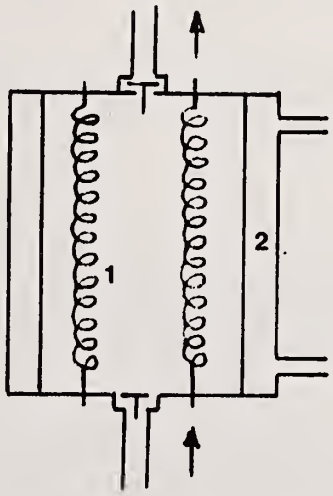

Figure 13 : *Thermocompressor*
1. *heating wire*
2. *water or liquid nitrogen for cooling.*

The second system is a thermocompressor : a gas volume is warmed by a short ohmic heating of a wire placed in this volume, the resulting increase of pressure opens the exhaust valve and pushes out a part of the gas. The subsequent cooling induces a depression which opens the inlet valve and restores the initial conditions. This system has the advantage of extreme simplicity. It is silent and is readily apt, by adding stages, to produce arbitrarily high compression ratios. It can even be used at very low pressure (≃ 1 Torr), subject to the use of actuated valves.

References

[1] P. Roubeau, G. deNigohossian, and O. Avenel, Adsorption de L'helium 4 par le charbon actif - Colloque international "Vide et Technicens", Grenoble, 1969. Supplement to "Le Vide" No. 143.

REFRIGERATION REQUIREMENTS FOR SUPERCONDUCTING COMPUTERS

R. W. Guernsey and E. B. Flint

IBM Thomas J. Watson Research Center
Yorktown Heights, New York 10598

High speed, low power Josephson junction logic and memory chips densely packed into a structure immersed in liquid helium may constitute the high performance computer of the future. In this paper we discuss chip cooling, input/output cable requirements, computer cryosystem design considerations, and refrigeration requirements.

Conventional gas expansion refrigeration should be suitable for medium to large size superconducting computers (0.5 to 10 watts). Small systems, such as a 25 mW future minicomputer, will require innovative refrigerator design that achieves high reliability at low cost.

Key words: Cryogenic equipment; 4K refrigeration; Josephson junction devices; superconducting computers; thermal contact.

1. Perspective

Research is in progress on a wholly new integrated circuit technology that may eventually replace semiconductors in high performance digital equipment [1]. The basic elements are Superconducting QUantum Interference Devices (SQUID) that can be switched from a non-resistive to a resistive state in roughly 10 ps by the magnetic field from a nearby control line. From these elements, one can build a very high-speed logic family and memory to match [2].

High-speed switches (or gates) alone, however, do not guarantee a high-speed computer. Intercircuit signals, typically travelling at half the speed of light, take 10 ps to go only 1.5mm. In order to avoid excessive signal propagation times, then, one must pack the circuits (and chips) closely while managing to get power in and the heat out. For example, in making an ultra-high performance computer one would want to package the logic and memory in a cube 9 cm on a side. Such a machine made with present semiconductor technology might dissipate as much as 20kW [2]. The delivery of this amount of power and its removal as heat in such a small package would be impossible with today's technology. A comparable machine made with superconducting circuits might dissipate roughly 10W [2] which would be easy to remove, even at 4.2K. The power distribution [3] would be via fine superconducting lines. It is the combination of the high speed and the low power of superconducting circuits that may put them in future computers.

An obvious consideration in judging the practicability of a superconducting computer is the refrigerator, and so there is interest in the state of this technology and in what improvement in reliability and reductions in cost could come in the next ten years. We present in this paper, as best we can predict, what a superconducting computer's cryosystem requirements might be. Let us take a more detailed look at these by starting at the heat source.

2. Heat transport: circuit to sink

Most of the heat generated by the circuits travels through several thin film layers to the chip substrate (a 6.4 mm square of silicon) which is isothermal because of its high thermal conductivity (~ 2 W/cmK). Most of this heat

then passes out the non-circuit side of the chip to a refrigerated heat sink such as a liquid helium bath. Heat transport in the bath is by natural convection, and heat transfer at the chip surface is aided by the stirring action of local boiling.

Figure 1 shows the expected chip temperature rise as a function of the chip power [4], and also shows anticipated power levels for logic, fast memory (cache), and main memory chips. These are essentially the same whether or not computations are taking place. The somewhat poorer heat transfer obtained as the chip power is brought up initially probably is due to incompletely developed nucleate boiling. Note that the substrate temperature for the three kinds of chips should run from 7 mK to 240 mK higher than the bath temperature. Note also that the highest chip power is only about 4% of the nucleate boiling limit, and if this power were increased tenfold then the chip temperature would be less than 400 mK above the bath.

In a small computer, one might choose to dispense with the bath and make a greased thermal contact to the chips. At 4.2K, the grease to silicon boundary resistance is negligible compared to the resistance of practical thicknesses of grease. The heat transfer characteristic for a 2μm thick, 6.4 mm square of silicone grease [5] is shown in Fig. 1.

For the interferometers currently in use at IBM, the maximum desirable chip substrate temperature is 4.5K, and one can expect successful operation of a machine whose chips vary in temperature from 4.0 to 4.5K. Then, for example, one could operate with a total spacial and temporal temperature variation from 4.0K to 4.2K, and so the variously loaded chips could run up to 0.3K warmer.

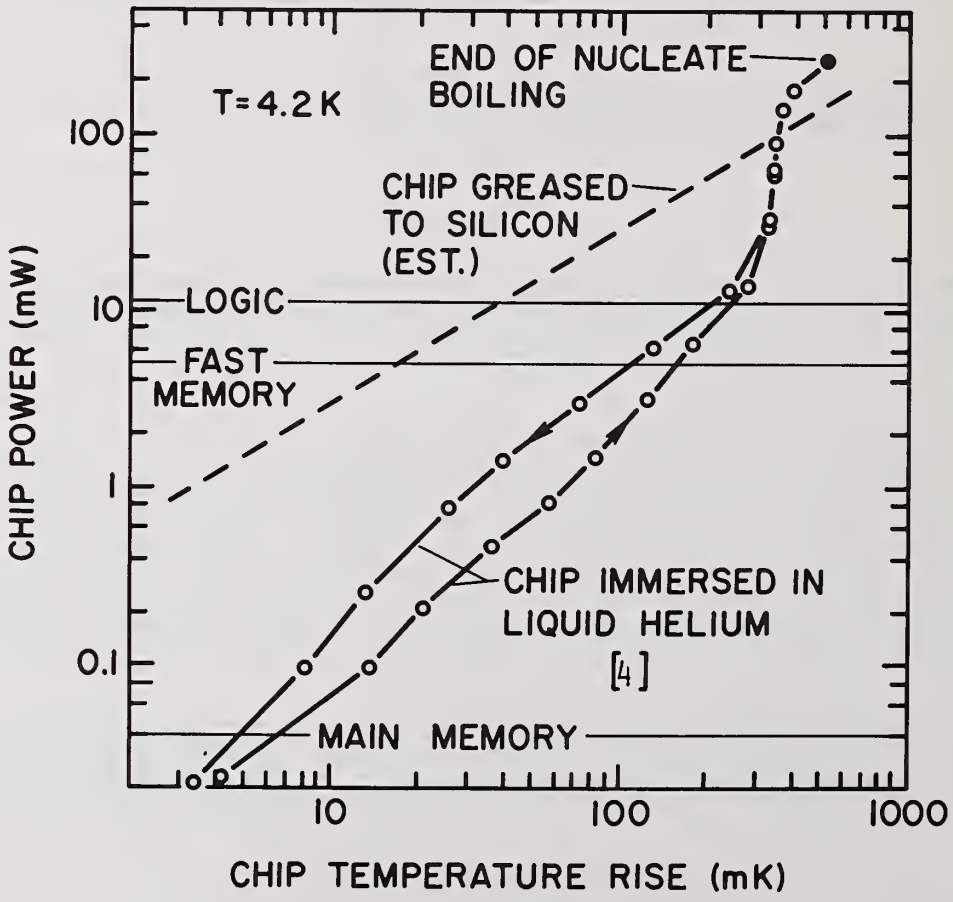

Figure 1: Chip Cooling Characteristics

3. Medium to large computer cryosystem

The logic and memory chips of a medium to large computer might be mounted on cards that plug into a box-like structure as shown in Fig. 2. This would be immersed in liquid helium, and the chips would be cooled by natural convection of the liquid up the vertical channels. A large computer might require a box structure 9 cm on a side and would dissipate approximately 10W of heat into the bath. A medium capacity computer might dissipate 0.5W to 2W.

Communication to room temperature support equipment would be via a multiple stripline input/ouput cable as shown in Figs. 2 and 3. Each copper line and associated groundplane would have a cross-sectional area of roughly 6.1×10^{-5} cm^2, and an ultra-high performance computer might have 400 lines. If these were thermally grounded at 75K and 18K as shown in Fig. 3, with a 20 cm length between stages, then the heat leak to these grounds would be 1.2W and 1.0W, respectively, and the heat leak to the 4.2K bath would be 0.3W which is small compared to the computer's 10W. Perhaps 20 of these lines would supply the power and so would have noticeable resistive heating that could bring the total I/O heat loads for the large system to 4.7W, 2.0W and 0.8W at 75K, 18K and 4.2K, respectively. One sees that the I/O lines will have little effect on the 4.2K refrigeration requirement.

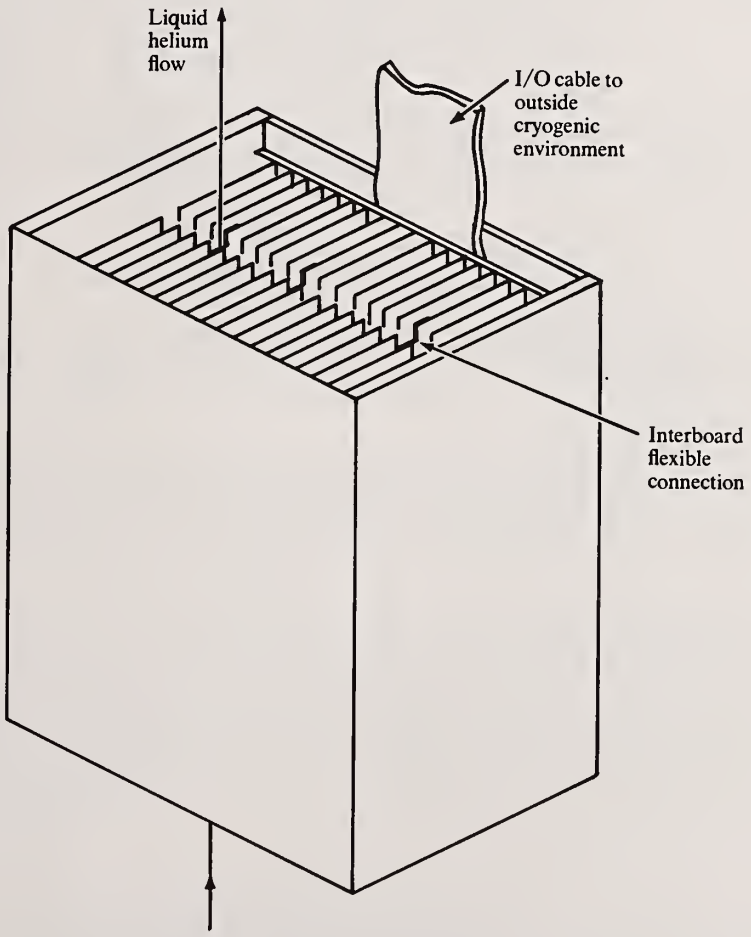

Figure 2: A Superconducting Computer Package Unit

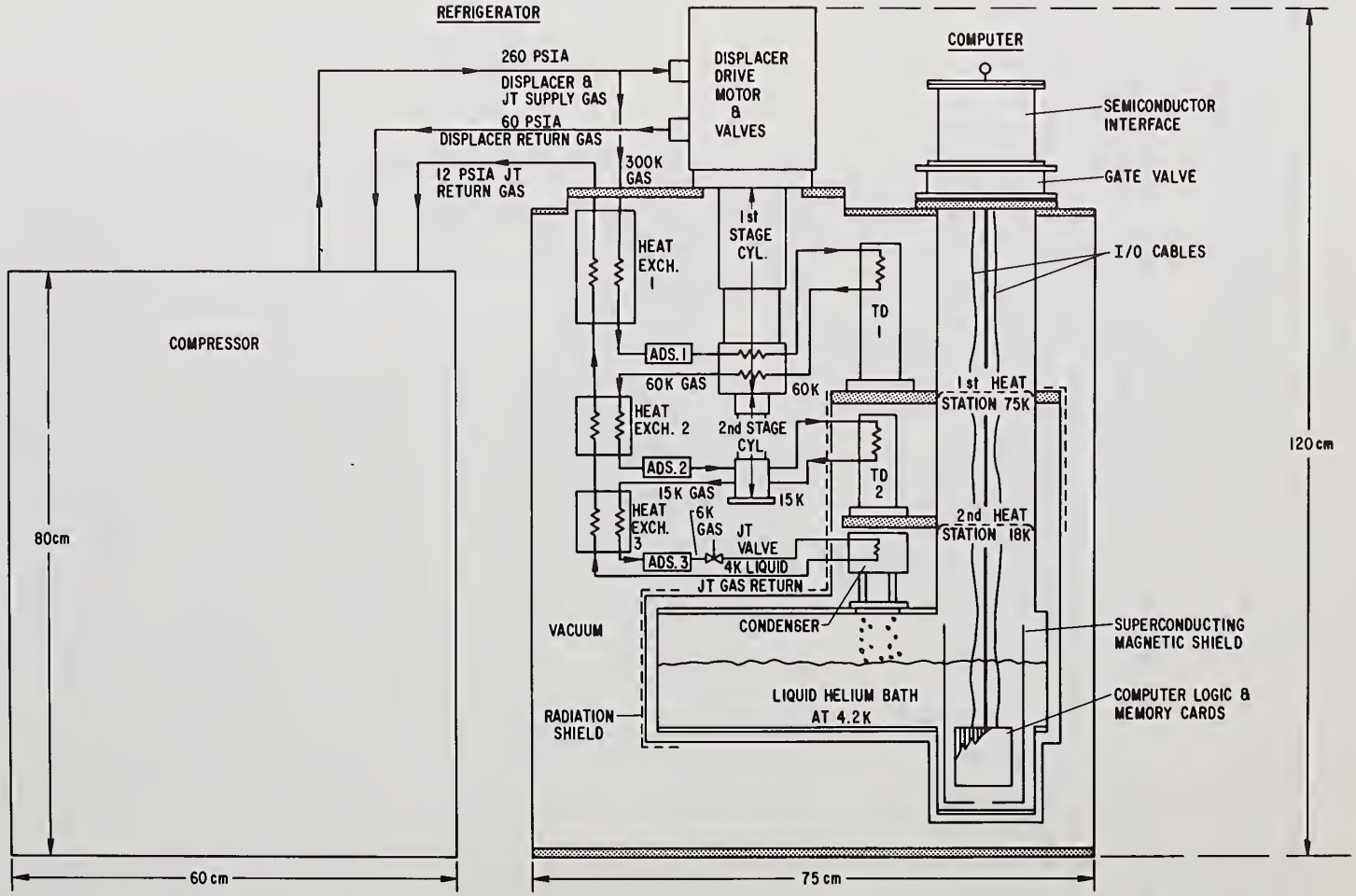

Figure 3: A Cryogenic System for Medium (0.5W) to Large (10W) Superconducting Computers.
JT = Joule-Thompson expansion valve, ADS = adsorber, TD = thermal diode.

There are three principal functions that we wish to achieve in a medium to large sized computer cryosystem:

(1) Uninterrupted computer operation during refrigerator servicing,
(2) Uninterrupted refrigeration operation during computer removal, and
(3) A semi-annual or longer service interval

An integral refrigerator/dewar cryosystem that should meet these requirements is shown in Fig. 3. If the refrigerator should fail or be shut down, then the thermal couplings (TD1, TD2, and condenser) isolate it from the bath which then provides temporary refrigeration by gradually boiling away. When the refrigerator is returned to operation, helium gas is liquefied to replenish the bath. The computer can be removed by pulling it up into a special room temperature service housing (not shown) that serves as an air lock. Heat from the I/O cable and from radiation and conduction in the dewar neck is intercepted by 75K and 18K heat stations that are part of the computer support structure. Each of these delivers its heat across a narrow annular gap to a refrigerated ring in the dewar neck wall. The compressor, refrigerator, and thermal couplings as shown schematically in the figure have been designed and built for IBM by the Advanced Products Division of Air Products and Chemicals. Further discussion of the design and performance is given by R. Longsworth and E. Flint et al. elsewhere in these proceedings.

An important feature of the refrigerator/dewar interface scheme is the simplicity of the connection between the refrigerator and the couplings. This consists of six small lines that carry the JT gas at various temperatures, and these can be made flexible (for vibraton isolation) or longer (for remote refrgerator placement). For example, in order to simplify dewar design or to make the system fit in tight quarters, one might place the refrigerator in a separate enclosure joined to the dewar by an evacuated link that carries the interconnecting tubing.

Good magnetic shielding is requried for the logic and memory devices. This can be provided by ferromagnetic shields and/or a superconducting shield as shown in Fig. 3. Materials having low remanent magnetization such as silicon, glass, polymide, aluminum, selected beryllium and copper, and molybdenum must be used for structures within the shield.

4. Cryogenic challenges

Refrigerator, interface, and dewar technology suitable for commercial medium to large superconducting computers is available, and we look for continued improvement in reliability, efficiency, and cost. Obtaining high reliability is of greatest importance. Installations in aircraft or satellites will pose obvious additional problems that challenge present day cryogenic technology.

The commercial viability of small superconducting computers (power < 0.5W) depends on both the reliability and the cost of the cryogenic system. In the extreme case of a future minicomputer, one would like to have a 25 to 50 mW 4K refrigerator for a few thousand dollars. This calls for real engineering innovation. One could think of simply using a large dewar, but a reasonably sized system is likely to need monthly fillings and the logistics of this for a machine destined for a diverse market look unattractive.

A schematic drawing of a hypothetical future minicomputer is given in Fig. 4. There would be no liquid helium bath and the chips would be cooled by greased contact to a silicon heat sink. The refrigerator would be capable of rapid cooldown ($\sim$ 10 min with the computer off). It might be a gas cycle machine depending on an external compressor, or it might be an innovative self-contained system where only exhaust heat and electrical or mechanical power pass through the interface. While magnetic, para-electric, and other cooling techniques are possible, gas expansion may be the most practical. An isothermal expansion of 13 mg of helium gas at 4K from 1 cm^3 to 2 cm^3 in one second can, in principle, produce 80 mW of refrigeration. The challenge is in delivering the expansion work out of the system and in recycling the gas.

5. Summary

Superconducting computers requiring closed cycle 4K cryosystems of up to 10W capacity may be on the market in the future. The medium to large size machines will be cooled by convection in a refrigerated liquid helium bath. Current refrigerator, interface, and dewar technologies are adequate for this application, although improved reliability, efficiency, and cost would be desirable. The future commercial viability of small superconducting computers depends on the development of new low capacity, low cost, but highly reliable 4K refrigerators.

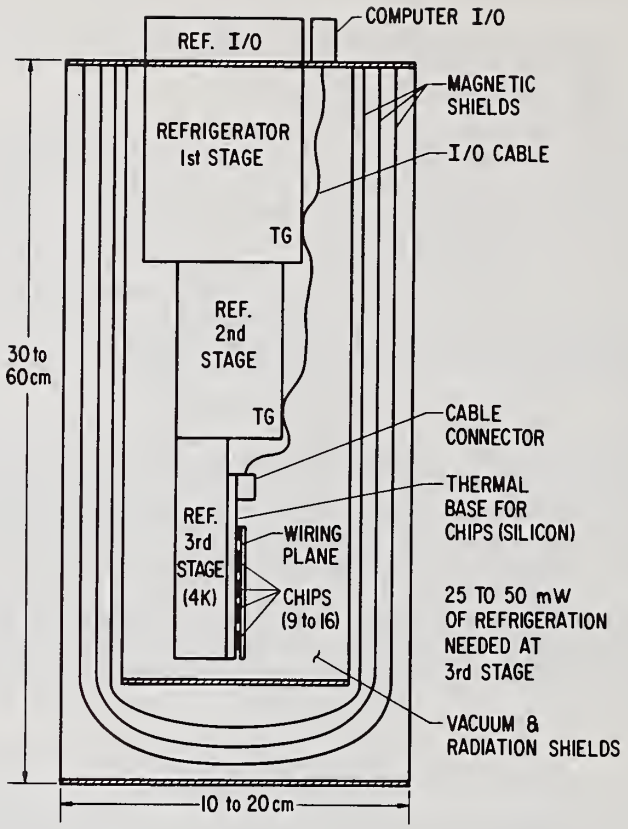

Figure 4: A Hypothetical Superconducting "Future Minicomputer". TG = thermal ground

6. References

[1] Matisoo, J., The Superconducting Computer, Sci. Am. 242, [5], 50-65 (May 1980).

[2] Anacker, W. et al., Josephson Computer Technology, IBM J. Res. Dev., 24, [2], 107-264 (March 1980).

[3] Arnett, P. C and Herrell, D. J., Power Design for Gigabit Josephson Logic Systems, IEEE Trans. Microwave Theory Tech., MTT-28, [5], 500-508 (May 1980).

[4] Flint, E. B., Jenkins, L. C, and Guernsey, R. W., to be published.

[5] Kreitman, M. M. and Callahan, J. T., Low Temperature Thermal Conductivity of Several Greases, Rev. Sci. Instrum., 40, 1562-1565 (1969).

DEVELOPMENT APPROACHES FOR LONG-LIFE CRYO-COOLERS

Ronald White
William Haskin

Flight Dynamics Laboratory
Air Force Wright Aeronautical Laboratories
Wright-Patterson Air Force Base, Ohio 45433

Development of cryogenic refrigerators (cryo-coolers) capable of operating for over three years without maintenance is being sponsored by the Flight Dynamics Laboratory for several Air Force missions. Future cryo-coolers for superconducting devices will need similar high reliability and durability. Therefore, the general approaches used and the lessons still being learned will be described as they apply to all long-life cryo-coolers.

Highly reliable and durable cryo-coolers are developed in a carefully planned and controlled process. Required operating conditions will influence the selection of the basic type of cooler, but the selected concept must have an inherent long-life potential. The principal long-life cryo-coolers being developed by the Flight Dynamics Laboratory are the Vuilleumier (VM), turbo-Brayton and rotary reciprocating refrigerators. These machines either use gas film bearings to avoid rubbing contact or have lightly loaded bearings and seals with low wear rates.

Careful development is necessary to realize the long-life potential of the coolers. This includes detailed analysis of stress levels for all parts of the cooler, adequate quality controls, contamination control, and reliability analysis. Final verification of adequate durability, with acceptable cooler performance, is demonstrated by reliability growth in a test, analyze, and correct program.

Key words: Component development; contamination control; cryogenics; helium retention; long-life; refrigerators; reliability; rotary-reciprocating; turbo-Brayton; Vuilleumier.

1. Introduction

Cryogenic refrigerators (cryo-coolers) capable of operating for over three years without maintenance are being developed by the Flight Dynamics Laboratory for several Air Force missions. Other applications may permit occassional maintenance, but good reliability and dependability will always be essential. This is especially true for future superconducting devices. The experience gained and the lessons still being learned in the development of long-life cryo-coolers will benefit future programs.

Active development of several types of long-life cryo-coolers is in progress. Different design approaches are being pursued until sufficient success is obtained to satisfy various requirements. Air Force efforts include Vuilleumier (VM) cycle, turbo-Brayton and rotary-reciprocating (R^3) Brayton cycle refrigerators. These coolers produce temperatures as low as 10°K with cooling capacities ranging from 0.1W at 10°K to over 10W at temperatures between 70° and 100°K. The turbo-Brayton and rotary-reciprocating refrigerators can be designed to produce temperatures down to 4°K or lower, and component development is planned for improved refrigerators to provide cooling at 4°K. The cryo-coolers presently being developed will be used to describe the approaches for obtaining long-life.

The VM cooler achieves internal pressure changes by gas displacement to different temperature volumes rather than by mechanical compression. The total gas volume in the cooler remains constant. Forces on bearings and seals are therefore sufficiently low to allow long operating times. Heated cylinders with domes maintained at 960°K are used for thermal compression, and gas expansion in the cold cylinder provides refrigeration. A small electric motor is used to overcome friction and control the motion of the displacers in the cooler. Thermal regenerators are used to exchange heat between incoming and exiting gas streams, to obtain adequate efficiency, for this reversing flow refrigeration cycle in much the same way as counterflow heat exchangers do in continuous flow refrigeration cycles. Figure 1 shows a schematic of a VM cooler which has two hot cylinders and three stages of expansion. This cooler [1] is being developed at the Hughes Aircraft Company for long duration Air Force missions.

The turbo-Brayton cooler uses small, high speed turbine wheels supported on gas film bearings to achieve compression and expansion of the working gas in the machine. Since there are no rubbing parts, the cooler should be capable of long term operation. A two-stage development model turbo-Brayton cooler [2] is being assembled at the AiResearch Manufacturing Company of California. Figure 2 shows a schematic for the arrangements of this cooler.

The concept of combining the efficiency of recpirocating refrigerators with the long-life capability of components suspended on gas film bearings provided the basic approach for rotary-reciprocating refrigerators (R^3). This type of machine is characterized by pistons rotating on their central axes at 1200-1400 RPM as they reciprocate at a cycle rate twice their rotational speed. This motion provides porting action to control the flow of the working gas which is compressed and expanded in different sections of the machine to produce refrigeration. The pistons are driven by electromagnetic actuators. Counterflow heat exchangers are used to implement the reverse Brayton cycle. A two-stage unit of this type has been tested and components are being developed by Arthur D. Little, Inc. [3] for a three-stage unit. Figure 3 shows the basic arrangement for a R^3 system.

The Stirling cycle is often used for comparison because it is potentially the most efficient. It is a refrigerative cycle with a cold section very similar to the VM cooler. However, the gas is compressed by a mechanical piston instead of heated cylinders. The forces on the bearings and piston seals are therefore significantly higher than the VM which has resulted in wear and shorter life. Recently NASA contracted with Philips Laboratories[4] to design and build a long life linearly driven Stirling cooler utilizing non-contacting magnetic bearings and clearance seals. This cooler will be described in another paper at this conference.

As indicated above, there are reasons to expect each type of cooler to be capable of operating for long periods of time. However, careful development is necessary to determine the true long-life potential. Methods used in these developments are described in the next section.

2. Development approach

In planning the development of a long-life cryo-cooler, the first essential step is to choose a type of machine which has an inherent capability to operate for long periods of time under expected environmental conditions. Although this is obvious, the applicable technology may need to be examined in some detail before making a decision. For example, an oil lubricated reciprocating compressor is generally accepted as having better durability and reliability than a dry lubricated reciprocating compressor. However, use of the oil lubricated compressor depends on the ability to separate the oil from the working gas in the refrigerator. Periodic replacement of the oil separation filters will be necessary. Thus, the oil lubricated compressor is not acceptable for use in a location where equipment cannot be maintained. The maintenance problem might be circumvented by use of devices such as rolling diaphram seals, but these add further complications which must be considered. These include a full-time oil support for the diaphram seals, a system to dispose of the helium that permeates into the oil through the diaphram seals, a helium makeup and control system, and devices to compensate for oil displacement and expansion.

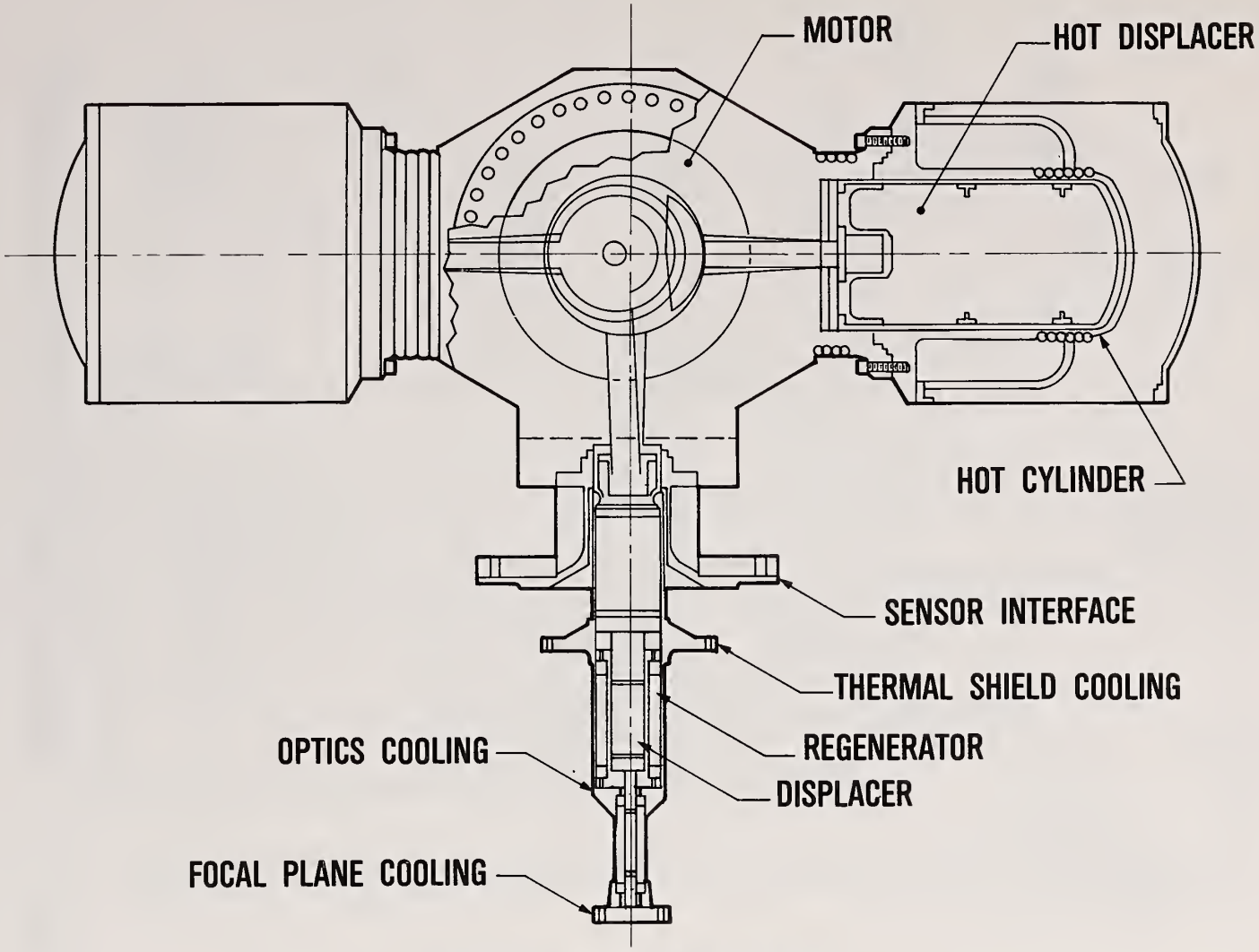

FIGURE 1. VM COOLER

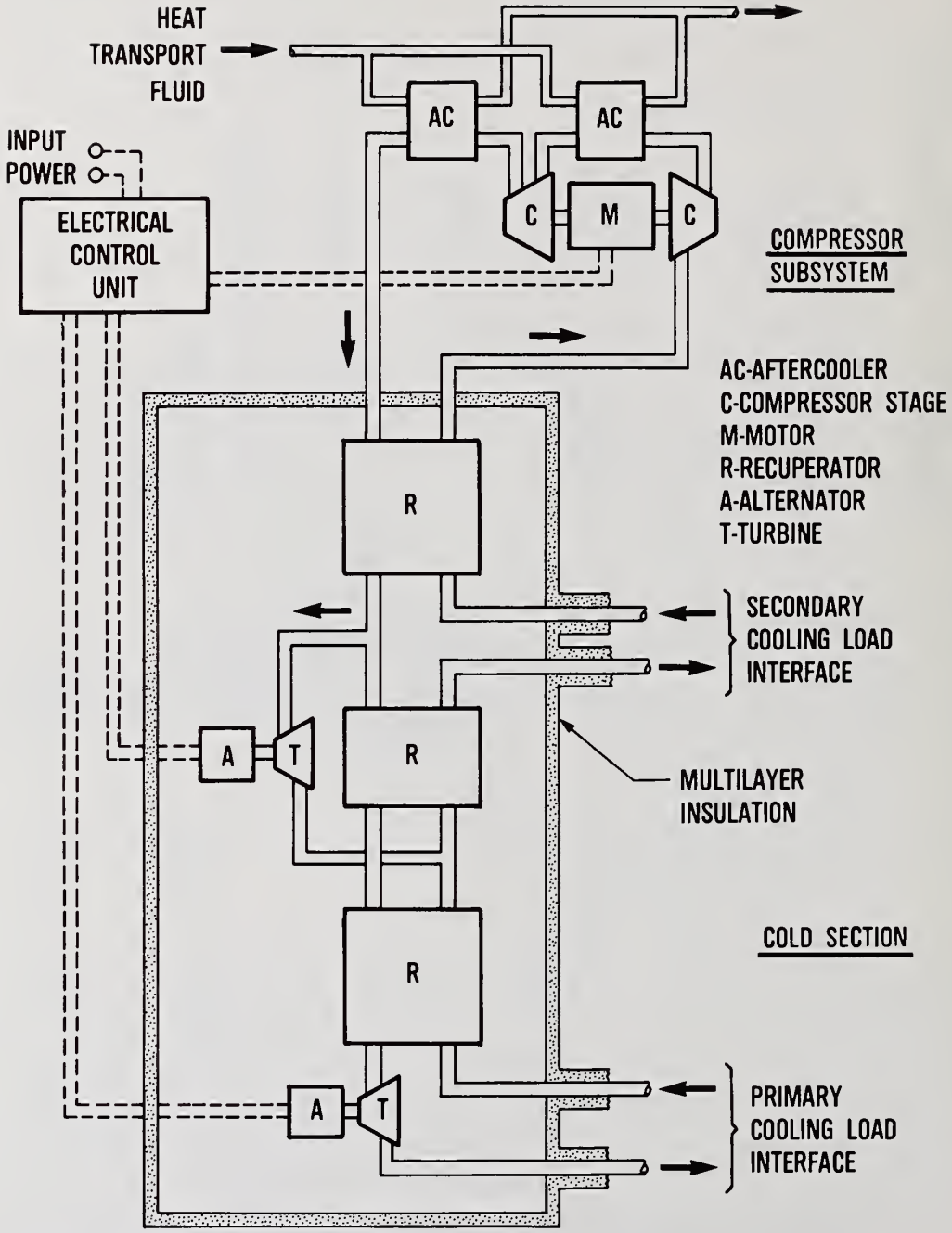

FIGURE 2. TURBO-REFRIGERATOR SYSTEM SCHEMATIC

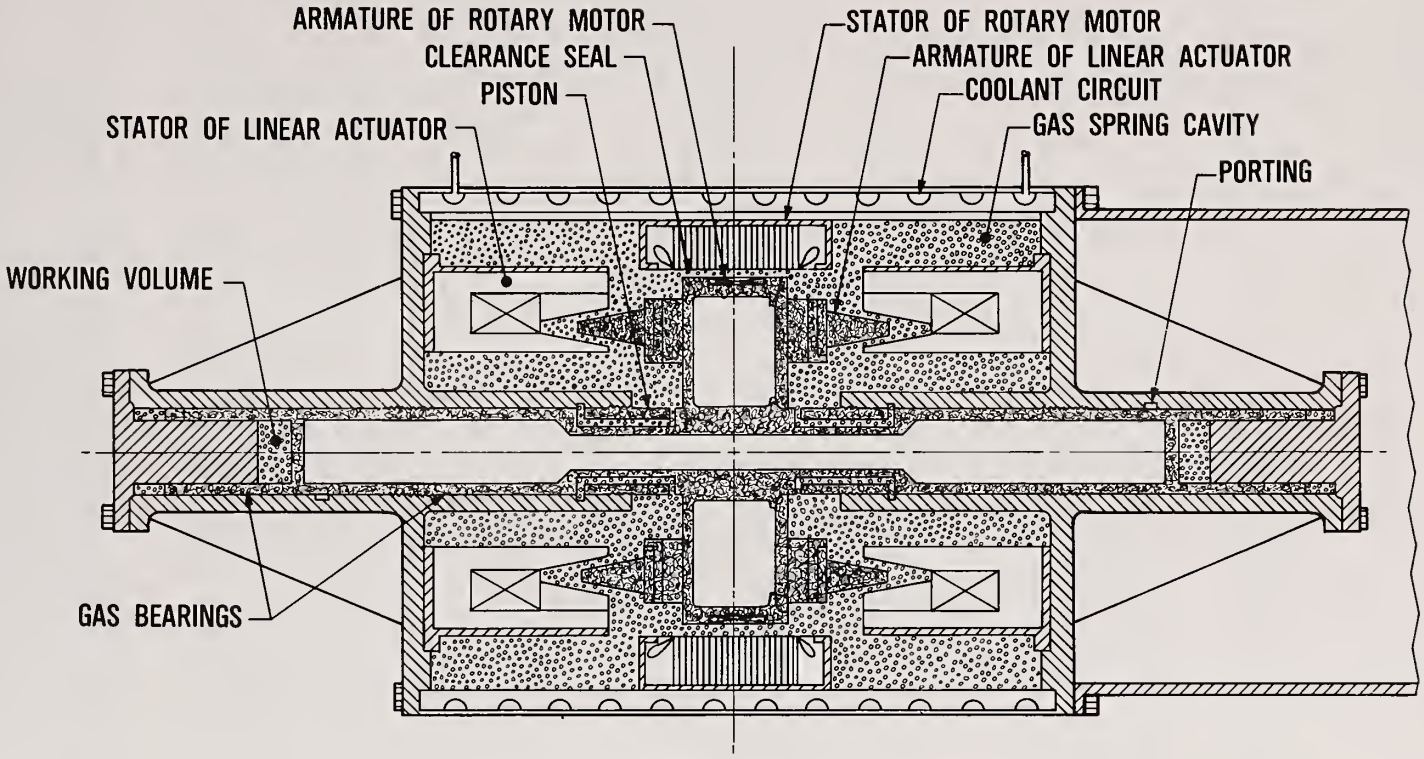

FIGURE 3. ROTARY-RECIPROCATING REFRIGERATOR COMPRESSOR

Other factors which influence the choice of a basic concept for a long-life cryo-cooler include power consumption and weight restraints which may be imposed. Turbine machinery with gas film bearings should operate for very long periods of time, but the efficiency is low unless a high cooling capacity is needed. The rotary-reciprocating refrigerator has a potential for very long-life and high efficiency but with higher weight and more complicated control circuits than other coolers. The VM cooler does not have as great a life potential as the gas bearing coolers, but it will have significant life because of the light loads. Its efficiency will not be as high as the R^3, but its weight is considerably less, the controls are simple, and the design more mature. Much better efficiency should be obtainable with Stirling cycle machines if novel means can be implemented to achieve long-life. The relative importance of different factors must be evaluated in making a decision.

Cryogenic refrigerators being developed by the Flight Dynamics Laboratory for long term continuous operation generally use gas film bearings to avoid rubbing contact or use lightly loaded bearings and seals with low wear rates. The turbo-Brayton and rotary-reciprocating refrigerators with gas film bearings may be subject to long term gas erosion and contamination effects, but their good durability potential is generally recognized. Durability of VM coolers may be somewhat questionable, but thermal compression and the constant volume aspect of the VM cycle provide significant benefits. Bearing loads and operating speeds can be an order of magnitude lower than for conventional Stirling coolers with equivalent capacity. The low forces permit long-life to be achieved with dry lubricated bearings. A low pressure drop across the sliding seals allows innovative, long lasting seal designs. Careful material selection along with thorough component specifications to assure adequate quality are leading to significant progress in extending the demonstrated life of VM coolers.

Other concepts for long-life coolers are being pursued by other organizations in relation to their particular requirements. NBS has demonstrated a low speed, low capacity Stirling cycle cooler [5] that is well suited to laboratory or similar use. NASA is sponsoring the development of a Stirling cycle cooler [4] which employs magnetic bearings to avoid rubbing contact. The combined efforts of all organizations should provide the technology to increase the potential for long life coolers in the next five years.

2.1 Component development

After the basic cryo-cooler concept is chosen, the long-life potential can be realized only by careful analysis and controlled fabrication of each part or component. Sufficient analyses must be performed to determine the mechanical and thermal stress levels for each part. The fatigue or wear limits for each part must then provide a margin of safety when compared to the durability requirements of the cooler. Those parts which may cause failures are identified for special emphasis in the development phase.

During the development of VM coolers, many early problems, such as heater life and mechanical interference forces, were eliminated by bench testing and analysis. A special material had to be found for the rider rings which guide the hot end of the displacers in the hot cylinders. Experience with sliding seals in the coolers indicated that simply finding a better material would not provide adequate life. Therefore, new designs are being evaluated along with new materials and better control of the surfaces on which the seals rub. These are examples of the detailed effort which is now showing a payoff for the total cooler.

In the case of the rotary-reciprocating refrigerator, technical issues include the design and fabrication of gas film bearings, the complexities of electrical drive circuits, and the fabrication of high effectiveness heat exchangers. Contamination control is also very important in relation to materials selection, assembly methods, and gas management. These problems have been identified, and solutions to them are being verified as development continues. Since the electrical control circuits for the rotary-reciprocating refrigerator are rather complicated, special emphasis has been placed on the basic design of these circuits to provide highly derated part operation with well established functions. Electrical problems with other coolers have shown that reliability and durability problems are not limited to mechanical devices. Technical issues for the turbo refrigerator include design and fabrication of compliant gas bearings, design and fabrication of high effectiveness heat exchangers, development of a high speed motor and controller, and the design and

fabrication of small turbine wheels. Quality control and contamination have been given a high level of attention. Included also, is a continuing effort to increase the efficiency of individual components such as heat exchanger effectiveness, compressor adiabatic efficiency, turbine adiabatic efficiency, and reduction of seal leakage and bearing losses.

2.2 Quality assurance

An adequate quality assurance program must be implemented during the development of a cryo-cooler. This program provides for verified identification of materials and complete inspection of all purchased and fabricated parts. This information is necessary to assure a reasonable probability of successful cooler operation and to help analyze the cause of difficulties which do occur. Part failures have been caused by materials which did not actually contain a specified constituent. In a similar manner, machined parts must be inspected for proper dimensions and quality of workmanship. Component assembly procedures must be reviewed for adequate process control, and the components should be inspected to assure that specified steps, such as heat treatments, were actually accomplished. Acceptance of this extra quality control burden is essential to the final success of a long-life cryo-cooler.

2.3 Contamination control

One of the most significant problems in developing long-life coolers is the elimination and control of contamination. The problem is usually broken into two categories: particulate contamination and gaseous contamination. Particulate contamination can result from inadequate cleaning, manufacturing defects, flaking of coatings and wear debris from bearings, riders, and seals. The effect of particulate contaminates varies from the scratching of highly finished close tolerance bearing and seal surfaces to the partial or total plugging of heat exchangers, regenerators, and other small gas passages. Scratching of surfaces can result in accelerated seal wear, bearing failures, additional particle generation, and the jamming of the refrigerator mechanism.

Advanced design concepts, cleanliness standards, and particle traps are utilized to eliminate or reduce particulate contamination. Design techniques include the elimination of rubbing parts by the utilization of gas bearings and non-contacting seals. Examples of this technique are the turbo-Brayton and rotary-reciprocating refrigerators.

In coolers that do have rubbing parts, the quantity of particulate contamination can be reduced by reducing the load on the parts and by dry lubrication. An example of this is the Vuilleumier refrigerator which utilizes heat instead of mechanical energy as the primary input power. Inside the refrigerator, the pressure drops across the thermal regenerators are only a few pounds per square inch. This results in low loads on the dynamic (sliding) seals, displacer riders, and bearings which, coupled with their slow speed, results in low wear, low contaminate production, and long-life.

Other techniques to reduce particulate contamination are to keep trapped dirt sources, such as motor windings, out of the working fluid (helium) or to hermetically seal the contamination source. Successful techniques have been to place the pressure wall between the solid metal motor rotor (inside the cooler) and the motor stator with its windings outside the cooler or to "can" the motor stator.

Cleaning prior to and during assembly is required for all cryogenic coolers but is especially critical for the extremely close clearance gas bearing refrigerators. Clearances in these bearings are typically measured in millionths of an inch.

Once assembled, the continuous flow coolers utilize filters to trap particulate contamination missed by cleaning or generated within the cooler. Reversing flow refrigerators such as the VM and Stirling utilize thermal regenerators which, because of the reversing flow, tend to be somewhat self-cleaning. Particulate traps can be created by adding small, deep groves perpendicular to the working fluid flow that allow contaminate or wear particulates to drop in and become trapped. The location and number of these type of particle traps must be carefully considered since they decrease refrigerator performance by increasing refrigerator dead volume and pressure drop.

Condensation or freezing of gaseous contamination is an even more severe problem than particulate contamination in cryogenic coolers since, at the very low temperature that some of these coolers produce, everything except helium is a liquid or a solid. Gaseous contamination can clog Joule-Thomson valves, clog heat exchangers, partially clog thermal regenerators, create thermal shorts from cryogenic regions to warmer regions of the refrigerator, and possibly even stall the refrigerator mechanism. Sources of gaseous contamination include organic materials such as seals, riders, bonding agents, plastic parts, motor wire insulation,and the gaseous contaminates adhering to the surfaces of the metal parts during assembly. Gaseous contamination has also been obtained from untested dirty helium fill bottles. Due to the difference in partial pressures of the contaminates, between the pure helium inside the refrigerator and the atmosphere outside, refrigerators with large static seal areas may experience additional long-term gaseous contamination problems caused by permeation of contaminates past the seals. Design techniques to reduce gaseous contamination include: elimination of organics within the refrigerator, hermetically sealing the motor windings or placing the windings outside the working fluid, and the use of welded joints whenever possible. Operational techniques include testing, certifying, or cold trapping the helium fill gas, careful purging of the cooler after assembly and after break-in, and bakeout of the cooler parts and the assembled cooler, which is limited by the high temperature tolerance of the seals and epoxy or solder bonding agents.

2.5 Helium retention

All of the refrigerators of interest utilize gaseous helium as the working fluid. Since helium molecules are small single atoms, it is one of the most difficult gases to contain for long periods of time. Techniques to maintain adequate working fluid within the refrigerator are helium makeup and helium retention. Helium makeup has been confined to large refrigerators and utilizes a high pressure bottle, pressure reducing regulator, valves, pressure sensors, and control logic. This adds parts to the refrigerator which in turn can affect system reliability. Helium retention has been accomplished by various means. For short life coolers, single or double "O" rings have been used. Since rubber "O" rings are permeable to helium, longer life coolers may have an "O" ring to withstand the internal refrigerator pressure fluctuations backed by a soft metal cut ring seal or indium coated metal "K" seal for positive sealing. These seals require careful preparation of the sealing surfaces and replacement of the seal after the joint is opened. The best way to seal joints is by welding. This can be considered after the refrigerator development phase has been completed and there is no longer a need to frequently disassemble the refrigerator. Clever weld flange designs allow the weld to be ground off and opened and then rewelded one or more times without destroying the expensive parts.

The detection and location of very small leaks is always a challenge especially on refrigerators of complex geometry. Leak isolation is currently being investigated under the VM effort.

2.6 Reliability

Reliability can be enhanced if the refrigerator designer pays careful attention to the environments and conditions that the cooler will experience during developmental testing and its ultimate use. Design simplicity with attendant low parts count enhances reliability. Since long-life coolers are not high production rate items, 100% inspection is possible and appropriate. Inspection records of wearing parts can be used to establish wear rates that may be extrapolated to indicate refrigerator life. The use of flight qualified electronic parts, although more expensive, appears to prevent numerous breakdowns later during refrigerator life testing or use.

In selecting the type of cooler to be developed, it is sometimes necessary to choose between a cooler that has good reliability associated with simplicity and a low number of parts but is limited by wearout of parts as compared to a more complicated machine that has lower reliability but better durability. Awareness of this conflict in relation to operational requirements can aid in selecting the best cryo-cooler for a particular application.

The quality of the support equipment should also be carefully considered before acquisition. Cooling cart (for heat rejection) breakdowns have been a continuing problem that

interrupts cooler testing and causes delays. Power supply and instrumentation malfunctions have resulted in many lost hours of operation and have confused the malfunction analyses. Adequate spares should be acquired to prevent long term breakdowns of the entire system.

Reliability and durability can be verified in several ways. Current Flight Dynamics Laboratory programs use the Test, Analyze, and Correct (TAC) method to demonstrate the life and increase the reliability of long-life refrigerators. This method provides reliability information on the failure modes and mechanisms of critical components while undergoing development and life testing. Reliability improvement (growth) results when failure modes and mechanisms are discovered, identified, and their recurrence prevented through implementation of corrective action.

3. Conclusion

In summary, working across all refrigerator technical fronts, there is a high expectation that the technology for five year coolers will be available within the next five years. Development of a highly reliable, long-life cryo-cooler must be a carefully planned and controlled process. Required operating conditions will influence the selection of the basic type of cooler, but the selected concept must have an inherent long-life potential. This potential is then realized through careful analysis of stress levels for each part and adequate quality control. Contamination control must also be implemented. Good reliability can be obtained by limiting the number of parts in a relatively simple cooler and by assuring adequate design margins for all parts. Final verification of adequate durability with acceptable cooler performance is demonstrated by reliability growth in a test, analyze, and correct program.

4. References

[1] Doody, R. D., The High Capacity Spaceborne Vuilleumier Refrigerator, Paper No. 245-15 presented at the SPIE Annual Technical Symposium, July 1980.

[2] Wapato, P. G. and Norman, R. H., Long Duration Cryogenic Cooling with the Reversed Brayton Turbo-Refrigerator, Paper No. 245-17 presented at the SPIE Annual Technical Symposium, July 1980.

[3] Breckenridge, R. W., Refrigerators for Cooling Spaceborne Sensors, Paper No. 245-16 presented at the SPIE Annual Symposium, July 1980.

[4] Sherman, A., Gasser, M., Goldowski, M., Benson, G., and McCormick, J., Progress on the Development of a 3-5 Year Lifetime Stirling Cycle Refrigerator for Space, Paper No. KC-1 presented at the Cryogenic Engineering Conference, August 1979.

[5] Sullivan, D. B., and Zimmerman, J. E., Very Low-Power Stirling Cryocoolers using Plastic and Composite Materials, International Journal of Refrigeration, Volume 2, No. 6 pp 211-213, November 1979.

THEORETICAL ANALYSIS OF A 3-STAGE STIRLING CYCLE CRYOCOOLER

Stuart B. Horn
Mark S. Asher
Far Infrared Team, Systems Integration Division
Night Vision & Electro-Optics Laboratory
Fort Belvoir, Virginia

Previous analyses of three stage coolers have neglected the real gas equation of state of helium. Those analyses have therefore neglected the compressibility effects that occur below 20K. This paper derives the thermodynamic performance of three stage Stirling type coolers using the real gas equation of state. An analysis of a small, efficient three stage cooler is given with the low temperature gas effects illustrated.

Key words: Cryocooler; cryogenic; helium; low temperature; refrigerator; Stirling cycle.

The three stage Stirling Cryocooler (Fig. 1) consists of a motor driven reciprocating helium compressor and a cold finger containing three expansion chambers separated by porous regenerators. The displacer-regenerator assembly may be driven by a cam or slider crank mounted on the same shaft as the compressor motor. Alternatively, a linear solenoidal drive may be used to drive the displacer assembly with no side thrust. The motion of the displacer could be easily changed with the solenoidal drive whereas a new lobe would have to be ground if a cam were used to drive the displacer.

Cooling is produced in the three expansion chambers by phasing the displacer motion with the pressure pulse generated by the compressor so that the working gas expands at high pressure and contracts at low pressure (Fig. 2). The regenerators serve to maintain the temperature difference between the three expansion spaces in the cold finger. As gas travels down toward the cold end of the cold finger it is precooled by the porous regenerator matrices. The matrices are recooled by the gas after expansion as it flows back to the ambient end. The matrix materials should have high volumetric specific heats relative to the compressed helium. If this is so, the axial temperature distribution in the regenerator matrices will be essentially constant in time and linear between the expansion spaces. Because the heat capacity of the solid drops so severely at low temperature (below 30K) and the helium heat capacity is pressure dependent in the same range, this assumption is clearly not exact at the lower end of the machine.

In most cases, refrigeration will be required only at the cold end of the cold finger. The upper two stages should then be designed to produce no net refrigeration. They should serve only to eliminate the flow losses associated with the regenerators.

The computer program used to predict the performance of the cryocooler is a modified version of the one described by Horn & Lumpkin (1) of the Army Night Vision Laboratories. This is a second-order isothermal analysis with decoupled losses. The original program was modified to include a three stage cold finger and real gas equations of state in the cold end. The program contains an iterative procedure to find the correct mass distribution in the machine and in iterative solution to the real

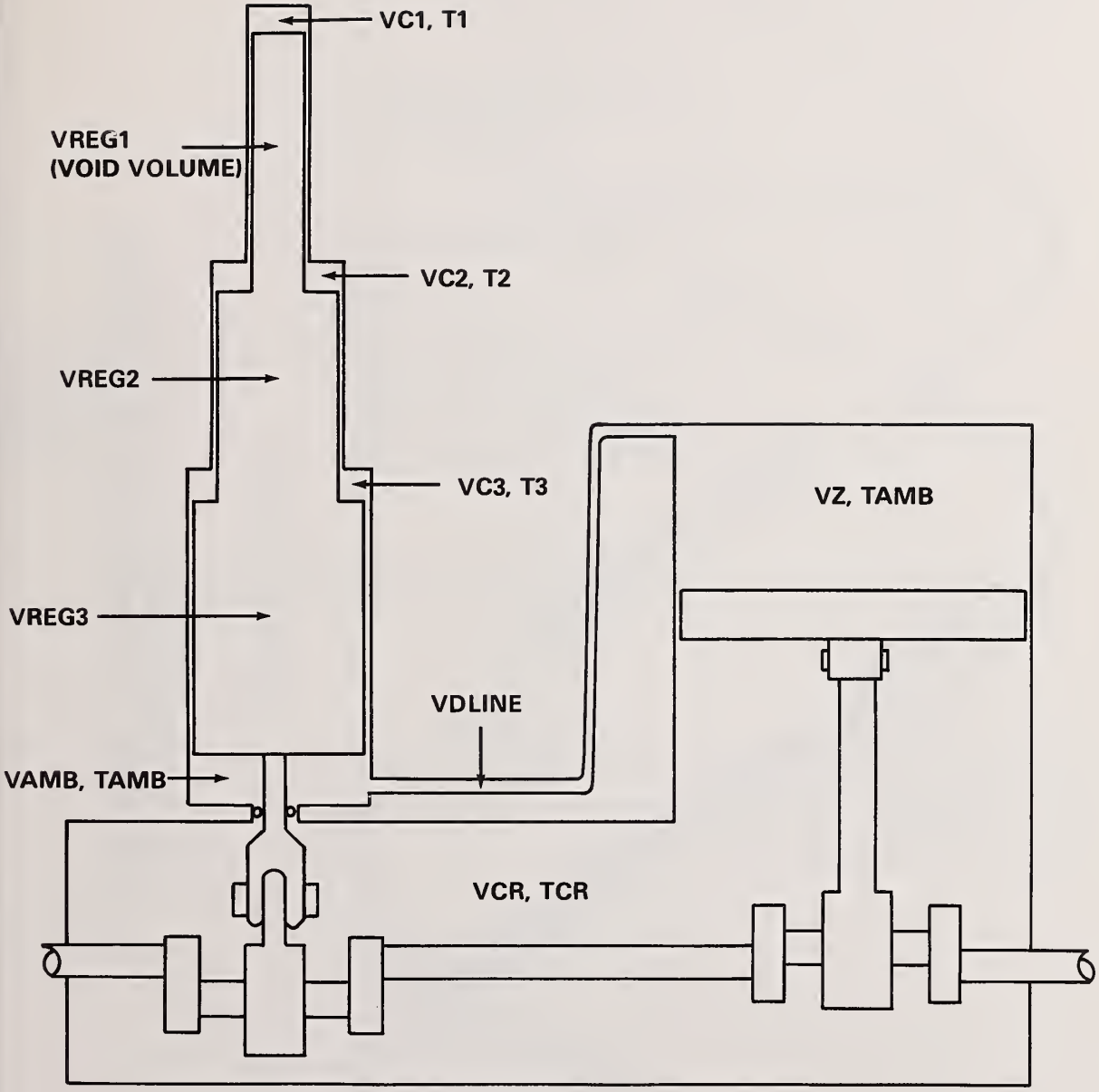

FIG. 1. THREE STAGE STIRLING CRYOCOOLER

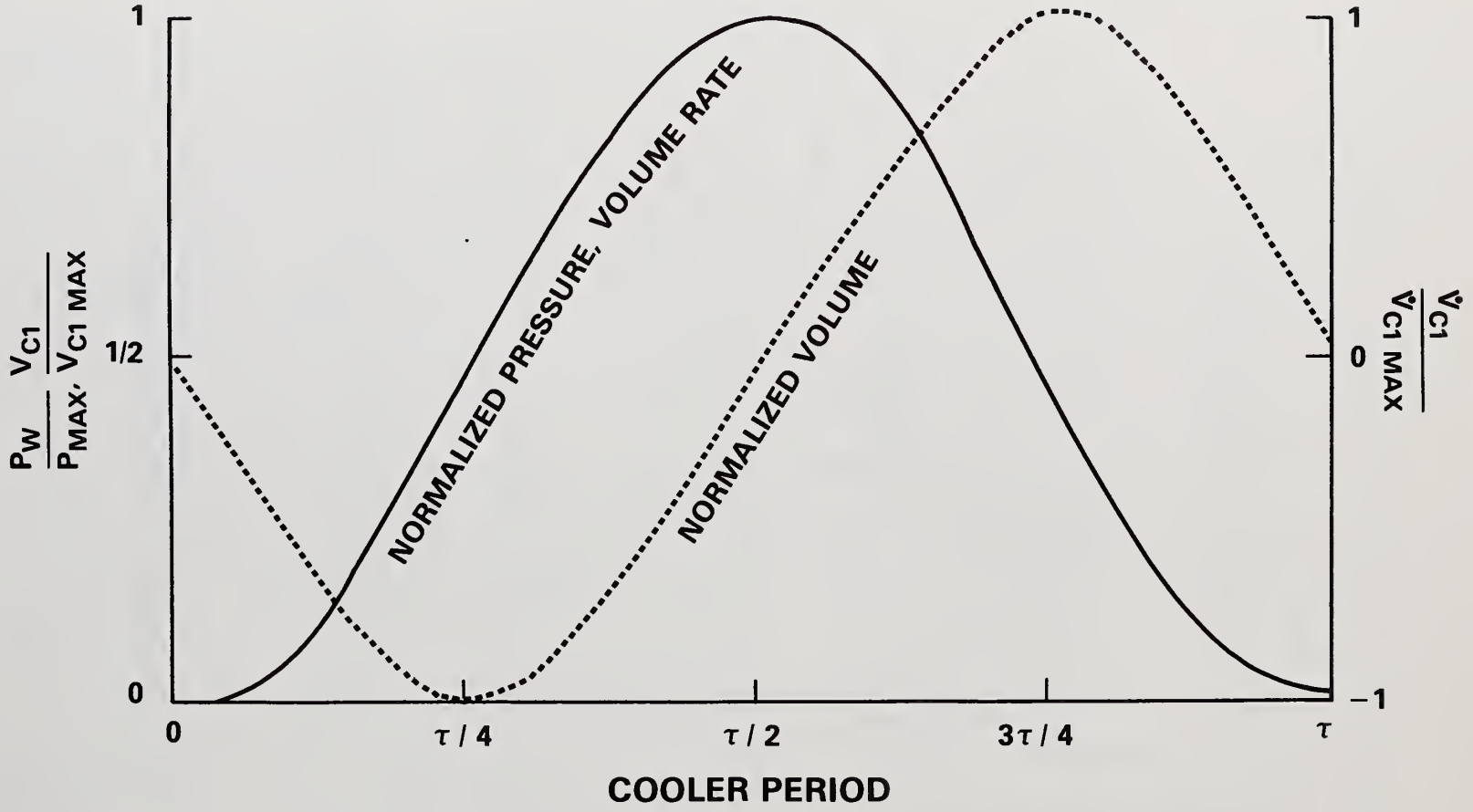

FIG. 2. NORMALIZED EXPANSION SPACE PRESSURES, VOLUMES, AND VOLUME RATES

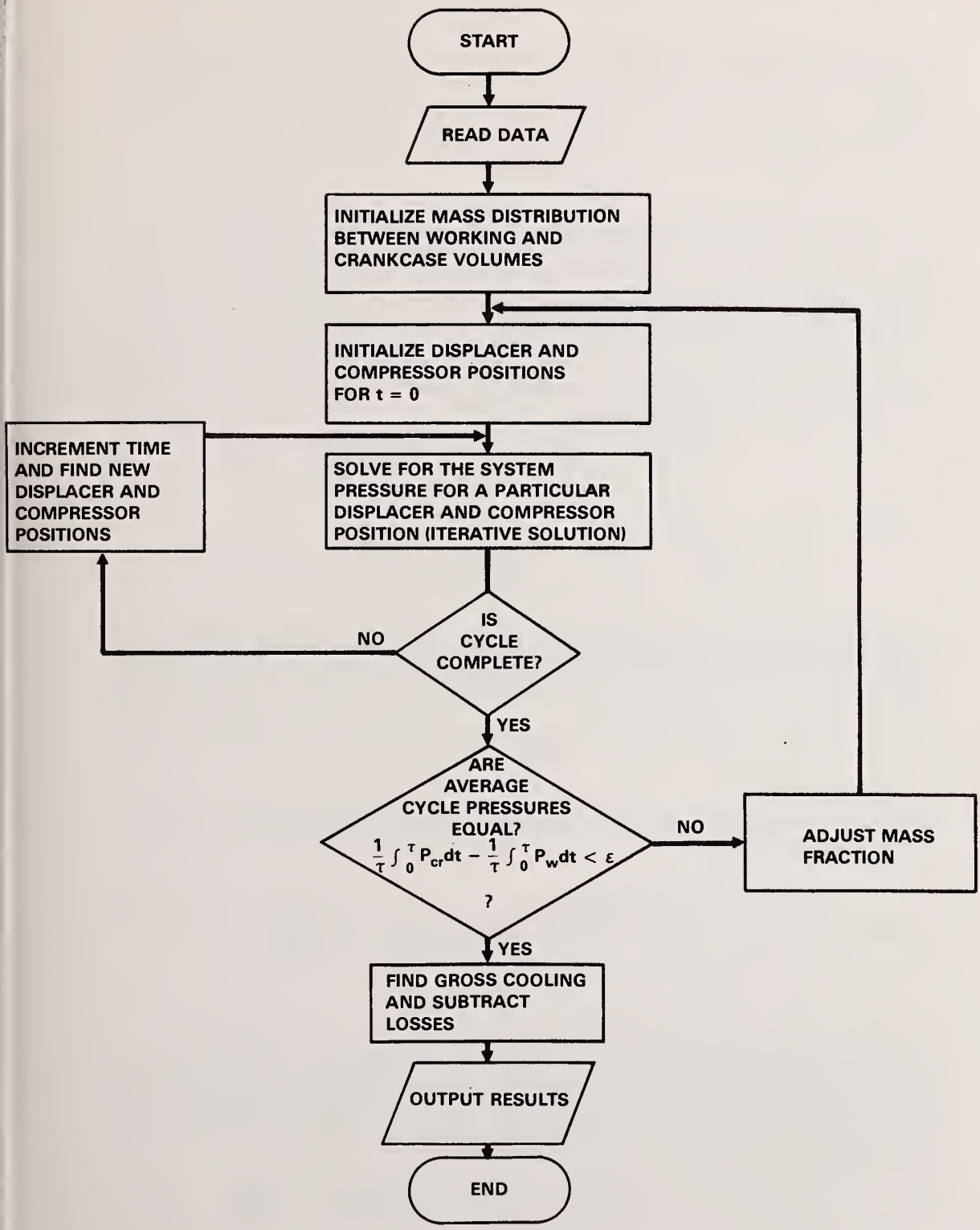

FIG. 3. PROGRAM FLOWCHART

gas equation of state. The non-zero Joule-Thomson coefficeint has not been completely included in this model.

A thermodynamic model of the cryocooler is shown in Fig. 1. In order for there to be no long term leakage of gas around the compressor piston seals, the time averaged pressure in the crankcase must be equal to the cycle averaged pressure in the working volumes:

$$\frac{1}{\tau}\int_0^{\tau} Pcr\ dt \quad = \quad \frac{1}{\tau}\int_0^{\tau} P_w\ dt \tag{1}$$

To satisfy this condition the program solves these integrals numerically and adjusts the amount of mass present in the working and crankcase volume. In order to evaluate the cycle averaged pressure the program solves the real gas equation of state numerically for every time step. There are then three nested iterative procedures contained in the program as shown in the flow chart (Fig. 3).

First, a rough estimate must be made of the mass distribution in the machine. The total amount of mass that should be present in the entire working volume can be found by summing the masses in the separate subvolumes:

$$Mw_1 = \frac{Pc}{R}\left[\frac{\bar{V}c2}{T2} + \frac{2\ Vreg2}{T2+T3} + \frac{\bar{V}c3}{T3} + \frac{\bar{V}c1}{T1} + \frac{2\ Vreg3}{T3+Tamb} + \frac{Vdline}{Tamb}\right. \tag{2}$$

$$\left. + \frac{Vamb}{Tamb} + \frac{\bar{V}z}{Tamb} + \frac{2\ Vreg1}{T1+T2}\right]$$

It has been assumed that the machine begins its cycle with both the compressor and the displacer at mid-stroke. Also, all isothermal subvolumes are assumed to already be at their equilibrium temperatures. The subscript 1 refers to the first mass distribution iteration. The mass in the crankcase can be found from the following relation:

$$Mcr_1 = \frac{Pc}{R}\ \frac{Vcr}{Tcr} \tag{3}$$

Where the volume of the crankcase is assumed to be essentially constant. The total mass of the system is then:

$$M_{TOT} = Mw_1 + Mcr_1 \tag{4}$$

We now define the first estimate of the working gas mass fraction as:

$$F_1 = \frac{Mw_1}{M_{TOT}} \tag{5}$$

In order to proceed further we must find the pressure in the working space as a function of time for one complete cycle. During this first cycle we will assume that there is no leakage of mass from the compression space into the crankcase. For some general point in the cycle, then, we can relate the instantaneous pressure in the working space to the mass fraction by again summing up the mass contributions of the subvolumes:

$$Mtot\ Fj = \frac{Pw_i}{R}\left[\frac{Vc2_i}{T2} + \frac{2\ Vreg2}{T2+T3} + \frac{Vc3_i}{T3} + \frac{2\ Vreg3}{T3+Tamb} + \frac{Vdline}{Tamb}\right. \tag{6}$$

$$\left. + \frac{Vamb_i}{Tamb} + \frac{Vz_i}{Tamb}\right] + \rho reg1\ \ Vreg1 + \rho c1\ \ Vc1_i$$

Where the following assumptions have been made:

1) All subvolumes are isothermal.

2) All subvolumes in the working space are in pressure equilibrium (no pressure drops).

3) The gas in the regenerators is at the arithmetic mean temperature of the expansion spaces that they connect. This is a simplifying assumption. While the temperature is a linear function of position, the gas density varies logarithmically with z.

4) The ideal gas law is correct in all subvolumes except the cold expansion space and the cold regenerator.

The subscript i in Eq. (6) refers to a particular instant in the cycle while the subscript j refers to a mass fraction iteration. The motion of the compressor and the displacer can be either sinusoidal or matched constant acceleration parabolic sections. The displacer and compressor motions define the instantaneous volumes Vcl_i, $Vc2_i$, $Vc3_i$, Vamb, and Vz_i. Solving Eq. (6) for the system pressure we have:

$$Pw_i = \frac{\left[Mtot \quad Fj - (\rho regl_i \quad Vregl + \rho cl_j \quad Vcl_i)\right] R}{Denom} \tag{7}$$

where:

$$Denom = \frac{Vc2_i}{T2} + \frac{2Vreg2}{T2+T3} + \frac{Vc3_i}{T3} + \frac{2\ Vreg3}{T3+Tamb} + \frac{Vdline}{Tamb} + \frac{Vamb}{Tamb} + \frac{Vz_i}{Tamb}$$

All terms in Eq. (7) are known except for $\rho regl_i$ and ρcl_i. An iterative procedure must be used to find a ρcl_i and a $\rho regl_i$ that result in pressure equilibrium throughout the machine. The flowchart in Fig. 4a shows how this procedure works.

First, a rough estimate of the instantaneous pressure in the machine is made by using the ideal gas law to find ρcl and $\rho regl$ in Eq. (7):

$$Pw_i = \left[Fj \quad Mtot - \left(\frac{2Pw_i \ Vregl}{R(T1+T2)} + \frac{Pw_i \ Vcl_i}{R \ T1}\right)\right] \frac{R}{Denom} \tag{8}$$

Solving for Pw_i we have:

$$Pw_i \ (guess) = \frac{R \ Mtot \ Fj}{Denom} \left[1 + \frac{1}{Denom}\left(\frac{2 \ Vregl}{T1 + T2} + \frac{Vcl_i}{T2}\right)\right] \tag{9}$$

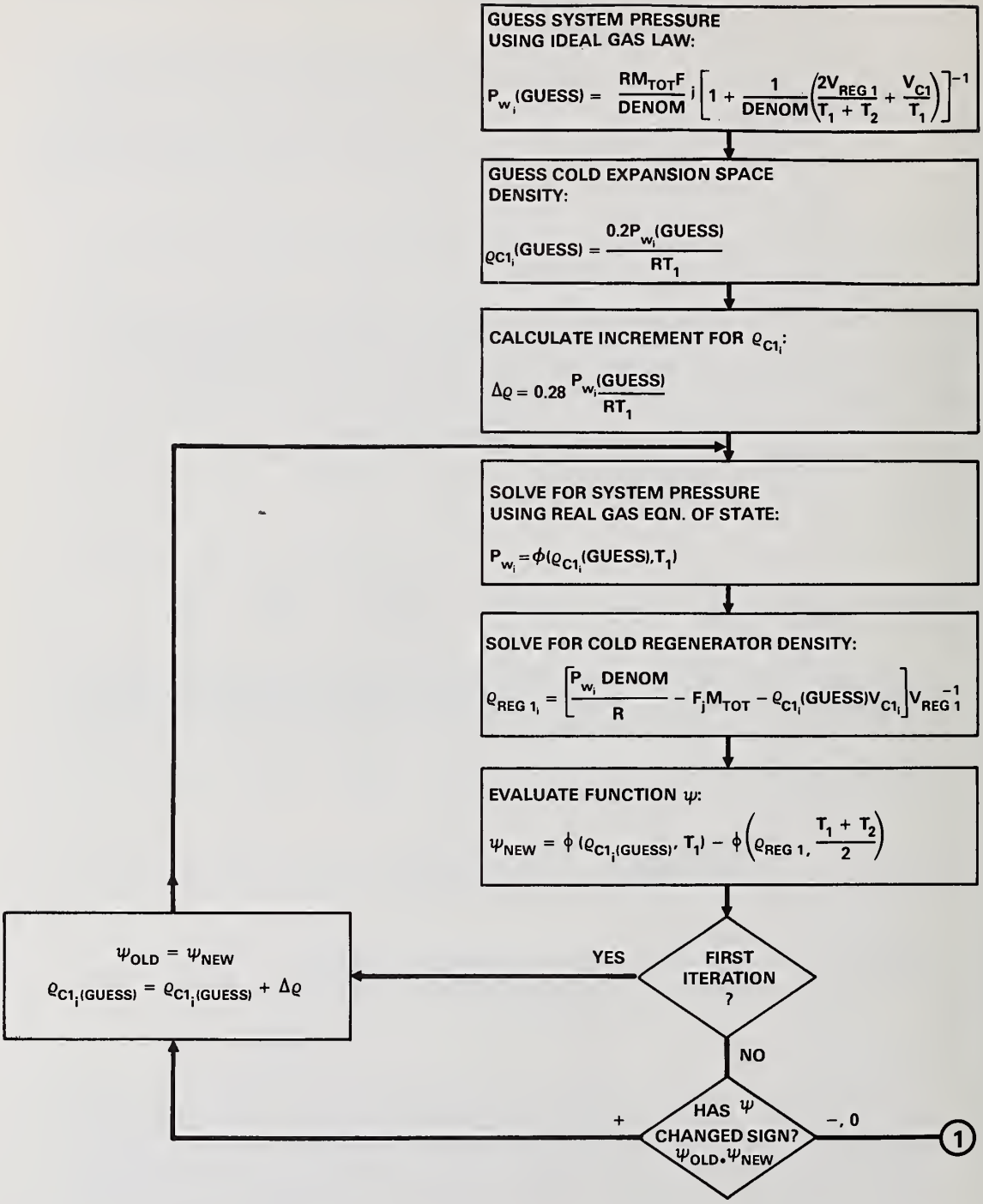

INCREMENTAL SEARCH

FIG. 4a. FLOWCHART FOR FINDING SYSTEM PRESSURE

An initial guess is then made for the instantaneous density in the cold expansion space:

$$\rho cl_i \text{ (guess)} = 0.2 \quad \frac{Pw_i \text{ (guess)}}{R\ T1} \tag{10}$$

The factor of 0.2 is present to insure that the initial guess of ρcl_i is below the actual value. Once ρcl_i (guess) is known we can solve for a new pressure from a real gas equation of state.

The equation of state that we will use is presented by Mann (2). The equation contains seventeen terms and is contained in the Appendix for continuity. It is accurate from 4K to 300K and to pressures of 100 atm. This equation is explicit in pressure; that is, pressure is found as a function ϕ of density and temperature:

$$P = \phi \ (\rho, T) \tag{11}$$

We can now substitute our first guess for the density in the cold expansion space along with the temperature in this space in Eq. (11):

$$Pw_i = \phi \ (\rho cl \text{ (guess)}, T1) \tag{12}$$

Next Eq. (6) is solved for $\rho regl$ in terms of ρcl and Pw_i:

$$\rho regl_i = \left[\frac{Pw_i \ Denom}{R} - Fj \ \ Mtot - \rho cl_i \text{ (guess)} \ \ Vcl_i \right] Vregl^{-1} \tag{13}$$

We now define a function ψ that will be zero when the appropriate denstities are found:

$$\psi = \phi \left[\rho cl_i, T1 \right] - \phi \left[\rho regl, 1/2 \ (T1+T2) \right] \tag{14}$$

Note that ψ is really a function of ρcli only because ρ regl can be found from knowledge of $\rho\ cl_i$. We can now define an increment by which to sequentially increase $\rho\ cl_i$ until we have found an interval of values of $\rho\ cl_i$ that contain a root to Eq. (14):

$$\Delta\rho = 0.28 \quad \frac{Pw_i \text{ (guess)}}{R\ T1} \tag{15}$$

We now increment $\rho\ cl_i$ successively by $\Delta\rho$ until the function Ψ changes sign. This defines an interval which contains a root of ψ and we can quickly converge on this root by the bisection method. The bisection procedure is illustrated in the flowchart shown in Fig. 4b.

This process is continued until the pressures and densities are known for each time step in a cycle of the machine. The integrals for the time averaged pressure in the working space and crankcase in equation 1 can then be evaluated numerically:

$$\frac{1}{n} \sum_{i=1}^{n} Pw \ = (1-Fj) \ Mtot \ R \ Tcr \ / \ Vcr \tag{16}$$

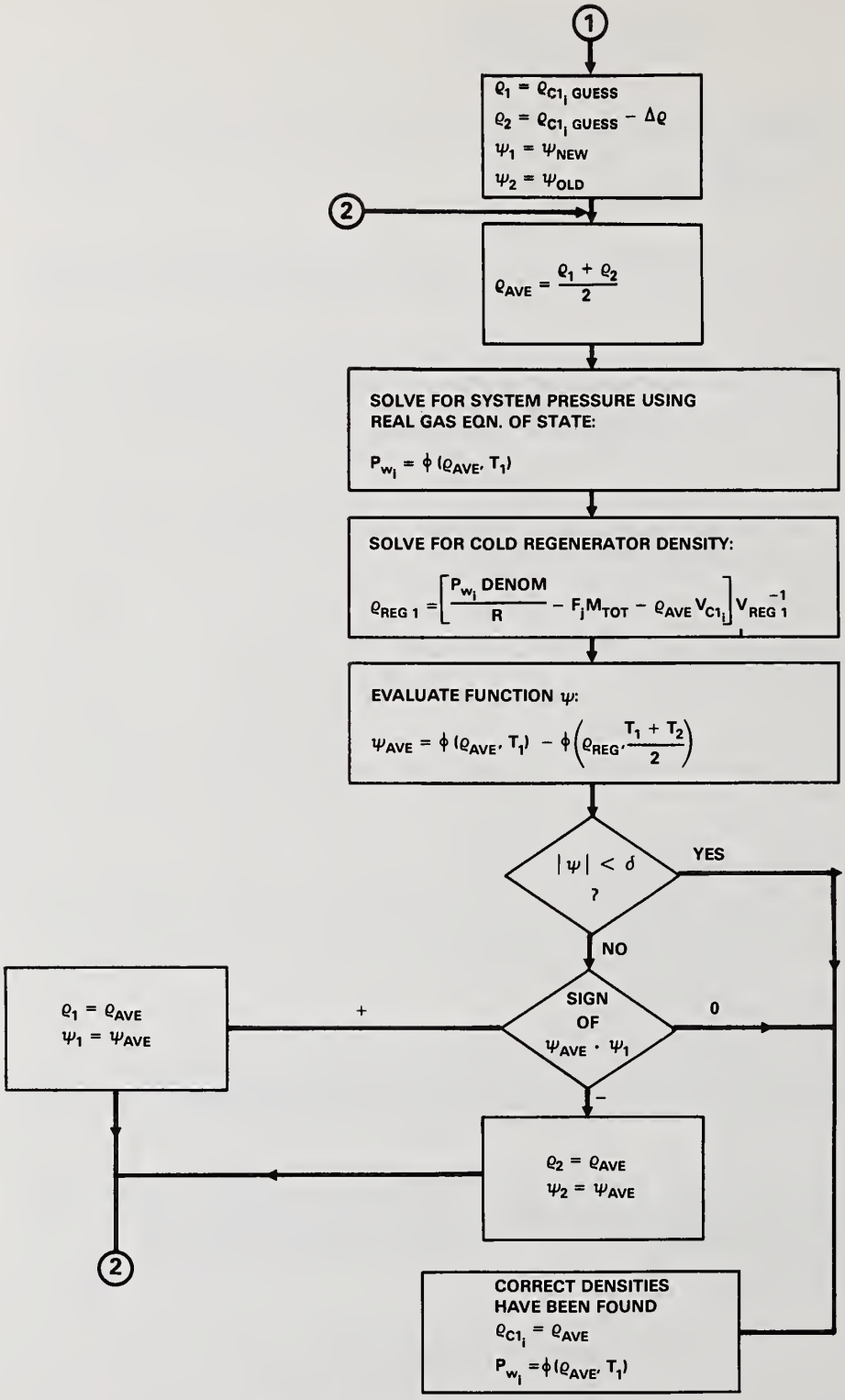

FIG. 4b. BISECTION SEARCH

where we have assumed that the crankcase volume is essentially constant. The term on the left represents the working space average pressure ($\bar{P}w$) while the term on the right is the crankcase average pressure ($\bar{P}cr$). If the time averaged pressure is not the same in the working space we must adjust the mass fraction. This is done by relating the pressures in the (j+1)th iteration to the pressures in the jth iteration as follows:

$$Pw_i\Big|_j = Pw_i\Big|_{j+1} \left(\frac{Fj+1}{Fj}\right) \tag{17}$$

$$\bar{P}cr\Big|_j = \bar{P}cr\Big|_{j+1} \left(\frac{1-Fj+1}{1-Fj}\right) \tag{18}$$

We can solve for Fj+1 by substituting equations (17) and (18) into (16), resulting in:

$$Fj+1 = \frac{(1-Fj)\ \bar{P}w}{Fj\bar{P}cr} \tag{19}$$

After adjusting the mass fraction the progam goes through another cycle and calculates the system pressures for each time step. This process is repeated until the time averaged pressures in the working space and the crankcase are within some specified error $\bar{\varepsilon}$.

The gross cooling for each stage is found by integrating the system pressure with respect to the expansion space volume:

$$\dot{Q}g1 = \frac{A1}{n} \sum_{i=1}^{n} Pw_i\ \dot{X}i \tag{20}$$

$$\dot{Q}g2 = \frac{A2}{A1}\ \dot{Q}g1 \tag{21}$$

$$\dot{Q}g3 = \frac{A3}{A1}\ \dot{Q}g1 \tag{22}$$

These expressions are valid because the expansion spaces are assumed to be isothermal; the cyclic integral of the work done by the gas is then equal to the heat absorbed by the gas. However, enthalpy is a function of pressure and since the ingoing and outgoing streams are at different pressures, this leads to an incomplete account of the Joule-Thomson effect.

After finding the gross cooling for each stage the net cooling is found by subtracting off the various thermal losses presented in Table 1:

$$\dot{Q}net = \dot{Q}g - \dot{Q}\ loss \tag{23}$$

The thermodynamic work done by the compressor is found by numerically integrating the system pressure with respect to the compression space volume:

$$\dot{W}c = \frac{Az}{n} \sum_{i=1}^{n} Pw_i\ \dot{Z}i \tag{24}$$

The net work done by the compressor is found by adding the thermodynamic work to the flow by adding the thermodynamic work to the flow losses of the gas in the transfer line and regenerators:

$$\dot{W}c(net) = \dot{W}c + Flow\ losses \tag{25}$$

TABLE I - Thermal Losses

LOSS	CAUSE
Shuttle	Regenerator motion causes heat to be transferred from warm to cold end.
Regenerator Heat Transfer	Irreversible heat transfer between regenerator matrix and helium.
Temperature Swing	Temperature cycling of regenerator matrix
Pressure Drop	Viscous drag in flow passages causing reduction in gross cooling.
Conduction	Irreversible heat transfer between warm end of displacer assembly and cold end.

TABLE II - Summary of Optimized Three-Stage Cooler Design

a. Data for Various Stages

Stage	1	2	3
Temperature, ^{o}K	10	25	123
Swept Volume, in^3	2.04×10^{-3}	4.38×10^{-3}	7.73×10^{-3}
Dead Volume, in^3	8.16×10^{-5}	1.75×10^{-4}	3.09×10^{-1}
Regenerator Void Volume, in^3	3.70×10^{-3}	1.16×10^{-2}	3.80×10^{-2}
Regenerator Flow Area, in^2	4.74×10^{-3}	1.32×10^{-2}	4.09×10^{-2}
Regenerator Matrix Material	Lead-Antimony Spheres	Nickle Spheres	Nickle Spheres
Regenerator Length, in.	0.780	0.880	0.930

b. Ambient End Data

Charge Pressure - 500 Psia
Ambient Temperature - 300K
Cycle Speed - 25 Hz
Compressor Swept Volume - 0.131 in^3
Compressor Dead Volume - 2.98×10^{-3} in^3
Connecting Line Dead Volume - 5.65×10^{-2} in^3

RESULTS

Airborne SQUIDS require small, efficient cryocoolers with small magnetic signatures. To achieve the small packaging requirement designs utilizing high charge pressures and cycle speeds to compensate for the lack of physical size were examined.

The optimized three stage cooler design is summarized in Table 2. The design was optimized by adjusting the length of the regenerators and the stage temperatures until the desired net cooling was obtained at the coldest stage. The performance of the machine is shown in Table 3.

The program was re-run using the same data except that the real gas equation of state was replaced with the ideal gas equation of state. The results are shown in Table 4. It is clear that the effect of compressibility in the cold stage expansion space and regenerator substantially altered the performance of the machine. The pressure ratio and gross cooling were reduced when compressibility was not included in the analysis. Compresssibility effects tend to magnify the swept volume in the cold expansion space relative to the other subvolumes in the machine. The compressibility factor Z is defined by:

$$PV = ZMRT \tag{26}$$

The effective temperature weighted swept volume of the cold expansion space is then given by:

$$\Delta V_{c1}' = \frac{\Delta V_{c1}}{\bar{Z}_{c1}\, T_1} \tag{27}$$

where $\bar{Z}_{c1}$ is the cyclic average compressibility factor. In the cold expansion space, similarly, the effective temperature weighted dead volume of the cold end regenerator is:

$$V_{reg1}' = \frac{V_{reg1}}{\bar{Z}_{reg1}\, T_1} \tag{28}$$

As can be seen from Fig. 5, the compressibility factors for both the cold end expansion space and the cold end regenerator are always less than unity. However, the average compressibility factor for the cold end expansion space is less than that of the cold end regenerator (since the regenerator is at a higher temperature). This causes the total temperature weighted swept volume of the machine to increase at the expense of the total temperature weighted dead volume. The pressure ratio and gross cooling are thus increased.

Several runs were also made using various displacer motions other than sinusoidal. Motions were found that gave substantial increases in net cooling. The compressor swept volume was then reduced until the net cooling was close to its original value, but because of the smaller compression space the input power was reduced. The performance characteristics of this design are listed in Table 5 and the optimized displacer waveform is shown in Fig. 6. The optimum waveform has short dwells at the ends of the stroke that tend to round off the work curve in the cold expansion space. By using the optimized waveform, the COP of the cooler was increased by 9%.

TABLE III - Performance Characteristics of Three Stage Cryocooler

Stage	1	2	3
Gross Cooling, W	0.972	2.09	3.68
Shuttle Loss, W	8.26×10^{-3}	0.191	0.320
Regenerator Heat Transfer Loss, W	0.130	0.714	0.400
Regenerator Temperature Swing, K	0.804	0.180	2.56×10^{-2}
Temperature Swing Loss, K	0.268	4.73×10^{-2}	2.35×10^{-3}
Pressure Drop Loss, W	0.283	0.539	0.488
Total Conduction Loss, W	4.50×10^{-2}	5.86×10^{-1}	2.43
Pumping Loss, W	1.70×10^{-2}	7.66×10^{-3}	3.51×10^{-2}
Net Cooling, W	0.220	1.44×10^{-3}	6.55×10^{-3}

Pmax - 46.1 atm
Pmin - 26.9 atm
Pressure Ratio - 1.71
Motor Shaft Power - 54.4 W
Flow Losses - 3.10 W

TABLE IV - Performance Characteristics of Three-Stage Cryocooler Ignorring Compressibility

Stage	1	2	3
Gross Cooling, W	0.833	1.79	3.16
Shuttle Loss, W	8.26×10^{-3}	0.191	0.320
Regenerator Heat Transfer	0.148	0.646	0.366
Regenerator Temperature Swing, K	0.938	0.190	2.63×10^{-1}
Temperature Swing Loss, K	0.337	4.99×10^{-2}	2.37×10^{-3}
Pressure Drop Loss, W	0.303	0.570	0.507
Total Conduction Loss, W	4.50×10^{-2}	5.86×10^{-1}	2.43
Pumping Loss, W	1.41×10^{-2}	8.34×10^{-2}	0.906
Net Cooling, W	-2.30×10^{-2}	-0.259	-0.497

Pmax - 44.0 atm
Pmin - 27.5 atm
Pressure Ratio - 1.62
Motor Shaft Power - 52.2W
Flow Losses - 3.77 W

TABLE V - Performance Characteristics of the Three-Stage Cryocooler with Non-Sinusoidal Displacer Motion

Stage	1	2	3
Gross Cooling, W	0.889	1.91	3.37
Shuttle Loss, W	8.27×10^{-3}	0.192	0.320
Regenerator Heat Transfer Loss, W	0.124	0.613	0.312
Regenerator Temperature Swing, K	0.830	0.183	2.64×10^{-2}
Temperature Swing Loss, K	0.271	4.48×10^{-2}	2.18×10^{-3}
Pressure Drop Loss, W	0.206	0.382	0.336
Total Conduction Loss, W	4.50×10^{-2}	5.86×10^{-1}	2.43
Pumping Loss, W	2.11×10^{-2}	9.61×10^{-3}	4.41×10^{-2}
Net Cooling, W	0.213	8.24×10^{-2}	-7.47×10^{-2}

Pmax - 48.0 atm
Pmin - 25.8 atm
Pressure Ratio - 1.86
Motor Shaft Power - 48.6 W
Flow Losses - 1.66 W

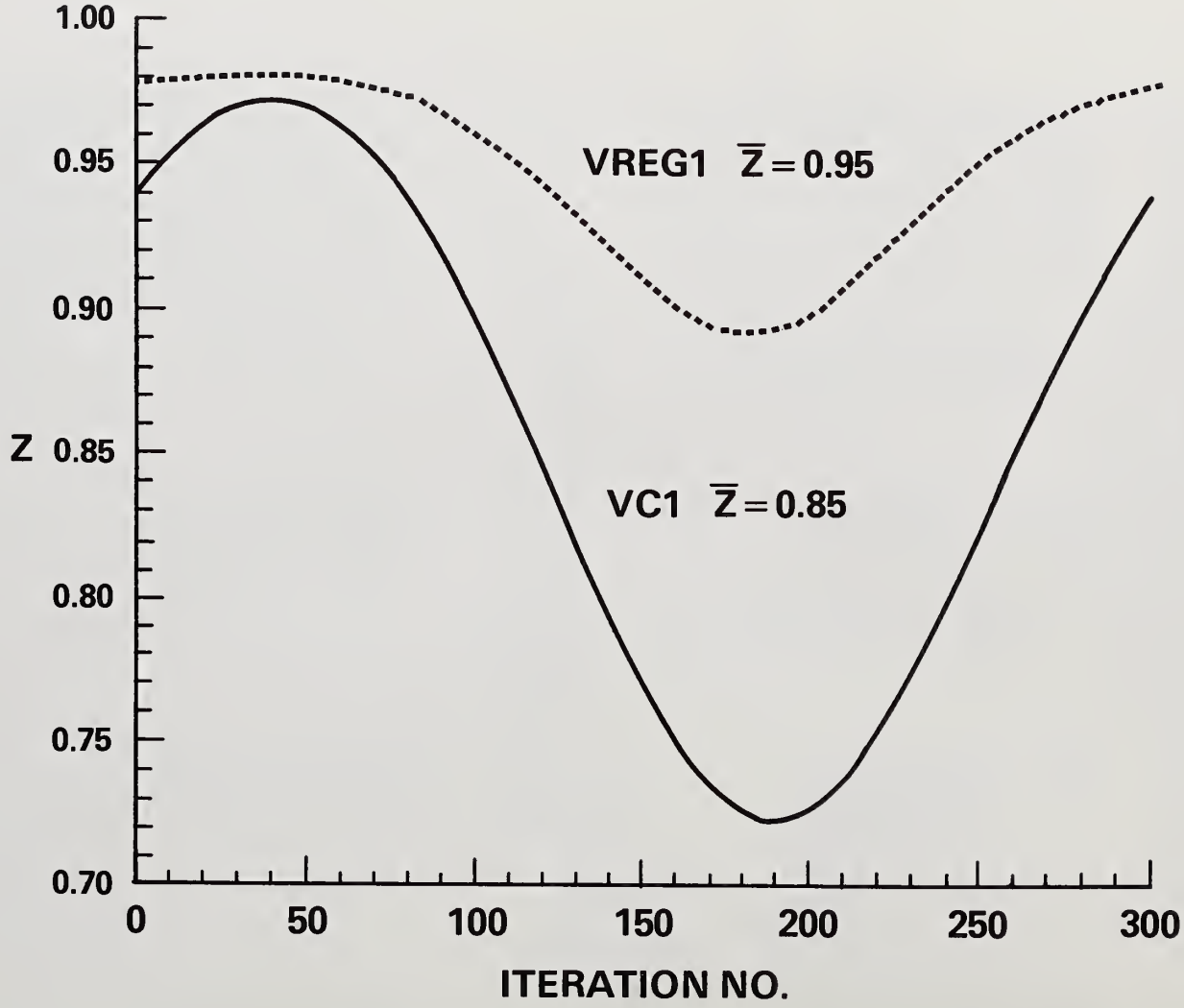

FIG. 5. COMPRESSIBILITY FACTORS FOR COLD EXPANSION SPACE (VC1) AND COLD REGENERATOR (VREG1)

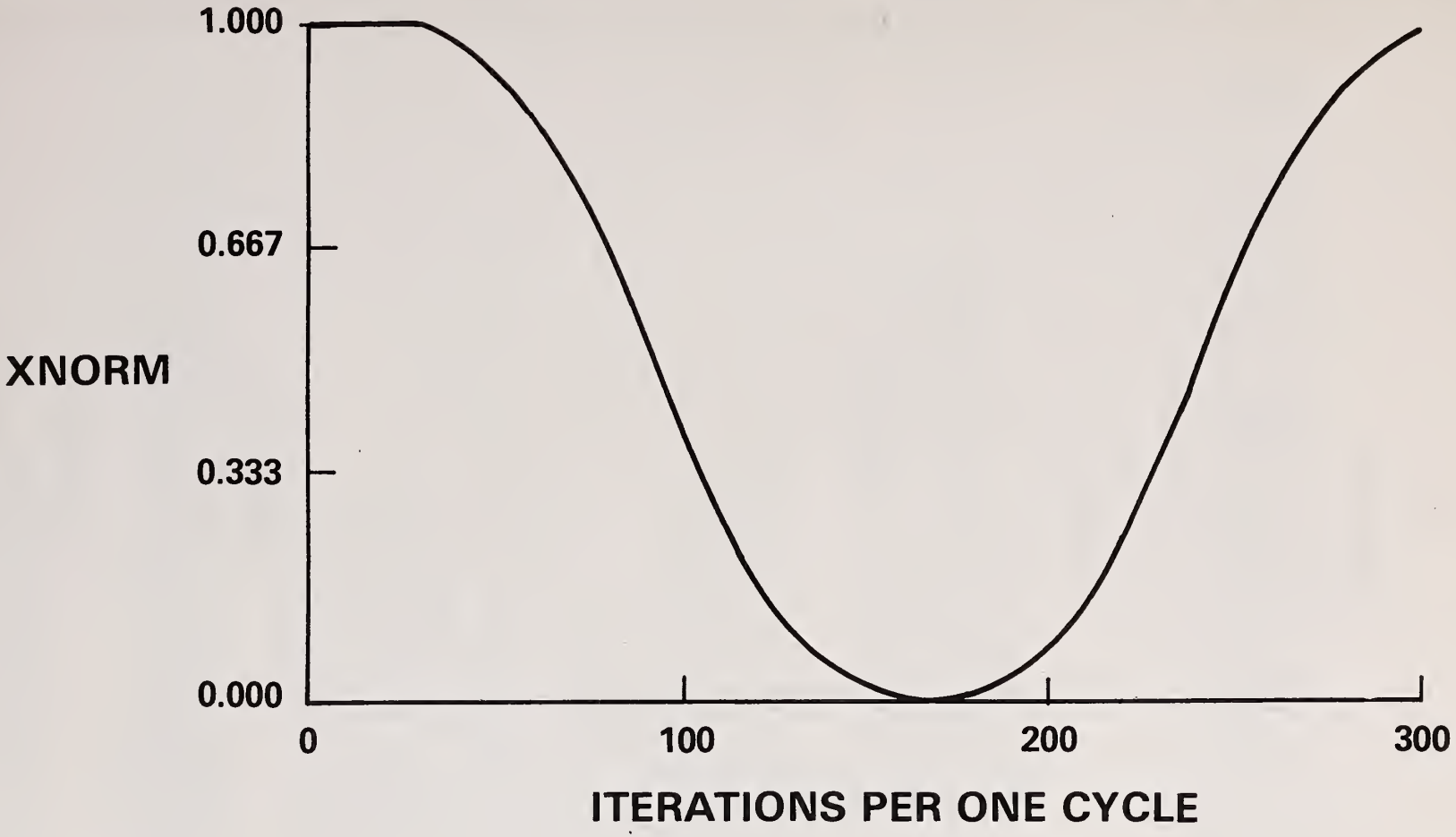

FIG. 6. OPTIMIZED DISPLACER WAVEFORM

CONCLUSION

This investigation demonstrates the feasibility of constructing a small, efficient three stage 10K Stirling Cryocooler. Compressibility should be taken into account when writing computer simulations for cryocoolers operating in this temperature range. Also, the displacer motion can be optimized to increase the performance of the machine.

NOMENCLATURE

Az - Swept area in compressor piston (m^2)
Al,2,3 - Swept area of expansion spaces 1, 2, and 3 (m^2)
Fj - Mass fraction in working volume for jth mass fraction iteration
Mcrj - Mass in crankcase volume in jth mass fraction iteration (kg)
Mtot - Total mass of helium charge (kg)
Mwj - Mass in working volume in jth mass fraction iteration (kg)
n - Number of discrete time steps per one cooler period
P - Pressure (Pa)
Pc - Charge Pressure (Pa)
Pcr - Crankcase Pressure (Pa)
Pw_i - Instantaneous working volume pressure (Pa)
Qg1,2,3 - Gross cooling in stages 1, 2 and 3 (W)
Qnet - Net cooling in a particular stage (W)
Qloss - Cooling losses in a particular stage (W)
R - Ideal gas constant for helium (J/kg K)
T - Temperature (K)
Tamb - Ambient temperature (K)
Tcr - Crankcase temperature (K)
T1, T2, T3 - Temperature in expansion spaces 1, 2, and 3 (K)
V - Volume (m^3)
$Vamb_i$ - Instantaneous ambient end volume (m^3)
$\bar{V}c1$, $\bar{V}c2$, $\bar{V}c3$ - Midstroke volume in expansion spaces 1, 2, and 3 (m^3)
Vcr - Crankcase volume (m^3)
Vreg 1, 2, 3 - Void volume in regenerators 1, 2, and 3 (m^3)
Vz_i - Instantaneous compressor volume (m^3)
Wc - Thermodynamic work done by compressor (W)
Xi - Instantaneous displacer velocity (m/s)
Z_i - Instantaneous compressor velocity (m/s)
Z - Compressibility factor
$Vc1_i$, $Vc2_i$, $Vc3_i$ - Instantaneous volume in expansion spaces 1,2, and 3

GREEK LETTERS

ρ - Density (kg/m^3)
$\rho reg1_i$ - Instantaneous gas density in regenerator 1 (kg/m^3)
$\rho c1_i$ - Instantaneous gas density in expansion space 1 (kg/m^3)
τ - Cooler period (sec)

SUBSCRIPTS

i - Associates a quantity with the ith time step
j - Associates a quantity with the jth mass fraction iteration

APPENDIX: Equation of State for He^4

Mann (2) presents the following equation of state for He^4 between 4.0K and 300K. This equation shows good correlation with experimental data for pressures up to 100 atm:

$$P = RdT + (Rn_1 T + n_2 + n_3/T + n_4/T^2 + n_5/T^4)d^2$$
$$+ (Rn_6 T + n_7)d^3 + n_8 d^4$$
$$+ (n9/T^2 + N_{10}/T^3 + n_{11}/T^4)d^5$$
$$+ \exp(-n_{12} d^2/T)$$
$$+ (n_{13}/T^2 + n_{14}/T^3 + n_{15}/T^4)d^5$$
$$+ \exp(-n_{12} d^2/T) + n_{16} d^5 + n_{17} d^6$$

Where d is in gmol/liter, T in K and

$R = 0.820575\ (10^{-1})$

$n_1 = 0.1627693557(10^{-1})$

$n_2 = -0.3700903492(10^{-1})$

$n_3 = 0.1567259965(10^{-2})$

$n_4 = -0.1887566673(10^{-1})$

$n_5 = 0.4792344640(10^{-1})$

$n_6 = 0.1560344984(10^{-3})$

$n_7 = 0.9274298542(10^{-3})$

$n_8 = -0.2833997045(10^{-4})$

$n_9 = -0.5002871627(10^{-2})$

$n_{10} = 0.3451283837(10^{-1})$

$n_{11} = 0.1008924438$

$n_{12} = 0.65\ (10^{-2})$

$n_{13} = -0.1851562535(10^{-4})$

$n_{14} = 0.4204351888(10^{-4})$

$n_{15} = -0.1712445150(10^{-3})$

$n_{16} = 0.7739390202(10^{-6})$

$n_{17} = -0.2870693948(10^{-8})$

BIBLIOGRAPHY

(1) S.B. Horn and M.E. Lumpkin, Advances in Cryogenic Engineering, Vol. 14, Plenum Press, New York (1974), p. 221.

(2) D. B. Mann, NBS TN 154, 1962.

SOME THERMODYNAMIC CONSIDERATIONS OF HELIUM TEMPERATURE CRYOCOOLERS*

D. E. Daney

Thermophysical Properties Division
National Bureau of Standards
Boulder, Colorado

Attempts to reach liquid helium temperatures with regenerative cryocoolers have been generally unsuccessful. The principal and well known cause of this failure is the decay of the regenerator matrix heat capacity at low temperature. As the regenerator effectiveness decreases, more and more of the refrigeration effect goes to the regenerator losses rather than to the load. A less well-recognized problem for some cryocoolers has been operation under adverse thermodynamic conditions. For example, operation at high pressure (40 bar) can decrease the calculated efficiency of the lowest stage by a factor of 10 or more - primarily because of the strongly negative Joule-Thomson effect of helium at low temperature and high pressure.

We first investigate the effect of the operating regime on the efficiency of helium temperature cryocoolers. Next, we propose two schemes of hybrid regenerative-counter flow cryocoolers as solutions to the problem of low helium-temperature regenerator heat capacity. Finally, we calculate the net mass flow through a typical hybrid regenerator-heat exchanger for one of the schemes that we propose.

Key words: Cryocooler; hybrid cryocoolers; refrigeration; regenerator; regenerative cooler; Stirling cooler; Stirling cycle.

1. Introduction

Much of the interest in reliable, low power, and compact cryocoolers for cooling smaller superconducting devices is focused on regenerative devices such as the Stirling machine. These coolers have a proven record of performance at temperatures above 20 K, and their relative simplicity is particularly appealing because it offers the potential of high reliability. However, attempts to reach liquid helium temperatures with regenerative cryocoolers rejecting heat to ambient temperature have failed[1]. Although temperatures as low as 6.5 K have been achieved, the efficiency falls rapidly at temperatures below 10 K [1,2,3].

---

[1]Temperatures as low as 3.1 K have been achieved by Zimmerman and Sullivan [8] with heat rejection at 8.6 K. This was achieved by operaton at low pressure - a very original approach to alleviating both of the thermodynamic problems discussed in this paper.

The principle and well known cause of this failure is the decay of the regenerator matrix heat capacity at low temperature. An accompanying loss in regenerator effectiveness results in more and more of the refrigeration effect going into regenerator losses rather than the load. A less well understood problem for some cryocoolers has been operation under adverse thermodynamic conditions, i.e., operation at pressures and pressure ratios where the efficiency is poor.

This paper proposes an alternative approach to the problem of diminishing low temperature regenerator heat capacity. Instead of searching for new regenerator materials, I suggest using hybrid cycles with helium counterflow in the final stage of the refrigerator. Two schemes which embody this principle are given.

2. Regenerator heat capacity

The requirement of high regenerator heat capacity has long been recognized, and we discuss it here only in sufficient detail to define the magnitude of the problem for helium temperature regenerative coolers. An empirical expression for the effect of heat capacity on regenerator effectiveness is given by Kays and London [4] for rotary regenerators:

$$\varepsilon = \varepsilon_0 \left(1 - \frac{0.11}{C_r^2}\right)$$

where ε is the regenerator effectiveness, ε_0 the effectiveness for infinite regenerator heat capacity and C_r is the heat capacity of the regenerator divided by heat capacity of the gas passing through in one direction during one cycle. Using this expression we find that C_r must be greater than 3 for the degradation in ε to be less than 0.01. By comparison, the experimental results of Gifford and Acharya [5] give C_r greater than 5 for a lead sphere regenerator operating between 80 K and 20 K. Whatever the exact values, both results support the conclusion that C_r should be several times greater than one if a significant deterioration in effectiveness is not to occur.

Comparing the volumetric heat capacity of helium with that of lead (the best common regenerator material), figure 1, we note that high losses may be expected below about 10 K. Although much may be accomplished through system optimization and materials research, figure 1 offers little hope for efficient regenerative cryocoolers operating at 4 K. This, of course, is not a new opinion.

3. Thermodynamic regimen

Because of their great complexity, regenerative cycle calculations are usually made using the simplifying assumption of an ideal gas equation of state. So long as the operating temperature is well above the critical point, little error is generally introduced by this assumption. As the operating temperature approaches the critical temperature, however, the error introduced in some cases may be large enough to make the calculations meaningless.

In order to characterize the effect of the operating conditions on the performance of the final stages we analyze a final Brayton cycle stage using real helium properties and methods described previously [6]. Although not a substitute for detailed regenerative cycle calculations, the results for a 6 K operating temperature, given in figure 2, clearly illustrate a strong effect of operating regimen on performance.

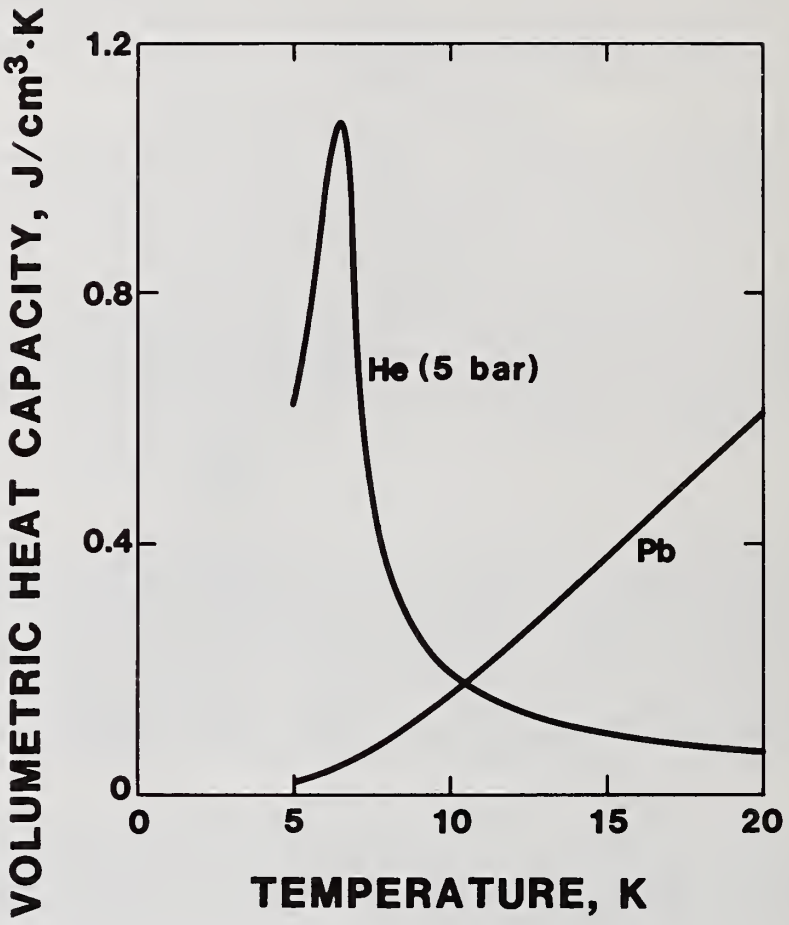

Figure 1. Volumetric heat capacity of helium and lead.

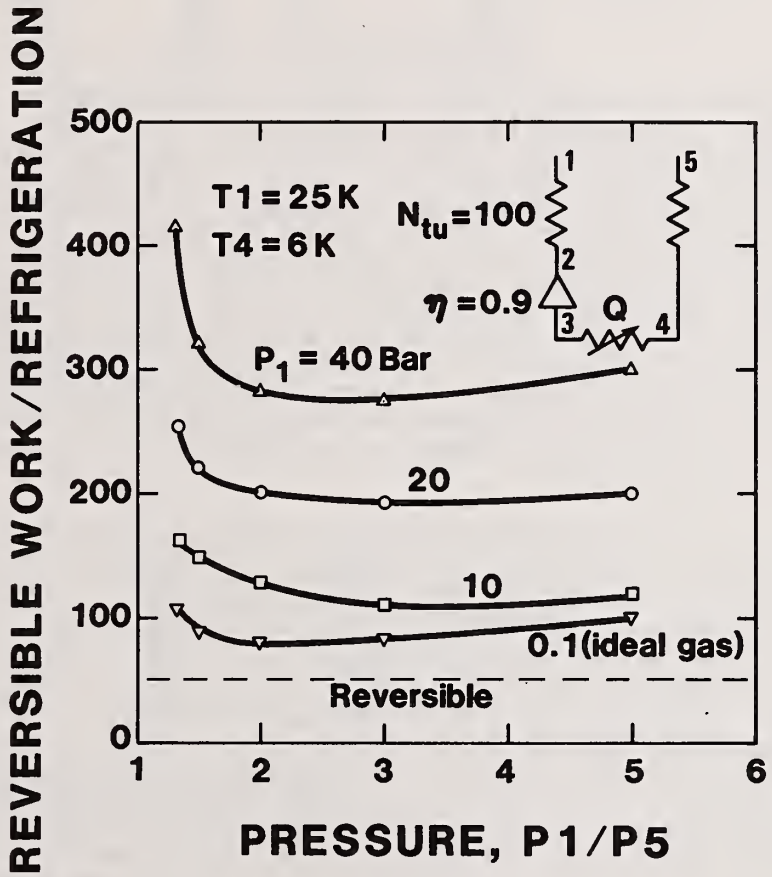

Figure 2. Performance of final refrigerator stage as a function of pressure and pressure ratio.

The dependence of the ideal work on the pressure is primarily due to the increasingly negative Joule-Thomson effect of helium with increasing pressure. The result is progressively less cooling as the pressure increases. Low pressure ratios are less efficient because a high fraction of the refrigeration is lost in the heat exchanger (regenerator). For less effective heat exchange, the effect of pressure ratio is even stronger. For the model used here, at least, relatively low operating pressures and modest pressure ratios are favored.

4. Hybrid regenerative coolers

As an alternative to the search for a high heat capacity regenerator material, we propose a hybrid machine with counterflow heat exchange in the final stage. Such an arrangement largely eliminates the need for a high heat capacity regenerator because heat is transferred directly from one helium stream to another. Figure 3 shows two possible arrangements for achieving such counterflow. In Scheme A, two regenerative coolers operating 180 degrees out of phase share a common counterflow heat exchanger, or hybrid heat exchanger-regenerator in the final stage. The gas entering one expansion space is cooled in counterflow by the gas flowing from the second expansion space. The mass flow wave-form is distorted from the sinusoidal, so that some instantaneous localflow imbalance occurs. Thus, a hybrid heat exchanger-regenerator (e.g. - a heat exchanger with high heat capacity) is desirable. Although a single pair of displacers are shown in the figure, any number could be coupled in a similar fashion. For example, for three displacers the phase angle would be 120 degrees and for four displacers the phase angle would be 90 degrees in order to further reduce any flow imbalance. Scheme A was suggested to me by Ray Radebaugh of NBS; its exact origin is unknown to us.

In Scheme B the last stage of the displacer is tightly sealed from the rest of the system so that it may act as a conventional expansion engine. During the high pressure part of the cycle, gas is admitted to the plenum via valve 2. When the piston-displacer reaches bottom dead center, valve 3 opens and admits gas to the cylinder until the piston rises to the cut-off position. As the piston continues upward, the gas cools by expansion; and a portion is liquefied. At top dead center the exhaust valve (4) opens, and two-phase helium is discharged into the load heat exchanger-plenum. Return of the gas to the main working volume occurs through valve 1 during the low pressure part of the cycle. Counterflow heat exchange between the high and low pressure streams occurs in a somewhat conventional heat-exchanger. However, because the mass flow in the two heat exchanger streams is not instantaneously equal, one side (the low pressure side) should have a volume much greater than the other side to provide additional heat capacity. Because of its complexity, Scheme B is probably feasible only for coolers with a capacity near one watt and above. Scheme B is an extension of a concept suggested by S. C. Collins some years ago [7].

In order to calculate the reduction in the regenerator load accomplished by Scheme A, we calculated the pressure and mass flow for a 3-stage Stirling cooler using real helium properties and sinusoidal movement of the displacer and piston. The following characteristics were assumed:

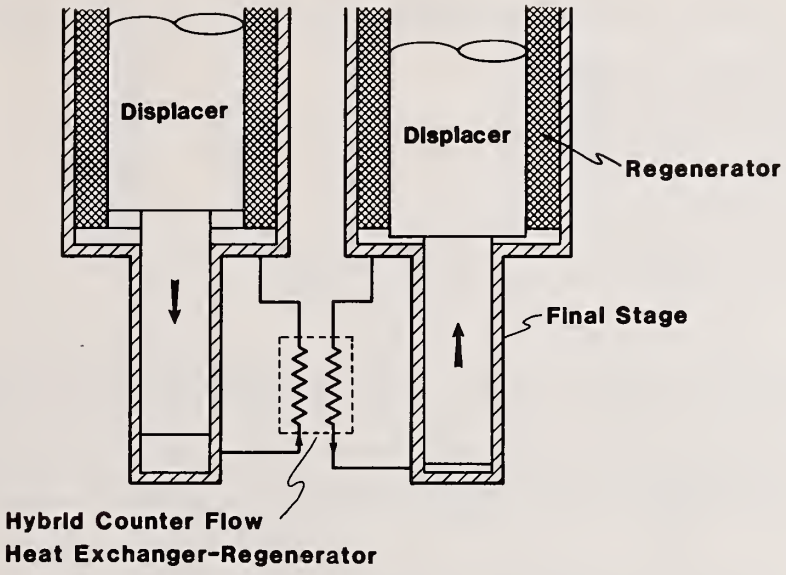

Scheme A. Displacers 180° out of phase.

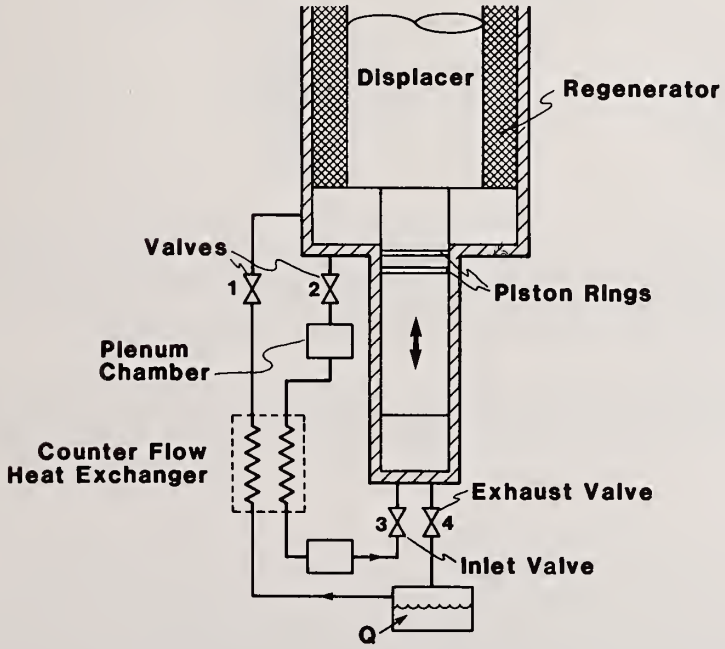

Scheme B.

Figure 3. Hybrid refrigerator schemes for the final stage of regenerative cooler.

Table 1. Split-Stirling cooler parameters for sample calculation of mass flow

Isothermal compressor temperature	300 K
1st expansion space temperature	100 K
2nd expansion space temperature	25 K
3rd expansion space temperature	6 K
Compressor volume	300 cm^3
1st expansion space volume	17 cm^3
2nd expansion space volume	4 cm^3
3rd expansion space volume	1 cm^3

Regenerator void volume = 1/2 expansion space volume.

Figure 4 shows that the mass flow rate is nonsinusoidal with the flow maximum and minimum separated by the compressor-displacer phase angle, 90 degrees in this case.

It is the total cyclic mass flow through the regenerator, not the instantaneous flow rate, that determines the load on the regenerator heat capacity. Thus, in Table 2 we compare the effect of the number of displacers on the cyclic change in the third stage expansion space mass.

Table 2. Cyclic mass flow with multiple displacers

Number of Displacers	Compressor-displacer angle 90 degrees Flow ratio	90 degrees 1/N x flow ratio	120 degrees Flow ratio	120 degrees 1/N x flow ratio
1	1.0	1.0	1.0	1.0
2	0.66	0.33	0.38	0.19
3	0.25	0.12	0.03	0.01
4	0.06	0.02	0.01	0.004

The column denoted flow ratio is the cyclic change in the total third stage mass compared to the change for a single displacer. Since multiple displacers would give N times the capacity of a single displacer, a further reduction in mass flow is achieved by the reduction in the size of each displacer when multiple displacers are used. Thus, the column denoted 1/N x flow ratio gives the total reduction cyclic mass flow for Scheme A.

A dramatic reduction in mass flow occurs when the number of displacers gives a phase angle between displacers equal to the compressor-displacer phase angle. Four displacers (with a 90 degree compressor-displacer phase angle) give a fifty fold decrease in the regenerator heat load.

5. Summary

In summary, I have proposed an efficient helium temperature regenerative cryocooler. It is a hybrid device using counterflow heat exchange in the final stage. It should have a maximum cycle pressure below 10 bar, and a pressure ratio above 2.

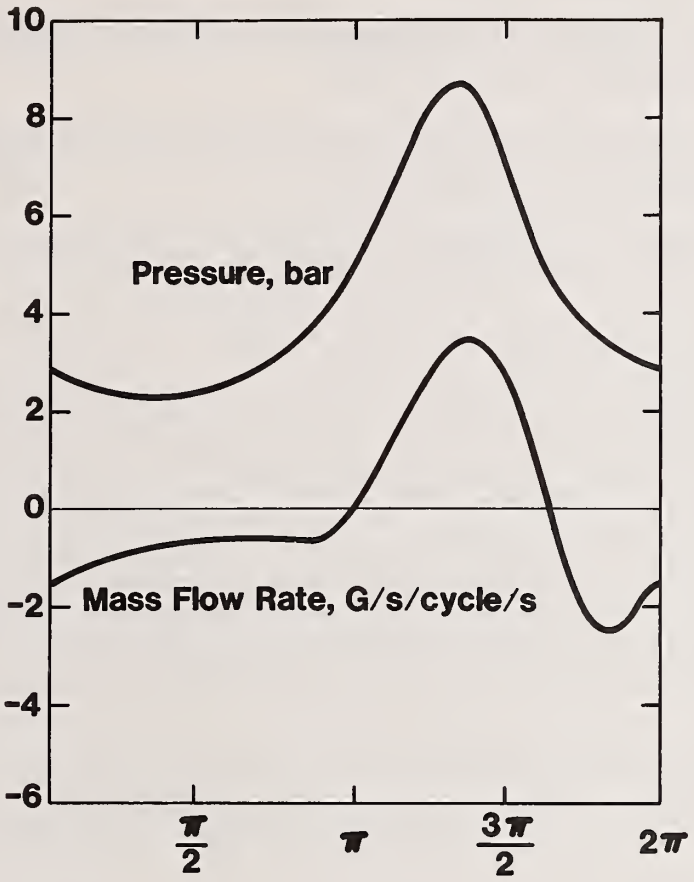

Figure 4. Pressure and mass flow waves for a Stirling cooler.

6. References

[1] Stuart, R. W. and Cohen, B. M., Operation of a Three Stage Closed-Cycle Regenerative Refrigerator in 6.5 K Region, in Advances in Cryogenic Engineering, Vol. 15, edited by K. D. Timmerhaus (Plenum Press, New York, 1970).

[2] Daniels, A. and du Pre", F. K., Triple-Expansion Stirling-Cycle Refrigerator, Advances in Cryogenic Engineering, Vol. 16, edited by K. D. Timmerhaus, 178-184 (Plenum Press, New York , 1971).

[3] Zimmerman, J. E. and Radebaugh, R., Operation of a SQUID in a Very Low-Power Cryocooler, NBS Special Publication SP-508, edited by J. E. Zimmerman and T. M. Flynn, National Bureau of Standards (1977).

[4] Kays, W. M. and London, R. L., in Compact Heat Exchangers, 20 (McGraw-Hill Book Co., Inc., New York, New York, 1978).

[5] Gifford, W. E. and Acharya, A., Low-Temperature Regenerator Test Apparatus, in Advances in Cryogenic Engineering, Vol. 15, edited by K. D. Timmerhaus, 436-442 (Plenum Press, New York, New York, 1976).

[6] Daney, D. E., Low-Temperature Losses in Supercritical Helium Refrigerators, in Advances in Cryogenic Engineering, Vol. 15, edited by K. D. Timmerhaus, 205-212 (Plenum Press, New York, New York, 1976).

[7] Daney, D. E., Design, Construction, and Testing of a Small Novel Air Liquefier, S. M. Thesis, Massachusetts Institute of Technology, 1962.

[8] Zimmerman, J. E. and Sullivan, D. B., A milliwatt Stirling cryocooler for temperature below 4 K, Cryogenices 19, 170-171 (1979).

DYNAMIC ANALYSIS OF A SMALL FREE-PISTON RESONANT CRYOREFRIGERATOR

R.A. Ackermann, Ph.D

Mechanical Technology Incorporated
Latham, New York 12110

The development of small, cryogenic refrigerators is receiving increased attention through the use of linear resonant machinery which has the potential for increasing the reliability and efficiency of these devices. The use of linear machinery, however, presents a complex second dimension to the analysis of the system's dynamics and thermodynamics which are implicitly tied together through the pressure wave produced in the refrigerator. This paper describes the dynamics of a linear cryogenic refrigerator and presents the analytical development of the equations of motion through the use of phasor notation. Solutions for both the transient and steady-state motions are presented, and the conditions of stability and selection of key operating parameters such as frequency, piston-displacer amplitudes and phase angles are discussed.

Key words: Displacer and piston drives; linear resonant machinery; linear free-displacer cryorefrigerator; linear electric motors; phasor notation; thermodynamic and dynamic analyses.

1.0 Description of a linear resonant cryogenic refrigerator

A schematic for a free-piston linear resonant refrigerator is shown in Figure 1. The machine consists of two dynamic components: a compressor piston which is electromagnetically actuated at resonance by a linear electric motor, and a displacer which is actuated at resonance by the pressure wave developed in the machine. Refrigeration is produced in the device by the expansion and compression of the working fluid at different temperature levels and by the controlled flow of the working fluid between the temperature levels due to volume changes in the expansion and compression spaces. The operation of the refrigerator is defined by the following set of equations.

1.1 Volume equations

The equations defining the changes in the expansion and compression volumes for sinusoidal motion of the piston and displacer are:

$$V(\text{expansion}) = V_e = \frac{1}{2}(V_e)_o \ (1 + \sin\omega t')$$

$$V(\text{compression}) = V_c = \frac{1}{2}(V_c)_o \ (1 + \sin(\omega t' - \theta))$$

where:

$(V_e)_o$ = Swept volume in the expansion space

$(V_c)_o$ = Swept volume in the compression space

ω = Operating frequency (rad/sec)

θ = Angle by which volume variations in the expansion space lead those in the compression space.

$t' = t + t_o$

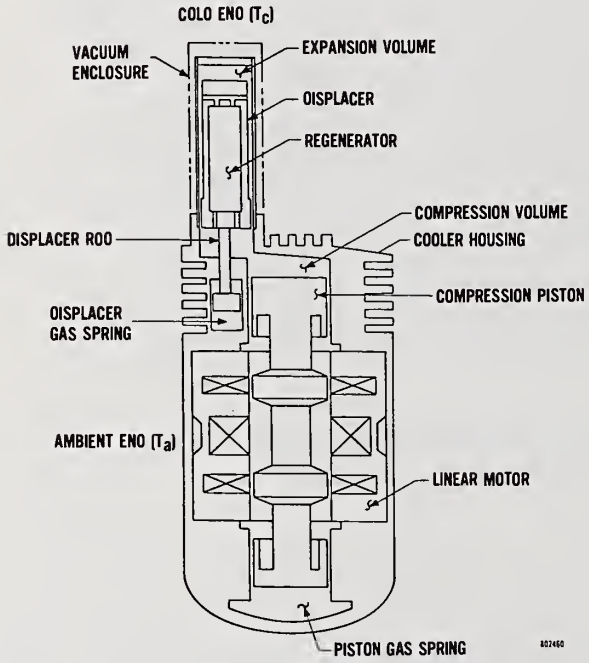

Fig. 1 MTI Single-Stage Linear Free-Displacer Cryorefrigerator

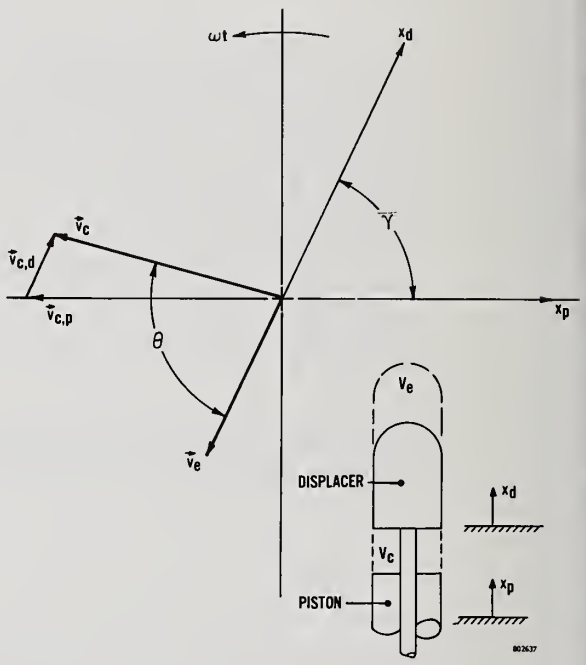

Fig. 2 Displacer and Volumetric Phasor Diagram

1.2 Pressure equation

The pressure equation is derived from the mass continuity equation for the system and is given by

$$M_T = \frac{P_{ch} V_{To}}{RT_a} = \frac{P_e V_e}{RT_e} + \frac{P_c V_c}{RT_c} + \sum^{n} \frac{P_v V_v}{RT_v} \qquad (1)$$

where:

M_T = Total mass in the system
P = Pressure
T = Temperature
V = Volume
R = Gas constant

subscripts:

ch = Charge pressure
e = Expansion space
c = Compression space
v = Void volume
To = Initial charge volume
a = Ambient

The conversion of the absolute volume expressions to phasor notation is made through the transformations:

$$V_e = \frac{1}{2}(V_e)_o + \vec{v}_e$$

$$V_c = \frac{1}{2}(V_c)_o + \vec{v}_c = \frac{1}{2}(V_c)_o + \vec{v}_{c,d} + \vec{v}_{c,d}$$

where:

V = Absolute volume variations

$\vec{v}_e$ = The phasor expansion space volume variation due to the displacer motion

and

$\vec{v}_{c,d}$ = Compression space volume variation due to the displacer motion

$\vec{v}_{c,p}$ = Compression space variation due to the piston motion

The advantage of this phasor notation is that the amplitude and phase relationship of each of the system operating parameters may now be represented on a phasor diagram that provides physical insight into the mathematics. The phasor diagram for a cryogenic refrigerator is shown in Figure 2. The development of this diagram proceeds from the relationship between the two position phasors.

Piston Motion

$$x_p = (x_p)_o \sin\omega t$$

Displacer Motion

$$x_d = (x_d)_o \sin(\omega t + \gamma)$$

where:

$(x_d)_o$ and $(x_p)_o$ = the amplitudes of the motion

γ = the angle by which the displacer motion leads the piston motion.

From these motions, the expansion and compression volume phasors may be located on the diagram (Figure 2) as follows:

- The expansion volume variation is produced by the displacer and is 180° out of phase with the displacer motion.

$$\vec{v_e} = -A_d(x_d)_o \sin(\omega t + \gamma) = A_d(x_d)_o \sin \omega t'$$

A_d = the displacer frontal area

- The compression volume variations are produced by both the displacer and piston motions.

$$\vec{v}_c = \vec{v}_{c,d} + \vec{v}_{c,p}$$

where $\vec{v}_{c,p}$ is the variation produced by the piston motion, which is represented by a phasor that is 180° out of phase with the piston motion

$$\vec{v}_{c,p} = -A_p (x_p)_o \sin\omega t$$

A_p = the piston frontal area

and $\vec{v}_{c,d}$ is the variation produced by the displacer, which is in phase with the displacer motion

$$\vec{v}_{c,d} = (A_d - A_{ROD})(x_d)_o \sin (\omega t + \gamma)$$

A_{ROD} = the displacer rod area as shown in Figure 1. The function of the displacer rod will be covered in a later discussion.

The third dimension in the analysis is the development of the pressure phasor, which is the resultant of the pressure variations caused by the displacer and piston motions. This relationship is shown in Figure 3, and is defined as

$$\vec{p} = \vec{P}_{e,d} + \vec{p}_{c,d} + \vec{p}_{c,p}$$

where:

- The displacer motion produces two pressure effects. First, variations in the expansion space produce a pressure change because of the temperature difference between the expansion and compression volumes and the shuttling of the working fluid between these volumes by the displacer motion. For a cryogenic refrigerator, where the expansion volume is at the cold temperature, the expansion volume component of the pressure wave is a phasor in phase with the displacer motion. This pressure component is represented by $\vec{p}_{e,d}$. Secondly, the volume variations produced by the displacer motion on either end of the displacer differ by the volume occupied by the displacer rod. Thus, neglecting the temperature difference, the displacer motion also causes a pressure change 180° out of phase with its motion. This pressure component is represented by $\vec{p}_{e,d}$.

- The piston motion produces a pressure change due to volume changes of the compression space. This motion produces a pressure change in phase with the piston motion, which is represented by $\vec{p}_{c,p}$ in Figure 3.

The sum of these three components produces the ideal pressure phasor. In an actual machine a pressure drop will occur across the regenerator, producing a phase lag between pressure changes in the expansion and compression spaces. The pressure drop is represented by $\Delta\vec{p}$ in Figure 3, and the expansion and compression space pressure phasors are given by

$$\vec{P}_e = (P_e)_o \sin(\omega t' + \alpha)$$

$$\vec{P}_c = (P_c)_o \sin(\omega t' - (\beta + \theta))$$

where

α = angle by which the pressure phasor ($\vec{p}_e$) leads the expansion volume phasor

β = angle by which the pressure phasor ($\vec{P}_c$) lags the compression volume phasor.

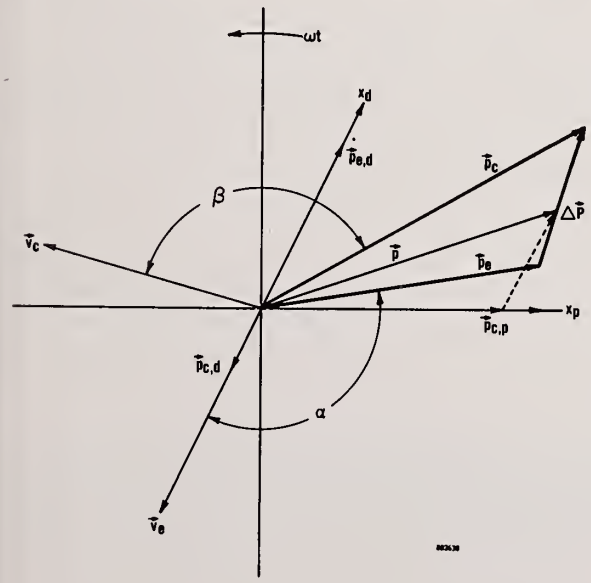

Fig. 3 Pressure Phasor Diagram

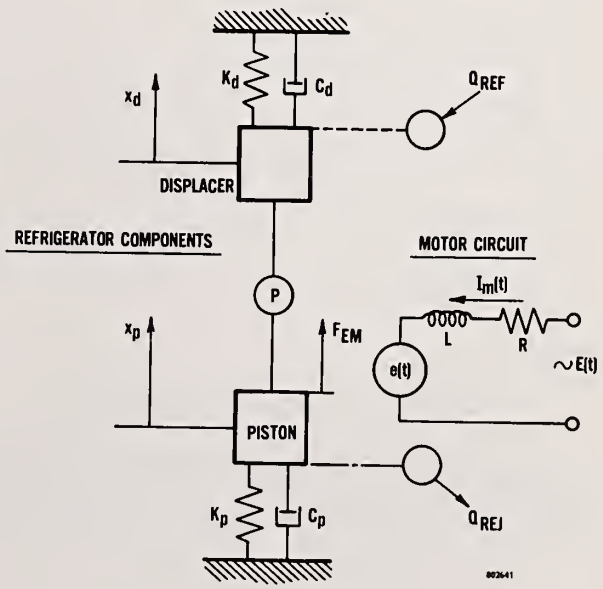

Fig. 4 Dynamic Free-Body Diagram

Up to this point in the analytical development, the equations apply for both a kinematic or free-piston machine. In a kinematic machine the proper amplitude and phase separation of the piston and displacer are established by a system of mechanical linkages. In a resonant machine the mechanical linkages are replaced by an equivalent set of dynamic components (springs, masses, dampers, and a displacer drive). Dynamically, the free-piston, linear resonant cryogenic refrigerator may be represented by the spring, mass, damper system shown in Figure 4. The link between the piston and displacer is a pneumatic linkage created by the engine pressure wave; thus, the additional complexity in analyzing this device becomes evident. Analysis of a kinematic device is less complicated because the linkage (drive mechanism) is an independent variable controllable through the positioning of the linkage on a crank mechanism. In a free-piston machine the pneumatic linkage is a dependent variable established by the dynamics of the system. Thus, the thermodynamics and dynamics are tied together through the pressure phasor.

1.3 Thermal equations

Having established the pressure and volumetric phasor relationships, definition of the power input, refrigeration capacity, and equations of motion for a resonant machine now are possible. An overall energy balance of the system gives the power delivered to the machine as the difference between the heat rejected to ambient and the refrigeration capacity.

$$\dot{P}_{IN} = \dot{Q}_{REJ} - \dot{Q}_{REF} = F_{EM} \cdot \dot{x}_P$$

where

F_{EM} = the electromagnetic driving force

$\dot{x}_P$ = piston velocity

Considering isothermal compression and expansion processes

$$\dot{Q}_{REJ} = \oint P_c \cdot dV_c$$

$$\dot{Q}_{REF} = \oint P_e \cdot dV_e$$

By applying the following phasor relationships to these integrals,

$$dV = d\vec{v}$$

$$P = P_o + \vec{p}$$

where

P_o = mean system operating pressure

and integrating over a full cycle leads directly to the following expressions for the refrigeration and heat rejection

$$\dot{Q}_{REF} = \pi f \cdot A_d \cdot (x_d)_o \ (p_e)_o \sin\alpha$$

$$Q_{REF} = \pi f \ A_p (P_c)_o \left[(x_p)_o \sin(\gamma - (\theta + \beta)) + \frac{A_d - A_{ROD}}{A_p} (x_d)_o \sin(\beta + \theta) \right]$$

where

f = the operating frequency in cycles/sec

These two equations define the difficulty in designing a resonant cryorefrigerator. First, the only independent variables are the frequency (f), and the cross-sectional areas, A_d, A_{ROD}, and Ap. Second, the five variables $(x_d)_o$, $(x_p)_o$, α, β, and γ are all dependent variables that are functions of the dynamic components, i.e., the masses, spring components, and damping. Finally, the pressure is a function of the temperatures and volumetric changes as defined by the mass continuity equation, Equation 1. Therefore, the performance of a linear resonant cryorefrigerator is defined by a minimum of 3 simultaneous equations. These are

1. The thermodynamic equations defining the refrigeration capacity
2. The mass continuity equation
3. The equations of motion

1.4 Equations of motion

The equations of motion are derived from the dynamic free-body diagram presented in Figure 4. The equation of motion for the displacer is given by

$$M_d\ddot{x}_d + C_d\dot{x}_d + K_dx_d + F_d = 0$$

in which $M_d\ddot{x}_d$ is the inertia force on the displacer, $C_d\dot{x}_d$ is the damping force which results from the viscous losses in the gas springs, K_dx_d is the conservative spring force, and F_d is the displacer driving force that maintains the displacer motion. The equation defining the driving force is found from a force balance on the displacer as shown in Figure 5.

This balance is

$$F_D = P_e \cdot A_d - P_c(A_d - A_{ROD}) - P_oA_{ROD}$$

In terms of the phasors described in Figure 3, this reduces to

$$F_D = -\Delta\vec{p} \cdot A_d + \vec{p}_c \cdot A_{ROD}$$

where

$$\Delta\vec{p} = P_c - P_e$$

$$\vec{p}_c = P_c - P_o$$

Referring again to the phasor diagram in Figure 3, it may be seen that the pressure phasors $\vec{p}_e$, $\vec{p}_c$, and $\Delta\vec{p}$ can be written as linear combinations of the conservative (displacement) and nonconservative (velocity) components as shown in Figure 6. The figure shows that the following relationships exist.

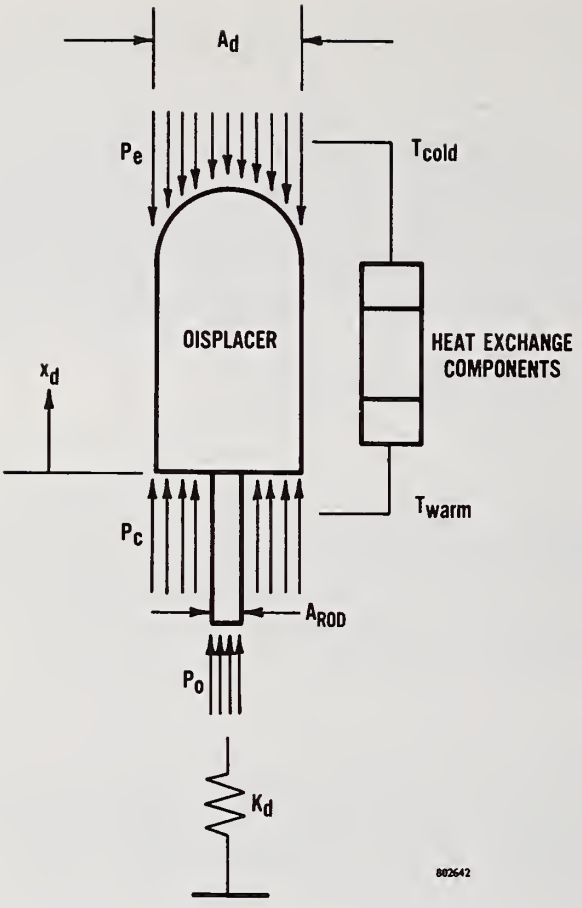

Fig. 5 Displacer Force Diagram

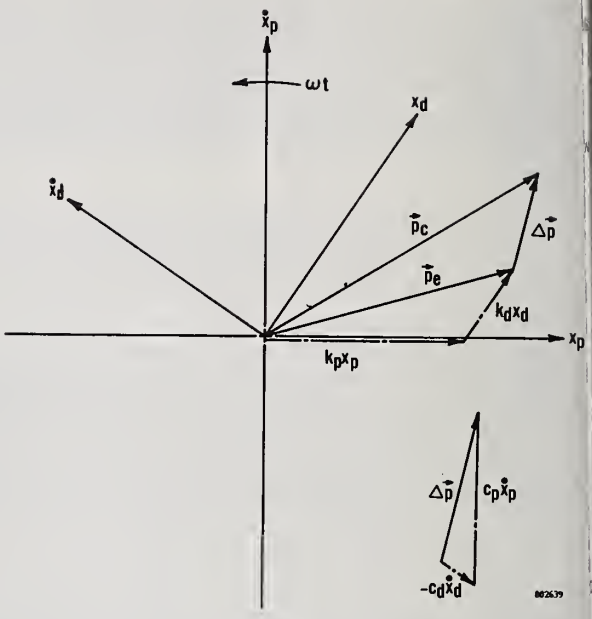

Fig. 6 Pressure Phasor Components

$$\vec{p}_c = \vec{p}_e + \Delta\vec{p} = k_p \cdot x_p + k_d \cdot x_d$$

$$\Delta\vec{p} = -c_d\dot{x}_d + c_p\dot{x}_p$$

Substitution of these expressions into the displacer equation of motion leads directly to

$$M_d\ddot{x}_d + (C_d + c_d \cdot A_d)\dot{x}_d - c_p \cdot A_d \cdot \dot{x}_p + (K_d + k_d \cdot A_{ROD})x_d + k_p \cdot A_{ROD} \cdot x_p = 0 \qquad (2)$$

in which the term $c_d \cdot A_d \cdot \dot{x}_d$ represents a nonconservative restoring force on the displacer produced by the viscous drag in the heat exchanger components; and $c_p \cdot A_d \cdot \dot{x}_p$ and $k_p \cdot A_{ROD} \cdot x_p$ represent the driving forces on the displacer produced by the pressure drop across the displacer, i.e., the heat exchanger $\Delta\vec{p}$, and the pressure force on the displacer rod.

The equation of motion for the piston is given by

$$M_p\ddot{x}_p + C_p\dot{x}_p + K_p x_p + F_p - F_{EM} = 0$$

in which the inertia, damping, and spring forces are described as above. The pressure force on the piston is

$$F_p = \vec{p}_c \cdot A_p = \bar{k}_p \cdot x_p + \bar{k}_d \cdot x_d$$

and the electromagnetic driving force for the motor is given by

$$F_{EM} = aI_m(t)$$

where:

$a = e/\dot{x}_p$

e = Voltage drop across the motor

$I_m(t)$ = Current in the motor circuit shown in Figure 4.

For our case, where the electromagnetic driving force is produced by a linear induction motor, the current is found from

$$L\frac{dI_m}{dt} + RI_m + e(t) = E(t)$$

or, by differentiating

$$L\frac{d^2I_m}{dt^2} + R\frac{dI_m}{dt} + a\,\ddot{x}_p = E_o\omega\cos(\omega t + \eta)$$

where:

L = the motor inductance
R = internal electrical resistance
E_o = the amplitude of the applied voltage $E(t)$
ω = the operating frequency
η = the phase angle between the applied voltage and the piston displacement

Then, the three equations defining the system dynamics are

$$\begin{bmatrix} M_d & o & o \\ o & M_p & o \\ o & a & L \end{bmatrix} \begin{bmatrix} \ddot{x}_d \\ \ddot{x}_p \\ \ddot{I}_m \end{bmatrix} + \begin{bmatrix} \bar{C}_d & -\bar{c}_p & o \\ o & C_p & o \\ o & o & R \end{bmatrix} \begin{bmatrix} \dot{x}_d \\ \dot{x}_p \\ \dot{I}_m \end{bmatrix} + \begin{bmatrix} \bar{K}_d & \bar{k}_p & o \\ \bar{k}_d & K_p & a \\ o & o & o \end{bmatrix} \begin{bmatrix} x_d \\ x_p \\ I_m \end{bmatrix} = \begin{bmatrix} o \\ o \\ E_o\omega\cos(\omega t + \eta) \end{bmatrix}$$

where:

$$\bar{C}_d = C_d + c_d \cdot A_d$$

$$\bar{c}_p = c_p \cdot A_d$$

$$\bar{K}_d = K_d + k_d \cdot A_{ROD}$$

$$\bar{K}_p = K_p + k_p \cdot A_p$$

$$\bar{k}_d = k_d \cdot A_d$$

$$\bar{k}_p = k_p \cdot A_{ROD}$$

The solution to the dynamic equation, in matrix form, is

$$\bar{x} = \bar{x}_t + \bar{x}_s$$

in which $\bar{x}_t$ represents the transient solution, and x_s represents the steady-state solution. A discussion of these two solutions follows.

1.4.1 Transient solution

The transient equation is

$$\begin{bmatrix} M_d & o & o \\ o & M_p & o \\ o & a & L \end{bmatrix} \begin{bmatrix} \ddot{x}_d \\ \ddot{x}_p \\ \ddot{I}_m \end{bmatrix} + \begin{bmatrix} \bar{C}_d & -c_p & o \\ o & C_p & o \\ o & o & R \end{bmatrix} \begin{bmatrix} \dot{x}_d \\ \dot{x}_p \\ \dot{I}_m \end{bmatrix} + \begin{bmatrix} \bar{K}_d & \bar{k}_p & o \\ \bar{k}_d & \bar{K}_p & a \\ o & o & o \end{bmatrix} \begin{bmatrix} x_d \\ x_p \\ I_m \end{bmatrix} = \begin{bmatrix} \bar{0} \end{bmatrix}$$

In the matrix form given, the transient equation represents a typical eigenvalue problem in which the eigenvalues represent the principal modes of vibration, and the eigenvectors define the amplitudes of the frequency response curves. In solving this set of equations the electromagnetic force coefficient, a, in the mass and spring matrices prevents a closed-form solution from being found and numerical techniques must be used to find the eigenvalues. In order to simplify the problem and gain some insight into the dynamics of the mechanical system, we shall assume that the electromagnetic force may be represented as a forcing function of the form

$$F_{EM} = F_o \sin(\omega t + \eta)$$

where

η = the phase angle between the force and piston motion.

With this assumption the transient equation becomes

$$\begin{bmatrix} M_d & o \\ o & M_p \end{bmatrix} \begin{bmatrix} \ddot{x}_d \\ \ddot{x}_p \end{bmatrix} + \begin{bmatrix} \bar{C}_d & -\bar{c}_p \\ o & C_p \end{bmatrix} \begin{bmatrix} \dot{x}_d \\ \dot{x}_p \end{bmatrix} + \begin{bmatrix} \bar{K}_d & \bar{k}_p \\ \bar{k}_d & \bar{K}_p \end{bmatrix} \begin{bmatrix} x_d \\ x_p \end{bmatrix} = \begin{bmatrix} \bar{0} \end{bmatrix}$$

Also, by drawing the force diagram for the displacer (Figure 7, which is the phasor representation of Equation 2), the term $c_p A_d \dot{x}_p$ can be expressed as

$$c_p \cdot A_d \cdot \dot{x}_p = c_p \cdot A_d \cos\gamma \cdot \dot{x}_d + c_p \cdot A_d \cdot \sin\gamma \cdot x_d$$

This substitution leads to a closed-form solution and the following eigenvalues

$$\alpha_{1,2} = -\frac{(\bar{C}_d - \bar{c}_p\cos\gamma)}{2M_d} \pm i\sqrt{\frac{(\bar{K}_d - \bar{c}_p\sin\gamma - \bar{k}_p)}{M_d} - \left(\frac{\bar{C}_d - \bar{c}_p\cos\gamma}{2M_d}\right)^2}$$

$$\alpha_{3,4} = -\frac{C_p}{2M_p} \pm \sqrt{\frac{\bar{K}_p - k_d}{M_p} - \left(\frac{C_p}{2M_p}\right)^2}$$

From necessary criteria for dynamic stability, the system is stable if the eigenvalue coefficients

$$\alpha_j = -a_j \pm i\sqrt{b_j}$$

satisfy the following conditions

If a_j is negative the solution is unstable
If a_j is positive the solution is stable
If b_j is positive the solution is harmonic

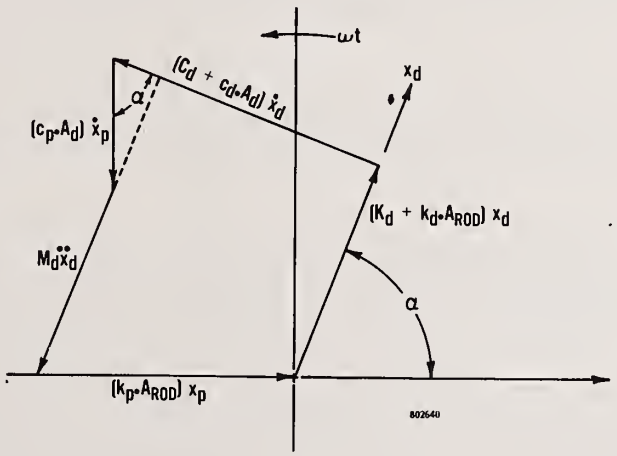

Fig. 7 Displacer Force Phasor Diagram

If b_j is negative the solution is not harmonic, and
If b_j is negative and $a_j < b_j$ the solution is unstable.

Thus, we see that in order for the mechanical system to be harmonic and stable, the necessary conditions are

$$\bar{C}_d > \bar{c}_p \cos\gamma$$

$$\bar{K}_d > \bar{c}_p \sin\gamma + \bar{k}_p$$

which essentially says that the displacer driving forces due to the pressure differential across the heat exchange components and the displacer rod must not exceed either the conservative spring or nonconservative damping forces.

1.4.2 Steady-state solution

The steady-state solution is found by substituting for the motions

$$x_p = (x_p)_o \sin\omega t$$

$$x_d = (x_d)_o \sin(\omega t + \gamma)$$

This substitution leads to the steady-state equation

$$\begin{bmatrix} M_d & o \\ o & M_p \end{bmatrix} \begin{bmatrix} -\omega^2 (x_d)_o \sin(\omega t + \gamma) \\ -\omega^2 (x_p)_o \sin\omega t \end{bmatrix} + \begin{bmatrix} \bar{C}_d & -c_p \\ o & C_p \end{bmatrix} \begin{bmatrix} \omega(x_d)_o \cos(\omega t + \gamma) \\ \omega(x_p)_o \cos\omega t \end{bmatrix}$$

$$+ \begin{bmatrix} \bar{K}_d & \bar{k}_p \\ \bar{k}_d & \bar{K}_p \end{bmatrix} \begin{bmatrix} (x_d)_o \sin(\omega t + \gamma) \\ (x_p)_o \sin\omega t \end{bmatrix} = \begin{bmatrix} o \\ F_o \sin(\omega t + \eta) \end{bmatrix}$$

The solutions to this system of equations are given in terms of the piston-displacer ratio and the phase relationship between the piston and displacer. The solution for the amplitude ratio is

$$\left(\frac{x_p}{x_d}\right)^2_o = \frac{\omega^4 \left[1 - \left(\frac{\omega_{dd}}{\omega}\right)^2\right]^2 + \left[2\int_d \left(\frac{\omega_{dd}}{\omega}\right)^2\right]^2}{\left[\frac{\bar{k}_p^2 + (c_p\omega)^2}{M_d^2}\right]}$$

where:

$$\omega_{dd}^2 = \frac{\bar{K}_d}{M_d} = \text{the natural frequency of the displacer}$$

$$\int_d = \frac{\bar{C}_d\, \omega_{dd}}{2M_d} = \text{damping coefficient}$$

And the solution for the phase angle is

$$\text{Tan}\gamma = \frac{\dfrac{F_o \sin\eta}{M_p\omega^2(x_p)_o} - 2\int_d\left(\dfrac{\omega_{dd}}{\omega}\right)}{\dfrac{F_o\cos\eta}{M_p\omega^2(x_p)_o} + \left(1 - \left(\dfrac{\omega_{dd}}{\omega}\right)^2\right)}$$

2.0 Conclusions

The phasor analysis described presents a useful tool for analyzing and understanding the operation of small, free-piston Stirling refrigerators. The usefulness of the approach has been demonstrated by the insight it has given to the operation and selection of important dynamic components. However, several assumptions were made in the analysis that have a bearing on its accuracy. These were:

1. The motions were described by a set of linear differential equations in which the conservative force terms are linear functions of displacement and nonconservative terms are linear functions of the velocity. Nonlinear effects are assumed negligible.

3. Only the first harmonic of the motions was used to describe the piston and displacer motions. Higher order terms were considered negligible.

3. To simplify the analysis, it was assumed that the electrical circuit could be represented by a sinusoidal forcing function on the piston. The effect of this assumption would be to decouple the motor's electrical circuit from the machine dynamics, making the mathematics manageable. The operation of a real machine is effected by this coupling where the interaction will influence the dynamics of the piston and displacer.

The effect of nonlinearities on the equations of motion is the possible introduction of additional instabilities into the dynamic behavior; the effect of higher order terms is to introduce additional terms into the steady-state solution that may be of the same order of magnitude as those given. A complete and thorough analysis of the device, therefore, must rely on numerical procedures, and these procedures must integrate the dynamics and thermodynamics of the refrigerator.

References

[1] Walker, G., Stirling-Cycle Machines, University of Calgary, Canada, 1978.

[2] De Jonge, A.K., "A Small Free-Piston Stirling Refrigerator," 14th Intersociety Energy Conversion Engineering Conference, American Chemical Society, Washington, D.C., 1979.

METHODS FOR THE MEASUREMENT OF REGENERATOR INEFFECTIVENESS*

Ray Radebaugh, Del Linenberger, and R. O. Voth

Thermophysical Properties Division
National Bureau of Standards
Boulder, Colorado 80303

The regenerator ineffectiveness is usually the dominant heat loss term in regenerative-cycle refrigerators which operate below about 15 K. Systematic measurements of regenerator ineffectiveness have never been done in this temperature range in spite of the fact that theoretical models are usually not adequate to fully describe and predict the thermal behavior of regenerators. The paper introduces the proper definition of regenerator ineffectiveness, which is valid for non-ideal gases and systems where a pressure wave exists. All parameters which influence the regenerator ineffectiveness are discussed. The concept of a temperature-dependent ineffectveness is proposed which simplifies computations of regenerator ineffectiveness when the material properties are temperature dependent and which yields the average ineffectiveness when it is integrated between the lower and upper operating temperatures of the regenerator. Previous methods used and proposed for the measurement of regenerator ineffectiveness at cryogenic temperatures will be reviewed and their limitations discussed. A new method will be presented which for the first time will allow measurements of regenerator ineffectiveness at all phase angles between the mass flow rate and the pressure wave, an important consideration with non-zero regenerator volumes. Temperatures considered are those beween 4 and 35 K.

Key words: Cryogenics; Gifford-McMahon cryocoolers; heat capacity; heat transfer; helium; refrigerators; regenerators; Stirling cryocoolers; thermal conductance; Vuilleumier cryocoolers.

1. Introduction

Small cryocoolers for temperatures down to about 7 K generally use a regenerative cycle. The most common examples are the Stirling, Gifford-McMahon, and Vuilleumier cryocoolers. Their potential for long life at relatively low capacities is one of the main attractions of the regenerative-cycle cryocoolers. They also have high overall efficiencies for temperatures down to about 15 K. At lower temperatures the efficiency drops rapidly because of the low specific heat of the regenerator matrix at those low temperatures. Presently, the lowest no-load temperature which can be achieved with these regenerative-cycle refrigerators is about 6 K, although Zimmerman and Sullivan [1] have operated a low-pressure single-stage device at 3.1 K with an upper temperature of 8.6 K. Higher pressures are required when the upper end is at room temperature, and the resulting higher heat capacity of helium gas in the system can become comparable to or greater than the matrix capacity for temperatures below about 10 K. Thus the overall performance of these refrigerators around 10 K and below is determined primarily by the effectiveness of the regenerator in transferring heat from the incoming warm gas to the outgoing cold gas.

* Work sponsored by Flight Dynamics Laboratory, Wright-Patterson Air Force Base, Ohio.

The theoretical behavior of regenerators is so complex that various simplifying assumptions are made in order to determine their behavior. Many of these assumptions are unrealistic for regenerators operating below about 15 K. Reliable experimental measurements of regenerator effectiveness have not been done at temperatures below 20 K. Generally comparisons between different regenerators are done by substituting them in an actual refrigerator and comparing the refrigerator performance. Such an approach is not very satisfactory because (i) several variables may be changed simultaneously, (ii) the range of variables is often limited, and (iii) it does not permit a separation of the various components which contribute to the regenerator ineffectiveness.

In this paper we describe a method for measuring regenerator ineffectiveness which allows the regenerator to be subjected to realistic operating conditions. These conditions can be varied independently in order to better understand the behavior of a regenerator. In addition, the method allows for the separation of various components of regenerator ineffectiveness.

2. Definition and Theory of Regenerator Ineffectiveness

The effectiveness ε of a heat exchanger is usually defined as

$$\varepsilon = \frac{\dot{Q}}{\dot{Q}_{max}} = \frac{\text{actual heat transfer rate}}{\text{maximum possible heat transfer rate}}. \tag{1}$$

The heat exchanger ineffectiveness λ is given by

$$\lambda = 1 - \varepsilon = \frac{\dot{Q}_{max} - \dot{Q}}{\dot{Q}_{max}} = \frac{\dot{Q}_{reg}}{\dot{Q}_{max}}, \tag{2}$$

where $\dot{Q}_{reg}$ is defined as $(\dot{Q}_{max} - \dot{Q})$. The term $\dot{Q}_{reg}$ then represents the heat load on the region of interest (the cold expansion space) caused by the excess enthalpy flow into this region. For a heat exchanger with a given λ we then find $\dot{Q}_{reg}$ from

$$\dot{Q}_{reg} = \lambda \dot{Q}_{max}. \tag{3}$$

The introduction of the terms ε and λ are generally useful since they are either independent of the temperature difference from one end of the heat exchanger to the other or a weak function of it. Thus the terms ε and λ are useful in the characterization of a heat exchanger since they eliminate one of the variables. The effectiveness according to Eq. (1) can be written as

$$\varepsilon = \frac{\dot{m}_h C_h (T_{h,in} - T_{h,out})}{(\dot{m}C)_{min}(T_{h,in} - T_{c,in})}, \tag{4}$$

where C is the fluid specific heat at constant pressure and $\dot{m}$ is the mass flow rate. The subscripts h and c refer to the hot and cold streams, respectively, 'in' and 'out' refer to the two ends of the heat exchanger, and $(\dot{m}C)_{min}$ refers to the minimum of $\dot{m}_c C_c$ and $\dot{m}_h C_h$. When C_h and C_c are temperature dependent, averaged values must be used, or the equation

$$\varepsilon = \frac{\dot{m}_h [H_h(T_{h,in}) - H_h(T_{h,out})]}{\{\dot{m}[H(T_{h,in}) - H(T_{c,in})]\}_{min}} \tag{5}$$

can be used where H is the fluid enthalpy.

For many regenerative heat exchangers the mass flow rate, temperature, and pressure are all functions of time. In that case Eqs. (4) and (5) can still be used for the regenerator effectiveness but now ε will be a function of time. In addition we must specify where $\dot{m}_h$ and $\dot{m}_c$ are to be measured since they will vary with position in the regenerator for the same instant of time, unless the gas volume in the regenerator is negligible compared with the gas volume passing through it. The most logical approach would be to choose $\dot{m}$ at the end of the regenerator next to the region of interest, i.e. the expansion space.

Usually the instantaneous effectiveness is of little interest. Instead a value averaged over a complete cycle is used to determine the average $\dot{Q}_{reg}$. The time averaged effectiveness is then

$$\varepsilon = \frac{\nu \int \dot{m}_h[H_h(T_{h,in}) - H_h(T_{h,out})]dt}{\nu \int \dot{m}[H(T_{h,in}) - H(T_{c,in})]_{min}dt} \tag{6}$$

where ν is the cycle frequency. In this expression $\dot{m}_h = 0$ during that part of the cycle when cold gas flows from the expansion space through the regenerator. Likewise $\dot{m}_{min}$ would be zero in part of the cycle. An energy balance on the regenerator requires that the heat transferred from the hot stream equals the heat transferred to the cold stream. Hence, the numerator in Eq. (6) could be replaced by the cold stream values.

We can simplify Eq. (6) whenever isothermal conditions exist for the gas inlets. In that case we let $T_{h,in} = T_U$ and $T_{c,in} = T_L$, where T_U and T_L are independent of time. Equation (6) then becomes

$$\varepsilon = \frac{\nu \int \dot{m}_h[H_h(T_U) - H_h(T_{h,out})]dt}{\nu \int \{\dot{m}[H(T_U) - H(T_L)]\}_{min}dt} \tag{7}$$

and the ineffectiveness becomes

$$\lambda = \frac{\nu \int \dot{m}_h[H_h(T_{h,out}) - H_h(T_L)]dt}{\nu \int \{\dot{m}[H(T_U) - H(T_L)]\}_{min}} \tag{8}$$

when the denominator refers to the hot stream. Additional terms arise in the numerator when the denominator refers to the cold stream and when the specific heat in the two streams are not equal. The terms $H(T_U)$ and $H(T_L)$ are independent of time if (a) the pressure is constant, or (b) the gas is an ideal gas since H is independent of pressure for an ideal gas. If either of those conditions is true, then Eq. (8) becomes

$$\lambda = \frac{\nu \int \dot{m}_h[H_h(T_{h,out}) - H_h(T_L)]dt}{\nu \{m[H(T_U) - H(T_L)]\}_{min}}, \tag{9}$$

where m is the total mass of gas passing by the end of the regenerator. The $m\Delta H$ product should be the minimum of $m_c\Delta H_c$ and $m_h\Delta H_h$, where

$$m_h = \int \dot{m}_h dt; \; m_c = \int \dot{m}_c dt. \tag{10}$$

Except for the case where some of the gas is being withdrawn (e.g. for producing liquid) $m_h = m_c$.

For regenerators with a finite gas volume and which are subjected to pressure variations, Eqs. (7) and (8) are still not satisfactory. Consider the case where $T_U = T_L$ in Eq. (8). The denominator then becomes zero and we would expect that the numerator would

also become zero in a manner such that λ remains finite as $T_U \rightarrow T_L$. However as the gas pressure in the regenerator changes it will change temperature and therefore $T_{h,out}$ will not be the same as T_L. Since the numerator in Eq. (8) remains finite as $T_U \rightarrow T_L$, the ineffectiveness approaches $\pm \infty$. Thus in such a regenerator there is an additional source of enthalpy flux besides the normal flux due to imperfect heat exchange in a temperature gradient. This additional enthalpy flux can be thought of as another heat flow term, but its presence still indicates imperfect heat exchange within the regenerator. This additional heat flow term can be understood by looking at the energy balance equations for the regenerator as shown below.

Gas Energy Balance Equation:

$$h\sigma_L(T_m - T_g) = \frac{\partial}{\partial x}(\dot{m}H) + A_g \frac{\partial}{\partial t}(\rho U)$$

Heat transfer	Enthalpy change	Energy storage

h = Heat transfer coefficient
σ_L = Surface area per unit length
T_m = Matrix temperature
T_g = Gas temperature
$\dot{m}$ = Mass flow rate
H = Gas enthalpy
A_g = Cross-sectional area of gas stream
ρ = Gas density
U = Gas internal energy

Matrix Energy Balance Equation:

$$h\sigma_L(T_g - T_m) = A_m \frac{\partial}{\partial t}(\rho_m U_m)$$

$$\approx A_m \rho_m C_m \frac{\partial}{\partial t} T_m$$

Heat transfer	Energy storage

A_m = Cross-sectional area of matrix
ρ_m = Density of matrix
U_m = Matrix internal energy
C_m = Matrix specific heat

We note that if the gas energy storage term were zero, i.e. $A_g = 0$, then a zero enthalpy gradient and zero temperature difference between T_g and T_m satisfy both equations. However when $A_g \neq 0$, the gas energy storage term will be finite whenever the pressure is a function of time. The finite gas energy storage term then forces all the other terms in both equations to be finite even for $T_U = T_L$. This effect becomes particularly important at low temperatures where the volumetric gas internal energy, ρU, is significantly larger than the matrix volumetric internal energy, $\rho_m U_m$.

In order to properly utilize the previous definitions for ε and λ, we must separate $\dot{Q}_{reg}$ into two parts

$$\dot{Q}_{reg} = \dot{Q}_T + \dot{Q}_U, \tag{13}$$

where $\dot{Q}_T$ is the heat load on the expansion space resulting from a temperature gradient in

the regenerator and $\dot{Q}_U$ is the heat load caused by the gas energy storage effects in the regenerator, which occurs when pressure waves exist. Figure 1 shows the expected dependence of $\dot{Q}_{reg}$ on the quantity $(\dot{m}C)_{min}\,\Delta T$, where ΔT is the temperature difference across the regenerator. We would expect that $\dot{Q}_U$ would depend on the absolute temperature and not on ΔT for small $\Delta T/T$. Thus the intercept in Fig. 1 should give $\dot{Q}_U$, and $\dot{Q}_T$ would then be $\dot{Q}_{reg} - \dot{Q}_U$. We shall then consider the regenerator ineffectiveness to be that associated only with $\dot{Q}_T$. The average ineffectiveness λ_a is just the slope of the straight line passing through the point P in Fig. 1. Note that according to Fig. 1, λ_a changes somewhat with ΔT. This behavior would occur when the thermal properties of the gas and the matrix are temperature dependent. In addition, λ_a also depends on both T_U and T_L when $T_U - T_L$ is large. Thus it is difficult to characterize a regenerator in a general sense with the term λ_a.

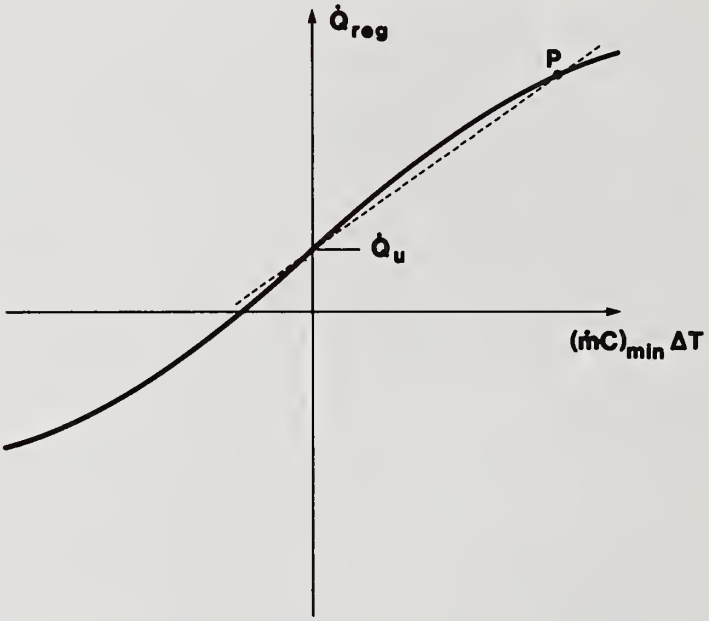

Figure 1. The dependence of $\dot{Q}_{reg}$ on the parameter $(\dot{m}C)_{min}\Delta T$. The intercept gives $\dot{Q}_U$, the heat load on the expansion space due to gas energy storage effects in the regenerator. The slope of the dashed line gives the average regenerator ineffectiveness at the point P.

We suggest that a regenerator is better characterized by using an incremental effectiveness ε_i or ineffectiveness λ_i, which is a function only of temperature. In Fig. 1 the slope at any point along the curve of $\dot{Q}_T$ vs. $(\dot{m}C)_{min}\,\Delta T$ is then λ_i. For some fixed T_L, e.g. 6 K, λ_i is then evaluated as a function of absolute temperature and the average ineffectiveness for a regenerator operating between any T_L and T_U is then

$$\lambda_a = \int_{T_L}^{T_U} \lambda_i dT/(T_U - T_L) \qquad (14)$$

whenever C_h and C_c are constant. When C_h and C_c are not constant the X-axis in Fig. 1 should be replaced by $\dot{m}[H(T_U) - H(T_L)]$ and the average ineffectiveness becomes

$$\lambda_a = \int_{T_L}^{T_U} \lambda_i C_{min} dT/[H(T_U) - H(T_L)]. \quad (15)$$

A regenerator is then best characterized by specifying $\dot{Q}_U(T)$ and $\lambda_i(T)$. Of course each of these quantities will also be functions of the heat capacity ratio, dead volume, pressure ratio, heat transfer units, pressure, and phase angle.

3. Measurement Methods

Figure 2 shows the schematics for three different methods of measuring regenerator ineffectiveness. Figure 2(a) shows the dual regenerator technique developed by Gifford [2,3]. In this scheme the gas first flows in one direction through the regenerators and then reverses direction after a period of time due to the rotary valve. The pressure is always constant in such a scheme. The heat flow due to ineffectiveness in the two identical regenerators causes boil-off of some cryogen. Gifford used liquid H_2 for the cryogen and so the value for T_L was fixed at 20 K. For lower temperatures liquid He can be used but then a semi-weak thermal coupling [4] must be placed between the heat exchanger and the helium bath so that the heat exchanger temperature will be high enough to prevent liquifying the working helium gas. The method used by Gifford and in that proposed by Walsh et al. [4] fixes the upper end of the regenerators at 77 K. The boil-off rate of the helium gives the time averaged value of the heat flow, which is just $\dot{Q}_{reg}$, or the numerator of Eq. (8). A measurement of $T_{h,out}$ would yield the instantaneous λ. This dual regenerator technique is simple to carry out but its disadvantage is that the pressure is constant, unlike that which exists in an actual refrigerator. Thus there is no way to study the effects due to gas energy storage.

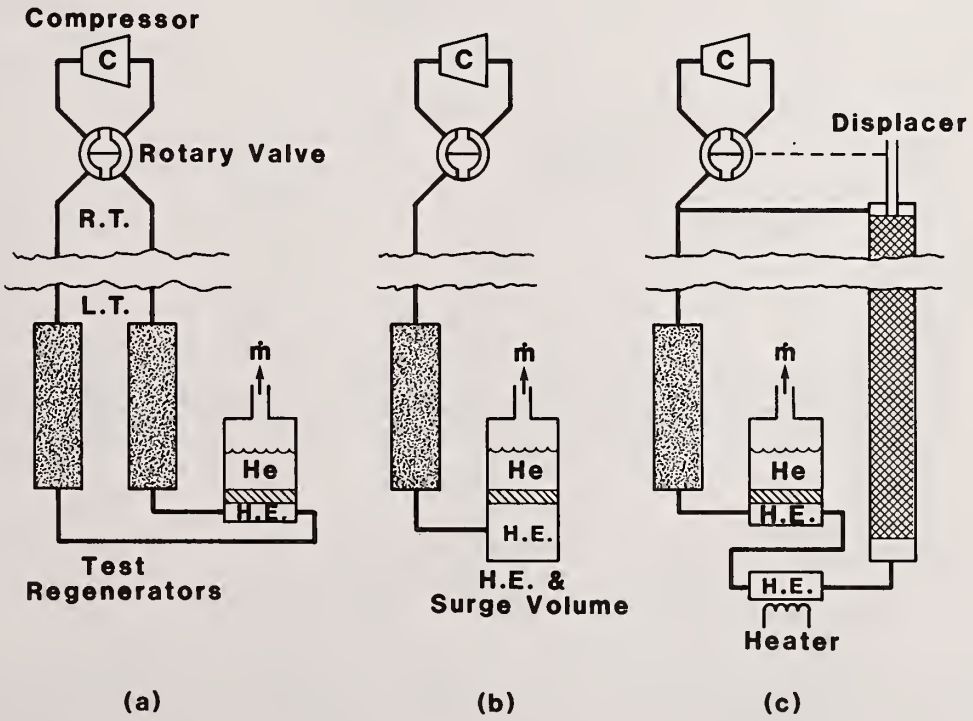

Figure 2. Schematics of three different methods of measuring regenerator ineffectiveness: (a) the dual regenerator method, (b) the surge volume method, and (c) the variable expansion space method proposed here.

Figure 2(b) shows a scheme used by Moore [5] whereby a single regenerator is closed off by a surge volume. That approach allows for a pressure wave within the system but the phase angle between the mass flow rate and the pressure wave is fixed at -90°. In a real refrigerator the phase angle is close to 0°. The gas energy storage contribution to the effectiveness is phase angle dependent and so the approach shown in Fig. 2(b) still does not allow for a proper characterization of regenerators with finite gas volumes.

The method shown in Fig. 2(c) is proposed here as one which will provide a measurement of the regenerator ineffectiveness and $\dot{Q}_U$ under conditions which exist in an actual refrigerator. The proper phase angle between the pressure wave and the mass flow rate is established by a variable expansion space, which in this case is done with a displacer. Heat supplied by the heater is absorbed by the refrigeration which occurs with proper phase angles. The regenerator ineffectiveness causes a helium boil-off. Both heat exchangers (H.E.) in Fig. 2(c) must be at the same temperature but yet they must be thermally isolated from each other. This approach allows the refrigeration power to be separated from the regenerator ineffectiveness. Figure 3 shows how this separation occurs. In this figure the heat exchangers are now isothermalizers since they also serve to bring the gas passing through them to the fixed temperature T_L. The cyclic nature of the process means that the isothermalizers must have a high heat capacity. In order to simulate Stirling and Vuilleumier cryocoolers the continuous compressor and rotary valve shown in Fig. 2(c) can be replaced by a compressor which operates synchronously with the displacer.

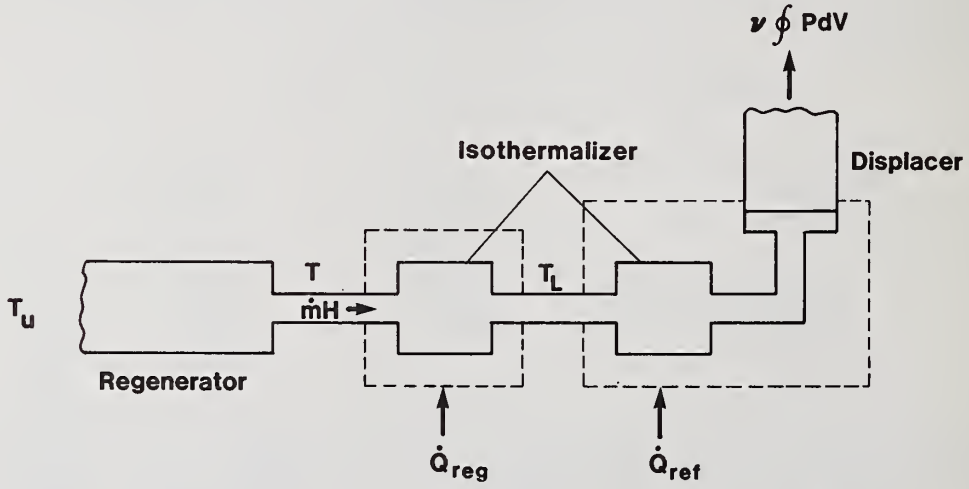

Figure 3. System boundaries for the energy balance equations which give $\dot{Q}_{reg}$ and $\dot{Q}_{ref}$.

An energy balance on the left isothermalizer shows that

$$\dot{Q}_{reg} = \nu \oint \dot{m}[H(T_L) - H(T)]dt, \qquad (16)$$

where $\dot{m}$ is positive for gas flowing to the right. For $\dot{m}$ positive $T \neq T_L$ because of the regenerator ineffectiveness. For $\dot{m}$ negative, $T = T_L$ for a perfect isothermalizer because the gas is leaving the isothermalizer. Thus $\dot{m}[H(T_L) - H(T)]$ is zero when $\dot{m}$ is negative, which means that Eq. (16) is the same as the numerator in Eq. (9) if we allow for a sign change in $\dot{Q}_{reg}$. Thus $\dot{Q}_{reg}$ is a direct measure of the heat flow due to regenerator ineffectiveness and $\dot{Q}_{ref}$ is a measure of the refrigeration rate. The ineffectiveness is then given as

$$\lambda = \frac{\dot{Q}_{reg}}{\nu \{m[H(T_U) - H(T_L)]\}_{min}} . \qquad (17)$$

An energy balance around the right isothermalizer and the displacer shows that

$$\dot{Q}_{ref} = \nu[\oint PdV - \oint \dot{m} H(T_L) dt], \qquad (18)$$

where P is the gas pressure at the displacer and dV is the volume change.

4. Description of Present Method

A detailed schematic of the low temperature parts of the proposed regenerator test apparatus is shown in Fig. 4. Each isothermalizer is connected to a helium bath via a variable thermal link, which will be discussed in more detail later. The variable thermal links allow the isothermalizers to be maintained at any temperature between about 5 K and 35 K with varying amounts of heat dissipation (up to 2 W) within each isothermalizer. It would be possible to maintain isothermalizers #1 and #2 at 77 K to provide a comparison with results from tests where the upper end is at 77 K. The heat dissipation from isothermalizer

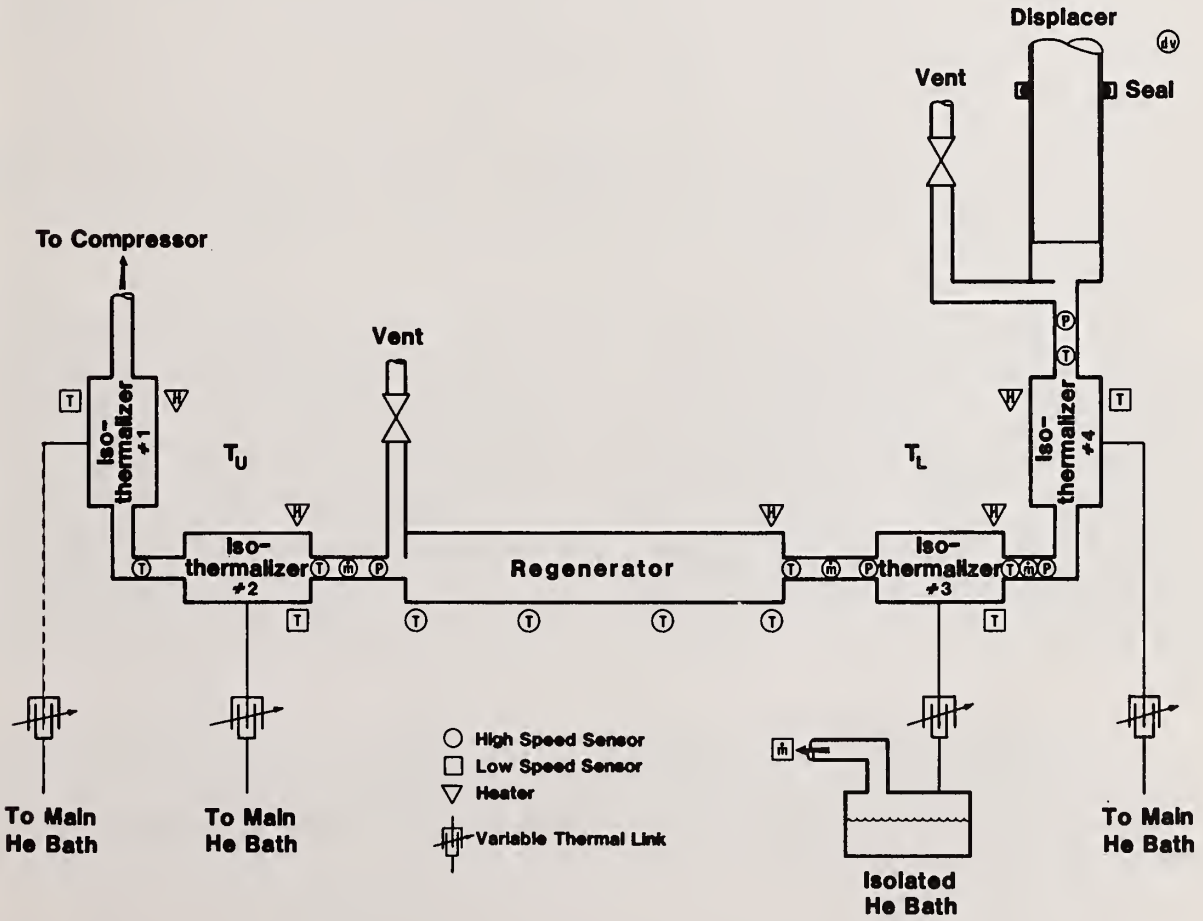

Figure 4. A schematic of the low temperature part of the regenerator test apparatus proposed here which shows the placement of $\dot{m}$, P, and T transducers.

#3 is $\dot{Q}_{reg}$ and so improved resolution is provided by using an isolated and shielded helium bath to absorb the heat. A small amount of heat supplied by a heater on each isothermalizer is used for temperature control. Isothermalizer #1 is included so that heat input to isothermalizer #2 gives $\dot{Q}_{reg}$ on the hot side of the regenerator. The facility has the capability to make $(T_U - T_L)/T_L << 1$ in order to measure incremental ineffectiveness at all temperatures between 5 and 35 K. In addition the temperature gradient can be reversed so that $\dot{Q}_{reg}$ is measured by applying heat to isothermalizer #3. A heat input can be measured much more accurately than a helium boil-off rate caused by heat dissipation. The change in the sign of dT/dx through zero also allows us to determine $\dot{Q}_U$, the heat load due to gas energy storage.

High speed sensors within the gas stream at several places allow us to measure the instantaneous T, P, and $\dot{m}$ for frequencies up to 20-30 Hz. Slow speed germanium thermometers on the isothermalizers are used to measure their temperature. Temperature control of the isothermalizers is critical to the operation of the system. For measurements of incremental ineffectiveness at, for example, 10 K the temperature difference $T_U - T_L$ may be about 1-2 K. For an ineffectiveness of 2% the difference of $T - T_L$ may be about 20-40 mK. Thus temperature control to within ± 1 mK at 10 K is needed in order to measure the ineffectiveness to within ± 5%. Temperature control of isothermalizers #2 and #3 is done in the usual fashion using PID controllers and carbon thermometers as sensors. Isothermalizers #1 and #4 are to be maintained at the same temperature to within ± 1 mK as their adjacent isothermalizer. However, the calibration accuracy of germanium thermometers is not good enough to yield temperature differences less than 1 mK at 10 K. We thus propose to use a differential gas thermometer. Each isothermalizer has a gas bulb of nominally the same size. The capillary lines from each pair of gas bulbs go to opposite sides of a sensitive differential pressure transducer. The room-temperature volume on one side of each transducer is made adjustable so that the low-temperature volume to room-temperature volume ratio on each side of the transducer can be made exactly equal. The correct volume is determined by a calibration at room temperature and at liquid He temperature. For a volume ratio of 0.05 and a filling pressure of 1 atm at room temperature a 1 mK change in temperature causes a pressure difference of about 2.7 Pa (0.02 torr). The room temperature volumes must be kept to within about ± 0.01°C of each other to keep differential pressure fluctuations less than the 2.7 Pa (0.02 torr). The electrical outputs from the two differential pressure transducers are fed into separate PID temperature controllers, which in turn control the heat input to isothermalizers #1 and #4.

The two vents shown in Fig. 4 allow the apparatus to measure the regenerator thermal conductance, heat capacity, and heat transfer coefficient. To measure the thermal conductance, heat is applied to the right side of the regenerator and the heat is absorbed at the left side by the gas stream flowing continuously through isothermalizers #1 and #2 and out through the vent. The heat capacity of the regenerator (including that due to adsorbed He and boundary layer He) is measured by passing He gas continuously through the regenerator and out through the vent next to the displacer. After the gas and regenerator are in thermal equilibrium, heat is suddenly applied to the gas upstream from the regenerator to provide a quasi-step function in temperature vs. time. The gas temperature at the regenerator inlet, T_i, and the outlet, T_o, are then measured as a function of time. Figure 5 shows the typical behavior for these two temperatures. The time lag is that associated with the wave front passing through the regenerator. The total heat capacity of the regenerator is given by

$$C_{reg} = \frac{\dot{m}C_p}{\Delta T_i} \int_0^\infty (T_i - T_o)\,dt, \tag{19}$$

where C_p is the specific heat of the gas at constant pressure. The number of heat transfer units, N_{tu}, is defined as

$$N_{tu} = h\sigma/\dot{m}C_p, \tag{20}$$

where h is the heat transfer coefficient and σ is the heat transfer surface area. The term N_{tu} can be determined from the temperature-time curves in Fig. 5 from the relation

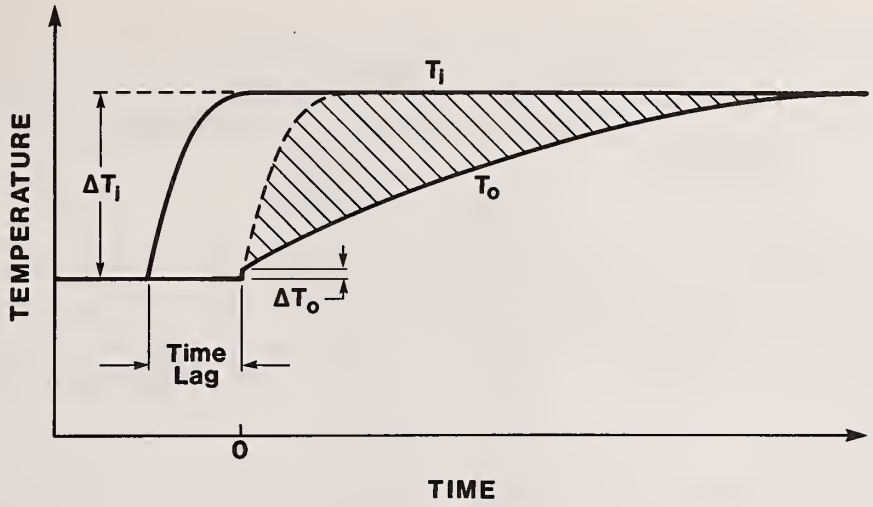

Figure 5. A temperature vs. time plot for the regenerator inlet and outlet temperatures after a quasi-step change in temperature. The regenerator heat capacity and N_{tu} are derived from the temperature behavior.

$$N_{tu} = (\Delta T_i - \Delta T_o)/\Delta T_o. \tag{21}$$

High values of N_{tu} will be difficult to measure accurately since ΔT_o will tend to be smeared out in practice. If σ is known, then h can be determined from Eq. (20).

The two critical parts of the regenerator test apparatus are the variable thermal links and the isothermalizers. For the variable thermal links we propose to use gas gap heat switches like that described by Bywaters and Griffin [6], in which heat is transferred between several concentric copper cylinders by helium gas in the gaps. Figure 6 shows the arrangement. For pressures below about 130 Pa (1 torr) the thermal conductance across the helium gap is proportional to the gas pressure. The variable pressure is achieved by the use of a molecular sieve adsorbant which can be heated to some temperature above 4.2 K [7]. When the molecular sieve is held at about 20 K by a heater, it adsorbs little He gas and so the pressure remains high. As the heat to the molecular sieve is decreased, the temperature of the sieve decreases and the resultant adsorption causes the gas pressure to decrease. In the full 'off' condition the only heat leak is through the fiberglass-epoxy support tube. Below 35 K radiation is negligible for polished surfaces. Measurements of the electrical conductance between the two ends would show whether the copper cylinders are touching each other. For long life (i.e., time greater than a few months) it is necessary to imbed a thin foil of Cu-Ni or stainless steel within the fiberglass-epoxy tube in order to prevent the diffusion of He gas through the tube walls.

The isothermalizers are the other set of critical components. Their design is not easy because of the following four requirements: a) high heat capacity, b) high N_{tu}, c) small pressure drop, and d) small gas volume. The first two and the last two requirements generally work in opposition to each other. The temperature difference between the gas and the isothermalizer at the outlet, ΔT_o, is related the inlet temperature difference, ΔT_i, by

$$\Delta T_o/\Delta T_i = \exp(-N_{tu}). \tag{22}$$

Thus for $\Delta T_o/\Delta T_i = 10^{-4}$, we need $N_{tu} = 9.2$. With such values the gas outlet temperature is within 1 mK of the isothermalizer even for $\Delta T_o = 10$ K. To calculate the required heat capacity of the isothermalizers we estimate the total heat to be stored in each cycle.

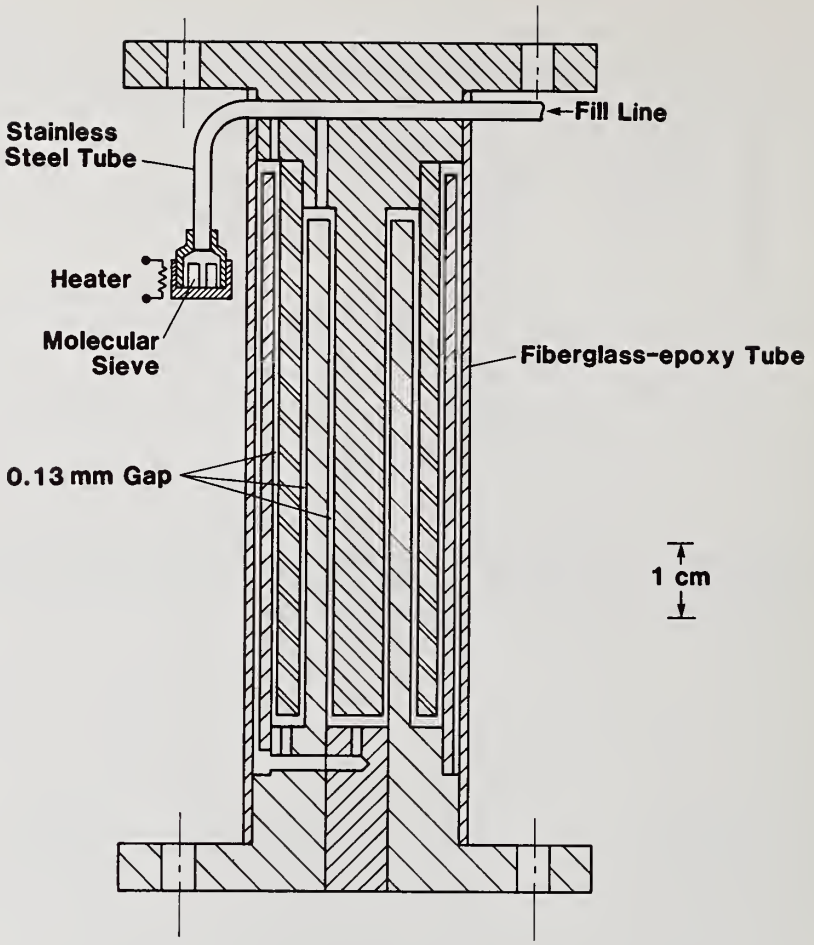

Figure 6. Drawing of a gas-gap heat switch used for the variable thermal link. The helium gas pressure between the concentric copper cylinders is controlled by the temperature of the molecular sieve adsorbent.

For a refrigeration rate of $\dot{Q}_{ref}$ the total heat to be stored is $\dot{Q}_{ref}/\nu$. For a total heat capacity of C_i the temperature fluctuation δT in the isothermalizer is then given by

$$C_i \delta T = \dot{Q}_{ref}/\nu. \tag{23}$$

For a fixed $\dot{Q}_{ref}$ the largest C_i is needed at the lowest ν. For $\dot{Q}_{ref}$ = 1 W and C_i = 50 J/K we get δT = 5 mK at ν = 4 Hz but δT = 1 mK at ν = 20 Hz. Further reductions in δT can be achieved by staging. A total heat capacity of at least 40 J/K between 5 K and 40 K can be achieved with the use of 50 cm^3 of Pb and 100 cm^3 of He gas at a pressure of 2 MPa (20 atm). The dimensions of the Pb and the He space must not be larger than the thermal penetration depth at the working frequency range, which at 10 Hz is about 1 mm in Pb at 35 K and 50 μm in He below 20 K.

Design calculations show that an N_{tu} value of 9.2 can be achieved with pressure drops generally less than 1% of the pressure for pressures greater than about 1 MPa (10 atm) and temperatures up to 35 K. A flow rate of 1.5 g/s can be accomodated with a gas volume in the isothermalizer of about 0.3 cm^3. We propose to use an annular gap of about 28 μm thickness, 31 cm effective width, and 3.5 cm long to provide the necessary surface area.

5. Conclusions

The regenerator test apparatus proposed here should be capable of measuring regenerator ineffectiveness in the range 4-35 K with variable phase angle between the mass flow rate and the pressure wave. Thus the conditions can be made to match very closely that which occurs in an actual refrigerator. In addition, the apparatus would be capable of separating out all of the sources contributing to the overall ineffectiveness and show their dependence on various parameters.

6. References

[1] Zimmerman, J. E. and Sullivan, D. B., A Milliwatt Stirling Cryocooler for Temperatures Below 4 K, Cryogenics 19, 170-171 (1979).

[2] Gifford, W. E., Basic Investigation of Cryogenic Refrigeration Methods, Air Force Flight Dynamics Laboratory, Wright-Patterson Air Force Base, Ohio, 45433, AFFDL-TR-68-61, (1968).

[3] Gifford, W. E. and Acharya, A., Low-Temperature Regenerator Test Apparatus, Adv. Cry. Eng. 15, 436-442 (1970).

[4] Walsh, P. J., Wade, L. A., and Chaudhary, T. M., Cryoregenerator Heat Capacity Enhancement, Air Force Flight Dynamics Laboratory, Wright-Patterson Air Force Base, Ohio, 45433, AFFDL-TR-80-3034 (1980).

[5] Moore, R. W., Jr., An Investigation of Thermal Regenerators for the 4 to 20 K Temperature Range, Air Force Flight Dynamics Laboratory, Wright-Paterson Air Force Base, Ohio, 45433, AFFDL-TR-70-64 (1970).

[6] Bywaters, R. P. and Griffin, R. A., A Gas-Gap Thermal Switch for Cryogenic Applications, Cryogenics 13, 344-349 (1973).

[7] Castles, S., private communication (1980).

SERVICEABLE REFRIGERATOR SYSTEM FOR SMALL SUPERCONDUCTING DEVICES

Ralph C. Longsworth

Air Products and Chemicals, Inc.
APD Cryogenics
P.O. Box 2802
Allentown, PA 18105

The design of a refrigeration system for cooling small superconducting devices such as Josephson Technology computers which can be serviced while the superconducting device remains in a cold operating state is described. The refrigeration system incorporates new (passive) thermal couplings which permit the Displex® expander and JT circuit to be warmed up, the expander serviced, and the JT circuit purged, while helium boils off at a relatively low rate from the bath that is cooling the superconducting device.

When connected to the 1.4 L test pot, a warmup-purge-cooldown test was run. Helium was initially condensed in the pot by the refrigerator at the rate of 0.3 L/hr then the refrigerator turned off. It took 7 hours to warm up and purge the refrigerator, followed by 3 hours to cool back down to 4K. Just a few minutes before reaching 4K, helium stopped venting and started to be drawn into the test pot indicating that slightly more than 1.4 L of helium was used during the service cycle.

Key Words: Cryogenic refrigerator; liquid helium; Josephson technology; serviceable; superconducting device; thermal coupling.

1. Introduction

As applications for small superconducting devices become commercial, there will be a need for closed-cycle refrigerator systems that permit such a device to be maintained in a cold operating state continuously, including periods when the refrigerator is off and being serviced. At the 1977 meeting of this group, van der Hoeven and Anaker [1] described the refrigerator requirements for a Josephson technology data processing system with particular emphasis on reliability and serviceability. At the same meeting Longsworth [2] described means of refrigerating small superconducting devices, while providing isolation from vibration and electromagnetic "noise".

This paper describes the design of the refrigerator system developed for this application which incorporates new thermal couplings that permit the expander and JT circuit to be warmed up, the expander serviced, and the JT circuit purged, while helium boils off at a relatively low rate from the bath that is cooling the superconducting device. A companion paper to this reports on test results which show reasonably good agreement between calculated values and actual performance.

2. System Description

The basic refrigerator system is an APCI Model CS-308 two-stage Displex® refrigeration system with a JT loop to provide refrigeration at ~ 4.2K. Refrigeration capacity ratings are 2.5 watts at 4.5K plus 2 watts at <20K and 10 watts at <77K. The original JT circuit which was designed for cooling samples at 4.5K has been modified to permit remote cooling of a liquid helium dewar using the first and second stage refrigeration to intercept heat leak and 4K refrigeration to recondense helium boil-off.

The compressor is a three-stage oil-lubricated reciprocating unit that supplies gas at 17.7 atm and receives gas from the expander at 4.1 atm and from the JT loop at 0.8 atm. In addition to the compressor, the standard CS-308 system includes a two-stage Displex expander, the three JT heat exchangers and adsorbers, manually adjustable JT valve, a 4K heat station, a hydrogen filled thermal switch connecting the second and 4K heat stations (for cooldown), a radiation shield attached to the first stage, and the gas ballast tank.

Figure 1 is a piping schematic of the present system. The helium pot simulates the helium dewar in the final system and serves the purpose of enabling the performance of the thermal coupling system and thermal losses during servicing of the refrigerator to be measured. The basic CS-308 system is thus modified by adding or substituting the following components:

a) thermal couplings 1 and 2 are added

b) a helium condenser replaces the standard 4K heat station

c) gas lines are added on the high pressure JT line to transport refrigeration to the separate thermal couplings and condenser

d) a bypass valve for cooldown is substituted for the H_2 thermal switch

e) a separate feed line for precooling and liquifying make-up helium is added

f) self-sealing gas couplings on the JT circuit are added to permit it to be isolated

g) purge lines on the JT circuit are added to permit it to be flushed

h) additional temperature sensors and heaters are added to permit control of rapid warmup for service and monitoring of performance

i) an absolute pressure JT bypass pressure regulator for automatic control of the liquid temperature is added

j) an experimental 1.4 L helium pot connected to a separate warm flange by a support tube, having its own radiation shield, is added.

Refrigeration systems similar to this are presently being built for cooling superconducting magnets and spectroscopy samples in which the refrigerator and magnet or spectroscopy sample holder are in separate enclosures connected by a flexible hose containing the gas lines.

An important design criteria that is adhered to is that the circulating refrigerant helium, which must be kept free of contaminants, is never mixed with the helium that is in contact with the superconducting device.

3. Refrigeration

Figure 2 shows the first and second stage capacity of the DE-208L Displex expander before adding the JT loop. The width of the capacity curve reflects a small interdependence of the heat load-temperature relation for the two stages and manufacturing variations from unit to unit. When the JT loop is added there are additional heat loads imposed, primarily heat exchanger losses on the first stage, and both heat exchanger losses and enthalpy difference loading imposed on the second stage.

In order to determine the complex relationship between first, second, and JT heat station heat loads versus temperatures, calculations were made of refrigeration losses in the JT heat exchangers assuming the following matrix of operating conditions.

- JT pressure at the compressor of 0.8 and 1 atm corresponding to 0.23 and 0.29 g/s flow respectively
- second stage temperatures of 16 and 20K
- first stage temperatures of 50, 65 and 80K

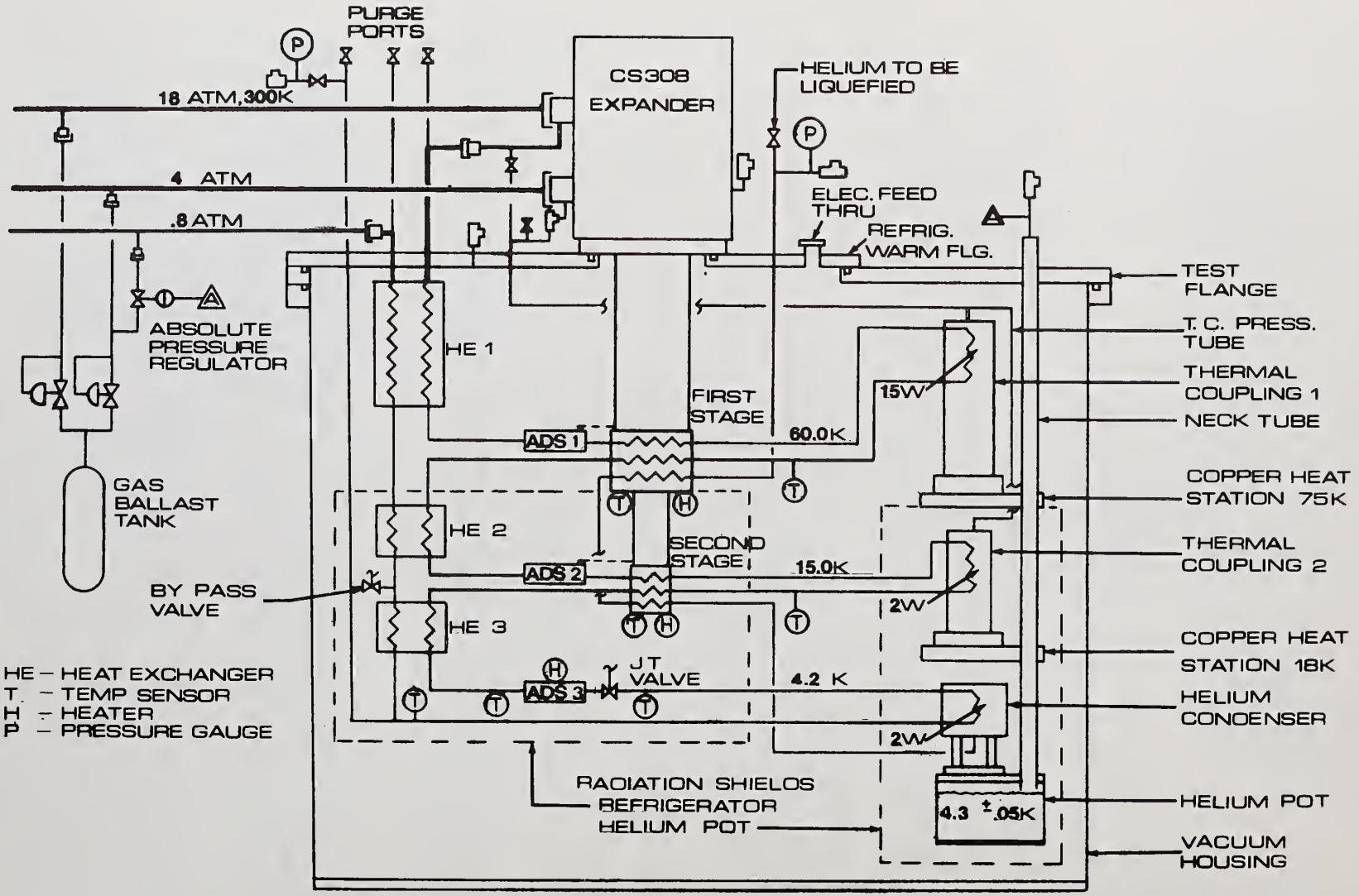

Figure 1. Refrigerator/Dewar Piping Schematic

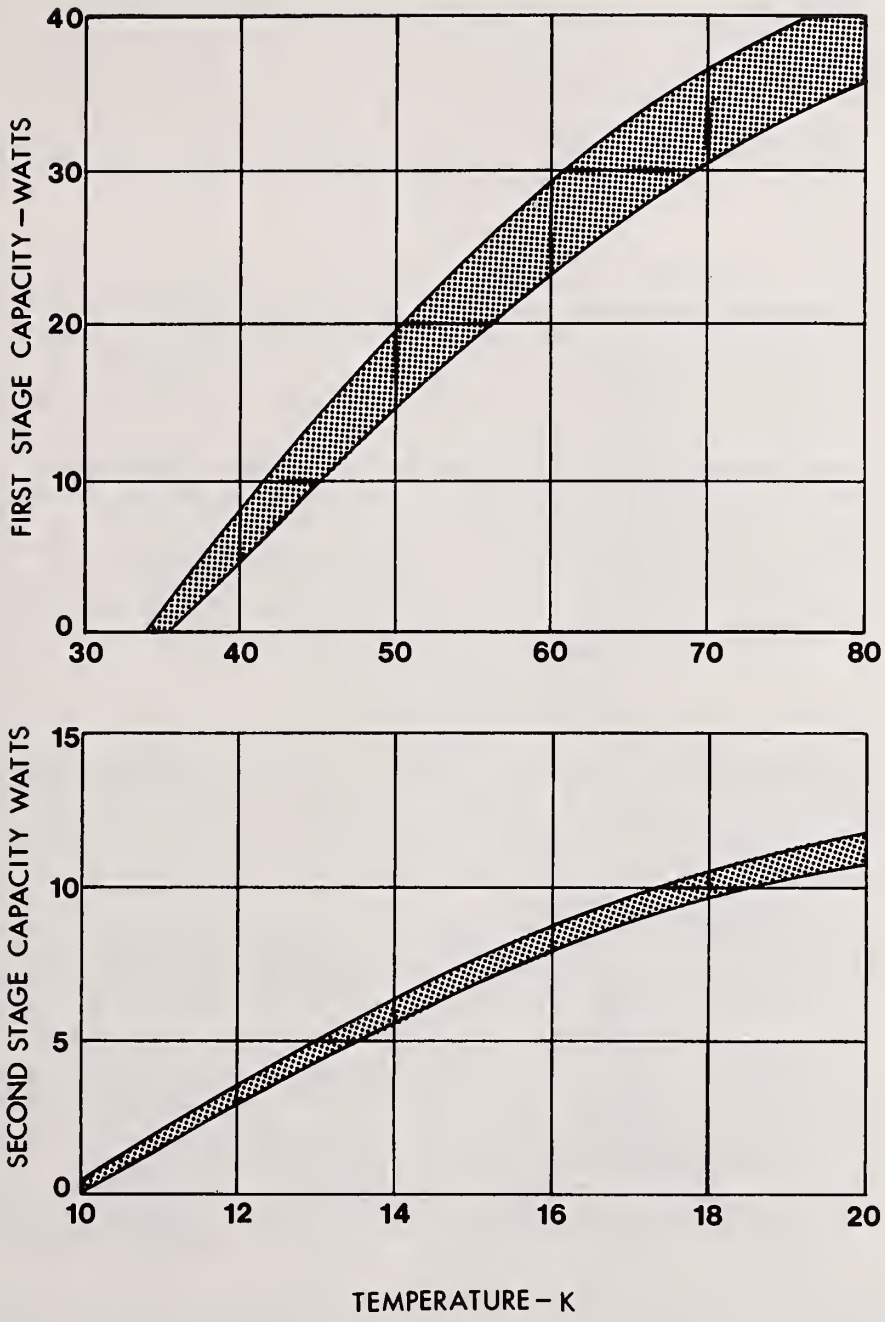

Figure 2. CS-208L Refrigerator Capacity

Heat exchanger and enthalpy losses calculated at these conditions are subtracted from the minimum capacity curve of Figure 2 to obtain the performance map shown in Figure 3. Figure 3 plots first and second stage refrigeration available versus first stage temperature for T_2 = 16 and 20K and P_{JT} = 0.8 and 1 atm. Refrigeration produced at the 4K heat station is also listed. Use of the curve is illustrated by assuming a 10 watt heat load on the first stage, second stage temperature of 16K, and 1 atm JT return pressure. First stage temperature is 56K, second stage capacity is 2.5 watts, and 2.3 watts is available at about 4.3K. There is a small pressure drop loss in the low pressure side of the JT loop, thus the saturation pressure at the 4K heat station is higher than the return pressure at the compressor.

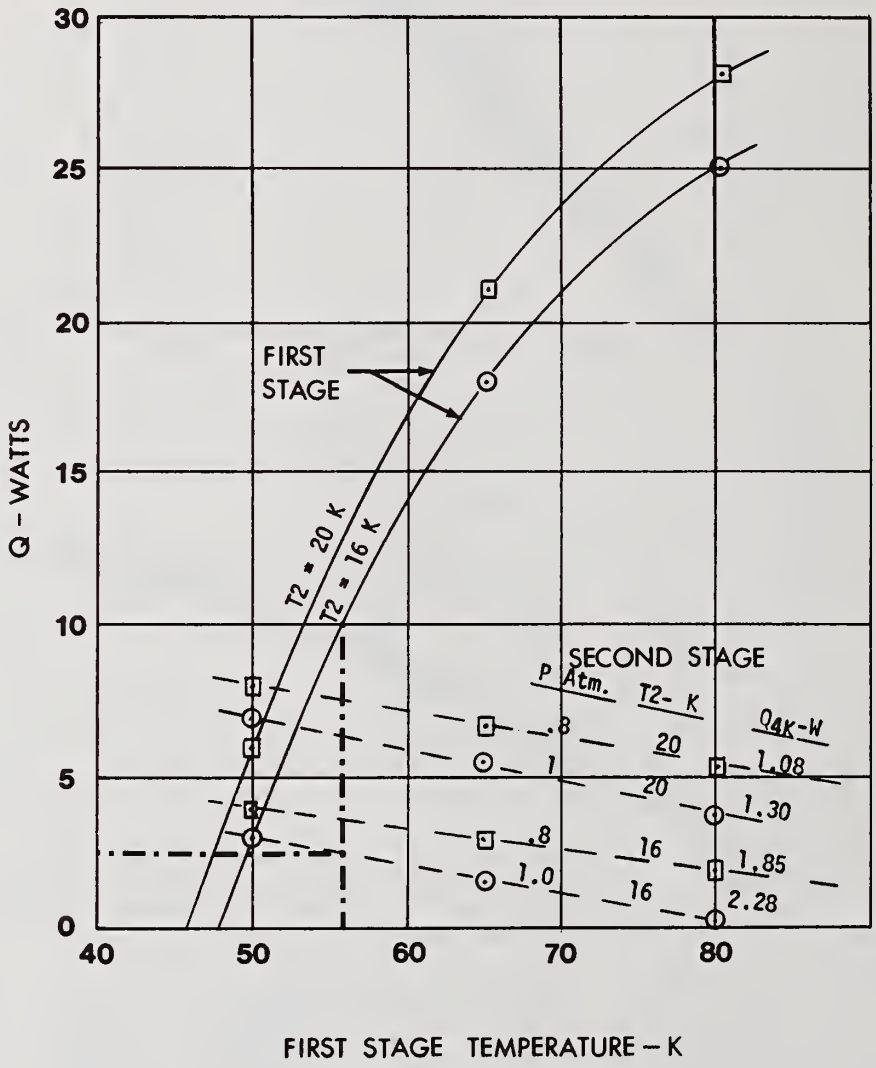

Figure 3. CS-308 Available Refrigeration of First and Second Stages Versus First Stage Temperature. Capacity of the 4 K stage is tabulated for second stage temperatures of 16 K and 20 K and return pressures of 0.8 and 1.0 atmospheres. The dashed lines at 56 K and 2.5 W refer to the example given in the text.

Figure 4 plots the refrigeration available at the second and 4K heat stations as a function of second stage temperature for 0.8 and 1 atm JT return pressure assuming a 15 watt heat load on the first stage. This plot shows that if there is a 2 watt heat load on the second stage and if the JT return pressure is 1 atm, then the second stage temperature is 16.0K and 2.3 watts is available at the 4K heat station.

These calculated capacities neglect conduction and radiation losses which can typically be kept relatively small by careful design.

4. Cooldown

It takes about 2-1/2 hours to cool down the standard CS-308 refrigerator and about 3 hours to cool down the refrigerator and thermal couplings. If additional mass is in good thermal contact with each of the heat stations then the first stage can cool 2.3 Kg of copper per hour and the second stage can cool .9 Kg of copper per hour. For the configuration shown in Figure 1, there is poor thermal coupling of the helium pot with the heat stations, thus the rest of the system cools down much faster than the helium pot.

In a dewar with a large neck tube it is possible to provide means for the first and second stage thermal baffles to cool down the helium pot by convection. Another option to cool the helium pot faster is to feed helium in through the liquefaction circuit and vent it through the top of the neck tube. A small circulating pump could be used to eliminate helium losses. Such an arrangement can be used as an alternate means to cool the leads from a superconducting device such as a magnet.

5. Thermal Couplings

Figure 5 shows a cross section view of the first stage thermal coupling which transfers heat by convection from the base to the finned tube in the top which in turn is cooled by flow from the JT loop. In the event that the refrigerator shuts down, the thermal coupling stays cold because gas circulation in the JT loop stops. Helium will typically boil off at a relatively low rate during this time, i.e., 0.1 to 0.5 L/hr.

The primary purpose of the convective thermal coupling is to enable the JT loop to be warmed to room temperature and purged without significantly increasing the helium boil-off rate. This is possible because the helium stratifies inside the thermal coupling when the top is warmer than the bottom so heat is only transferred by conduction in the gas and housing from top to bottom.

High heat transfer rates with modest temperature differences and relatively compact design are achieved by separating the hot rising gas from the cold down-flowing gas and locating extended surface heat exchangers in such a way as to promote convective circulation of the gas. Since the convective heat transfer rate is proportional to pressure, it is best to keep the pressure at the high pressure side of the system. In other applications the thermal convective coupling can be used as a variable thermal conductance device by adjusting the gas pressure.

The helium condenser shown in cross section in Figure 6 is designed with the JT stream cooling a finned tube in the top chamber which is separated from the main liquid helium pot by standoff tubes. These standoff tubes are designed to have a low heat leak to the liquid helium when the refrigerator is off and when the JT loop is warmed up to be purged.

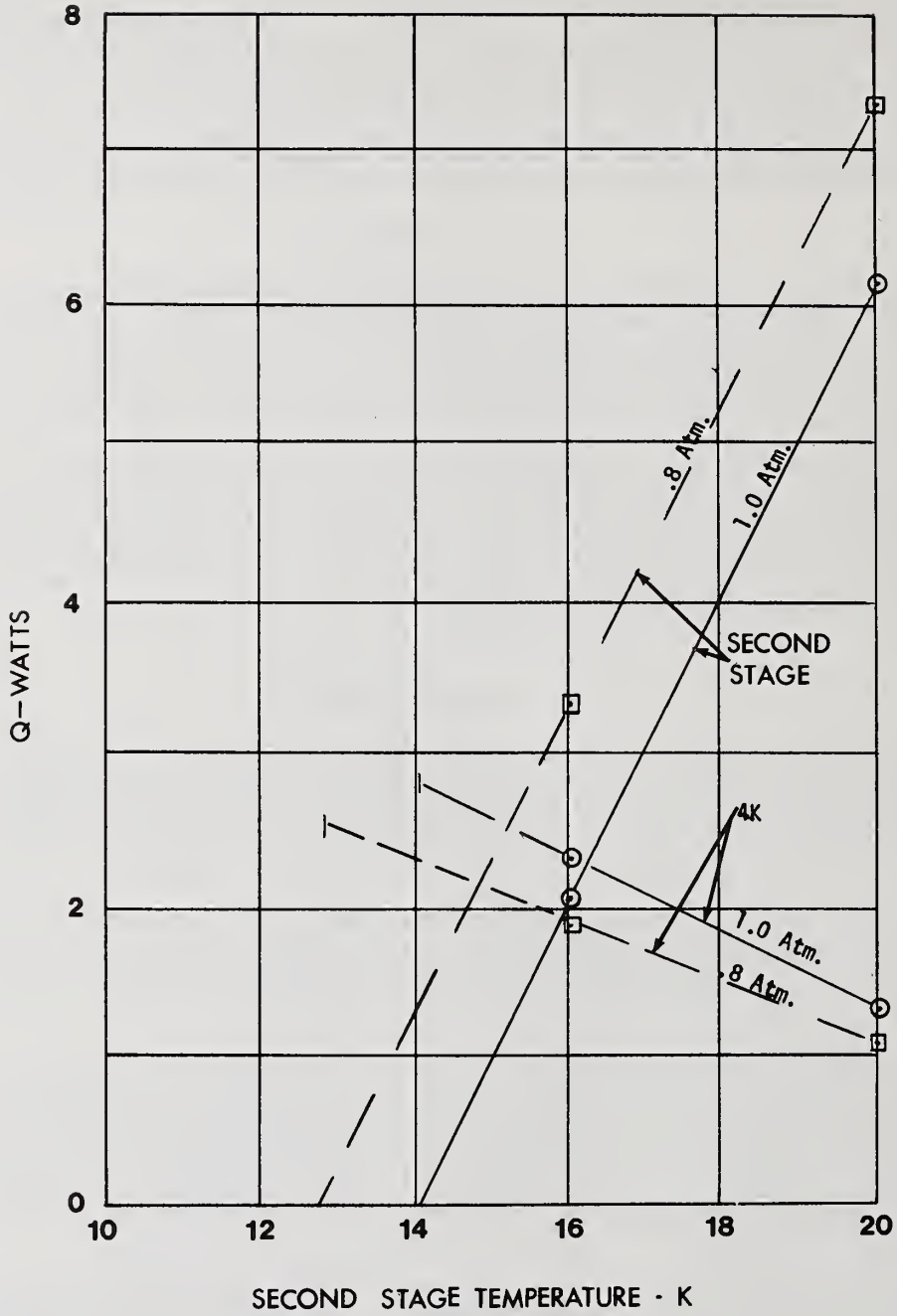

Figure 4. CS-308 Available Refrigeration of Second Stage and 4K Heat Station Versus Second Stage Temperature with 15 watts on First Stage.

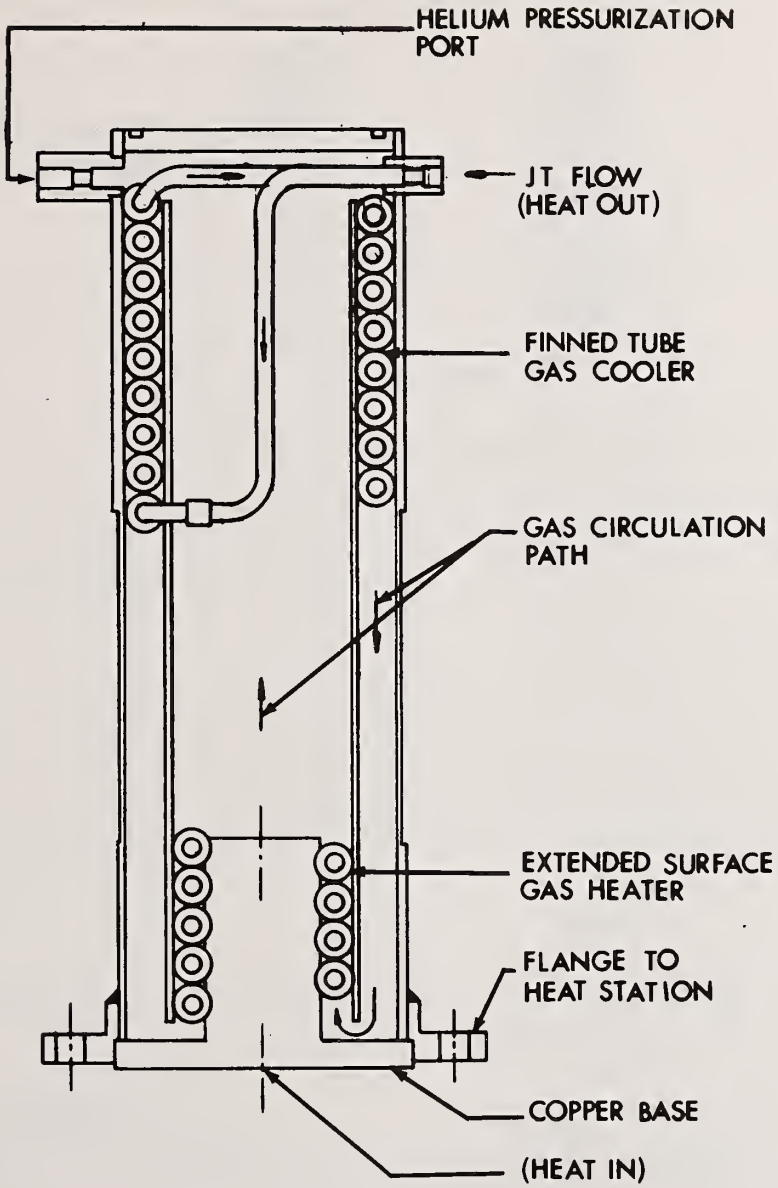

Figure 5. Convective Thermal Coupling for First and Second Heat Stations.

The JT loop gas coupling, the convective thermal couplings, and the helium condenser are all (passive) thermal disconnect switches that serve to thermally isolate the refrigerator from the liquid helium bath when the refrigerator shuts down and when it is being serviced.

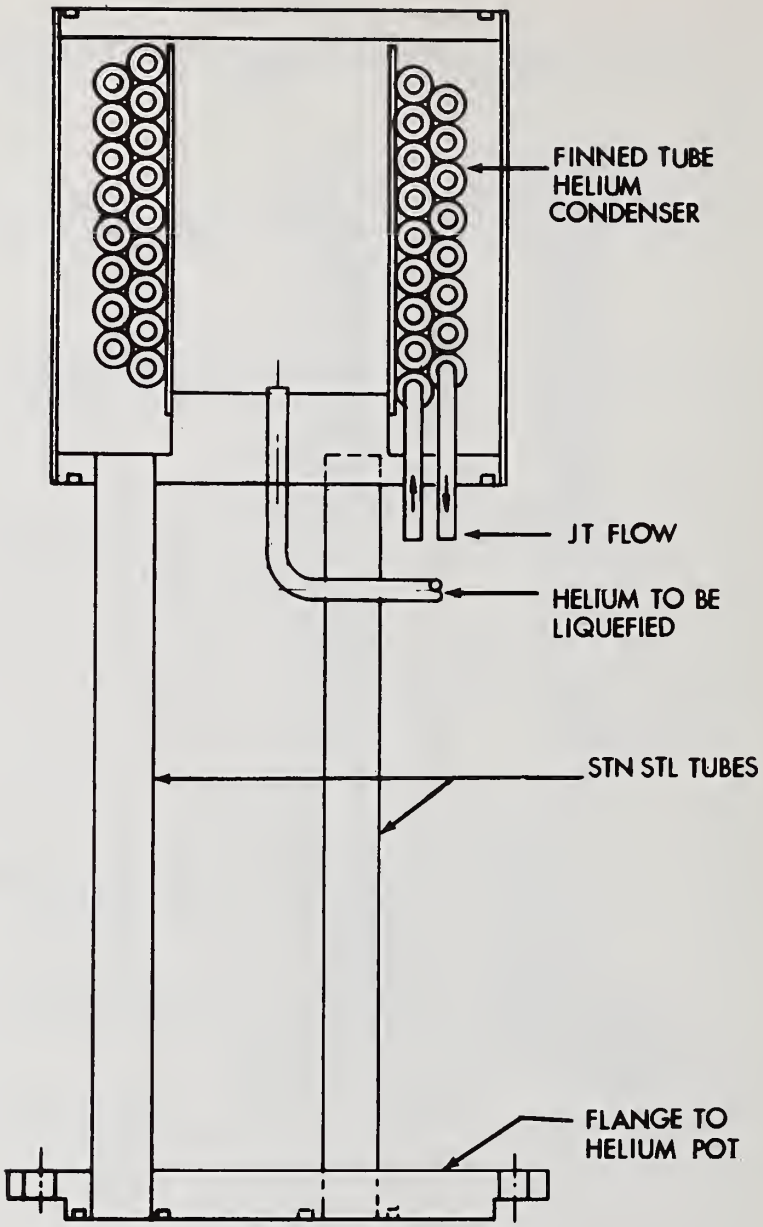

Figure 6. Helium Condenser.

6. Service

When one reviews failures in small closed-cycle coolers, it is seen that there are very few cases of leaks developing in the vacuum chamber if all the joints are properly made and carefully leak checked. It is thus sufficient to leave the piping in place and not break vacuum if a) the expander can be disassembled for service and, b) if the JT loop can be warmed and purged or possibly flushed.

Servicing a cold expander in less than an hour has been demonstrated. This was done in the following sequence:

a) disconnect gas lines to the expander and let gas out

b) remove valve motor (the displacer stays in place)

c) screw a special tool with purge gas flowing through it into the top of the displacer

d) with purge gas flowing pull the displacer into a sealed plastic bag

e) warm displacer and service it while keeping a cover on the cylinder with a small purge flow of helium

f) reassemble the expander in the reverse order

g) evacuate and purge the expander several times before reconnecting the gas lines.

The most common source of trouble with the JT loop is blockage due to freeze-out of contaminants. Servicing of the JT loop thus usually consists of warming it to room temperature and purging or flushing out contaminants. This is done in the following sequence:

a) Disconnect the gas couplings to isolate the JT loop.

b) Warm the heat exchangers with a back flow of gas through the low pressure side of the heat exchangers, venting out through the bypass line.

c) Simultaneously warm the refrigerator and adsorbers by turning on the heaters.

d) Warm the tops of the thermal couplings and helium condenser by flowing purge gas in through the bypass line and out through the high pressure lines. Adjust the heaters on adsorber 3 and the refrigerator while doing this to keep the heat exchangers at room temperature.

e) Reconnect gas lines after warmup and purging is complete.

Liquid helium boiloff is minimized by keeping the tops of the thermal couplings cold as long as possible - thus the refrigerator, heat exchangers, and adsorbers are warmed up first. Since the tops of the thermal couplings are relatively light they can be warmed fairly quickly.

When this procedure was first tried on the unit with 1.4 L of liquid in the test pot, it took a long time to adjust the helium purge flow rate and set the heaters. The total time from shutdown to return to 4.2K took 10 hours. Five hours were spent warming the refrigerator to room temperature. With the refrigerator warm and the thermal couplings cold, the boil-off rate was 0.13 liquid L/hr. The next 2.1 hours were spent warming the tops of the thermal couplings and cold adsorber during which time the boil-off rate increased to 0.24 liquid L/hr. Three hours were then required to cool back down to 4.2K.

Helium stopped venting and started to be drawn into the feed line about 15 minutes before the system reached 4.2K indicating that the entire warmup and purge consumed slightly more than 1.4 L of liquid helium. The unit then recondensed helium at a rate in excess of 0.3 L/hr.

The warmup and purge period can be reduced from 7 hours to about 2.5 hours with some small changes in instrumentation and practice.

7. Summary

Many thousands of small cryogenic refrigerators that operate at about 10K on the Gifford McMahon and modified Solvay cycles are in use today. The most common small 4K (systems) in use today use these 10K refrigerators as a base to achieve 4K by adding a JT loop. While it essentially doubles the complexity of the refrigerator, it is still possibl to achieve very high reliability, as described by Higa [3], if care is taken in the construction, operation, and maintenance of the units.

The refrigerator described in this paper extends the applications for this type of refrigerator to cooling small superconducting devices such as Josephson technology data processors, which in addition to high reliability, require an ability to service the refrigerator while the superconducting device continues to operate. This has been accomplished by means of thermal convective couplings which passively disconnect the refrigerato from a helium dewar when the refrigerator shuts down and permit the refrigerator circuit to be warmed and purged.

Warmup, purging, and cooldown back to 4.2K has been demonstrated with a total loss of about 1.4 L of liquid helium.

References

[1] van der Hoeven, B. J. C. Jr., and Anacker, W. "Refrigerator Requirements for Potential Josephson Data Processing Systems", NBS Special Publication 508, p. 213, April 1978.

[2] Longsworth, R. C., "Concepts for Cooling Small Superconducting Devices Using Closed-Cycle Regenerative Refrigerators", NBS Special Publication 508, p. 45, April 1978.

[3] Higa, W. H. and Wiebe, E., "One Million Hours at 4.5 Kelvin", NBS Special Publication 508, p. 99, April 1978.

PERFORMANCE OF A 1 watt 4K CRYOSYSTEM SUITABLE FOR A SUPERCONDUCTING COMPUTER

E. B. Flint, L. C. Jenkins, R. W. Guernsey

IBM Thomas J. Watson Research Center
Yorktown Heights, New York 10598

Superconducting computers of the future will require closed cycle refrigeration systems capable of removing 0.5-10 watts at 4K. The refrigerators must be reliable and the interface to the cryostat must allow continued computer operation during refrigerator shutdown. Such a system has been designed by R. Longsworth and one unit has been built by Air Products. This cryocooler is being operated now in a test configuration that allows detailed study and analysis of the design. The results of these studies, including cool-down times, refrigeration capacity, and interface performance will be discussed and compared with the design calculations.

Key words: Convective heat transfer; cryocooler; heat transfer by evaporating and condensing helium; helium refrigerator; superconducting computer; thermal couplings; thermal isolation.

1. Introduction

1.1 Desired cryosystem characteristics

In the future, one may be able to buy an extremely high-speed computer whose logic and memory chips operate at 4.2K. This might be packaged in a cube 9 cm on a side and would be immersed in liquid helium where it would dissipate about 10W of heat [1]. At this time, it is of interest to evaluate cryosystems that might be appropriate for such a machine. A general view of the requirements, as anticipated at this time, is given elsewhere in these proceedings.

Medium to large size superconducting computers are likely to need from 0.5W to 10W of refrigeration at 4.2K. The cryosystem should provide continued computer operation in the case of refrigerator shut down, and it also should allow one to service the computer without disturbing the refrigerator. A semi-annual service interval and a mean time between failure in excess of two years would be desirable. High reliability and fool proof service procedures are paramount. This paper documents the performance of a refrigerator and thermal interface designed to support a 1W, medium sized superconducting computer.

1.2 The interface concept

A study was done by R. Longsworth of Air Products, in which he developed a design for a complete cryogenic system using existing refrigeration technology which meets the requirements of a superconducting computer. The design he developed uses the Air Products CS-308, 4K refrigerator to which was added a thermal interface which couples the dewar and bath to the refrigerator. A schematic of the system is shown in Fig. 1. The interface provides good thermal coupling between the refrigerator and the dewar structure and processor during normal operation and good isolation when the refrigerator is warm for servicing. A companion paper by R. Longsworth [2] describes the design in some detail. Following the study, Air Products [3] built the system in a test configuration that now is undergoing extensive tests at IBM. While this work is far from complete (for example, there are few reliability data) there are data characterizing the refrigerator capacity and interface performance. In this paper we

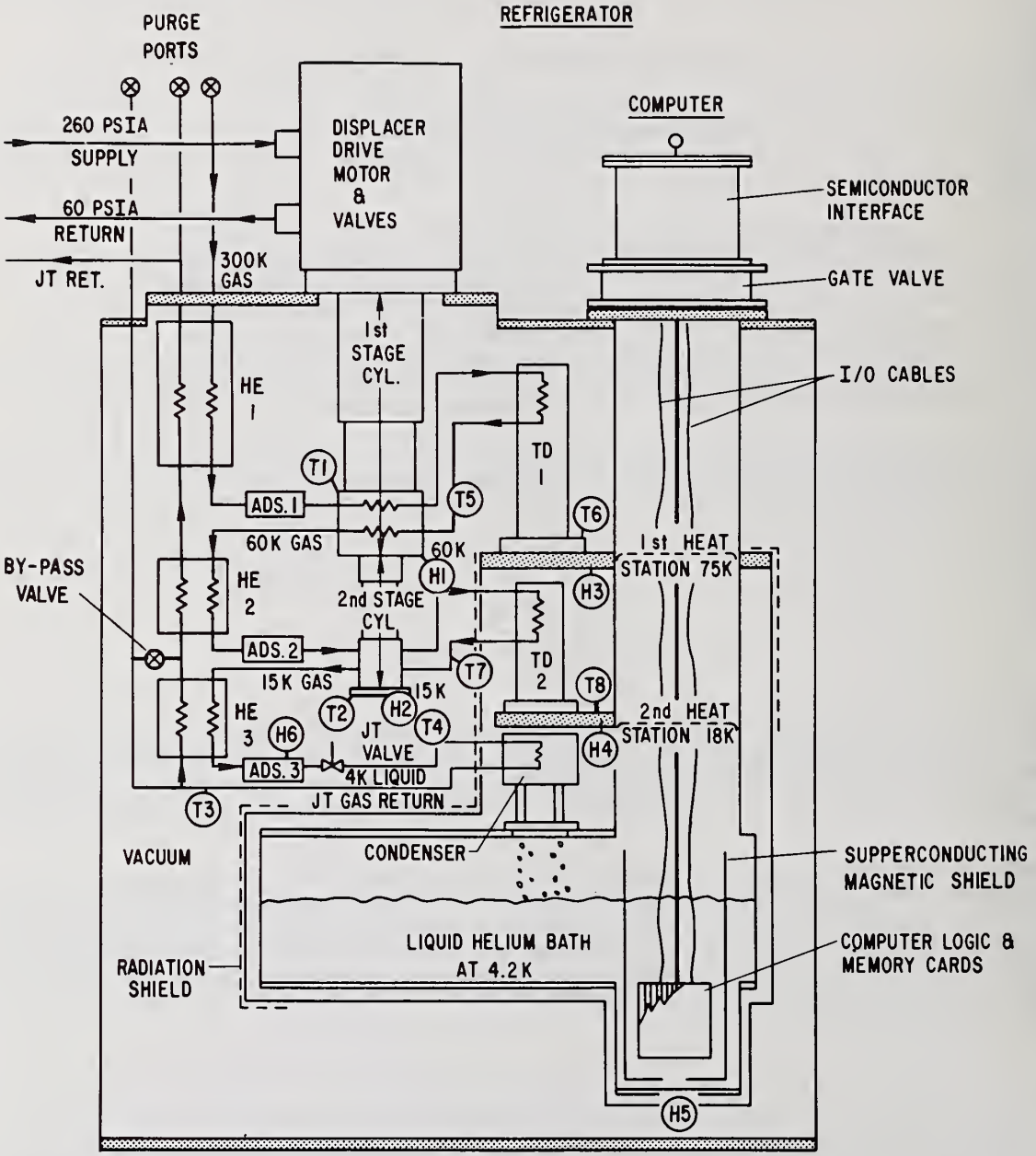

Figure 1: Shown is a schematic representation of a superconducting computer cryosystem with a large liquid helium reservoir for thermal ballast. The cryosystem under test has a 1.4 liter pot and includes thermometers T1-T8 and heaters H1-H6.

describe the cryogenic system and instrumentation used in the experiments, the performance data, and the areas where we believe the data indicate more work, both documentation and engineering, is required.

2. Description of the cryogenic system

In this section we describe the system including the refrigerator, the thermal interface, and the instrumentation used in the experiments. Figure 1 shows the refrigerator and interface with a dewar which might be suitable for a processor. The large liquid helium bath provides thermal ballast during periods when the refrigerator is shut down. In the test configuration a 1.4 liter helium pot replaces the bath shown.

The 4K refrigerator includes the 2 stage expander which provides refrigeration at 60K and 15K and a Joule-Thompson (JT) loop which produces the refrigeration at 4K. There is a by-pass line around the low pressure side of the third JT heat exchanger which is used for the cool-down from room temperature. The JT valve can be adjusted from the top of the cryostat so as to compensate for different load conditions.

The thermal interface consists of two gas thermal diodes and a condenser. The refrigeration available at the first and second expanders is delivered to the tops of the diodes via the JT gas stream. The diodes conduct by gas convection from bottom to top. When the temperature gradient is reversed the gas stratifies, providing relatively good thermal isolation. The condenser is similar to the diodes except that it is a two phase device. In normal operation (top cold) the boil-off gas from the bath is condensed on fins cooled by the JT stream and then runs back into the bath. Thermal isolation is, once again, provided when the top is warm because the helium gas in the support tubes stratifies.

The system performance has been studied using instrumentation which includes thermometers and heaters at each of the refrigerator stages. At the first and second stages silicon diode thermometers (numbers: T1, T2, T5, T6, T7, T8) are used to monitor the refrigerator temperature, the heat station temperature at the base of the thermal diode and the temperature of JT gas as it returns from the diode. The thermometer, T2, was calibrated between 4K and 100K. All other silicon diode thermometers have four point calibrations (4.2K, 20.4K, 77.4K and 273.2K) which were used to scale the T2 temperature vs. voltage curve to obtain temperatures from the measured voltages. The relative accuracy of the thermometers is probably less than 1K at 70K and less than 0.1K at 20K. Thermometers T3 and T4 are calibrated germanium resistance thermometers located inside the JT stream. The manufacturer quoted accuracy of these thermometers is 0.005K. The temperature of the bath was measured by monitoring the vapor pressure and using the 1958 helium temperature scale.

There are six heaters (H1 $\lesssim$ 60 watts, all others $\lesssim$ 20 watts) which were used to simulate heat loads and to warm the refrigerator for purging the JT loop and servicing the refrigerator.

3. Refrigerator performance

3.1 Capacity

The refrigerator was delivered with the thermal interface, test pot, and instrumentation in place. In order to determine the total cooling capacity at each stage, one must know the parasitic heat loads that result from these structures. We begin with a discussion of the methods used to measure these. At the first and second stages heat leaks are intercepted at the refrigerator stage and the coupling station. Those for the two couplings were determined from the temperature increase in the JT gas stream and the JT flow rate, and these values were confirmed by calculations of heat leak from the support structures and from radiation. An additional check was made by extrapolating the heat transport characteristic, $\dot{Q}(\Delta T)$, to $\Delta T = 0$ for the couplings. $\dot{Q}$ is the heat transported across the coupling and ΔT is the temperature difference between the JT gas (either entering or leaving the coupling) and base of the coupling. In the case of the first stage data, the parasitic loads are sufficiently large and the $\dot{Q}(\Delta T)$ characteristic sufficiently non-linear that it is possible to conclude only that there were no inconsistencies in the data. For the second stage coupling the loads (parasitic and applied) are smaller and the three determinations of the parasitic load were in reasonable agreement.

The parasitic load to the JT stream from the test pot was measured by noting the boil-off rate with the JT and the pot thermally decoupled. The result is in reasonable agreement with the calculated value. The parasitic load to the pot as indicated by the $\dot{Q}(\Delta T)$ characteristic for the condenser extrapolated to $\Delta T = 0$ was substantially higher and the difference is not understood. Offsets of $\sim$ 0.035K and $\sim$ 0.008K in the JT thermometers up and down stream of the condenser relative to the bath temperature would be required to explain the discrepancy. The parasitic loads at the three refrigerator stations are given in Table 1.

A complete map of the refrigeration capacity has not yet been made. The capacity at 4K, however, has been measured with the first and second stages loaded as they would be in an actual computer cryostat. Table 1 shows the results of these tests. With 9.9 watts applied to the first stage (22W total) and 0.5 watts to the second stage (1W total) the minimum temperature in the pot was determined with applied loads of 1.0W and 1.5W to the bath. At 1.03W total dissipation in the bath the minimum temperature, T_{min} was 3.82K and at 1.53W total dissipation T_{min} was 4.24K. A summary of data is given in Table 1.

The refrigeration at 4.2K is 25% less than anticipated but the refrigeration at the other stages is near the design values.

Table 1

Station	Parasitic Load (W)		Applied Heat Load	Total Heat Load (W)	Stage Temp.	Temperatures at Couplings and Pot
	Refrig-erator[1]	Coupl.[2]				
1st	5.5	6.5	9.9	21.9	59	86K (est)
2nd	0.2	0.24	0.5	0.94	14	15.5 (est)
JT	0	0.03	1.0	1.03	3.77 (est)[3]	3.82 (.57 atm at compressor)
1st	5.5	6.5	9.9	21.9	57	84K (est)
2nd	0.2	0.24	0.5	0.94	16.3	17.8 (est)
JT	0	0.03	1.5	1.53	4.18 (est)	4.24 (0.92 atm at compressor)

Notes:
1) heat load in this column are calculated;
2) heat loads in this column are measured and checked with calculation;
3) est. = estimated temperature. Temperature is determined from one measured temperature and the coupling heat transfer characteristic.

3.2 Reliability

It is important that a superconducting computer cryosystem be highly reliable and a maintenance interval of 6 months or longer is desired. Reliability studies will become a major part of our test program. When the refrigerator was delivered the compressor had run 1375 hours, and it has run an additional 1685 hours at IBM, bringing the total operation time to 3060 hours. Although this is only one third the scheduled maintenance interval, the refrigerator has been shut down and warmed to room temperature several times to correct problems, primarily with the instrumentation. Once the initial debug and performance mapping is completed, long term reliability testing will begin.

4. Interface performance

The thermal interface between the refrigerator and dewar is a key element of the cryosystem. It must deliver the refrigeration efficiently in normal operation and provide good thermal isolation during periods when the refrigerator is warm for servicing. It also must provide for liquefaction of make-up helium. The thermal contact provided during cool-down from room temperature must be good so that the cooling time required is reasonable. In this section we present the test results for the thermal interface system and the JT temperature regulator.

4.1 Thermal coupling heat transfer characteristics

The heat transfer characteristic, $\dot{Q}(\Delta T)$, for the first and second stage thermal diodes was measured by heating the base of the diode while monitoring the temperatures of the ingoing and outgoing JT gas and the diode base. For the second stage diode, thermometers T2, T7 and T8 were used to measure the temperatures. The results are shown in Fig. 2 where the heat transported through the diode is plotted as a function of the temperature drop across the diode. The circled points are taken from R. Longsworth's design calculations and their locations below the measured curves indicate that the diode performs somewhat better than anticipated. The two sets of data for this diode were fit to a straight line which gave slopes (diode conductance) of 0.81 W/K and 1.85 W/K and intercepts of -0.24W and -0.31W. The intercepts should be the parasitic load and in fact are in approximate agreement with the calculated value and also with that determined from the measured enthalpy increase in the JT gas.

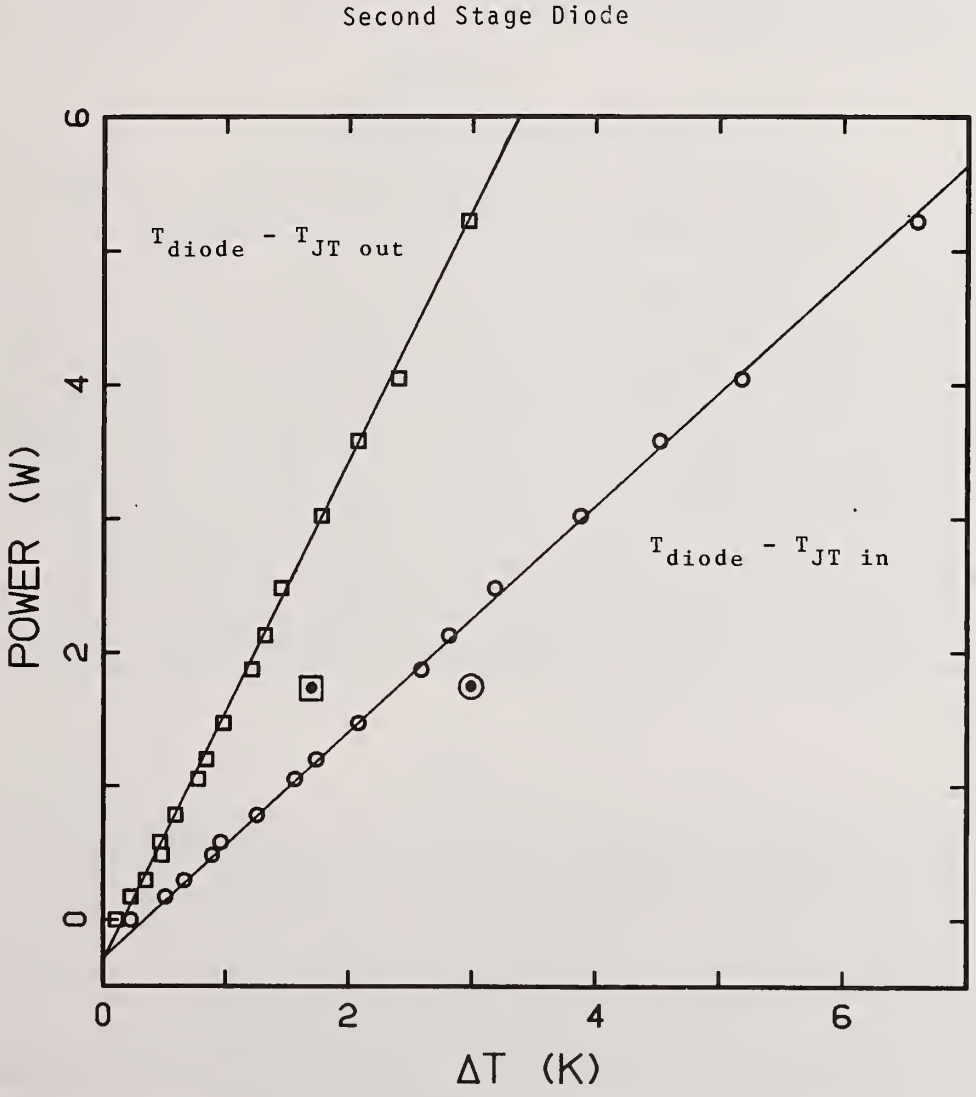

Figure 2: Heat transfer characteristic for the second stage diode.

Similar measurements and analysis were made for the first stage diode. There is some doubt as to the absolute accuracy of T6 which measures the diode temperature but it can be used to measure the temperature changes at the base of the diode. It therefore was not possible to obtaln parasitic losses from these data. In addition, the heat transfer characteristic for this diode is non-linear which makes the analysis more difficult. The slopes obtained from fitting the data through $\dot{Q}$ = 15W total load to a straight line give a measure of the diode's effective thermal conductivity. For $\Delta T = T_{diode} - T_{JT\ in}$ the conductivity obtained is 0.69 W/K and for $\Delta T = T_{diode} - T_{JT\ out}$ the conductivity is 1.11 W/K. If instead one fits the same data to a second order polynomial to allow for the curvature, the corresponding effective conductivities for 15W through the diode are 0.75 W/K and 1.22 W/K. The numbers obtained fromR. Longsworth's design calculations are 0.75 W/K and 1.9 W/K. One can conclude that the coupling performs substantially as designed.

The helium condenser used to couple the bath to the JT stream was tested similarly at several bath temperatures between 3.6K and 4.5K. The results for a nominal bath temperature of 4.0K are shown in Fig. 3. The squares represent the temperature difference between the bath and the JT loop upstream of the condenser, and the circles give the difference between the bath and the JT loop downstream of the condenser. R. Longsworth has calculated a temperature drop of 0.158K for 2 watts through the condenser. This is equivalent to a thermal conductivity of 12.7 watts/K. The values obtained from fits of the data to a straight line typically give 18-26 W/K with no discernable dependence on the operation temperature in the range of $3.6K < T_{bath} < 4.5K$. The condenser is at least 50% more effective than anticipated.

4.2 System performance of the interface

The performance of the thermal interface in normal operation is shown in Table 1. The temperatures marked "estimated" have been determined from the heat transfer characteristic for the appropriate coupling. As the temperatures in the table indicate, the refrigeration is very effectively coupled to the heat stations and the bath.

A test of the thermal isolation provided by interface when the refrigerator is warm was conducted as follows. With the refrigerator in its normal operating mode the 1.4 liter test pot was filled. The refrigerator was then turned off and warmed to room temperature with the heaters on the two expander stages, the heater on the third adsorber, and a flow of 6 SL/M of helium gas through the low pressure side of the JT loop. The average boil-off during the 2.5 hours required to warm the refrigerator to room temperature was 0.055 liters/hr. At 2.15 hours 2.4 SL/M of the He gas flow in the JT was directed out the high pressure side. This warmed the tops of the two couplings and the condenser and increased the boil-off from the pot to 0.15 liter/hr. The refrigerator was restarted at the end of the purge, 3.15 hours after it had been shut down. The total helium loss during this period was 0.25 liters. After the refrigerator was started the boil-off increased to 0.24 liter/hr. It is likely that this increase indicates that the tops of the couplings had not been fully warmed to room temperature and a longer purge is required. Assuming normal operation 3 hours after the restart of the refrigerator, as demonstrated by Air Products, and a 0.20 liter/hr average boil-off during this time the total helium loss would be approximately 0.8-1.0 liters. Some adjustments in the purge procedure may make it possible to reduce the time and/or helium loss further. It is worthwhile to note that the 1 liter of liquid which is lost due to the cryogenic structures and the reverse heat leak of the thermal couplings is small compared to 8.4 liters which would be boiled by a 1 watt processor whose operation is maintained during this time.

4.3 Liquefaction

The liquid lost during a refrigerator shut down must be replaced by the liquefaction of He gas supplied from room temperature. This is done by admitting the gas to the condenser via a tube that is thermally sunk at the first and second stages of the refrigerator. The liquefaction rate has been measured with and without additional heat loads applied to the three refrigerator stations. With no applied loads (parasitic losses only) the liquefaction rate is 6.7 liter/day. With simultaneous loads of 10W, 0.56W, and 0.23W applied to the first and second stages of the refrigerator and the helium bath, respectively, the liquefaction rate dropped to 3.9 liter/day. Assuming ideal heat exchange at the first and second stages the 6.7 liter/day liquefaction rate represents a load of 11.8W, 2.3W, and 1.05W to the three stages of the refrigerator. The 1.05W load at 4.2K is roughly 50% less than the measured refrigeration capacity at this temperature and suggests that the heat exchange at the second stage is not complete. It may be possible to increase the liquefaction rate through better exchange at the first and second stages and/or thermally sinking the condensing line to the third JT heat exchanger. It is not essential, however, in this application that the liquefaction rate be optimized.

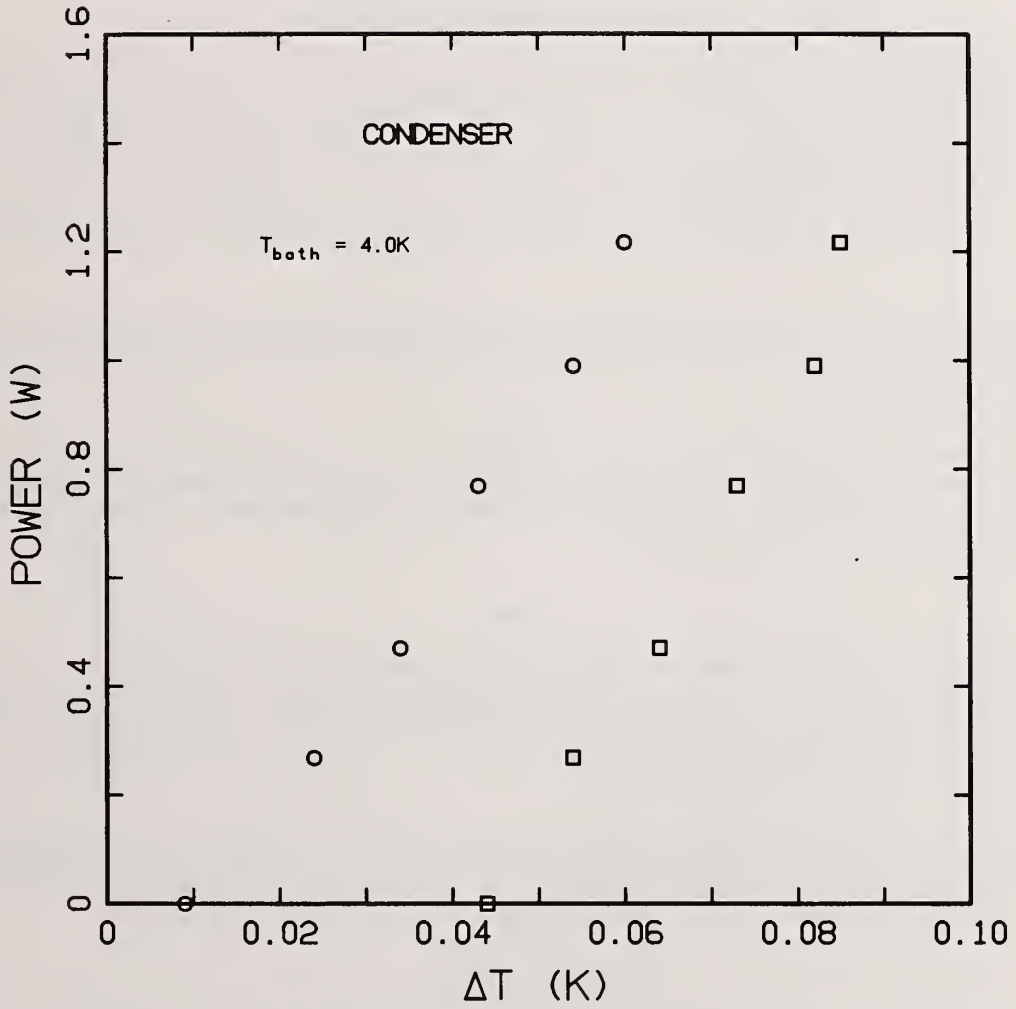

Figure 3: Heat transfer characteristic for the condenser. The squares are determined from the temperature difference between the bath and the JT temperature upstream of the condenser and the circles from the JT temperature downstream of the condenser.

4.4 Cool-down from room temperature

The time required to cool the helium test pot to 4.2K starting with the entire system at room temperature is approximately 10 hours. The first and second stages cool more quickly, nearing their operating temperatures in 3-4 hours. The difficulty is that the condenser is designed as a 2-phase device and provides only a very weak thermal link at higher temperatures. One could achieve a more rapid cool-down with the available refrigeration if, for example, a hydrogen gas thermal coupling were added betweeen the pot and the second stage. Another alternative would be to modify the condenser geometry to enhance gas convection. A model calculation, which assumes good contact between the He gas and the pot, indicates that such a modification could reduce the time required to cool the pot to 6 hours. The changes in the geometry of the condenser would not compromise its normal operation or the reverse heat leak. It is expected that the therml contact between the gas and pot would have to be improved with fins.

4.5 JT temperature regulator

A JT pressure/temperature regulator was supplied with the refrigerator. A sense pressure, referenced to vacuum, causes an increase or decrease in gas flow through the regulator from the expander return to the JT return which regulates the JT return pressure. In our tests the sense pressure was the saturated vapor pressure in the helium pot. Figure 4 shows the results of the tests. The horizontal axis is the heat applied to the liquid in the test pot and vertical axis shows the resulting temperature increase. The upper curve was taken with no regulation and represents the ability of the refrigerator to absorb the increased load. A linear fit gives a response characteristic of 0.039K/W. The lower curve gives a regulated response of 0.013K/W. This represents roughly a factor of 3 improvement.

There is a mechanical hysteresis in the regulator of about 20 mm Hg which corresponds to a temperature difference of 0.028K at 4.2K. In fact, it was necessary to tap the regulator continuously to obtain the data in the figure. Air Products had measured a substantially smaller hysteresis (8 mm Hg) prior to delivery. The cause of the hysteresis has yet to be studied.

The performance of the regulator has not yet been measured at lower bath temperatures. Since both the sense and the feedback response generated by the regulator depend on the slope of the saturated vapor pressure curve, $dP/dT|_{sat}$, the gain of the system may be essentially unchanged at lower temperatues. Mechanical hysteretic effects, however, are likely to be more pronounced.

Summary

Tests of an Air Products refrigerator and thermal interface designed to support a superconducting computer have given the following results. In normal operation the interface provides good thermal contact between the dewar structure and the bath with a minimal loss of refrigeration. The liquid bath can be maintained automatically between 4.20 and 4.22K for applied heat loads varying from 0 to 1.6W. The interface also automatically isolates the dewar and bath in the case of refrigerator shut down.

The procedure and/or instrumentation used to warm the refrigerator for servicing and purging should be improved to reduce the time and liquid lost. The time required to cool the system can be and should be reduced by the addition of a thermal switch between the second stage and the helium pot. This will require a change in the hardware. The long-term reliability of the compressor package and refrigerator has yet to be studied.

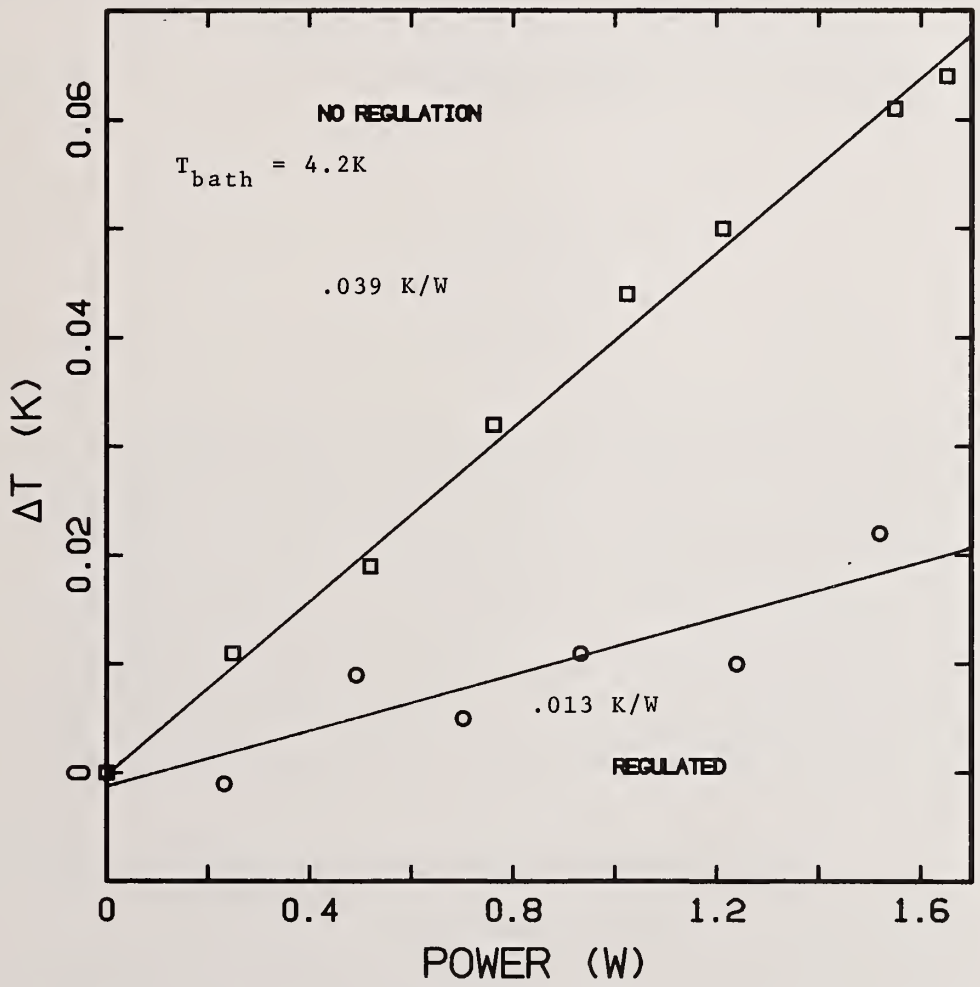

Figure 4: Increase in bath temperature, ΔT, as a function of the power applied to the bath with and without the JT regulator.

Acknowledgement

We would like to acknowledge the assistance given by J. Stasiak with the data acquisition.

References

[1] Anacker, W., et al., "Josephson Computer Technology," IBM J. Res. Dev., 24 [2], 107-264 (March 1980).

[2] Longsworth, R., "Serviceable Refrigerator System for a Small Superconducting Device," Proceedings of the Conference on Refrigeration for Cryogenic Sensors and Electronic Systems, NBS, Boulder, CO, Oct. 6 and 7, 1980.

[3] Air Products and Chemicals, Inc., APD Cryogenics, Allentown, PA, 18103.

DEVELOPMENTS TOWARD ACHIEVEMENT OF A 3-5 YEAR LIFETIME STIRLING CYCLE REFRIGERATOR FOR SPACE APPLICATIONS

Max G. Gasser
and
Allan Sherman

Cryogenics, Propulsion and Fluid Systems Branch
Space Technology Division
Goddard Space Flight Center
Greenbelt, Maryland 20771

and

William Beale

Sunpower, Inc.
Athens, Ohio

A major effort is underway at the NASA/Goddard Space Flight Center to develop a long lifetime Stirling cycle cryogenic cooler for spaceflight. The initial objective is a 3-5 year, 5 watts at 65°K, cooler to be followed by a 12°K cooler. The previous paper, "Progress on the Development of a 3-5 Year Lifetime Stirling Cycle Refrigerator for Space," presented at the 1979 Cryogenic Engineering Conference, outlined the approach [1]. During the past year, the design of a refrigerator with linear magnetic bearings has changed. The displacer rod no longer goes through the piston, resulting in a machine that is comprised of a compressor section and an expansion section bolted together. Each section has its own magnetic bearings, linear motor, displacement transducer (LVDT), and displacement volume. The phase angle and displacements of the two moving parts are electronically controlled, utilizing the signals from the LVDT's. Delivery of the engineering model magnetic bearing cooler is scheduled for March, 1981.

Work on the engineering model gas bearing cooler previously reported has ceased. However, an advanced concept for a gas bearing cooler is being studied.

Preliminary results indicate that the normal gas flow in a free displacer Stirling cycle cooler can be utilized to spin the displacer at a speed sufficient to form a self-acting hydrodynamic gas bearing with a clearance seal. The periodic gas flow from the cold end through the generator to the ambient end makes intermittent contact with a turbine located at the ambient end of the displacer. The induced spin is unidirectional.

Key words: Cryogenics; space application; long lifetime; Stirling cycle; linear magnetic suspension; clearance seals; hydrodynamic gas bearing.

1. Introduction

A wide variety of spacecraft instruments require cryogenic cooling to accomplish mission objectives. There are many cooler systems which have been developed or are being developed to satisfy these needs [2]. A particular critical area is the requirement for a system capable of providing high cooling-load (5-10 watts) for 3-5 year missions. A major effort is, therefore, underway to develop a long-lifetime Stirling cycle cryogenic cooler for spacecraft.

The basic problem is to develop a closed cycle machine with moving parts that will reliably run for billions of cycles while unattended. Past attempts to solve this problem have used liquid or semi-liquid lubricants, dry lubricants, and "hard-on-hard" bearings with little or no lubricants [3]. Various seal designs were also tried. To-date, these approaches have not yielded a long-lifetime spaceborne cooler system.

The new approach initiated by NASA/Goddard Space Flight Center hopefully eliminates the problem-causing features of the past. The key elements of the approach are: (1) The reciprocating components are driven directly with linear motors. (2) While operating, there is no contact between the moving components and the machine housing and motor. The noncontact operation can be achieved by either magnetic or gas bearings and clearance seals.

The magnetic approach is presently being developed into an engineering model cooler for test and evaluation. The fluidic approach is still in the technology phase.

2. Cooler Utilizing Magnetic Bearings

2.1 System description

Figure 1 is the schematic of the North American Philips single expansion cryogenic cooler with linear magnetic suspension. There are three subassemblies: (1) the compressor section, (2) the expansion section, and (3) the balancing device. The displacer rod does not go through the piston, and at no time do the piston and displacer occupy the same space. Each subassembly has its own linear motor, bearings, and displacement transducer. The phase angle can be changed by the input signals to the motor. The linear motions will be sinusoidal. The displacer and piston are free to rotate, but are not intended to do so. There are no springs on the displacer; it is driven in both directions. The piston operates with a gas spring. There are two pressure transducers (not shown in the figures): (1) to measure the static pressure, and (2) to measure the dynamic pressure cycles. Temperature transducers (not shown) are mounted on the exterior of the pressure shell at the cold end and the ambient areas. A small electric heater (not shown) is located at the cold end to simulate a load.

Figure 2 shows the compressor section at mid-stroke. The motor is the moving magnet type with the magnets and coils sealed in metal cans to prevent outgassing products from reaching the working fluid. The piston is hollow and vented to the motor housing. The close clearance (0.0025 cm) between the piston and its cylinder forms the noncontact seal with the piston centered in the cylinder by the magnetic bearings in the attraction mode.

The bearings are comprised of four nickel/iron poles acting on a vanadium Permendur shaft. Two eddy current sensors, positioned 90° apart around the circumference, measure the gap. The error signal from these sensors is then used to adjust the current in the magnets to prevent contact between the moving member and the cylinder wall. A redundant set of eddy current sensors is also incorporated in the design.

Figure 3 shows the expansion section at mid-stroke. The cold end has a heavy copper cap, which is connected to the ambient flange by a thin titanium tube for low thermal conductivity. The cold heat exchanger is the gap between the displacer and the copper cap. The cold end of the displacer is hollow and contains a vacuum. Regeneration is by the phosphorbronze screen matrix and also in the gap between the displacer and the cylinder. (Again, in the seal area, this gap is 0.0025 cm.) The ambient temperature flange supports a vacuum dewar (not shown) around the cold end. Starting at the cold end, the helium working fluid flows through a central passage in the displacer in the location of the magnetic bearing. This is the part of the displacer which constitutes the clearance seal. The working fluid flows outward through radial passages, over the linear motor, between the rear magnetic bearing, around the LVDT, and into the piston compression volume. The displacer motor is the moving magnet type with the coils and magnets sealed in metal cans. The displacer bearings operate in exactly the same way as that described for the piston.

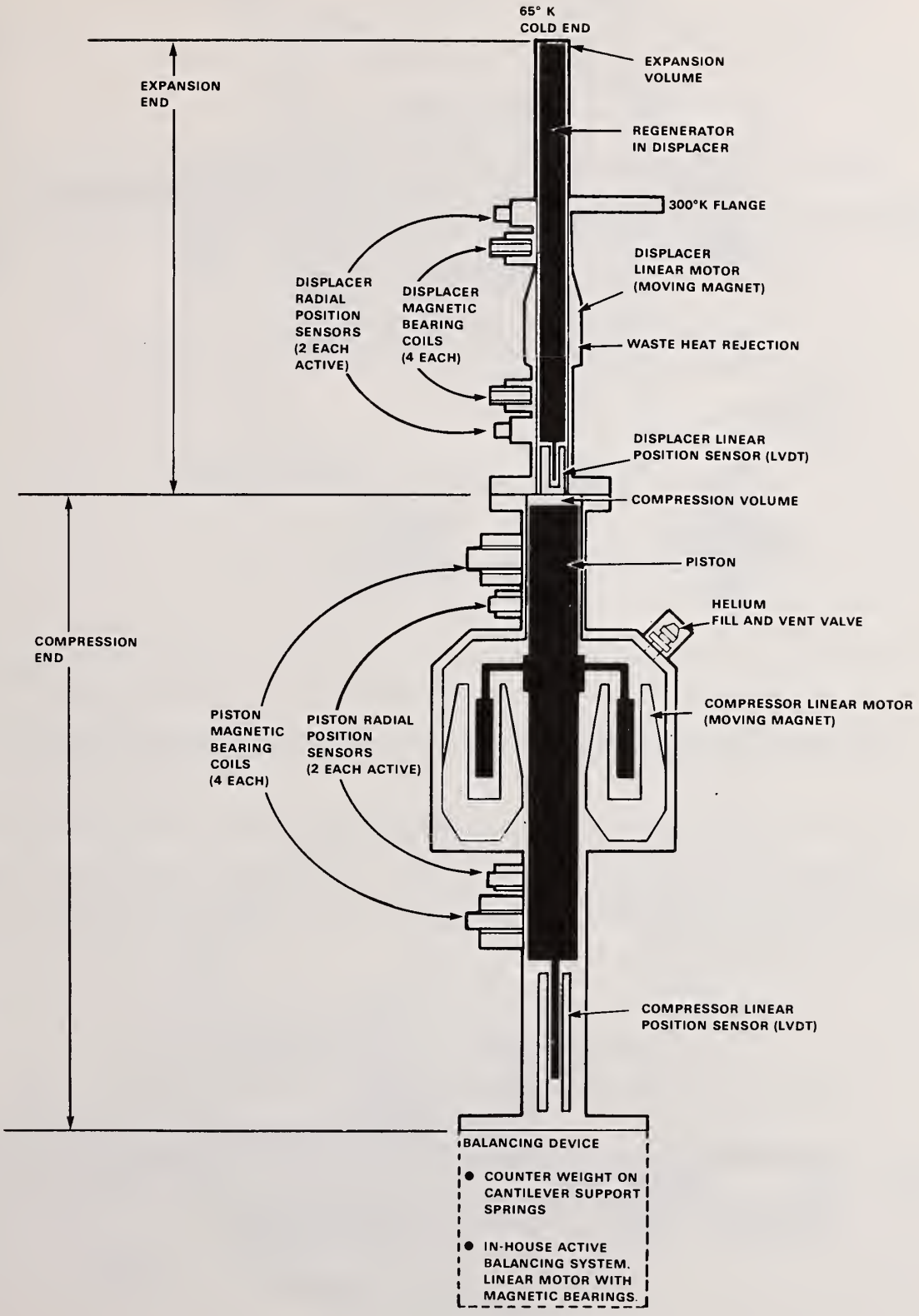

Figure 1. Schematic of the North American Philips single expansion cryogenic cooler with linear magnetic suspension.

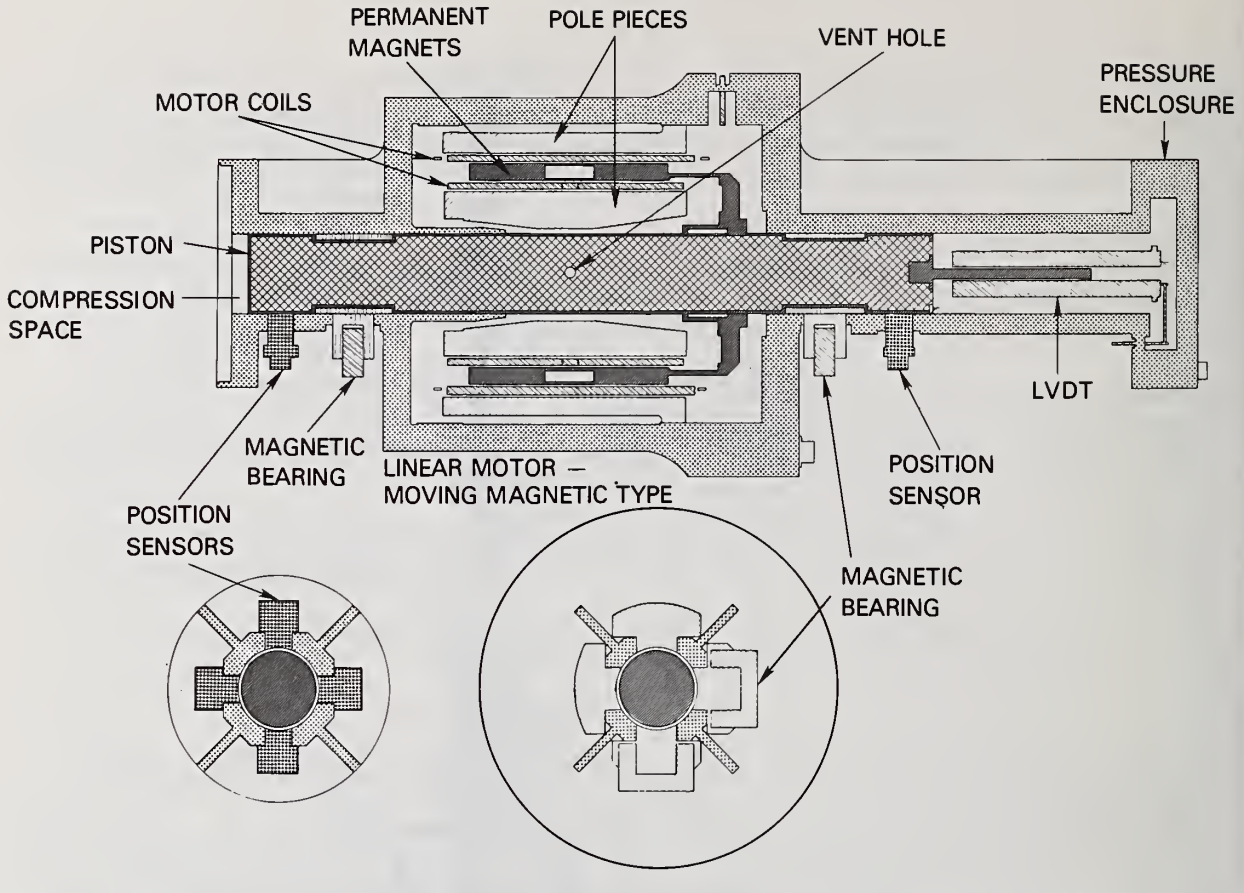

Figure 2. Philips Laboratories linear compression section of the Stirling cycle cooler shown in Figure 1.

All of the waste heat is removed by cooling jackets around the outside of both the piston and displacer housings.

Figures 4 and 5 show the passive counter-mass on cantilever support springs, which is one form of balancing device. The active balancing system, which utilizes accelerometers, a linear motor (moving iron type), and magnetic bearings, is described in reference [4]. The balancing device is bolted to the ambient end of the refrigerator. There is

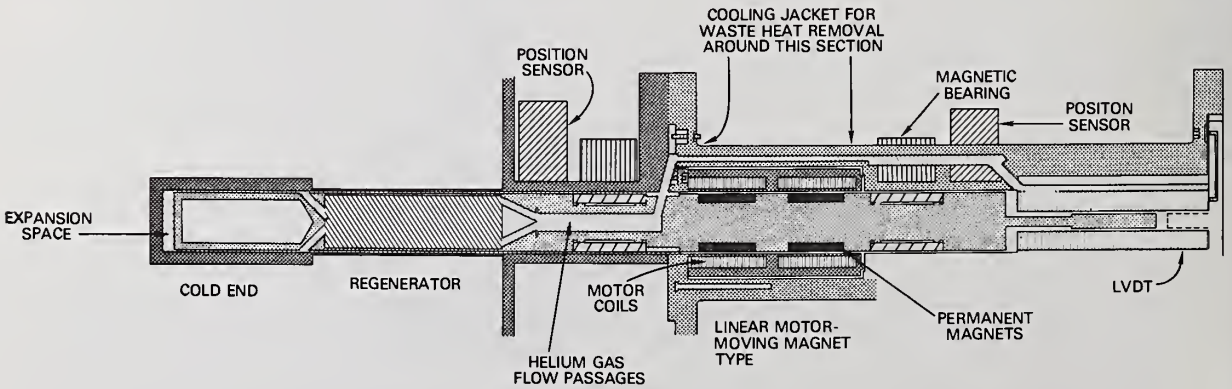

Figure 3. Philips Laboratories expansion section of the Stirling cycle cooler shown in Figure 1.

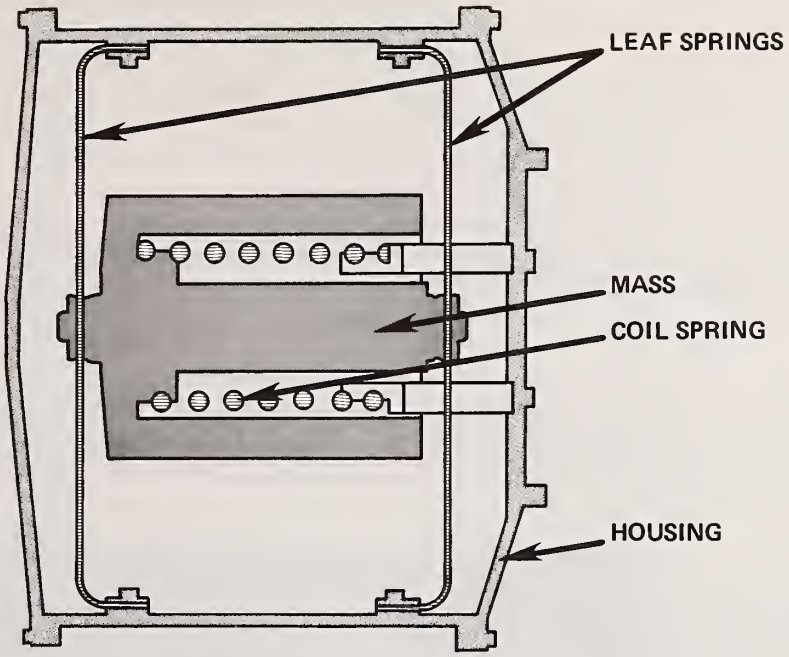

Figure 4. Cross-section of the counter-mass passive balance system for Figure 1.

no communication of the working fluid to the balancing device. The balancing could also be accomplished by two refrigerators back-to-back and operating in counter-phase.

The passive spring-mass system has been used on the Philips MC-80 (Einhoven) cryogenic refrigerator and is tuned to vibrate counter-phase to the piston.

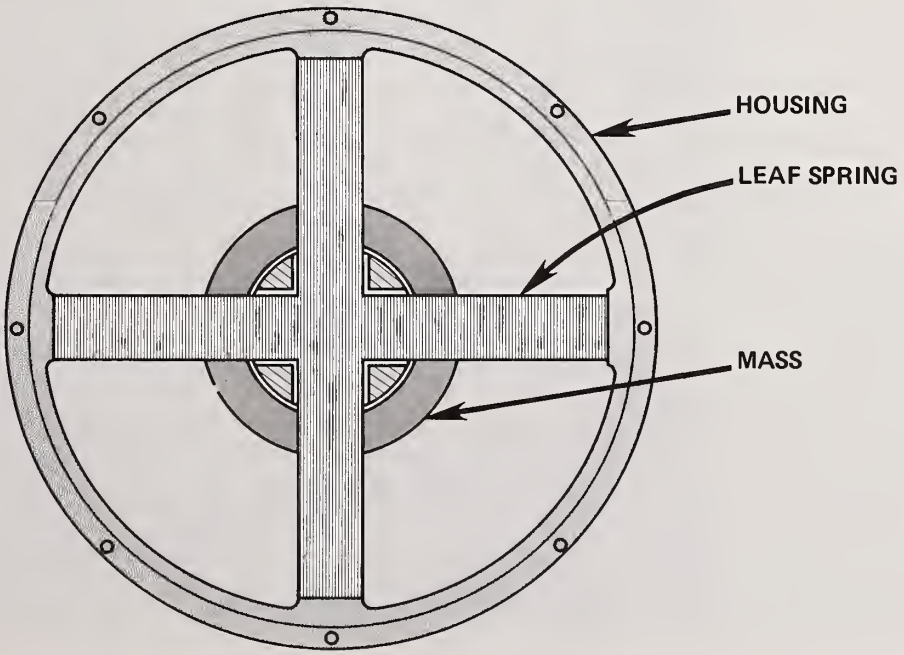

Figure 5. End view of the counter-mass passive balance system for Figure 1.

2.2 Performance characteristics

The refrigerator is designed to produce 5 watts of cooling at 65°K when operating at a resonant speed of 1700 strokes/minute. The helium charge pressure is 16 ATM. The refrigerator will be one meter long with the largest diameter about 20 cm. The expected lifetime is 3–5 years with either continuous operation or 1000 starts. Noncontact between moving and static components can be achieved for startup, steady operation, and shutdown because the bearings can be activated independent of the linear motors.

The piston and displacer can be locked in place for launch by (1) energizing adjacent magnetic coils or (2) using the motor to hold the moving part in one of its extreme positions or (3) a combination of the two.

2.3 Component testing

Figure 6 shows a test setup to verify magnetic suspension in a refrigerator configuration. A shaker with a linear DC motor was connected to the bearing shaft via an impedance head (an integrated accelerometer and force

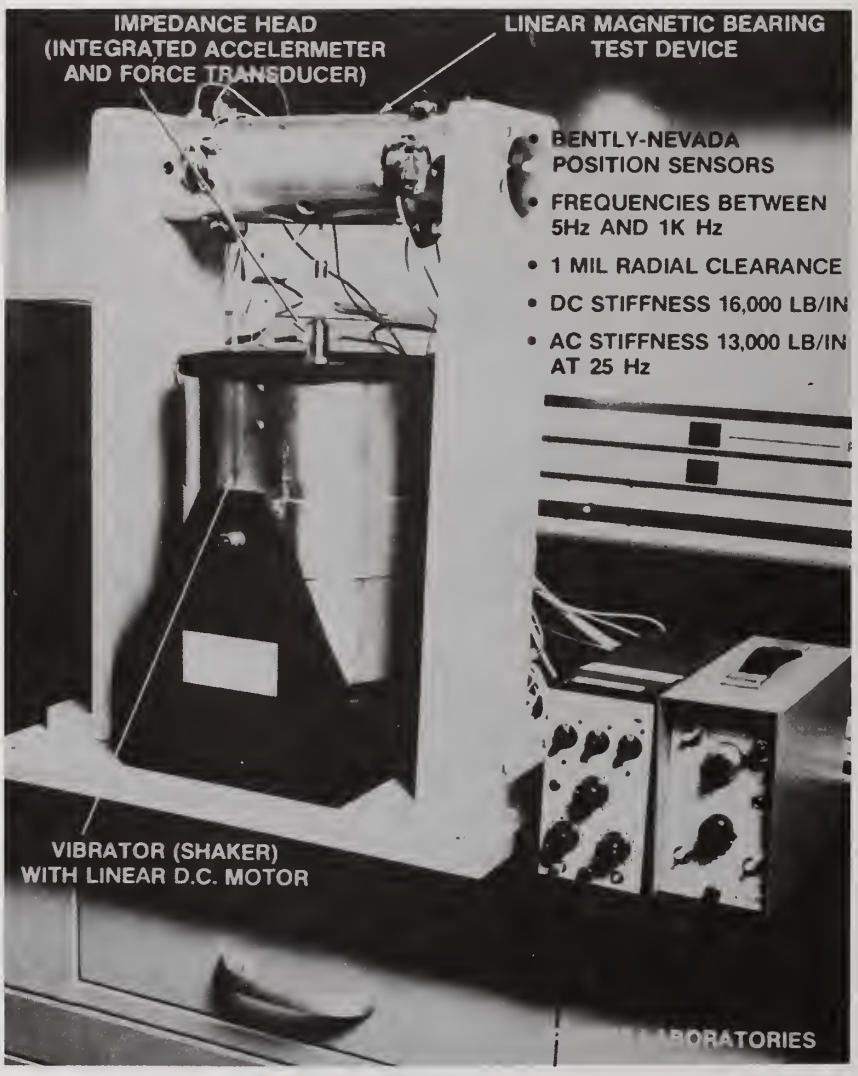

Figure 6. Test setup to verify magnetic suspension in a refrigerator configuration.

transducer). Two Bently-Nevada position sensors were mounted to measure the displacement of the shaft center-of-gravity and the shaker armature. An accelerometer was mounted to monitor the deflection of the bearing housing. The coil currents were observed with oscilloscope probes. Readings of the amplitude and phase of all quantities were taken with a gain/phase meter via a narrow band filter for frequencies between 5 Hz and 1 kHz. The shaker was set to produce a DC force to counteract the effects of gravity and oscillate about the center position since this is the minimum stiffness condition.

The preferred bearing configuration based on brazing tests and magnetic hysteresis measurements of ring samples is a combination of nickel/iron pole pieces and a vanadium Permendur armature with a 0.0025 cm radial clearance. Each side of the prototype of this configuration was found to have a DC stiffness of 16,000 lb/in. (28,000 Newtons/cm) and an AC stiffness at 25 Hz of 13,000 lb/in. (22,800 Newtons/cm).

Figure 7 shows the piston motor armature with the magnet segments mounted, but before enclosure in a metal can. The motor will be tested on a special test rig before assembly into the refrigerator.

For comparison purposes, Figure 8 shows parts of the displacer motor. No test is planned for it before assembly into the refrigerator.

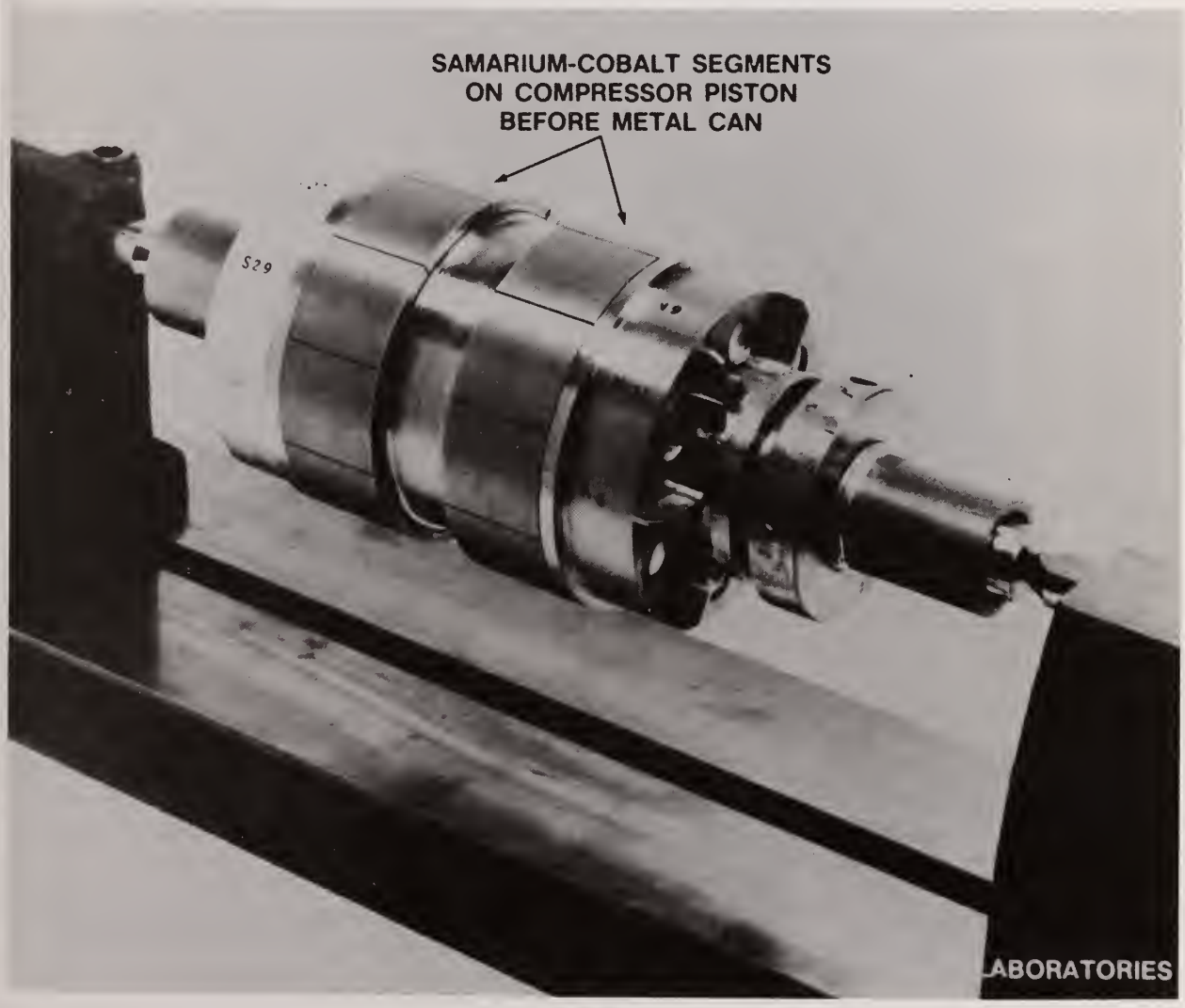

Figure 7. Piston motor armature under construction with magnetic segments mounted.

Figure 8. Displacer motor parts.

3. Self-Actuated, Spinning Gas Bearing Feasibility Study

Sunpower, Inc. made a study to determine the feasibility of spinning the displacer of a Stirling cycle cryogenic cooler by the interaction of the gas flow with a turbine mounted on the displacer. The turbine encounters the flow only at the outermost part of the displacer stroke, where gas flow is at its maximum rate, in such a way as to give a one-directional torque to the displacer.

The hydrodynamic bearing requirements for noncontact operation of the displacer could be met by such a turbine action, and the method indicates minimal penalty in flow losses. The bearing should be stable, and its fits and tolerance requirements should be well within manufacturing capability.

A design of a demonstration model has been made which is capable of showing hydrodynamic bearing operation, self-spinning and zero mechanical contact.

The concept of the turbine spun, hydrodynamic displacer system having a bearing and turbine design compatible with a single-stage Stirling cryocooler of 5 watt heat lifting capacity at 65°K is described in the following paragraphs.

3.1 Hydrodynamic bearing system concept

Figure 9 shows a turbine spun displacer and an electrically driven piston which may either be spun or supported by hydrostatic bearings or magnetic bearings. This is the concept which we would like to develop into a proof-of-principle device.

3.2 Proposed spin bearing demonstration model

Figure 10 shows the proposed proof-of-principle device.

The displacer has a mass of approximately 50 grams, and this can be sustained in a 1.5 g field with a slow speed gas bearing having a bearing gap of about 7 micrometers – a value typical of existing Sunpower seal clearances.

For purposes of turbine design, it would be desirable to spin the bearing more rapidly than the maximum stable 10 radians/second, but this, in theory at least, can lead to plain bearing instability (whirl) under low loading as would be in the case in space. The use of herringbone rather than plain bearing surfaces gives promise of elimination of whirl instability at low load and high speed.

The proposed design will be first tested with a plain bearing. If this proves unsatisfactory, a herringbone will be chemically etched on the plain bearing surface (the depth of the herringbone groove is only about 20 micrometers).

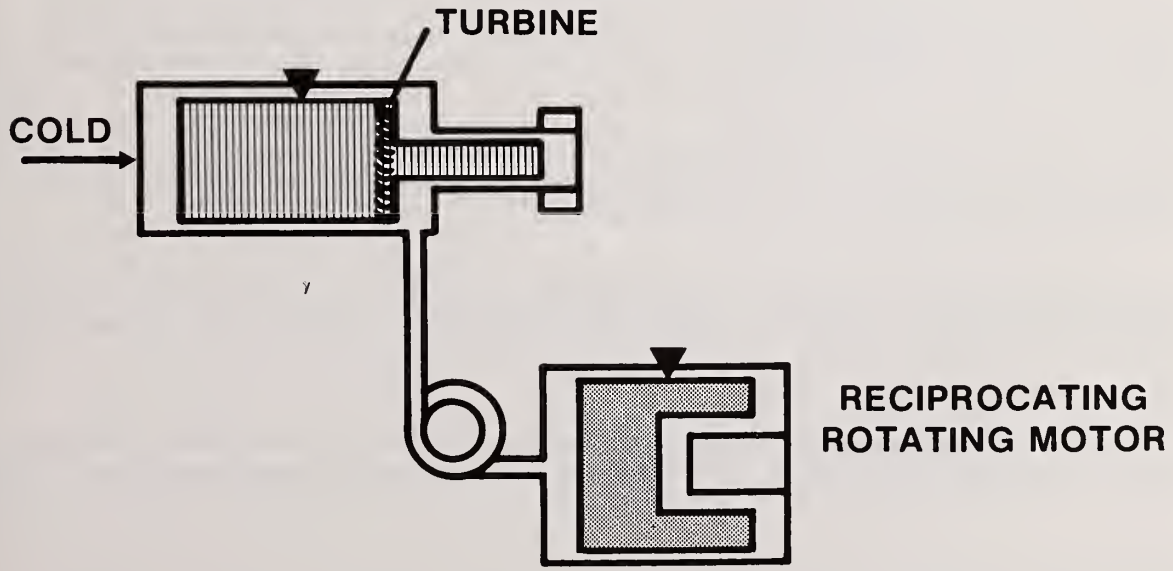

Figure 9. Sunpower, Inc. long life cooler concept.

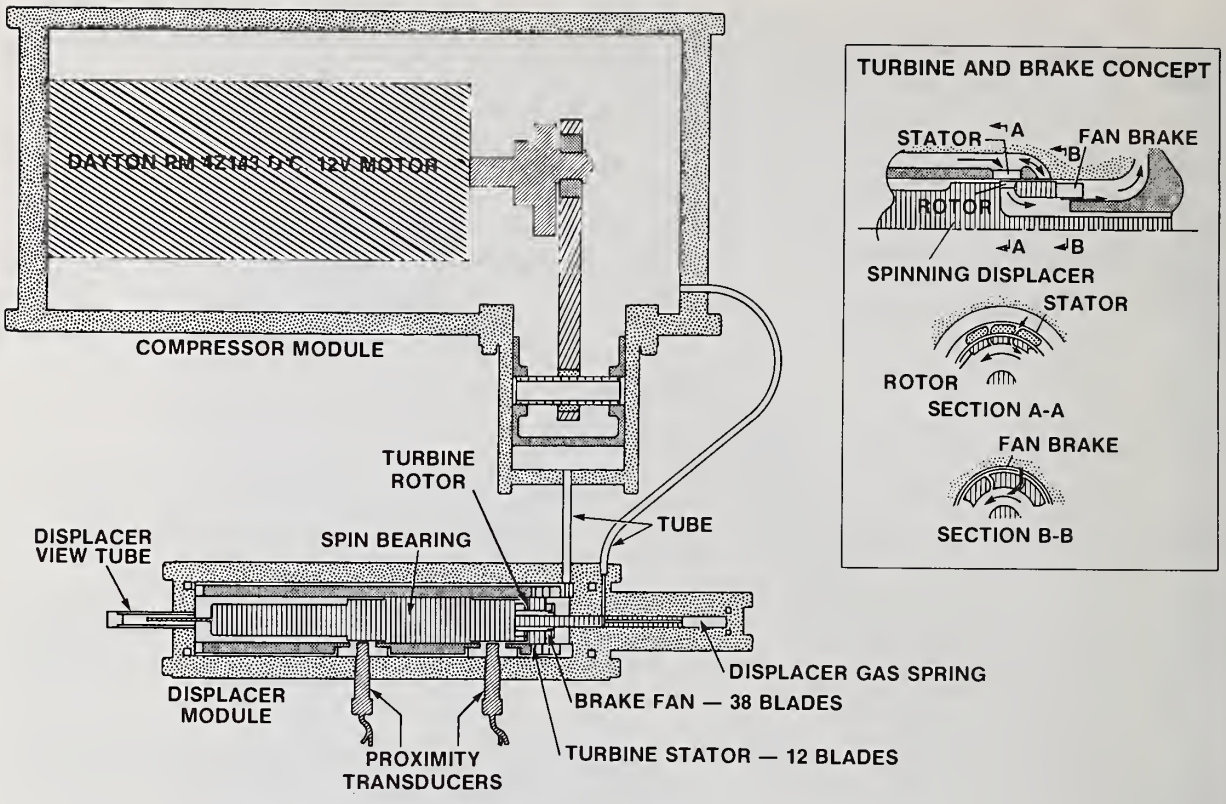

Figure 10. Sunpower, Inc. proposed spin bearing demonstration model.

3.2.1 Turbine design

The basic problem of the turbine spun bearing system is that while the spinning bearing requires very low torque to maintain its load carrying capacity, its static friction starting torque is many times greater, at least as indicated by elementary static friction estimates. The high starting torque requires a high tangential gas velocity impinging on the turbine, which would impose an excessively high running speed, possibly inducing large out of balance forces. But, this is by no means an intractable problem. Many solutions are possible of which the least complex might be a centrifugal brake (fan) on the displacer. However, one is reminded of the many occurrences in the past in which great effort was expended to solve on paper what in the lab was found to be a nonexistent problem. Just what the startup torque requirement is in a reciprocating spinning seal with a pressure difference across it is apparently not known, and it may be very much lower than the static friction torque.

The simplest approach is a plain bearing and a brute force turbine capable of overcoming full sliding friction and accelerating the bearing to a high speed. Combined with the strong turbine, a geometrically similar fan brake is included, which is intended to limit displacer angular velocity to one tenth of the theoretical velocity capability of the turbine. Both the turbine and brake were designed for ease of experimental variation, with the assumption that some modification would inevitably be required.

The turbine was designed such that it is energized only about 1/8 of the cycle time. Its loss is in the range of tenths of watts at most, and little effect on the thermodynamic performance of the cooler is expected.

3.2.2 Instrumentation

The purpose of the demonstration model is to show hydrodynamic lubrication without contact as the displacer cycles in a manner compatible with operational cryocooler performance. In order to show this, instrumentation must be provided which shows presence or absence of contact.

The system uses two proximity sensors at 90° separation in two separate planes perpendicular to the displacer axis. These show a circle on an oscilloscope within which a dot representing the center line of the displacer runs, with contact represented by the dot reaching the inner edge of the circle. This display would show not only contact, but also eccentricity and whirl, and would be very useful in diagnostics.

3.2.3 Characteristics of proposed designs

The characteristics of the demonstration model are as follows:

Operating pressure	13 bar (helium)
Frequency	25 Hz
Displacer diameter	20 mm
Bearing length	40 mm
Mass	75 grams (for demonstration purposes)
Rod diameter	5.3 mm
Stroke	8 mm
Rotation rate	300 radians/second (3500 RPM max)
Piston diameter	52 mm
Stroke	8 mm
Drive motor – Type	Dayton PM 42143, 12 volt
– Power	100 watts
– Speed	1750 RPM

The displacer is rotated by a turbine, which has gas flow for only 1/8 of the total stroke. During the remainder of the displacer motion, the turbine stators are short-circuited by the normal warm heat exchanger ports. Volumes are sized so that the mass flow through the ports is the same as would be present if the cryocooler temperature existed. This was done by enlarging the volume of the demonstration model cold end by the temperature ratio, so that it represents a larger mass flow source and sink, as does the cold end of the cryocooler.

The displacer has a fan brake which will initially be blocked. If experiment shows problems with overspeed, the dam will be progressively removed, and the brake brought into greater effectiveness until the desired displacer rotating speed is met. At full effectiveness, the brake is expected to limit rotating speed below 300 radians per second.

Materials are anodized aluminum and chrome-plated aluminum ground and honed to true roundness and straightness. These have given good service in past applications to small Stirling heat engines.

3.3 Sequence of operations of the spin mechanism

Figure 11 shows the sequence of operations which causes the displacer to spin as it reciprocates in the normal mode of the free displacer driven by fluidic forces.

The displacer motion leads the piston by 90°, that is to say, at a time when the displacer is at the midpoint of its motion, going out (to the right), the piston is at the innermost point of its motion, just starting its outward motion (out).

When the displacer is at its outermost point, where the turbine has come into register with the turbine stator, the piston is at its midpoint and moving with maximum velocity outward. At this point, the maximum flow rate of gas occurs from the cold expansion space, through the regenerator, through the stator and turbine blades (since the warm port is blocked by the displacer), and then through the connecting tube to the piston space.

It is useful to note that this maximum mass flow occurs at a point (about 190°) where the displacer is almost stopped, having just turned around and started in again. The flow occurs as a result of the influence of the motion of the piston, which is at its maximum rate. Cold gas in the expansion space moves through the regenerator, warming and expanding, then moving through the turbine toward the piston.

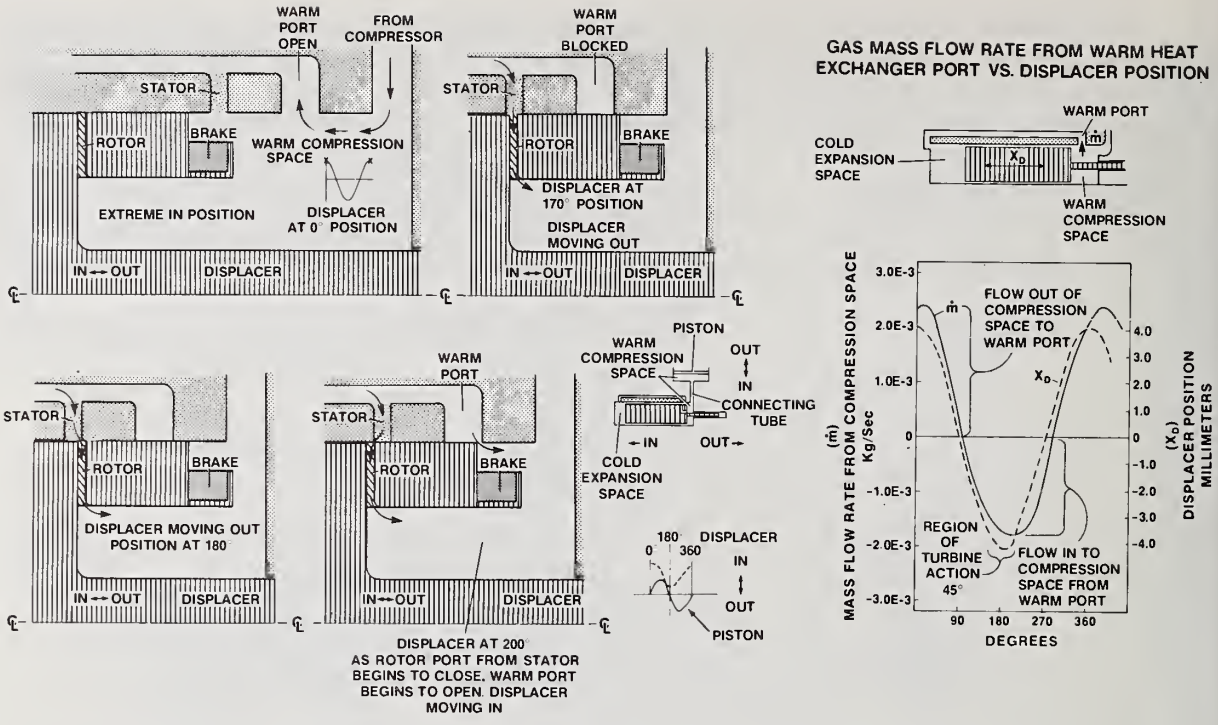

Figure 11. Sequence of operations of Sunpower, Inc. proposed spin bearing demonstration model.

The turbine is positioned so as to intercept this maximum flow of gas at a brief interval during the outermost point of its travel, thus imparting a spin to the displacer.

As the displacer moves back in again, it covers the stator, and once again uncovers the warm port so that normal flow through it can occur. Flow outward at its midpoint, and the piston has almost reached its outermost travel. As the component motions continue, the flow through the warm port reverses and now flows through the port toward the cold space, increasing in magnitude under the influence of the piston. The piston reaches its midpoint and maximum inward velocity at about the time the displacer reaches its innermost point and reverses its direction to come out again and repeat the cycle.

During the entire cycle, the displacer is spinning, even though it receives a spin impulse only during the 45° of its travel, and as it spins, it pumps gas through the brake after the manner of a squirrel cage fan. This brake is designed to limit maximum rotating speed to reasonable values fixed by bearing performance. The brake is only effective at high speed and has no retarding effect on the displacer during startup, when maximum turbine torque is applied to begin the spinning action.

4. Conclusion

The major effort in the Goddard program is to develop the magnetic bearing cooler. The self-actuated spin bearing approach is still in the study phase; however, initial analysis shows that the approach is promising.

5. References

[1] Sherman, A., Gasser M., Goldowsky, M., Benson, G. and McCormick, J., "Progress on the development of a 3-5 year lifetime Stirling cycle refrigerator for space," in Advances in Cryogenic Engineering, Volume 25.

[2] Sherman, A., "Cryogenic cooling for spacecraft sensors, instruments, and experiments," in Astronauts and Aeronautics, November 1978.

[3] Gasser, et al., "An approach to long-life Vm cryogenic refrigeration for space applications," Applications of Cryogenic Technology, Volume 4, 1971.

[4] Studer, P. and Gasser, M., "A bi-directional linear motor/generator with integral magnetic bearings for long lifetime Stirling cycle refrigerators," Topical Conference on refrigeration for cryogenic sensors and electronic systems, October 1980, at National Bureau of Standards.

THOR CRYOCOOLER

G. M. Benson, PhD and R. J. Vincent, PhD
ERG, Inc.
Oakland, CA 94608

A resonant, free-piston Stirling-cycle cryocooler driven by linear reciprocating synchronous electric motors and utilizing gas bearings and gas springs has been designed, and selected components tested. This hermetically-sealed, dynamically balanced design is based on ERG's previous work and has been engineered for long-life through use of: 1) non-contacting linear gas bearings and narrow clearance reciprocating seals, 2) brushless reciprocating electric motors with hermetically-sealed coil and core, 3) stationary external first-stage regenerator, and 4) solid-state controller. The design has been efficiency-optimized by 1) transferring heat nearly isothermally (to better approach Carnot efficiency), and 2) minimizing losses through use of advanced components of resonant free-pistons (which eliminate piston drive losses). The single-stage unit, designed to produce 10 watts at 65 K, may be expanded to three-stages, using a novel design, for producing 4.2 K. Designs and test results of selected components are described and compared with theoretical and computer modeled results.

Key words: Cryocooler; gas bearings; refrigeration; regenerator; resonant free piston; Stirling cycle.

A CRYOGENIC SYSTEM FOR THE SMALL INFRARED TELESCOPE FOR SPACELAB 2

E. W. Urban and L. Katz
Marshall Space Flight Center
Huntsville, Alabama

J. B. Hendricks and G. R. Karr
University of Alabama in Huntsville
Huntsville, Alabama

The cryogenic system for the small helium cooled infrared telescope for Spacelab 2 is described. The system consists of a 250 ℓ storage dewar containing superfluid helium at about 1.6K and a separate experiment cryostat. The liquid helium is confined within the dewar in zero-g by means of a porous plug. The cold vapor leaving the plug surface is split into two, not necessarily equal, flows. One flow path is through heat exchangers which cool the radiation shields of the storage dewar and, therefore, control the liquid storage efficiency. The second flow path is through a flexible joint to the independent set of heat exchangers for cooling the infrared optical apparatus and radiation shields in the cryostat. By means of commandable valves on the dewar and cryostat vent lines, the fraction of total helium boiloff used for cooling the dewar radiation shields can be controlled, and the cooling available at the cryostat can be adjusted from zero flow rate to nearly 50 mg/s of helium gas at 2K. A number of unusual cryogenic problems which have been solved in the development of this complex system are discussed.

Key words: Cryogenics, infrared telescope, Spacelab, superfluid helium.

1. Introduction

The Infrared Telescope (IRT) Experiment will first be flown on the Spacelab 2 mission in late 1983. It is a joint project of the Smithsonian Astrophysical Observatory (SAO), the University of Arizona (UA), and the NASA Marshall Space Flight Center (MSFC). Our responsibility at MSFC is the development of the cryogenic and mechanical systems of the IRT. The University of Alabama in Huntsville (UAH) is collaborating on the cryogenic design, fabrication of special cryogenic apparatus, and cryogenic performance testing. UA and SAO are responsible for the infrared instrument and data analysis. The NASA Ames Research Center is collaborating in the analysis of contamination and zodiacal light data. This paper describes the cryogenic apparatus, the status of assembly and testing, and a number of special cryogenic problems which we have faced during development.

2. Cryogenic System

The IRT experiment employs a very unusual cryogenic design which results from both the requirements of the infrared science and a desire to utilize commercial apparatus and fabrication technology wherever possible. Two views of a scale model of the IRT are shown in Figure 1, and a schematic of the cryogenic system is shown in Figure 2. A description of the mounting and operation of the 3.4m tall experiment in the Spacelab 2 payload was previously given [1] ,[2]. The two major cryogenic components, the dewar subsystem and the cryostat subsystem, are described below.

2.1 Dewar Subsystem

The dewar subsystem consists of two parts, a 250 liter liquid helium storage dewar and a transfer assembly (TA), which form a closely integrated thermal system. The result is essentially a single complex superfluid helium dewar with the liquid containment vessel at one end of a neck structure and a number of cold flow control components at the other; all are surrounded by a common thermal protection system, discussed below.

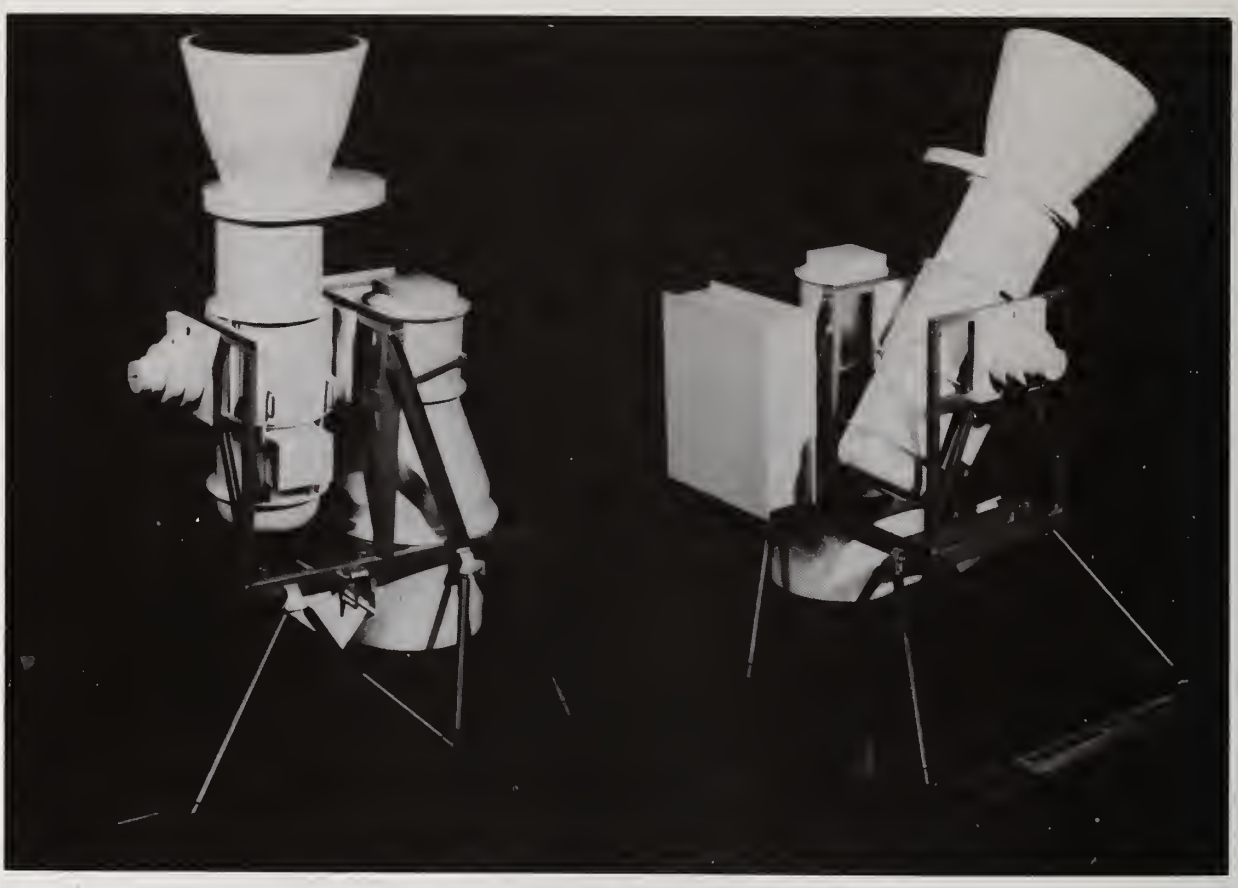

Figure 1. Two views of a scale model of the infrared telescope.

2.1.1 Dewar

In a conventional storage dewar of the type used to ship helium on the highways the liquid vessel is surrounded by a system of nested vapor cooled shields (VCS), separated by superinsulation and mounted within a high vacuum space. These shields serve to intercept heat being radiated and conducted in toward the cold liquid from the outer shell. The intercepted heat is then conducted up each shield to the dewar neck where it warms the venting helium gas. The dewar neck is a heat exchanger as well as the support for the liquid vessel. The source of the cold gas venting up the neck is the slow evaporation of the stored liquid by the unavoidable parasitic heat conducted down the neck tube and radiated in from the coldest VCS. A typical unmodified conventional 250 liter dewar achieves a steady state boiloff rate of 1% per day or 2.5 liters of liquid per day corresponding to a heat input to the liquid of 75 mW.

In order to utilize the basic features of a commerical storage dewar for the IRT, several modifications have been required as shown in Figure 3. To retain the stored LHe in the zero gravity of space, it is necessary to close off the dewar neck at the liquid vessel entrance. Liquid is filled and withdrawn through tubes which pass down the neck from the TA, and valving and flow control is accomplished by the cold components in the TA. These components are also insulated from the outside world by a VCS system, which is tied to the dewar shields within the neck tube. The TA and the interior of the dewar neck share a common vacuum independent of the dewar guard vacuum. Heat intercepted by the dewar shields is conducted up to the heat exchanger in the TA.

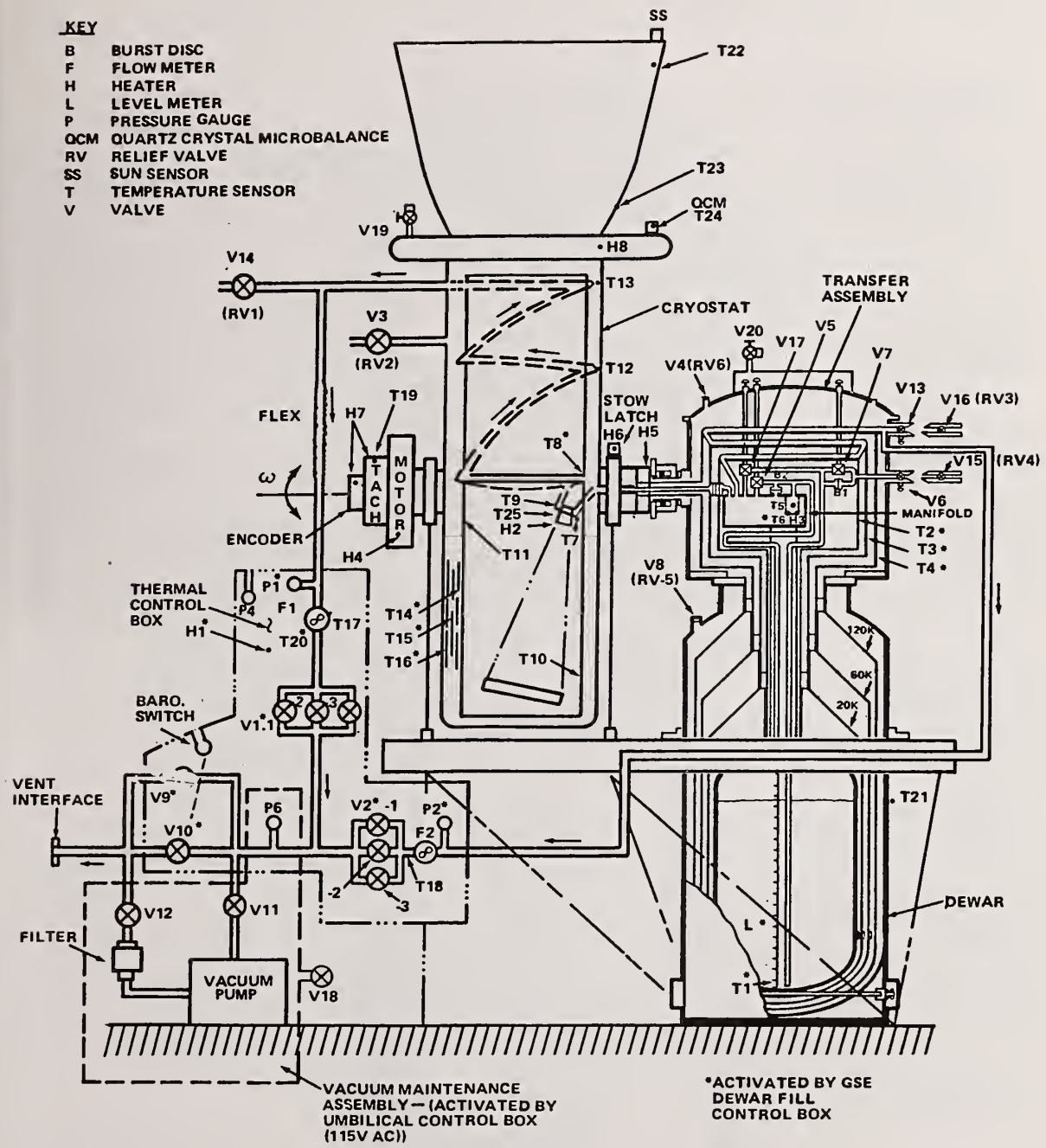

Figure 2. Schematic diagram of the infrared telescope system.

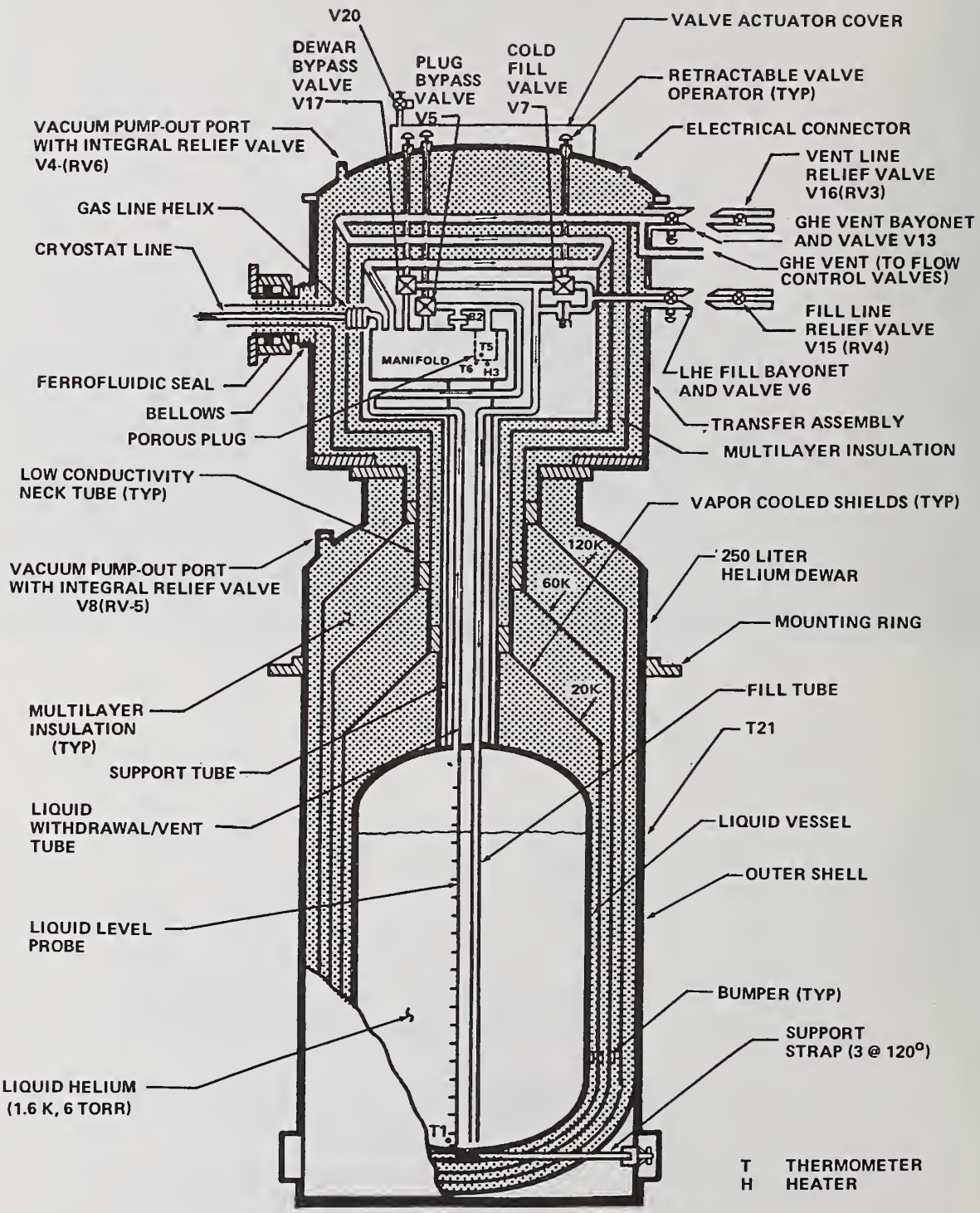

Figure 3. Schematic diagram of the IRT dewar subsystem.

When the experiment is launched in the Space Shuttle the dewar subsystem will be horizontal, and large accelerations will be applied transverse to the dewar axis. To aid in supporting the mass of the 250 liters of helium, the liquid vessel and the dewar VCS against these loads, three fiberglass/epoxy straps attach the bottom of the liquid vessel radially to the outer shell. Our dewar was fabricated by Cryogenic Associates, Inc. It has been vacuum leak tested, but cryogenic testing must await the assembly of the TA onto the dewar.

2.1.2 Transfer Assembly

The TA, designed and fabricated by UAH, is currently being assembled onto the dewar at MSFC. Within the outer case of the TA is a set of three nested heat exchanger tubs, shown in Figure 4, each with a gas tube welded to its upper circumference. Each tub will be wrapped with MLI and bolted to a dewar shield extending up from the neck. As described below, a portion of the dewar boiloff gas leaving the porous plug, is circulated in turn through the three heat exchangers and then to external valves.

Within the inner tube is a demountable plumbing module which is supported by the dewar neck. The module has five tubing connections, each utilizing a Varian mini conflat ultra high vacuum flange. These connections are to the dewar fill and vent tubes, the external fill line, the inner heat exchanger tub, and the gas line to the cryostat. The module components, shown in Figure 3, operate at the temperature of the liquid helium, nominally 1.6K. They are described below.

Liquid helium is introduced into the dewar subsystem through a standard bayonet and vacuum jacketed valve (V6), then through cold fill valve (V7) and the dewar fill tube. The cold fill valve (V7) prevents liquid helium from flowing out the fill line to the warm outer shell when the experiment is in space. A burst disk (B1) permits controlled venting through the fill line in the event of accidental overpressurization. In space, liquid flows into the TA through the withdrawal line and is restrained by the porous plug. The principle and operation of porous plugs, which are essentially liquid/vapor phase separators for superfluid helium are described elsewhere [3]. In the event of plug blockage and overpressurization a second bypass burst disk (B2) provides relief into the vent lines. When the dewar is being initially filled or when normal helium (4.2K, 1 atmosphere vapor pressure) is being converted to superfluid (1.6K, .008 atmosphere pressure), large gas flow rates must be vented. A bypass valve (V5) is opened in parallel with the porous plug to permit high flow rates and avoid possible contamination of the plug pores. A second bypass valve (V17) is opened when liquid topoff begins to prevent initial warm helium from the warm transfer line from entering the liquid vessel.

The cold valves, V5, V7, and V17 are operated by vacuum-tight, retractable actuator shafts having low thermal conductivity and low thermal mass. When retracted, the actuator shafts will be held in place by a cover box which can be evacuated through valve (V20) to prevent air leakage through the shaft retraction seals during the vibrations of launch. To reduce wear on the valve seats and minimize heat input when the valve actuators are engaged, the valves will be opened at the beginning of cryogenic operations and will not be closed except when the dewar subsystem must be turned on its side (launch attitude) for testing or just before the actual launch. Minor leakage past the seats of V5 and V17 can be tolerated, but V7 must remain sealed superfluid tight even in space to avoid heat conduction down the fill line from V6. To prevent the cold valves from vibrating open during launch we have designed a spring loaded detent lock operated by the valve actuator.

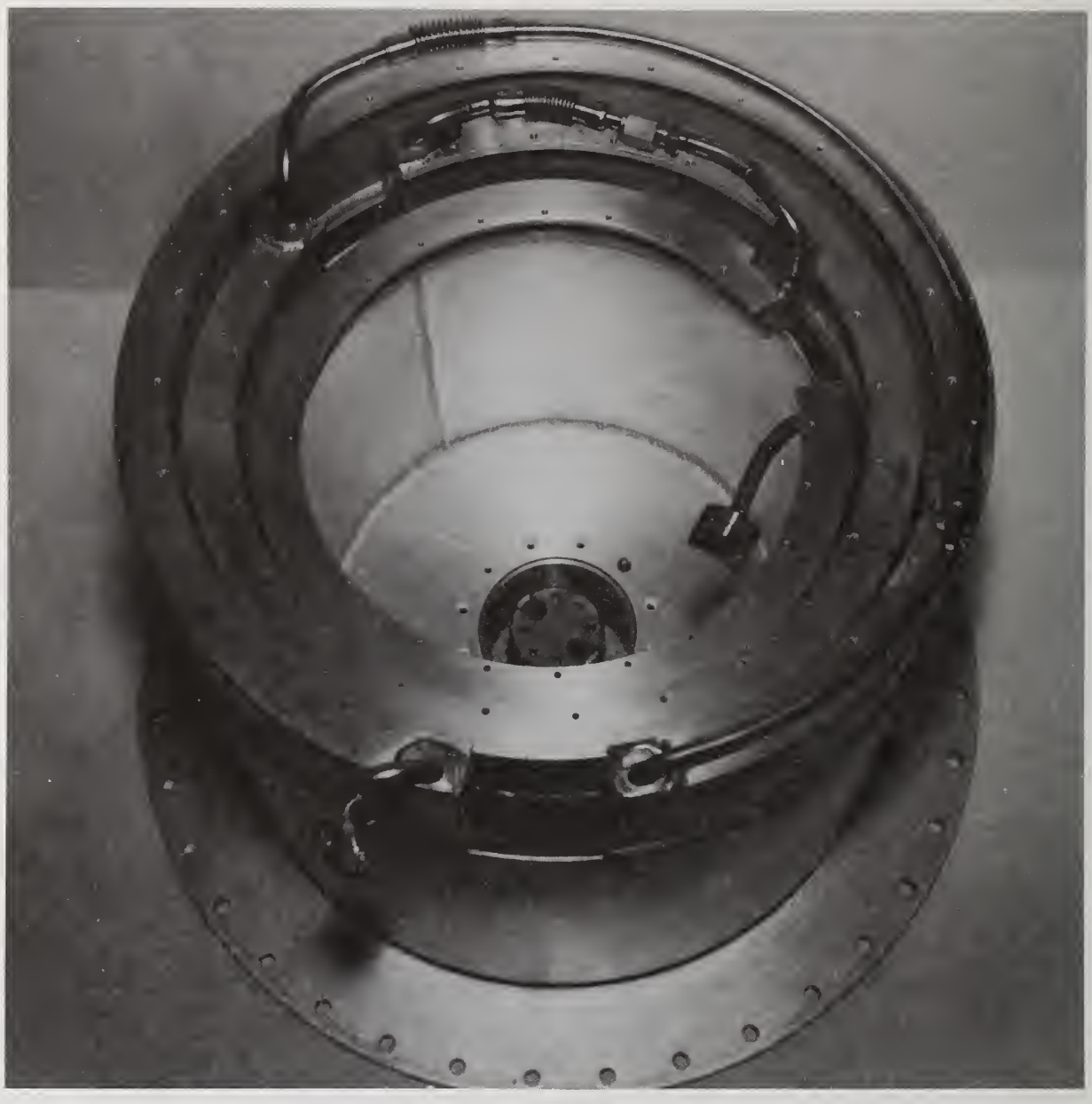

Figure 4. Transfer assembly heat exchanger tubs.

The liquid helium evaporates from the porous plug at a temperature of about 1.6K and enters a manifold from which it is divided into the dewar and cryostat vent flows discussed above. The cryostat vent tube is wrapped into a helical coil which flexes with the motion of the cryostat as the infrared instrument is scanned across the sky. The insulated cryostat line then passes through a ferrofluidic seal which joins the TA to the cryostat, accommodates the scanning motion, and maintains the high vacuum within the cryostat and TA before the experiment is carried into the vacuum of space.

The dewar subsystem has been instrumented to permit accurate measurement and control of its operation on the ground and on-orbit. A number of thermometers measure liquid and VCS temperatures. Thermometers T5 and T6 on the porous plug indicate the plug performance and a commandable heater gives us a means of plug flow control in addition to the external valves (see below). A thermometer (T1) and liquid level probe are inserted into the dewar from the TA and can be replaced in case of malfunction. Several superfluid tight electrical feedthrus are used to bring instrumentation leads from the liquid helium out into the vacuum space.

2.1.3 Dewar Subsystem Thermal Performance

The dewar subsystem will be tested by itself at MSFC while the infrared instrument is being installed in the cryostat in Arizona. Initially the gas line to the cryostat will be terminated within the TA and the dewar tested as a stand-alone subsystem. The dewar will be filled with normal helium and allowed to stabilize; then the helium will be converted to superfluid at about 1.6K by pumping through the vent line. A long term performance test will be made with the dewar upright (porous plug not wet by the liquid helium), tilted 90° into the launch attitude (plug may or may not be wet), and tilted beyond 90° to insure that the plug is wet and operating as it will in space where fluid flows easily to it. Actual performance will be compared to predicted performance.

Initial estimates of the thermal balance in this complex dewar led to the nominal temperatures indicated in Figures 2 and 3: 20K for the inner VCS, 60K for the middle VCS, and 120K for the outer VCS. The final configuration of the system, particularly the neck tube structure and the support straps, has led to a revision of the analytic predictions for steady state operation [2]. In the case in which all boiloff gas is used to cool the dewar VCS (none to the cryostat), the shields are predicted to operate at 30K, 126K, and 240K respectively. The corresponding predicted heat load on the liquid vessel is 152 mW and the boiloff rate is 6.7 mg/s, or 4.0 liter/day of superfluid helium.

When the stand-alone tests are completed, a cryostat substitute will be installed on the cryostat gas line of the TA. This test equipment will allow us to simulate the division of gas flow between the dewar and cryostat shields and to make preliminary tests of the flight situation.

2.2 Cryostat

The cryostat, shown schematically in Figure 5, will be a special modification of an open neck laboratory dewar. The essential special features include mounting flanges for the two sections of the infrared telescope, an access port for infrared detector installation, a side extension on the cryostat rotation axis through which the cold gas from the TA enters, and a gas heat exchanger and VCS system. A commandable vacuum cover insures that a high vacuum can be maintained within the cryostat and telescope before the experiment is in space. The cold gas from the TA is first delivered at a temperature of about 2K to a cold finger, designed to maintain a temperature of about 2.5K, to which the IR detector block will be clamped, and then to the heat shield system. The lower and upper telescope sections are designed to operate at maximum temperatures of 8K and 60K, respectively. They will be cooled by conduction to their mounting flanges. The two telescope mount flange rings, and two additional rings which are at temperatures of approximately 120K and 200K are suspended from the top of the cryostat on large diameter fiberglass-epoxy tubes. Each ring carries a VCS and each delivers its collected heat to the cold venting helium gas. The vent tube, after leaving the cold finger, is fastened to the four rings in turn, exits the cryostat at ambient temperatures, then connects to external flow control valves. Additional design information was given previously [1]. The cryostat was also built by Cryogenic Associates, Inc.

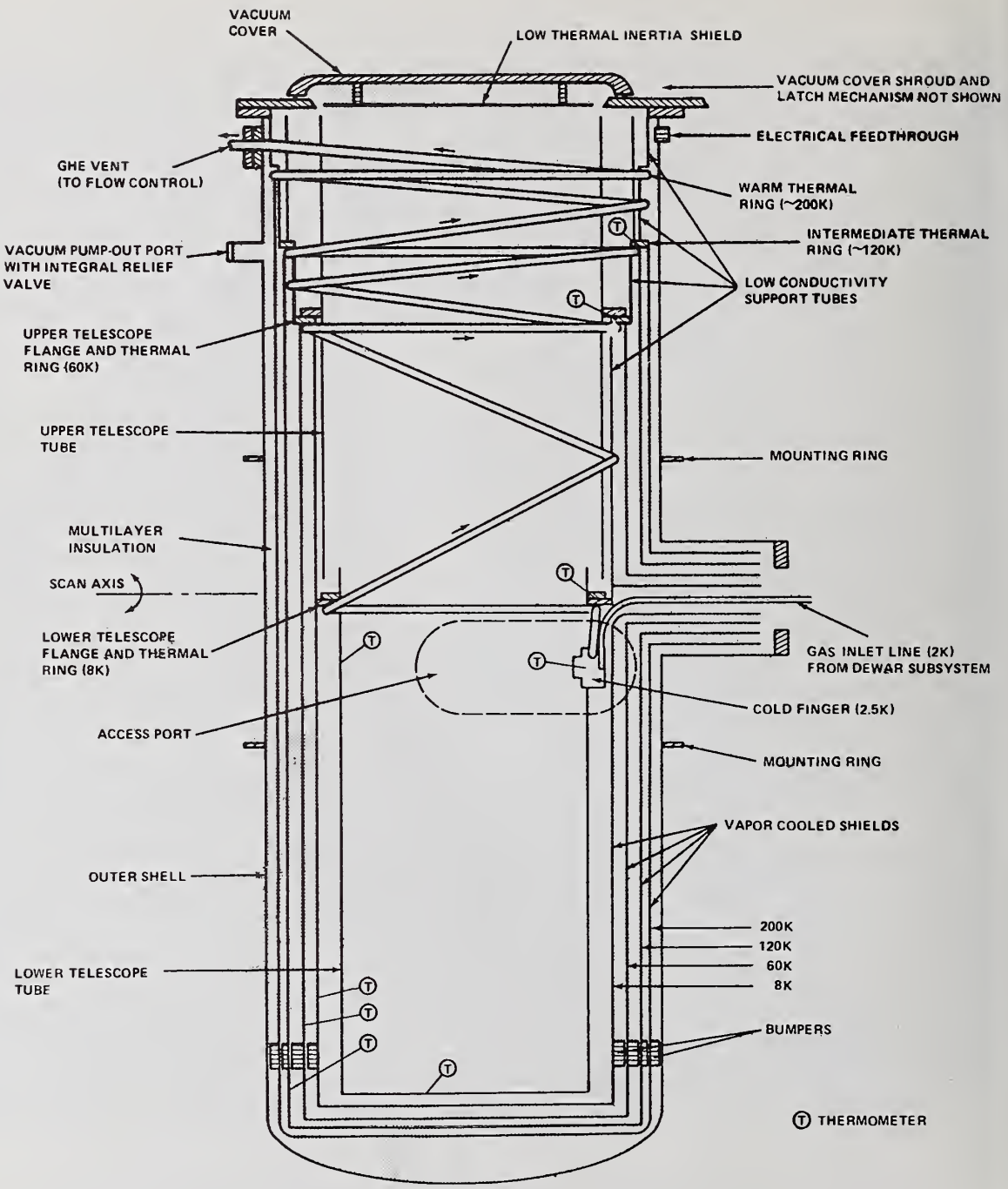

Figure 5. Schematic diagram of the IRT cryostat subsystem.

The cryostat was tested cryogenically, using a transfer assembly substitute which permitted the controlled flow of cold helium gas into the cryostat line from an ordinary helium dewar. The results of these tests, discussed elsewhere [2], indicate that a flow rate of about 17 mg/s will be required, at an inlet temperature and pressure of 2K and 6 torr (.008 atm), respectively, in order to maintain the infrared optical components at their design temperatures.

2.3 Cryogenic System Performance

After the cryostat and dewar subsystems are integrated together, a cryogenic system test will be run to verify the combined operation of the system. We will be particularly interested in confirming the predicted steady state and transient behavior as we vary the division of vent gas flow between the two heat exchangers. We must develop an optimum strategy for the experiment operations prelaunch and on orbit in order to conserve helium and still permit successful infrared observations whenever required. The only source of cold gas is vaporization of liquid helium from the dewar/porous plug by either parasitic heat, or electrical heat from the heater on the porous plug. The parasitic heat can, of course, be controlled over a wide range by varying the amount of gas in the dewar vent line. For a given rate of heat input, total pumping rate, and division of flow, the liquid will come to some equilibrium state. Regardless of the division of flow, total pumping rate must be adequate to keep the liquid in the superfluid phase.

When the 17 mg/s required for infrared observations is diverted to the cryostat, the dewar flow is predicted [2] to be only 3 mg/s. In this situation the dewar shields will warm to temperatures of 90K, 205K, and 260K respectively. The resulting total system flow rate of 20 mg/s or 12 liter/day could be maintained only for about 21 days, if the dewar were initially full of superfluid. With the Spacelab 2 on-orbit mission duration of 9 days and an anticipated prelaunch period after dewar topoff of as much as 15 days, it will not be possible, nor, in fact, necessary to fully cool the cryostat until after launch. As shown earlier, dedicating all flow to the dewar results in lowest dewar shield temperatures, a warm cryostat, and a total superlfuid boiloff rate of 4 liters/day or a full dewar lifetime of 62 days. Clearly an intermediate situation will be chosen with the infrared optics held at a fairly low temperature until the experiment is in space.

Adjustment of dewar and cryostat vent flows will be possible during the mission by operating a set of three commandable warm valves in each of the vent lines as shown in Figure 2. The three parallel on/off valves in each vent are sized with orifices allowing 14%, 29%, and 57% of full flow in the vent line. Thus, particular combinations of 0, 14, 29, 43, 57, 71, 86, or 100% of full flow can be selected for each vent line with the setting of three valves. The system, and particularly the telescope and liquid helium temperatures will respond rather slowly to changes in these valve settings. We anticipate the occasional need to rapidly deliver additional cooling to the cryostat as, for example, when closure of the warm cover dumps a burst of heat onto the cold optics. This rapid delivery of extra cooling can be achieved by activating a small heater on the vapor side of the porous plug. The well-known superfluid helium "fountain-effect" [3] then draws liquid through the plug.

3. Prelaunch Cryogenic Operations

Cryogenic servicing of the IRT experiment before launch presents a number of unusual and challenging requirements. The Spacelab 2 payload will be installed into the Space Shuttle Orbiter several weeks before launch. Perhaps 3 weeks before launch the IRT will be purged, filled with normal helium, and allowed to stabilize. Since the supply dewars must be located on workstands of limited weight carrying capacity at the sides of the Orbiter bay, several small supply dewars will be required and the vacuum jacketed flexible fill line will be 4.5 m long. Venting of the cold gas must be through long insulated hoses to prevent condensation and resulting dripping of water onto other experiments or orbiter hardware. The helium will then be pumped down to and maintained in the superfluid phase by means of large, remote vacuum pumps. As late as possible in the ground processing flow, nominally 15 days before launch, the dewar will be topped off with superfluid. Recent superfluid topoffs performed at Ball Aerospace Division on the superfluid helium dewar for the Infrared Astronomical Satellite (IRAS) have demonstrated that essentially 100% superfluid fill can be achieved.

The requirement that the liquid helium be held at a temperature and vapor pressure below 2.17K and 38 torr (.05 atm), respectively, (the superfluid transition) means that essentially continuous pumping must be maintained until launch. Pumping through long umbilical vacuum lines to overboard pumps is not feasible for the Spacelab 2 mission, so we must provide our own on-board vacuum maintenance system, powered almost continuously through an umbilical electrical line. This pump must operate satisfactorily when the Orbiter is horizontal and also when it is in the vertical launch attitude. Through this period the equipment is inaccessible. We are using a commercial, direct drive laboratory pump and valves for this purpose. The pump was found to operate satisfactorily over an angular range of about -50° to 45°, measured about the shaft axis from normal upright laboratory attitude. The pump is therefore mounted tilted -50° on a bracket; when the Orbiter is raised to the vertical, the pump is at 40° and still operates.

There will be a few unavoidable power outages for the vacuum maintenance assembly as the Orbiter is moved, raised to the vertical, mated to the External Tank and Solid Rocket Boosters, and rolled to the launch pad. When the pumping is thus diasbled, the helium will warm; it must not warm above the superfluid transition. We have estimated that one four-hour power outage and several shorter ones can be tolerated, if adequately separated to give the system time to recool. Pumping will be continued until a few minutes before launch. During ascent some heating of the liquid is expected, mainly due to the absence of vent flow. Recent vibration tests on the cold IRAS dewar indicate that very little frictional heating of the superfluid helium occurs. When the Orbiter reaches an altitude at which the atmospheric pressure is below five torr, a barostatic switch will open a valve between the experiment vent tube and the overboard vent. This will permit pumping on the superfluid to resume several hours before the Spacelab is activated.

We will monitor and control the cryogenics during the mission from the ground in the Spacelab Payload Operations Control Center (POCC). Emergency monitoring and control will also be possible by the on-board Payload Specialists (scientists). Shortly before landing the experiment will be stowed, the vacuum cover sealed, and the vent valves closed. The relief valves on the vent lines will permit the experiment to warm up safely and untended.

4. Conclusion

The cryogenic system for the Spacelab 2 Infrared Telescope Experiment has been designed as a low-cost approach to the storage of liquid helium during the preparation of a Spacelab payload for launch and the supply of adequate cooling to a separate Infrared Telescope for the duration of a typical Spacelab mission. The result is a system which will satisfy the scientific requirements of the IRT and also be capable of furnishing cooling to a variety of follow-on Spacelab experiments. It is expected that as the Spacelab and Space Transportation System flight program matures, flight durations will increase and prelaunch preparation times will decrease. The superfluid helium system described herein should be capable of satisfying experiment helium cooled refrigeration requirements for the next several years.

5. References

[1] Urban, E. W., Katz, L., Karr, G. R., and Hendricks, J. B., Spacelab 2 infrared telescope cryogenic systems, Society of Photo Optical Instrumentation Engineers, Volume 183 - Space Optics, 1979.

[2] Karr, G. R. et al., Cryogenic subsystem performance of the infrared telescope for Spacelab 2, Proceedings Eighth International Cryogenic Engineering Conference, ICEC-8, Genoa, 1980.

[3] Karr, G. R. and Urban, E. W., Superfluid plug as a control device for helium coolant, Cryogenics, 266-270 (1989).

Requirements for and Status of a 4.2°K Adsorption Refrigerator Using Zeolites

William H. Hartwig
Department of Electrical Engineering
The University of Texas at Austin
Austin, Texas 78712

Previous work by the author and his associates has demonstrated the feasibility of 77°K adsorption refrigerators using one N_2O stage which provides the adsorption temperature (185°K) for N_2. The concept of adding an H_2 stage and He stage has been examined theoretically and experimentally using zeolites and/or other molecular adsorbers. The results are described which shows the requirements for each stage and suggests that a reliable low-power 4.2°K non-mechanical refrigerator can be built with a considerable development effort and some additional research.

Key words: Adsorption; compressor; cryogenics; molecular adsorption; refrigeration; zeolites.

1. Molecular Adsorption/Desorption Compressors for Cryogenic Gases

It is well known [1] the clay minerals called Zeolites adsorb large volumes of such gases as N_2O, CO_2 and NH_3 at room temperature and pressure. For example, the synthetic sodium aluminum silicate zeolite NaY will adsorb 21% by weight of N_2O at room temperature and pressure. The family of adsorption isotherms for N_2O and the zeolite NaY is shown in Figure 1 as an example. The adsorption process is exothermic, generating a heat of adsorption, H_a, which is less than the heat of vaporization of the normal liquid. The adsorbed gas density is, however, approximately that of the liquified gas at its normal boiling point. For that reason, addition of heat will release a large mass of adsorbed gas in a small volume, creating a high pressure.

Cryogenic gases with lower boiling points can also be adsorbed with a useful mass fraction if the zeolite temperature is suppressed to about 2-3 times their normal boiling points in absolute degrees. The exact pressure ratios and desorption temperatures for nitrogen,hydrogen,and helium depend upon the choice of zeolite. The practical problem is to find adsorbing media for helium at 20°K, for H_2 at 77°K, and for N_2 at 185°K. A successful N_2O refrigerator has been built [2,3,4] which delivers 150 watts of cooling.

a. Advantages of Adsorption/Desorption Gas Compressors

The Molecular Adsorption Refrigeration System (MARS) is being developed to take advantage of several desirable features; no shaft seals or lubricant contamination, low-tolerance fabrication techniques, no mechanical vibration or acoustic noise background, long mean time to repair or failure, low cost materials, and the ability to use waste heat.

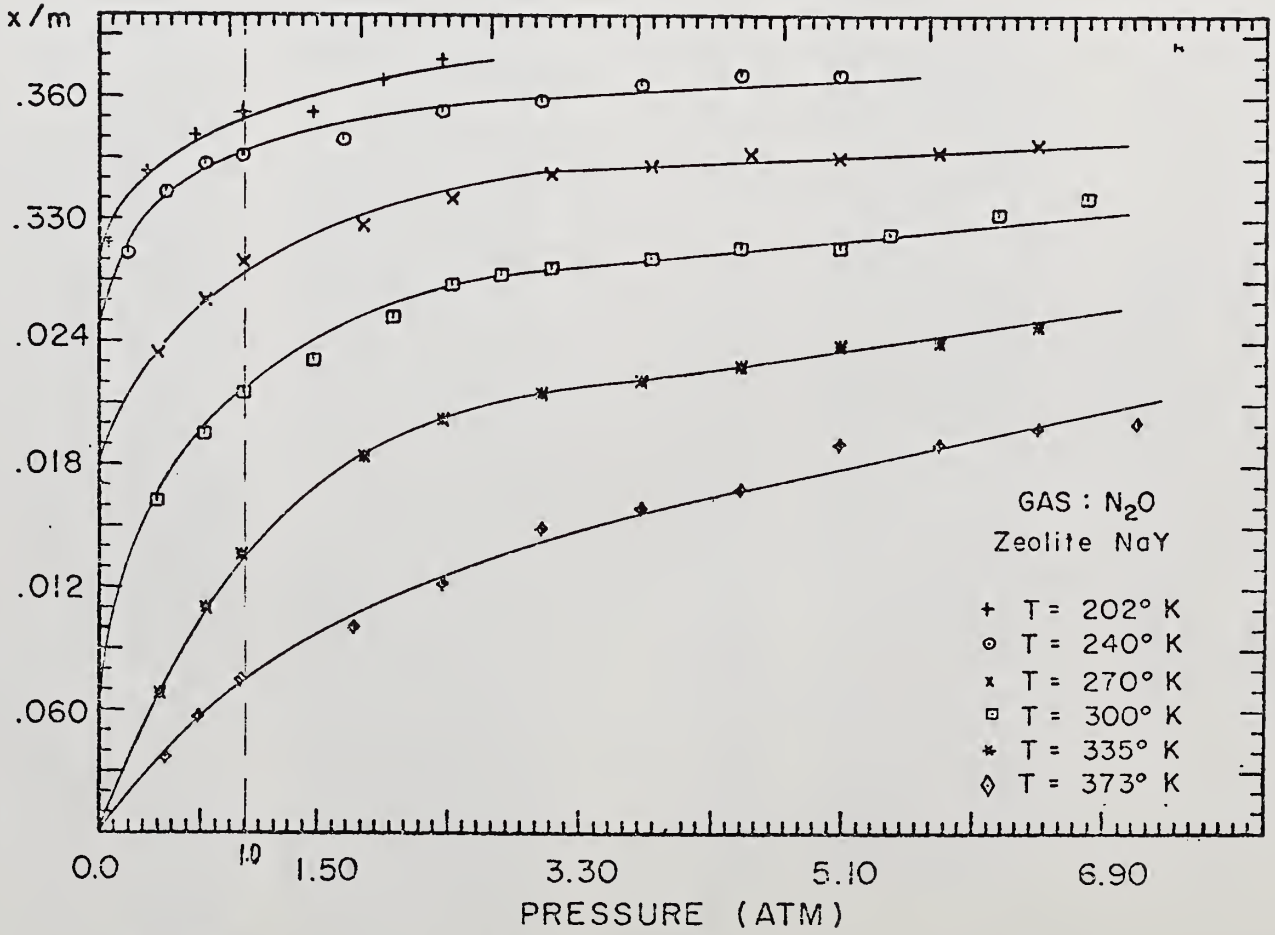

Fig. 1 Weight ratio of gas to zeolite, x/m for N_2O adsorbed in zeolite

The disadvantages include a lower C.O.P. than mechanical compressors, but this is partially offset by the large compression ratio. To operate with lower boiling point gases than N_2O the adsorption temperature must be suppressed below room temperature, but some of the heat can be cycled reversibly with proper design.

b. Theory of Gas Adsorption on Zeolites

The crystal structure of zeolite is that of an open lattice of Al, Si, and O atoms with dominant cations that may be Na, K, Cs, or other metals. The open structure is a three dimensional periodic array of voids, typically 13Å in diameter, with 5Å openings between adjacent voids. Normally each of these voids fill with 10-20 H_2O molecules. When heated in a vacuum the water is desorbed, and may then be cooled and filled with polar molecules of other gases. The adsorption of gas molecules on the interior surfaces of the voids is an ionic interaction with a characteristic potential energy for each different gas molecule at each different ion site. The functional relationship of amount of adsorption versus temperature and pressure for various zeolite-gas pairs is extremely complex, and as such emperical methods have been commonly used to generate adsorption data.

Recent work by Woltman and Hartwig [5,6] has led to a theory of gas adsorption derived from first principles. A lattice model of solutions is the basis of the theory, and it treats adsorbed gas molecules and the vacant sites where there are no adsorbed molecules as a two-component solution. The theory is capable of accounting for the detailed physical behavior over a wide range of pressures, and thereby establishes a reliable formalism to predict behavior and design apparatus.

c. Closed Cycle MARS Compressor Configurations

While many configurations are possible, a typical one consists of four cylindrical pressure vessels filled with zeolite. Each compressor is able to heat and cool the zeolite with a finned heat exchanger, using electric heat and circulating liquid coolants. Each compressor successively adsorbs gas, pressurizes with addition of heat, desorbs gas, and then cools to adsorption pressure. Figure 2 is a cycle diagram, where the vertical scale is heat power, positive if added and negative if removed.

In cryogenic refrigeration service the desorbed high pressure gas is delivered to a Joule-Thomson orifice or expansion engine, and the low pressure return gas is adsorbed. The adsorption cycle is illustrated in Figure 3. Gas is adsorbed at 1 Atm. pressure up to point a, where x/m is 0.15 grams of gas per gram of zeolite. Upon addition of heat, gas is desorbed and pressure rises to 21 Atm. at b. Gas is delivered at 21 Atm until x/m reaches c. The cooling interval removes heat and the pressure drops to 1 Atm. at d.

2. Compressor Design Theory

For a given mass flow, $\dot{m}_g$, the compressor delivers a fraction, $\Delta x/m$, of the adsorbed gas from M_z grams of zeolite in the desorption time, t_d. Hence

$$\dot{m}_g = \frac{M_z(\Delta x/m)}{t_d} \qquad (1)$$

To pressurize and desorb the gas, a fixed energy must be added to the compressor per gram of zeolite, or

$$q_d = K_1 C_p \Delta T \qquad (2)$$

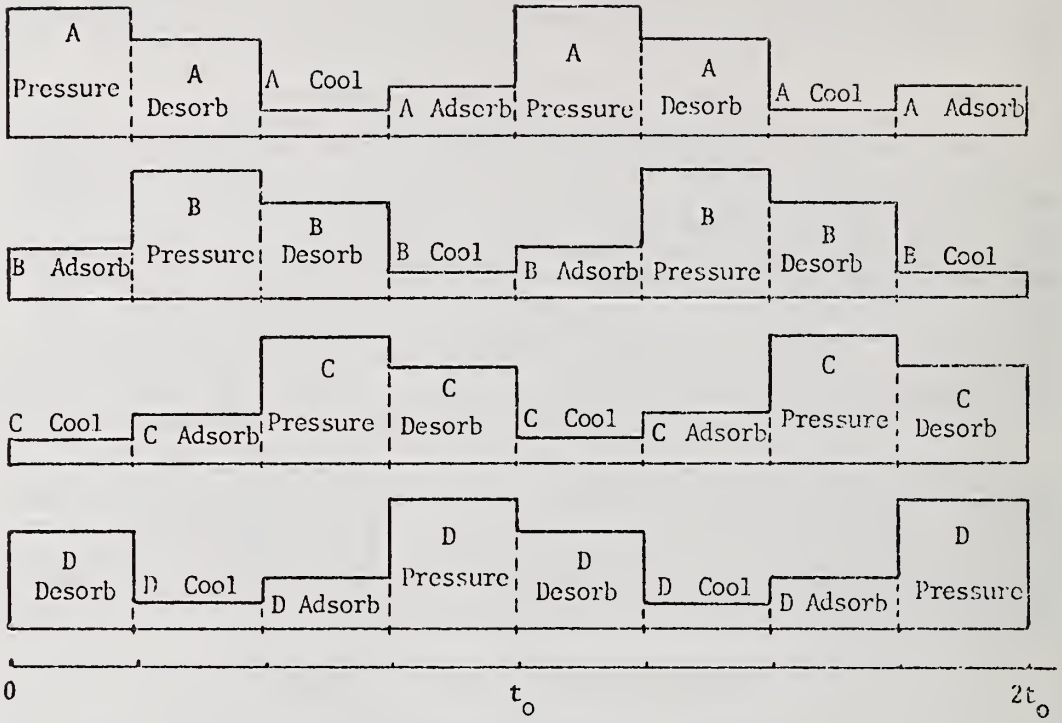

Fig. 2 Heat Cycle diagram for MARS compressors. Each one, A-D, is always in one of four states; (1) adsorbing gas at low pressure, (2) pressurizing by addition of heat with no flow of gas, (3) desorbing gas under pressure, and (4) cooling the zeolite bed to reach adsorption pressure.

where K_1 is a constant, C_p is the specific heat and ΔT is the zeolite temperature rise. The average power input during the pressurizing and desorbing intervals is

$$\dot{Q} = \frac{q_d M_z}{t_p + t_d} = \frac{K_1 M_z C_p \Delta T}{t_p + t_d} \tag{3}$$

Eliminating M_z between (1) and (3), the mass flow of gas is proportional to the input power, or

$$\dot{Q} = \frac{K_2 C_p \Delta T}{\Delta x/m} \dot{m}_g \tag{4}$$

where K_2 includes K_1 and $t_d/(t_p+t_d)$.

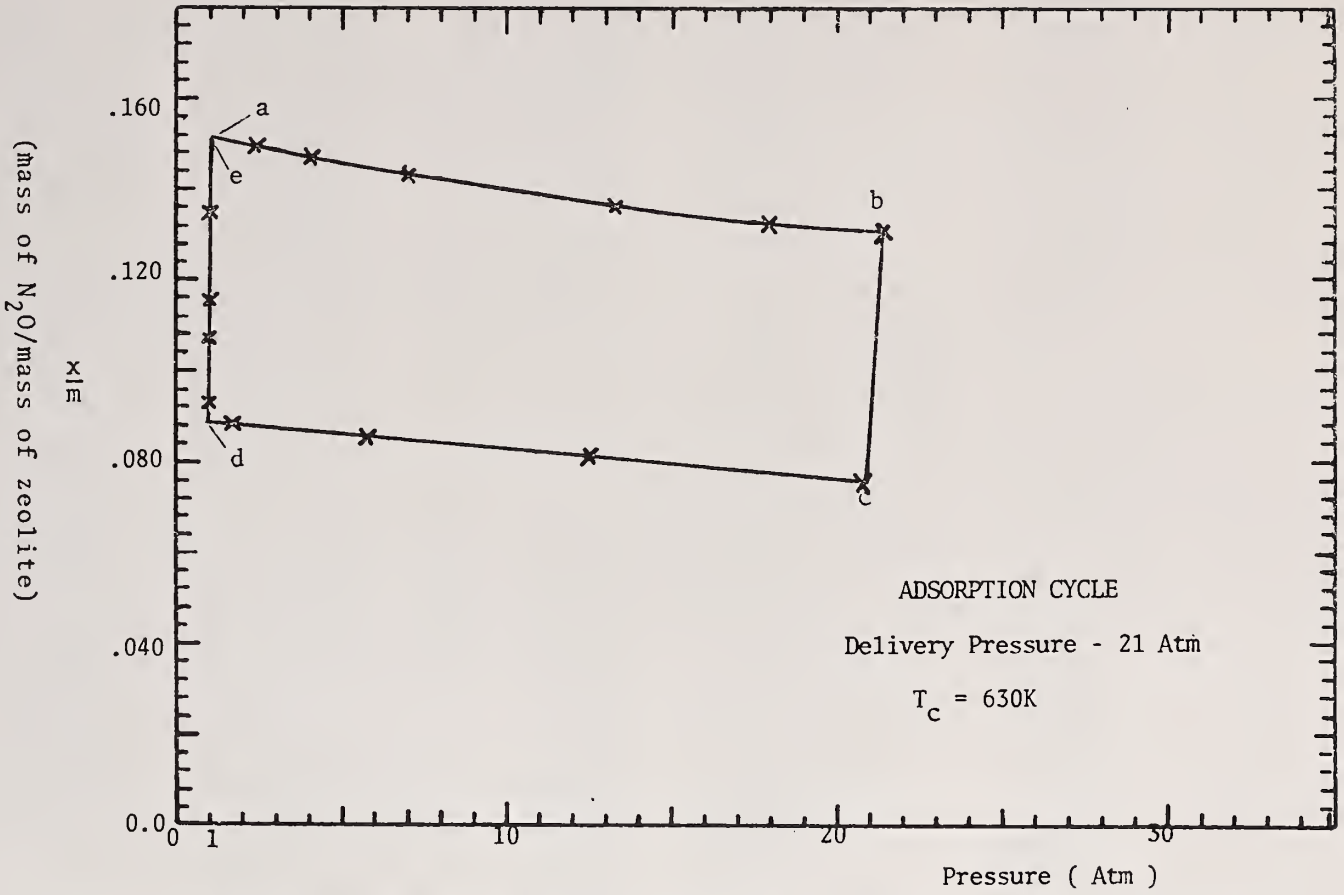

Fig (3) Adsorption cycle of N_2O in 13X with delivery pressure of 21 Atm. Temperature is peak value for zeolite at the end of the desorption phase, point "c".

Desorption pressure, P_a, is the dominant gas parameter that links gas flow to cooling power. By referring to the T-s or H-P diagrams of the cryogenic gases in their superheated regions, an emperical relation can be derived.

$$P_d \dot{m}_g = A\dot{Q}_o = \frac{P_d M_z \Delta(x/m)}{t_d} \tag{5}$$

where A is a constant over a wide range of pressure. Equation (5) can be solved for $\dot{Q}_o$,

$$\dot{Q}_o = \frac{P_d M_z \Delta(x/m)}{A t_d} \tag{6}$$

The Coefficient of Performance is the ratio of cooling power developed by the stage to the heat removal rate for adsorption, which means we divide Equation (6) by Equation (4).

$$COP = \frac{\dot{Q}_o}{\dot{Q}_i} = K \frac{P_d \Delta(X/m)}{\Delta T} \tag{7}$$

Good design practice will increase the constant, K, by reducing the relative mass of non-adsorbing materials, such as the compressor shell, using isentropic expansion instead of J-T orifices, and taking advantage of low Cp materials at low temperatures. As with conventional refrigerators, the COP of a multiple-stage MARS is the product of the separate COP's.

MARS compressors would be optimized in part, by selecting the lowest possible adsorption temperature to maximize the total adsorbed mass of gas; which in turn, insures the highest desorption pressure for a given zeolite. This choice is limited in practice to the boiling points of natural gases, such as N_2O, N_2, and H_2, but more favorable combinations may include Ne, argon, CH_4, and CO_2.

The optimum zeolite for each gas is the one that maximizes the combined COP, not necessarily the individual COP's. At the time of this report no definitive choices have been made between various synthetic and natural zeolites, and also charcoal.

Table 1 summarizes typical values found so far, for the parameters in the equations above, all using a J-T expansion orifice. The values selected for the various constants are realistic approximations in the present state of the art. The optimum energy budget for any design maximizes $P_d(\Delta x/m)/\Delta T$, and it is noteworthy to point out neither zeolite mass nor the cycle time appear in Equation (7). A critical parameter, concealed in K, is the effect of free volume in limiting the maximum value of desorption pressure.

Desorption pressure can be thought of as a function of gas temperature, free volume (exclusive of the zeolite and adsorbed gas volumes), and the mass of desorbed gas. The adsorption isotherms show the adsorbed mass is almost independent of pressure, so if more gas is "vaporized" by changing the zeolite temperature, the pressure will increase. To the extent this is true, MARS desorption pressure will be enhanced by limiting the volume of the external tubing and valves, and reducing the interstitial volume between zeolite grains.

TABLE 1

Stage	Gas	Adsorb. Temp. ^oK	Desorb. Temp. ^oK	P (atm)	K	$\frac{\Delta X}{m}$	ΔT (^oK)	COP	$\frac{\Delta x/m}{\Delta T}$
1	N_2O	300	575	21	23.8	0.10	275	0.050[4]	3.6×10^{-4}
2	N_2	200	475	30	0.62	0.10	70[1]	0.0067	3.6×10^{-4}
3	H_2	77	200	25	1.3	0.009	123[2]	0.0018	7.3×10^{-5}
4	He	20	77	25	0.42	0.028	57[3]	0.0052	4.9×10^{-4}

1. 70^o is the temp. reduction load on the first stage. Reduction from 475^oK to 270^oK is by thermoelectric-cooled circulating fluid.
2. ΔT for H_2 compressor may be less for some zeolites.
3. ΔT for He compressor can be less since $\frac{\Delta x}{m}$ is probably optimum at about 60^oK and the zeolite need not be taken to 77^oK.
4. COP of a working N_2O stage is experimental data. Energy for desorption was added by joule heat and dissipated to the ambient.

3. Conclusions

The data in Table 1 is not indicative of optimum performance because it was processed with equations for isenthalpic expansions. Some errors are possible, although the data is consistent with published values[7] for common zeolites. It is reasonable, we believe at this writing, that optimum COP's with the zeolites tested will be about twice those reported for N_2O, N_2 and He. The very low values for H_2 are not consistent with the others, and other zeolites will increase them. As it stands now, a 4-stage MARS could have an overall COP of about 10^{-6}. This would produce 10 mw of cooling at 4.2K with about 10 KW input power.

a. Directions for Future Research

The Woltman-Hartwig model for adsorption and an experimental program for verification is now appropriate to match all the cryogenic gases with particular adsorbers. This will produce a better understanding of the physics of adsorption/desorption systems, and permit the MARS compressors to achieve the maximum values of $\Delta(x/m)/\Delta T$ by improved design and temperature control.

b. Directions for Future Development

Many avenues for innovation and design remain for increasing the COP of multistage MARS. The H_2 stage has the lowest individual COP, and it can be increased by adsorbing at higher pressure, finding more effective zeolites, or substituting other technology. A $LaNi_5$ compressor which utilizes the reversible hydride formation is one possibility now being studied elsewhere [8]. It would operate with a room temperature heat sink but needs a very small 77^oK stage to get the H_2 gas below its inversion point. This could be supplied with a two-stage MARS. If metal hydride compressors prove to be feasible, the marriage of the two new technologies will be straightforward.

Many areas for compressor design improvements must be pursued to optimize the cycle and give proper attention to reliability and maintainability. Work by the author and his associates [9] has led to optimizing the heat exchanger geometry for MARS compressors. Other problems involve the logic of valve networks for routing gases throughout the system, and design of the valves themselves. The best design approach appears to be rotary ganged valves that synchronize the cycle in each stage.

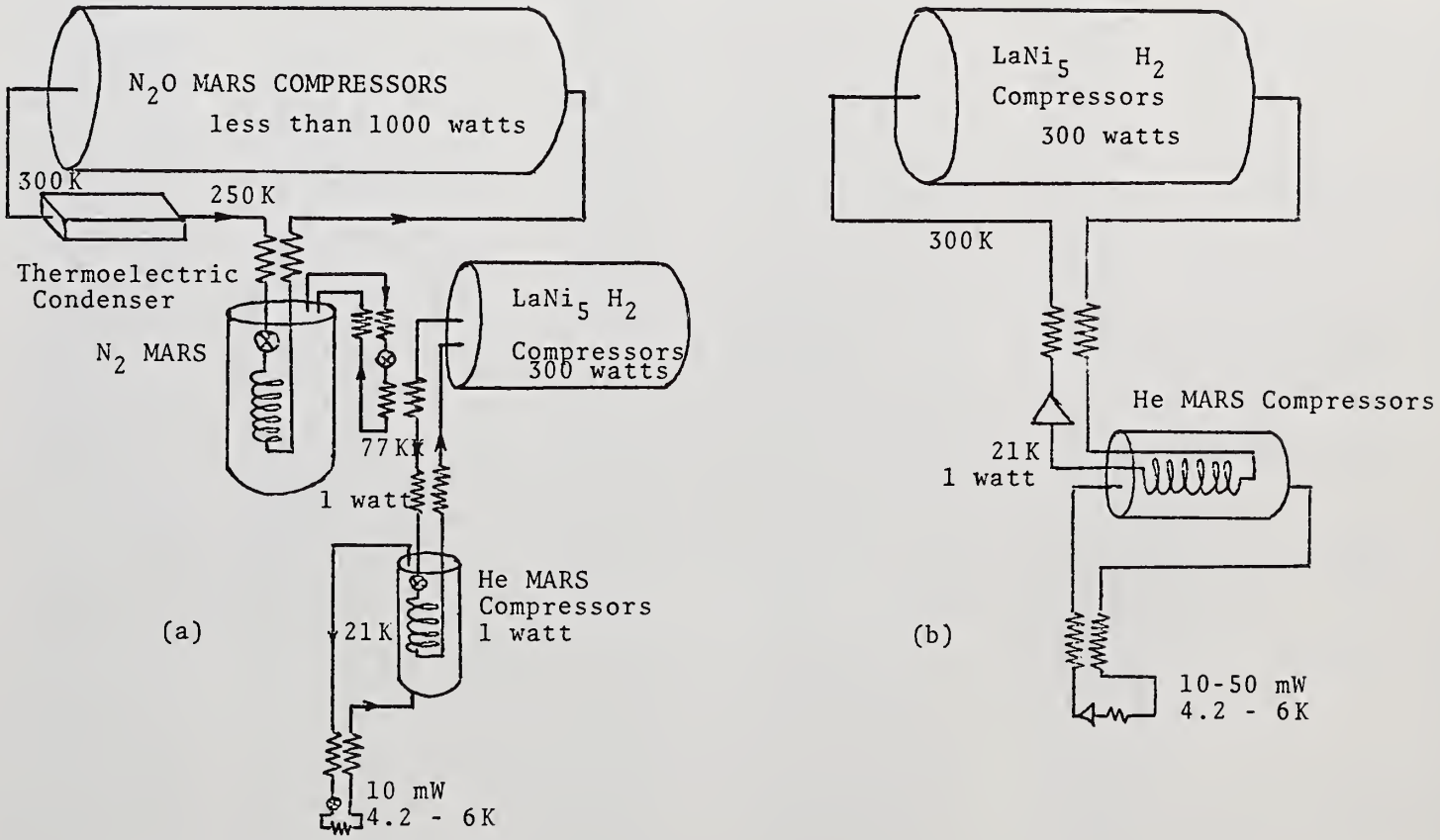

Fig. 4 Schematic diagrams of two configurations of cryocoolers which utilize non-mechanical gas compression. The system (a) has J-T expansion in four stages, and in (b) turbine expansion permits the system to be reduced to a single $LaNi_5$ compressor operating against ambient temperature followed be a He MARS adsorption/desorption stage using zeolite or charcoal. Power levels shown are approximate.

The use of simple expansion engines to improve the COP of each stage is an obvious choice. Miniature cylindrical or spherical rotors with gas bearings are possible configurations, but the development effort will be significant. Figure 4 is a schematic diagram of two He cryocoolers which compares JT and rotating expansion.

A most important problem, for a multistage MARS design that is otherwise feasible, is heat management. Advantage can be taken of heat leaks and waste heat in hotter stages to provide desorption heat in colder stages. If the optimum gas/zeolite combination is found for a particular stage the final desorption temperature can be controlled to achieve the optimum $P_d(\Delta x/m)/\Delta T$ and COP.

4. Acknowledgements

The work was supported by NASA-LBJ Space Center, Houston, and by Rockwell International, Anaheim, by a contract with the Navy. The author acknowledges their contributions to the work.

5. References

[1] D.W. Breck, Zeolite Molecular Sieves, John Wiley, New York, (1974)

[2] Hartwig, W.H., Steinfink, H., Masson, J.P. and Woltman, A.W., Proc. 1976 Region V IEEE Conf., IEEE Cat. 76CH1068-6Reg5, 1976, p. 80.

[3] Hartwig, W.H., "Adv. in Cryogenic Engineering," Ed. by K.D. Timmerhouse, Plenum Publishing Co., N.Y., 1978, 23, 435-447.

[4] Hartwig, W.H., Woltman, A.W., and Masson, J.P., Proc. 1978 Int'l. Cryogenic Eng'g. Conf., IPC Science and Technology Press Guildford, Surrey GU2 5AW, England.

[5] Woltman, A.W., Ph.D. Dissertation, The University of Texas at Austin, Austin, Texas, March 1978.

[6] A.W. Woltman and W.H. Hartwig, "The Solution Theory Modeling of Gas Adsorption on Zeolites," ACS Symposium Series 135, pp. 3-25, W.H. Flank, Ed., (1980)

[7] A.J. Kidnay and M.J. Hiza, "High Pressure Adsorption Isotherms of Neon, Hydrogen and Helium at 76°K," Adv. in Cryogenic Engineering, Paper K-5, pp. 730-740, (1978), K.D. Timmerhaus, Ed., Plenum, New York.

[8] William Steyert, Los Alamos Scientific Labs., (personal communication of a paper submitted for publication).

[9] R.M. Flores and W.H. Hartwig, "Optimization of Heat Exchangers in a Molecular Adsorption Refrigeration System," Rpt. No. TSR-3, Electrical Engineering Dept., The University of Texas at Austin, Austin, Texas 78712, (May 1980).

COOLING OF SQUID DEVICES BY MEANS OF LIQUID TRANSFER TECHNIQUES FOR REDUCED HELIUM CONSUMPTION AND ENHANCED TEMPERATURE STABILITY

Eldon A. Byrd

Naval Surface Weapons Center
White Oak, Silver Spring, Maryland 10901

R. G. Hansen

R. G. Hansen & Associates
Santa Barbara, California 93101

In an effort to establish a state-of-the-art SQUID device for both laboratory and field applications, a developmental effort has been undertaken by Naval Surface Weapons Center to utilize a liquid helium transfer system to perform cooling of SQUID devices in the temperature region of 4.5 to 16 Kelvin. Various techniques have been employed to enhance the temperature stability of the inherent system as well as to provide increased system portability and flexibility of application.

The specific refrigeration system used in this program has been further modified for expanded applications in the low temperature testing of infrared sensors, low noise amplifiers, and other devices.

This particular developmental effort has resulted in a system which allows the user to function in either a horizontal or vertical orientation. Operation had previously been limited to single axis orientation as a result of liquid cryogenic systems.

This paper presents a concept of utilizing state-of-the-art cryogenic systems to interface with diverse technical needs in the area of electro-optics, SQUID devices, and supporting electronic accessories.

Key words: Cryogenics, helium, infrared, SQUID, temperature sensors

This presentation, although originally intended to be a report on actual performance results of a functional system, is respectfully submitted as an interim report on "results to date" of a recently delivered system designed for both laboratory and field operation of SQUID devices.

In the initial definition of the cryogenic support requirements, considerations such as package size, system efficiency, cost of operation, and portability were defined as primary objectives. The specific function for the system was to perform the necessary refrigeration to operate SQUID magnetometers in both laboratory and field experiments.

Secondary application such as infrared detector cooling, sample cooling for cryospectroscopy, and the testing of low noise amplification systems were also envisioned for future use with the basic cryogenic system.

A refrigeration capacity of 0.250 watts at 4.2 Kelvin was the required refrigeration capacity with a goal of 2 watts at 4.2 Kelvin. Temperature indication and control over the entire range of 4.2 Kelvin to 300 Kelvin was necessary with desired stability of $\pm$ 0.001 Kelvin over the specific region of 4.2 to 16 Kelvin.

Refrigeration techniques such as closed cycle refrigeration systems, traditional dewars, and liquid transfer techniques were reviewed.

With all desired parameters being considered in view of available systems, the Air Products and Chemicals' Model LT-3-110 Heli-Tran liquid transfer refrigeration system was selected. Of particular importance in this selection were the following rather unique features of the Heli-Tran as it related to our needs.

1. The Heli-Tran's compact size and ability to operate in either a horizontal or vertical orientation was beneficial.

2. The "off-the-shelf" system was easily adaptable to our specific needs without costly alterations.

3. Rapid cooldown of samples could be effected within 45 to 60 minutes with cryogenic consumption of $\sim \leq$ one liquid liter of helium per hour of operation.

4. The "O" ring interface of the Heli-Tran cold head was readily adaptable to various vacuum shroud configurations, thus allowing versatility of applications within varying technologies.

5. Temperature control could be effected with rapid response time due to the "fine tune" controlability of the liquid helium transfer and the cold head tip heater circuit.

The commercially available Heli-Tran LT-3-110 liquid helium transfer system is shown in Figure 1 schematically. The functional system is shown in Figure 2.

In briefly summarizing the operation of the Heli-Tran, we provide the following:

A specially designed flexible transfer line is inserted into any standard helium storage container. An insertion tube on the dewar end of the line contains a fitting for pressuring the dewar from 3 to 5 psi and incorporates a safety relief valve. The line itself consists of two very small flexible tubes, one inside the other, and a separate return tube which acts as a heat shield. Operation of the line is as follows: liquid is transferred to the specimen through the innermost passage of the two concentric tubes at the pressure of the dewar. To ensure 100% liquid and extremely steady flow in the center tube, a second stream of helium is transferred at a slightly lower pressure through the annular space between the concentric tubes. This lower pressure (and therefore lower temperature) liquid is a result of flashing the liquid to a slightly lower pressure by means of a capillary tube through which the liquid enters the line from the dewar. Boiling and flow oscillations thus occur in the annular flow passage while the liquid in the center tube remains sub-cooled. The liquid to the specimen is expanded at the cold end through an adjustable needle orifice. This regulates the flow rate and therefore refrigeration to accommodate varying heat loads. The exhaust vapor from the specimen cools the radiation shield surrounding the specimen and is then heated as it vents from the cold end to avoid frosting. The pressure of the exhaust helium from the specimen may be lowered by connecting a vacuum pump permitting temperatures as low as 2 Kelvin to be achieved.

The shield liquid in the annular space is vaporized by the heat leak into the line. This consists primarily of conduction through the support system and radiation. Radiation is minimized by use of superinsulation around the concentric tubes. The cold gas from the annular flow passage is returned

through a tube parallel to the insulated concentric tubes. This further decreases radiation and support conduction losses by using the sensible heat of the shield flow. This gas is vented at the dewar end of the transfer line.

Temperature is monitored and regulated through temperature sensors and a heater mounted on the cold tip. The top of the conductively cooled unit has a 1/4"-28 UNF thread in a high conductivity copper tip at the cold end which permits a variety of specimen holders to be easily interchanged. [1]

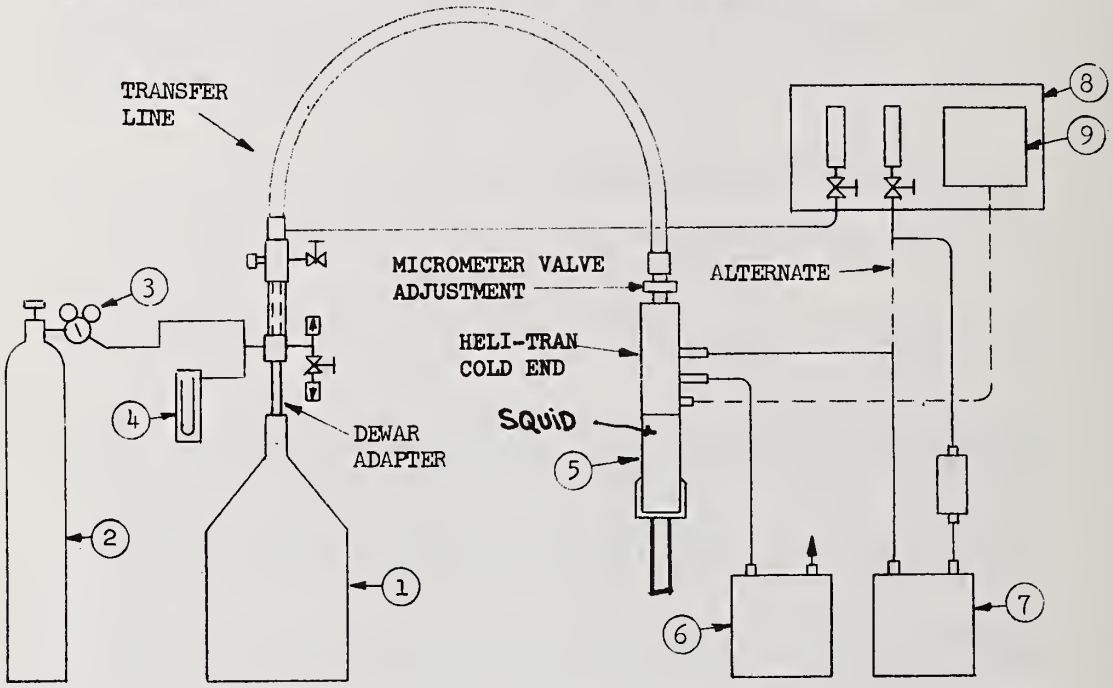

1. HELIUM DEWAR
2. HELIUM CYLINDER
3. PRESSURE REGULATOR
4. MERCURY MANOMETER, 0 to 20" Hg OR PRESSURE GAUGE ON HELIUM DEWAR
5. VACUUM SHROUD
6. VACUUM SHROUD PUMP
7. VACUUM PUMP FOR OPERATION BELOW 4.2°K
8. ACCESSORY FLOW CONTROL PANEL
9. ACCESSORY TEMPERATURE CONTROLLER, MANUAL OR AUTOMATIC

FIGURE 1

Typical Test Set Up [2]

In the interface of our particular SQUID device to the standard Heli-Tran, it was necessary to design a vacuum shroud approximately 46" in length so as to accommodate the required electrical feedthrough. This was accomplished by means of a two-piece telescoping vacuum shroud.

The heat loss or load for the electrical feedthrough was calculated to be 0.230 watts. This heat load was received on the incoming cable by means of a thermal attachment of the cable to the exhaust gas radiation station thus reducing the base load on the refrigeration system and effectively utilizing the refrigeration provided by the exhausting helium gas.

To provide for the temperature indication and control of the SQUID, a gallium arsenide diode thermometer was initially selected. Although not offering the most favorable

CRYOGENIC REFRIGERATION SYSTEM

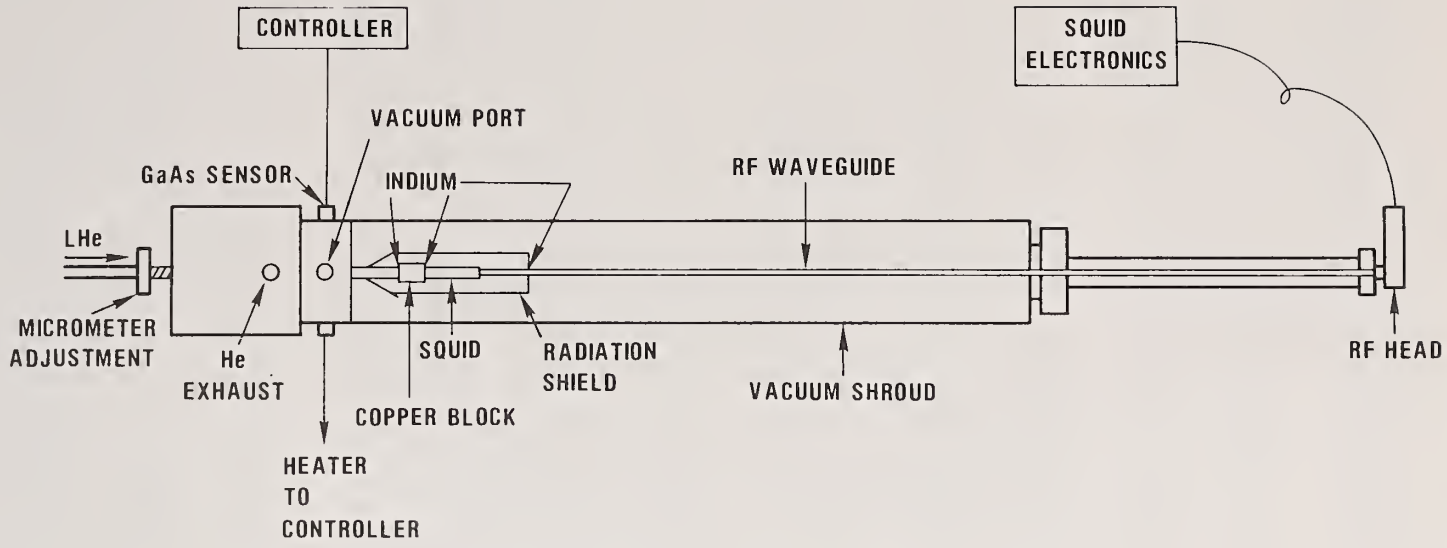

FIGURE 2.

sensitivity, this type of thermometer provided the most favorable non-magnetic interference for the SQUID.

As a secondary means of temperature monitoring, an iron-doped gold vs. Chromel thermocouple was also inserted in the cold head. At the present time we are installing a calibrated silicon diode thermometer into the SQUID interface in an effort to ascertain the ultimate stability of the system over the temperature region of 4.2 to 16 Kelvin.

To perform the required temperature display and control, the Scientific Instruments Incorporated Model 3800 Indicator/Controller was used. This particular instrument is compatible with either silicon diodes or gallium arsenide diodes and provides proportional heater output specified by the programmed temperature set point.

The salient parameters of the controller as it applies to our primary application (4.2 K to 16 K) are as follows:

1. Readout Resolution and Repeatibility (Kelvin)
   ± .002 K from 1K to 10K
   ± .010 K from 10K to 20K

2. With Si-400 Silicon Diode the Readout Accuracy in Kelvin is
   ± .005 K from 1K to 10K
   ± .010 K from 10K to 20K

3. Control Stability at Fixed Set Point with Constant Load and Ambient (in Kelvin units)
   ± .001 K ± .04% of temperature for one (1) minute
   ± .010 K ± .04% of temperature for one (1) hour

4. Power Output
   One (1) ampere at 30 volts
   (maximum for 46 ohm 20 watt heater integrated into Heli-Tran cold head.) [3]

Having had but one opportunity to functionally test the above system, we accomplished a cooldown from 300 Kelvin to 11 Kelvin within ninety (90) minutes after commencement of cryogenic transfer. Unfortunately the desired temperature could not be achieved due to a later discovered vacuum leak in a braze joint on the vacuum shroud. Temperature stability, however, over the temperature range of 11-17 Kelvin was recorded with a stability of greater than ± 0.01 Kelvin; this represented the GaAs readout accuracy.

At the present time the vacuum leak is being corrected and the additional silicon diode is being installed on the interface between the refrigeration assembly and the SQUID device.

References

[1] Meier, R. N. and KOURY, A. G., "Cryogenic Systems for Research at Helium Temperatures" Air Products & Chemicals, Inc., Advanced Products Department, Allentown, PA 18105

[2] Operation Manual for Model LT-3-110 Liquid Transfer Heli-Tran Refrigerators, Air Products & Chemicals, Inc., Advanced Products Department, Allentown, PA 18105

[3] Scientific Instruments Incorporated Data Sheet Number 301277 entitled "Model 3800 Temperature Indicator/Controller".

A CONTAMINATION FREE COMPRESSOR FOR SMALL SCALE STIRLING REFRIGERATORS

J.G. Daunt*, C. Heiden

Institut für Angewandte Physik der Justus-Liebig-Universität Giessen
Heinrich-Buff-Ring 16, D-6300 Giessen, West Germany

Contamination of the working gas appears to be a major problem encountered in the design of reliable small scale Stirling cycle refrigerators for cooling cryoelectronic devices over long uninterrupted periods. Seals for the reciprocating shafts of such a refrigerator may be a source for contamination due to lubrication and possible small leaks. The use of bellows provides the potentiality for a hermetically sealed refrigerator. As a first step towards such a system, a bellows compressor was designed. For increased lifetime, mechanical load on the bellows is reduced significantly by keeping the differential pressure acting on the membranes at a low level. This is achieved by placing the bellows in the volume of a conventional piston compressor. Such a compressor system is tried in connection with a three stage plastic displacer unit. First results on the performance of the scheme are reported and discussed together with possible design variations that may lead to a further reduction of mechanical vibrations and magnetic interference of the cooling unit.

Key words: Bellows; compressor; contamination; continuous operation; cryocooler; low power refrigerator; Stirling refrigerator.

1. Introduction

Low Power Cryocoolers such as developed by Zimmerman et al. [1], [2], [3] are very attractive for use with cryoelectronic components such as SQUIDs or other devices based on the Josephson effect. Long uninterrupted working periods of such a cooler are desirable not only when needed in continuous measurements but also from the point of view of the rather long cool down times of the order of several hours of the refrigerator. It may for example be more convenient to leave the cooling unit for a magnetocardiographic system using a SQUID running continuously than always turning it on many hours before actual use. Since one of the major problems encountered with the design of a continuously running small scale cryocooler is contamination of the working gas, efforts towards a hermetically sealed system were undertaken using bellows as a means for sealing. This paper reports first experiences made during this work.

2. Basic Low Power Cryocooler Design

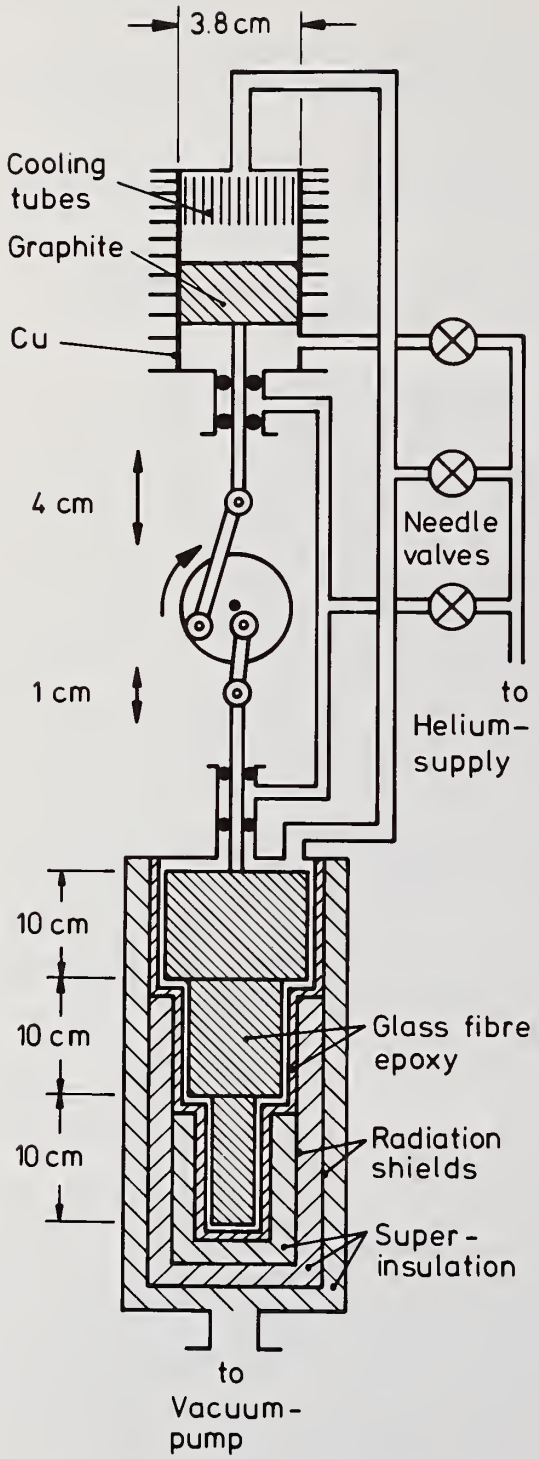

Fig. 1. Basic Stirling cryocooler design.

Our Stirling refrigerator is based on a design similar to that of Zimmerman [1]. The three stage displacer and surrounding cylinder are made of glass fibre enforced plastic (Cadillac G10) with close fit (cf. fig. 1). The lowest stage of the displacer has a bore which is filled with lead shot in order to increase the low temperature heat capacity. The displacer unit is connected to a small compressor which consists of a graphite piston moving with close fit in a copper cylinder. The compressed gas is cooled by a package of air cooled copper tubes located at the exit of the compressor. The piston shafts of displacer and compressor are sealed with double O-rings. The buffer volume between the O-rings is filled with helium gas of the same average pressure as in the compressor. The whole system is connected via needle valves to a helium supply cylinder.

Running this machine with 5 bar average helium pressure and a speed of 115rpm with a compression ratio of about 3:1 resulted in an almost linear initial cool down behavior with a temperature drop $\frac{dT}{dt} \approx 120K/h$, measured at the bottom of the lowest displacer stage. The final temperature was 24K. A reduction in average pressure by a factor of two then resulted in a further decrease of the lowest temperature towards a value near 18K. This is somewhat higher than the final temperature that was reached by Zimmerman and coworkers[1] We expect to obtain a lower temperature after optimization of the present displacer unit.

After an uninterrupted running period of three days, a noticeable reduction in performance however took place resulting in a slow temperature increase of the coldest stage. The origin of this was found in the formation of deposits at the lowest displacer stage causing increased friction. A possible source may be small leaks due to the O-ring seals and also due to some remaining porosity of the plastic material in the displacer unit that lead to losses of helium gas. They are compensated by connecting the refrigerator at appro-

priate locations with high flow impedance (needle valves) to the pressure cylinder of the helium supply. This however requires helium gas of high purity. Otherwise the refrigerator will act as a cryopump on the contaminations in the gas eventually leading to the observed deposits. The transport of air molecules through the O-ring seals along the greased shafts also has to be considered in this context.

3. Cryocooler Using a Bellows Compressor

Since contamination appears to be a fundamental problem with regard to long uninterrupted working periods a straight forward solution to it should be the construction of a hermetically sealed system or at least one that comes close to it. As a first approach we started to build a contamination free compressor. A simple well known means to separate different media for instance in pumps is the use of bellows. Using this principle the present set was modified by inserting a bellows into the piston compressor as shown in fig. 2. In addition to being rather simple, this design has the advantage of keeping the mechanical load on the bellows at a low level which should be of importance for a long lifetime of the bellows. Except for a difference due to the mechanical stiffness of the membranes, the pressure inside and outside the bellows is identical as long as it can breathe.

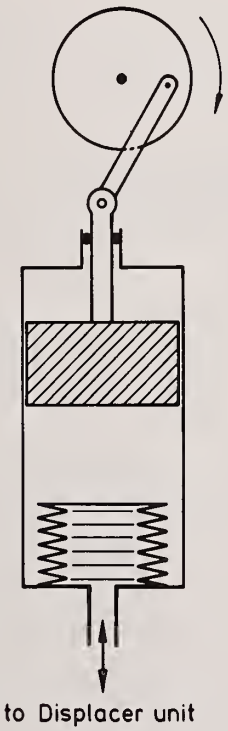

Fig.2: Sealing Bellows inside Piston Compressor

The experience with a stainless steel bellows used in the first experiment however was disappointing. Driven with a compression ratio of about 2 its lifetime was about 10^5 strokes, terminated by fatigue fracture along one of the welded seems.

A lifetime of 10^8 strokes on the other hand would be quite appropriate. A lifetime exceeding this is quoted for commercial bellows made of teflon. Using such a bellows the compressor has been operated with an average helium pressure of 5 bar and without apparent degradation in performance now for a period totaling more than 4 million strokes. Although the compression ratio due to increased dead volume in the compressor was reduced to a value of 2.3 resulting in a somewhat slower cool down rate of about 80K/h, the final temperature again was close to 18K. A problem encountered during the cool down period is the change of average helium gas pressure inside the bellows, which has to be accounted for by a corresponding reduction of the outside average gas pressure. So far this was done manually, but should be effected automatically in a more elaborated design. Much longer testing periods of course are needed before anything definite can be stated about the long term performance of the compressor system, and there may be still other materials superior to teflon for the bellows.

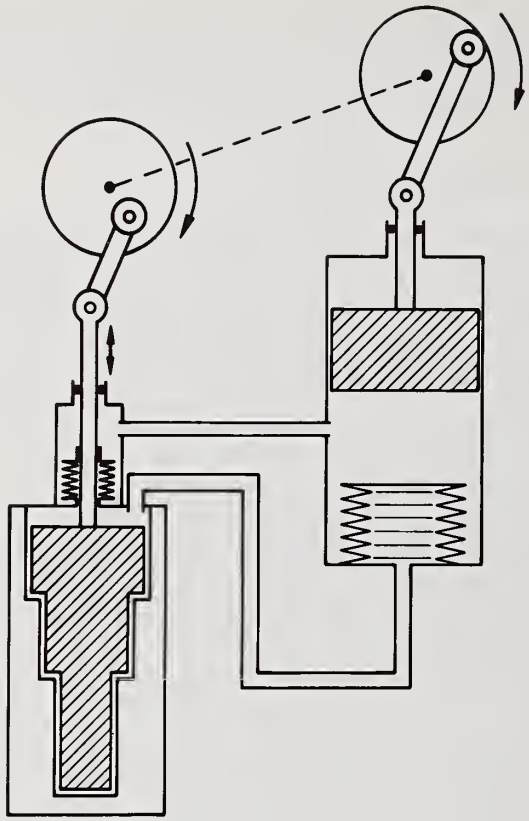

However, before any long period testing is reasonable, the other weak spot in the system has to be eliminated which is the seal at the displacer shaft. This can be done using the same principle (cf. fig.3). To reduce again mechanical load acting on the membranes the sealing bellows is surrounded by a pressure compensation cylinder connected to the outside volume of the compressor bellows. The time constants for filling the volumes of the displacer unit and of the compensation cylinder should of course have about the same value in order to avoid larger dynamic pressure differences at the second bellows.

Fig.3. Hermetically sealed Stirling cryocooler.

4. Refrigerator with Pneumatic Bellows Compressor

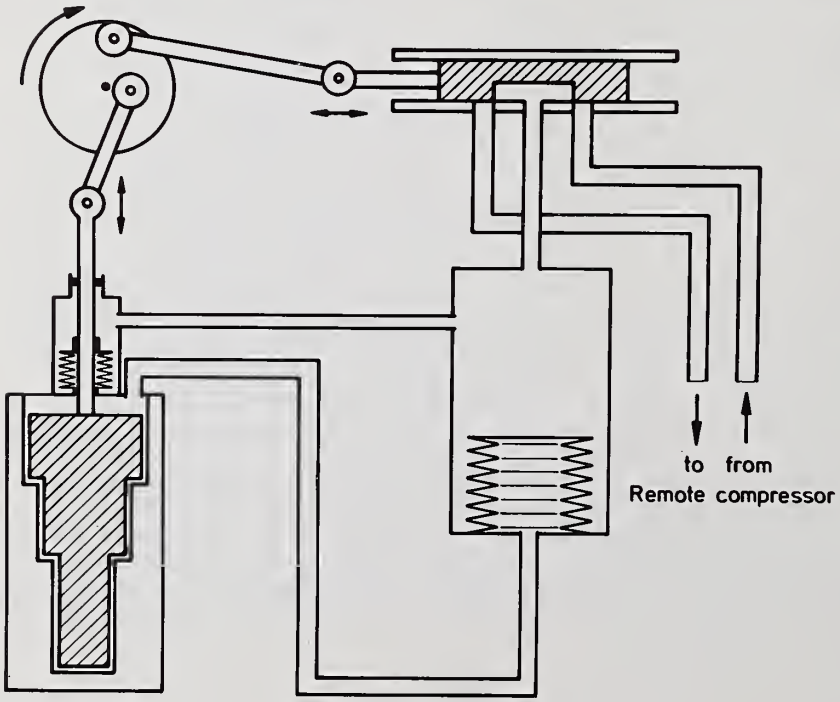

Instead of using a piston compressor to provide the driving pressure of the bellows, one could employ a pneumatic system as shown in fig.4. The compressor bellows is activated by periodically pressurizing and depressurizing the surrounding cylinder via two valves that are controlled by the crankshaft of the displacer unit. This can be done either mechanically as shown or by magnet valves. We tried a

Fig.4. Stirling refrigerator with pneumatic bellows compressor

setup with the latter valve type and found that such a system can be operated successfully with practically the same cooling performance as with bellows in the piston compressor. The inherent advantages of such a system are increased flexibility of design which allows for instance to place sources of electromagnetic interference and of mechanical vibration at locations remote from the cold end of the displacer unit.

Acknowledgements: Part of this work was made possible by a Senior US Scientist award granted one of the authors (J.G.D.) by the Alexander von Humboldt Foundation.

5. References

[1] Zimmerman, J.E., Radebaugh, R. and Siegwarth, J.D., Possible Cryocoolers for SQUID Magnetometers, Superconducting Quantum Interference Devices and Their Applications. Hahlbohm, H.D. and Lübbig, H., eds., Walter de Gruyter, Berlin (1977) p. 287.

[2] Zimmerman, J.E. and Radebaugh, R., Operation of a SQUID in a Very Low-Power Cryocooler, Applications of Closed-Cycle Cryocoolers to Small Superconducting Devices, Zimmerman, J.E. and Flynn, Th.M., eds., US Dept. of Commerce, NBS Special Publication 508, Washington DC 1978, p. 59

[3] Zimmerman, J.E., Cryogenic Techniques for SQUIDs, Proc. of the second intern. Conf. on Superconducting Quantum Devices, Berlin 1980, in print

* Present address: Physics Department, Queen's University, Kingston, Ontario, Canada K7L 3N6.

A BI-DIRECTIONAL LINEAR MOTOR/GENERATOR WITH INTEGRAL MAGNETIC BEARINGS FOR LONG LIFETIME STIRLING CYCLE REFRIGERATORS

Philip A. Studer and Max G. Gasser

Space Technology Division
Goddard Space Flight Center
Greenbelt, Maryland

Linear motors are well suited to drive Stirling Cycle machines since they reduce the machine dynamics to straight line motion. The first device is being constructed as a dynamic balancer for the Stirling Cycle cooler, which is described in a companion paper at this conference. The motor concepts also applies to Stirling Cycle cryogenic coolers, and its advantages in this application are presented. The permanent magnets, pole pieces and drive coils, which form the stator, are stationary and external to the working fluid. The only moving part is the iron piston, which is not in physical contact with anything except the working fluid. It is magnetically suspended and positioned to within 10 microinches by differential capacitive sensors. This allows the clearance between the piston and cylinder to be small enough to form a clearance seal. The piston is also driven electromagnetically and its axial position sensed capacitively. Heat generated in the motor coils does not enter the working fluid. Gas springs allow a controlled resonant drive to minimize power. The same magnetic structure is used for both the drive function and the magnetic suspension. The electromagnetic design along with the sensing and control implementation are described in the paper. Preliminary test data is presented. Magnetic bearing performance characteristics are discussed.

Key words: Clearance seal; gas compressor; linear motor/generator; magnetic bearings; Stirling Cycle.

1. Introduction

The linear motor/generator is the heart of a dynamic balancer which is one element of a long-life mechanical refrigerator system being developed by the Goddard Space Flight Center. The need for cooling capability in space is growing with the use of larger sensor arrays and larger optics as well as future plans for cooled instruments and superconducting devices. Long maintenance-free life is the prime goal since satisfactory short term missions can be accomplished with stored cryogens and satisfactory refrigeration systems are available where maintenance can be easily provided. The goals of this development are directed toward technological advancement of the state-of-the-art as well as providing an effective balancer. To illustrate, the motor concept was the result of an analysis of a basic limitation of linear moving magnet motors and an effort to minimize the mass of the moving element. It establishes a basis for significant system improvements in future refrigeration systems. The major thrust of this overall development is to eliminate all life limiting mechanical wearout phenomena by employing non-contacting bearings and seals and reducing the number of moving elements to a minimum. The first step in this direction is the linear drive motor which does away with the rotary to linear conversion mechanism. There is no crankshaft, connecting rod, or wrist pin, each of which requires a set of bearings. Also to this end, magnetic bearings, a development pioneered by the GSFC in the early 70's[1] for rotary devices, plays a major role. The close clearances imposed by the gas sealing requirements represent a new challenge in bearing design. Good thermodynamic performance requires additional analysis and tradeoffs to operate efficiently with clearance seals. The initial motor analysis rejected some motor types based on highly destabilizing side forces and focused on moving coil and moving magnet d.c. motors. Moving coil motors, which offer lower moving mass (at the expense of power) were discounted because of the need for flexing leads, a reliability hazard. A generalized expression for motor weight and power was programmed (Figure 1) based on fundamental motor equations.

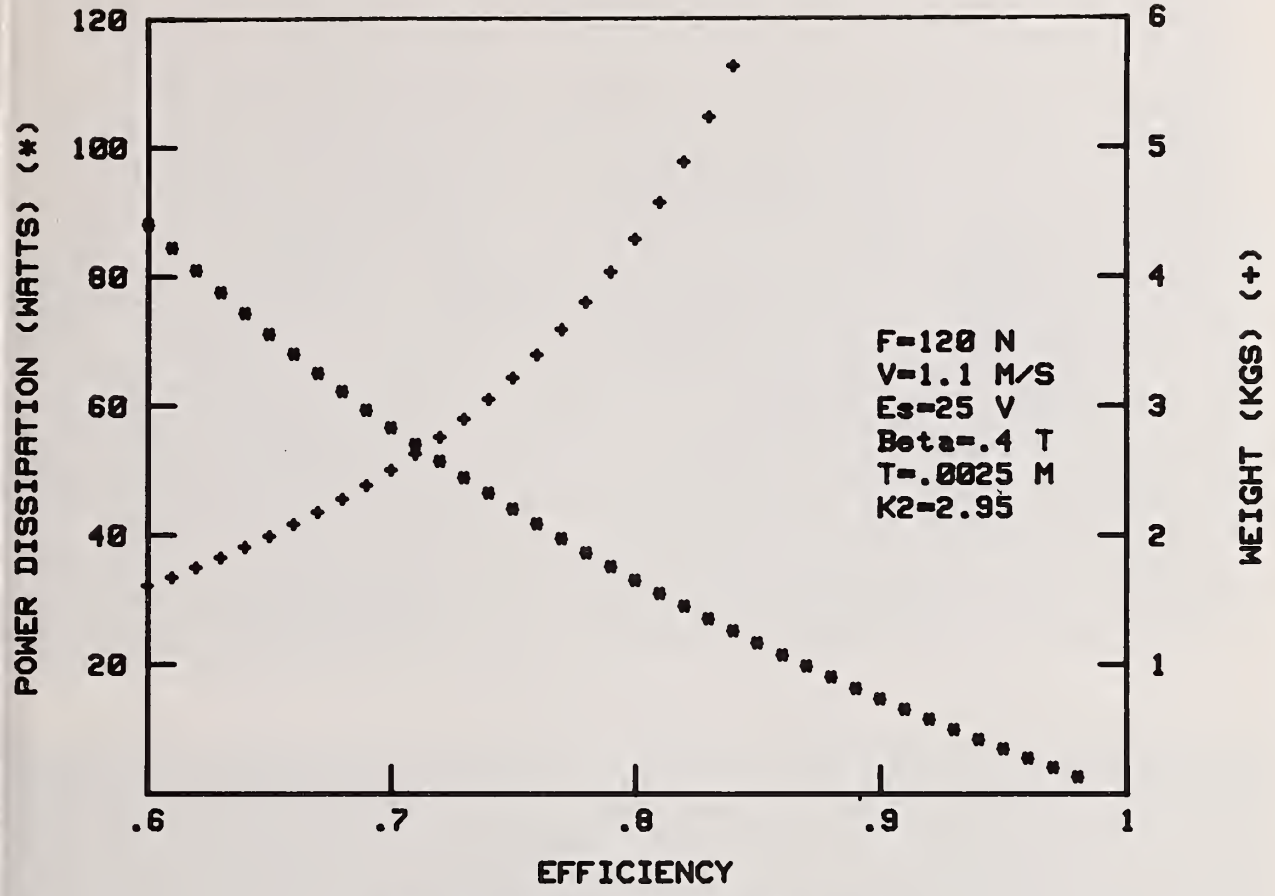

Figure 1. Typical Plot for Linear Motor Sizing

This plot is representative of the way power dissipation and the weight of the motor can be expected to vary for a given set of parameters meeting a particular refrigerator requirement. This procedure established a minimum weight for a given thrust and efficiency with currently available permanent magnet materials with the clear choice of rare-earth magnets. The flux density of these magnets is one fourth the saturation value of magnetically soft steels. These considerations led to the concept about to be described in which the piston is magnetically soft steel and both the permanent magnet and the drive coils are stationary.

2. Linear Motor Description

A permanent magnet biased electromagnet approach was selected. This allows the use of the highest magnetic flux densities, on which the force generation is dependent. The piston, illustrated in Figure (2) is essentially a solid iron bar with the maximum magnetic flux limited only by saturation of the central cross sectional area. This determines the peak axial force which can be generated. In the final design the two end portions are composed of thin ring laminations to reduce magnetic losses.

Figure (3) shows the bare stator structure which is symmetrical both axially and radially. This photograph was taken prior to coil winding to show the structural design. A pair of poles sandwich the permanent magnets at each end and produce a high airgap flux in the major diameter at each end of the piston when it is inserted in the bore. There is some magnetic axial centering force. The permanent magnet and pole assemblies are joined by four bridging elements whose functions will be explained later. A rather thick wall non-magnetic cylinder is interposed between the pole surfaces and the piston.

The magnetic circuit and typical flux paths are seen more clearly in Figure (4). On the right is a cross section of the stator assembly with the piston in place and the motor coil identified.

Figure 2. Piston (Motor Armature)

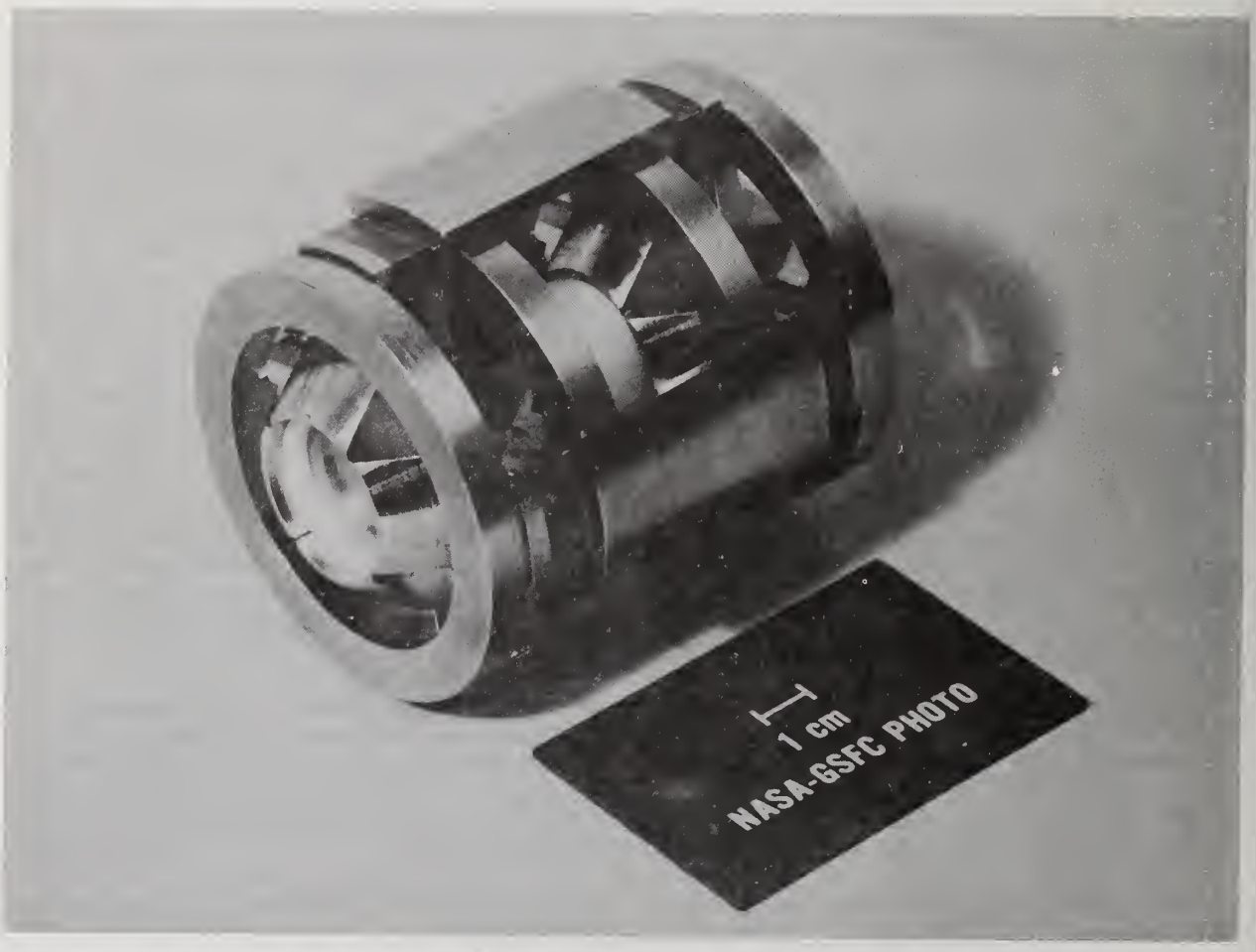

Figure 3. Stator Structure

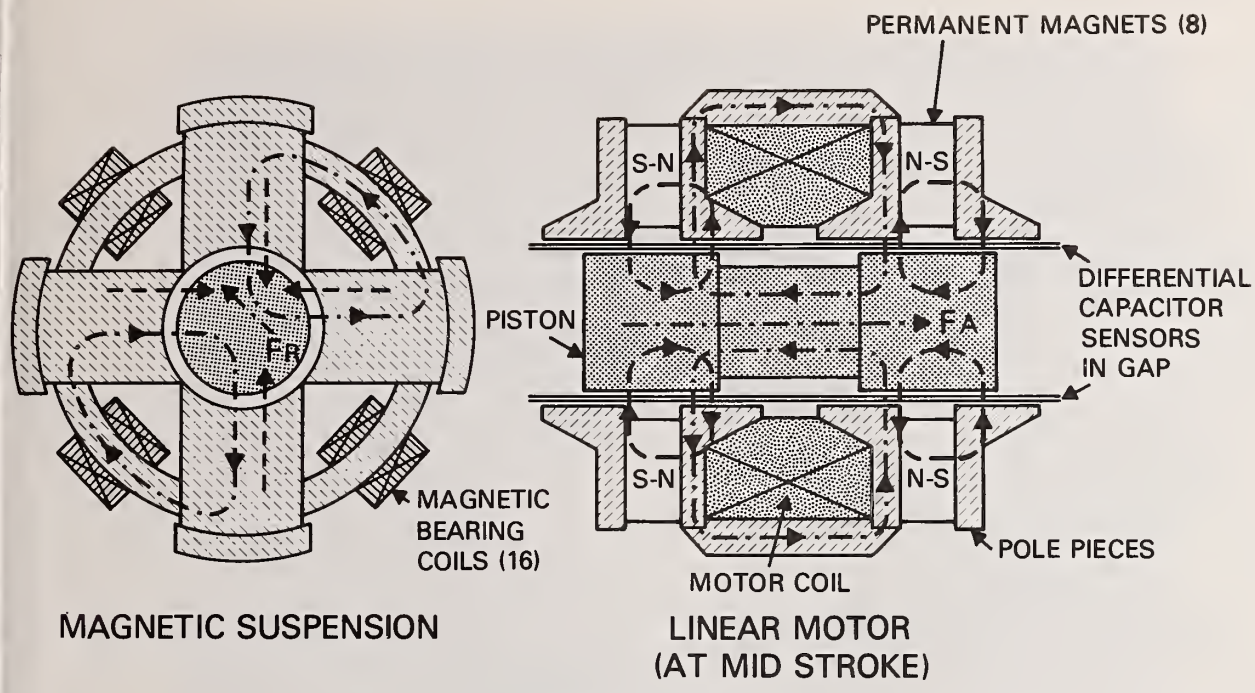

Figure 4. Cryogenic Cooler Balancer at Mid Stroke

Note that none of the permanent magnet flux passes axially through the length of the piston when it is at mid-stroke. The flux from the permanent magnets is radially outward in both of the central gaps which are also part of the motor coil circuit. When the motor coil is energized the flux level on one side increases with a decrease on the other resulting in an axial force. A good motor should also be a good generator and this equivalent reciprocal action is evident in Figure (5).

Here the piston is shown displaced to the left which causes permanent magnet flux to pass down the length of the piston following a path which encircles the motor drive coil. This change of flux occurring in the bore of the coil generates a voltage proportional to the rate of change. The magnitude of this flux change from one end of stroke to the other can be equal to twice the saturation flux level of the piston mid-section. And the mid-section of the piston can nearly fill the bore of the motor coil. Therefore, a highly effective generator and motor action occur. The efficiency of static force generation is the ratio of mechanical power generated to the input power and the differences in the electrical input and mechanical output is dissipation which results in heating. The drive coil resistance can be kept small because of the large volume available for the coil winding and, in contrast to rotary motors, there is no wasted energy in "end turns." All of the copper is effective at all times so that the electromagnetic efficiency can be very high. All of the stator structure in the final design is laminated to reduce magnetic losses. The permanent magnets are Samarium Cobalt, which has a coercive force ten times that of Al_{nicos}, which makes it possible to drive large airgaps.

On the left of Figure (5) you see that each of the poles is actually four elements forming a cruciform shape around the centered piston. The large magnetic gap of 0.25 cm is shown to scale. The piston, when radially centered, is at a point of unstable equilibrium. Huge side forces would be developed if the piston were free to move close to the poles in any direction.

The requirements of the long life refrigerator however, demand clearance seals and the piston is physically limited to move less than ±0.003 cm within the cylinder wall. This means that a relatively thick wall pressure cylinder can be interposed between the moving piston and the magnetic poles of the stator assembly removing all of the windings and magnets outside the pressurized working fluid. This is advantageous from several standpoints; contamination, heat rejection, minimization of dead volume and the structural weight of the pressurized envelope.

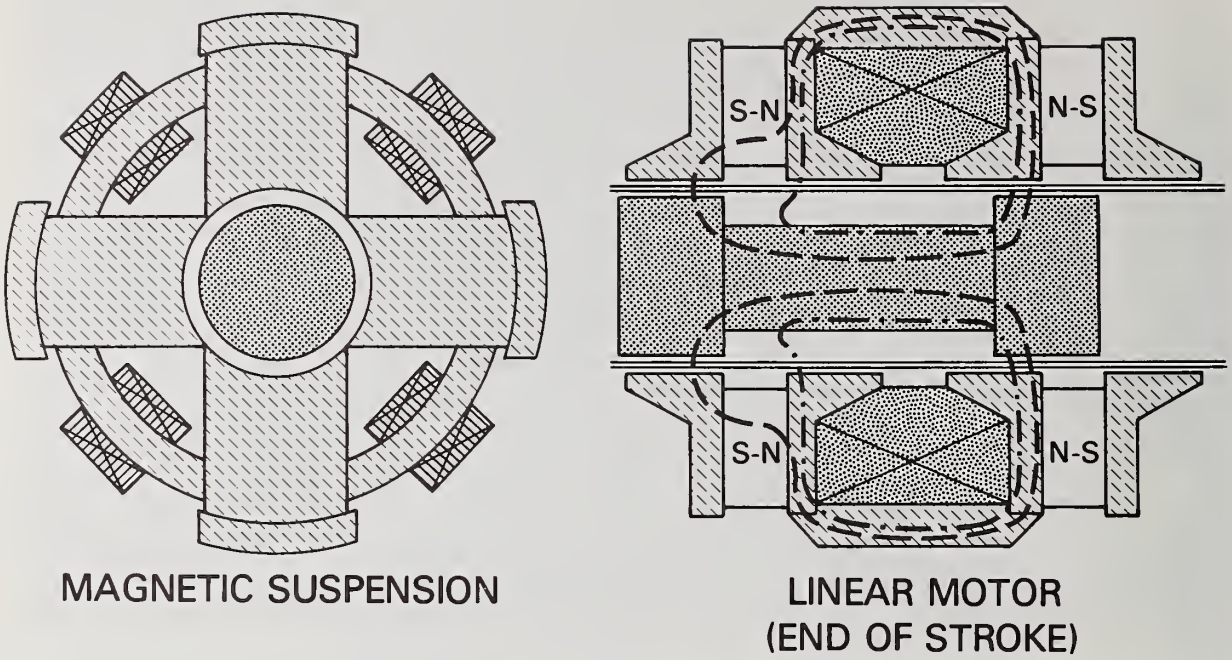

Figure 5. Cryogenic Cooler Balancer at End of Stroke

3. Magnetic Bearing Description

Referring back to Figure (4) left, note that the permanent magnet flux is always similarly directed radially from each of the four surfaces making up the cruciform shape (in this case inward). The suspension control coils are mounted on the ring which connects the outer ends of the cruciform. When a pair of these coils are energized, the normally symmetric flux distribution is altered with an increase in two sectors and a decrease in the other two. A force is generated in the diagonal vector shown which is proportional to the product of the permanent magnet flux and the control flux[2]. This force is directly proportional to the control ampere turns and, just as in this motor, provides linear control at high efficiency. The efficiency is due to the permanent magnet bias flux level for which no power is required.

Active (servo controlled) magnetic suspension is required to obtain the precision necessary to center the close fitting piston within the cylinder bore. Stiffnesses of the order of 1×10^6 Newton per meter are required to overcome static and gas dynamic loads anticipated while maintaining zero contact (displacements less than 20 micrometers). Also required are means to sense the displacement of the piston relative to the cylinder wall.

4. Sensing and Control

We have selected differential capacitive sensing to measure and control the wall clearances. Capacitive sensing is compatible with the large area short stroke requirements. The piston surface itself acts as the passive plate. Figure (6) illustrates the etched capacitor plates which are formed on the inner bore of the cylinder.

There are eight of the smaller plates encircling each end of the piston. Four of these are electrically common and are excited by an A.C. source in the mega Hertz range. The other four form two pairs of sensors whose coupling varies as a function of piston clearance. The inverse action in opposing gaps linearizes the output. A simple demodulation circuit[3] developed by H. Machlanski of Mac Bar Mechanisms, Inc., has been found to be a very effective signal source. Figure (7) shows schematically the four identical radial control channels and a diagramatically similar axial drive servo.

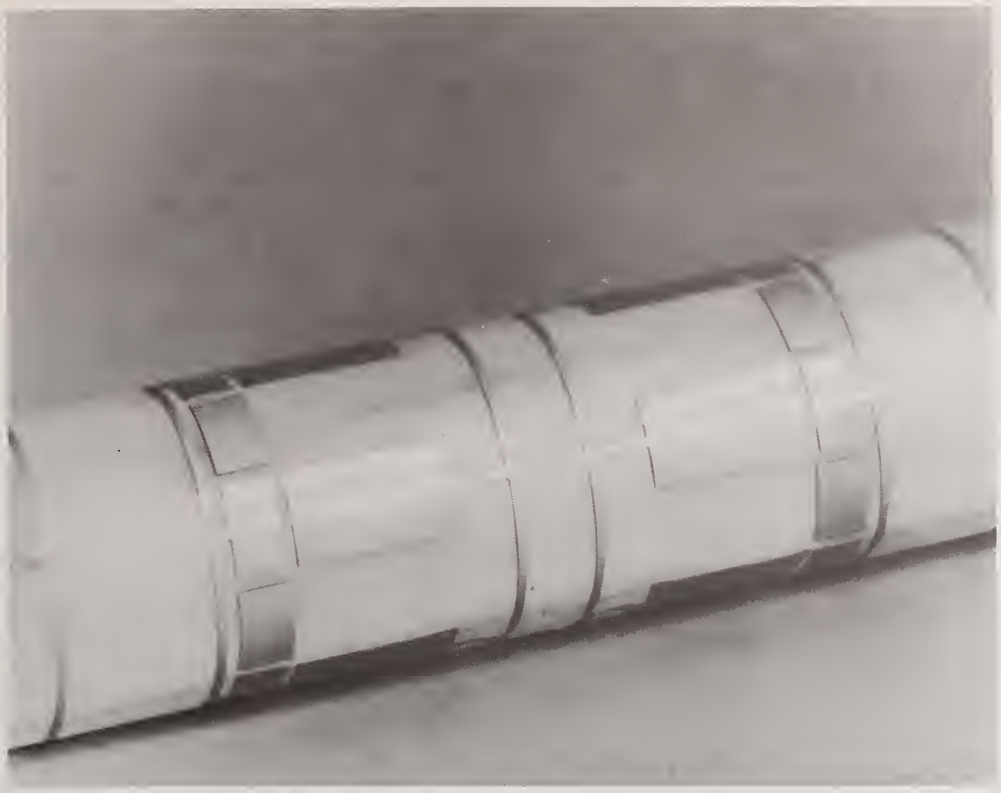

Figure 6. Capacitor Plates

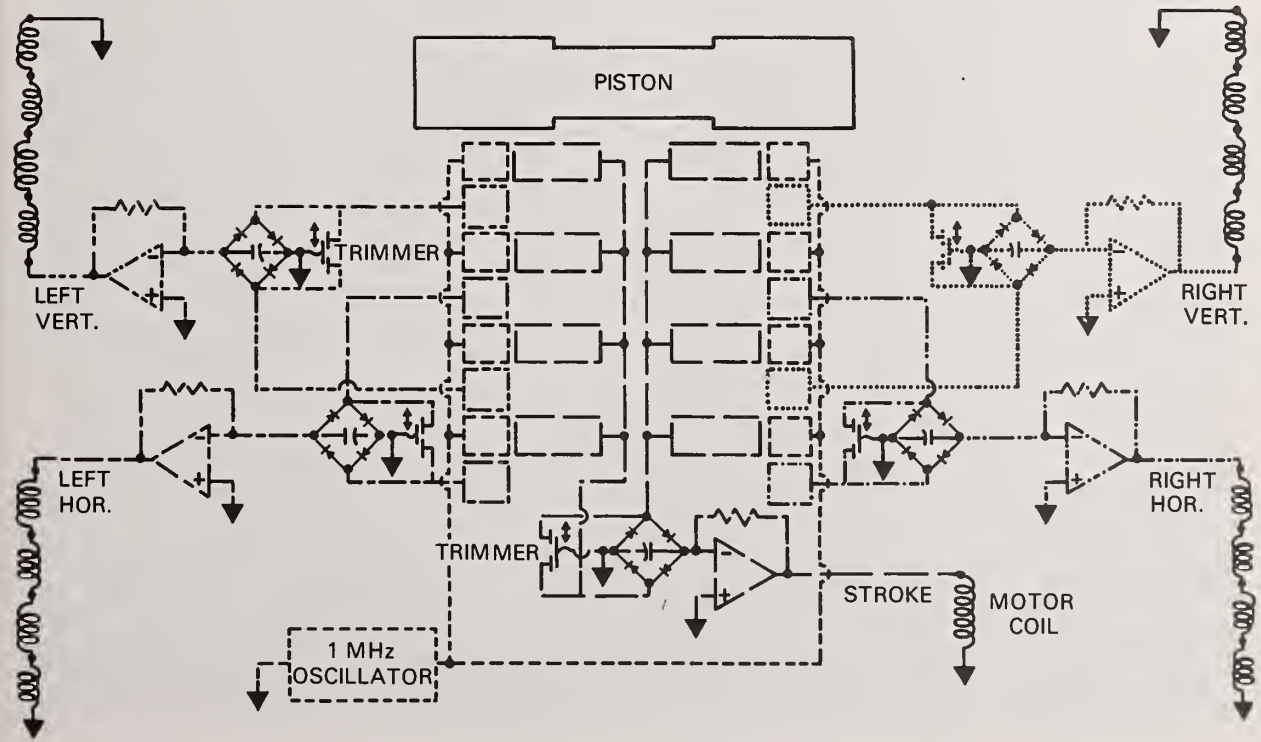

Figure 7. Momentum Balancing System Sensor Circuitry

The two sets of longer plates at each end receive the same excitation and provide an axial position output. For a resonant system only an output phase-shifted from the displacement signal is needed to maintain oscillating motion, in which case the input power is very much smaller than the instantaneous power of the piston. When the piston is doing work on the compressed gas, of course, drive power must be supplied to equal the work done per cycle and the losses. The device currently being developed at GSFC is intended to be used as a dynamic balancer for the Cryogenic Cooler which is the subject of another paper[4] at this conference. The motor drive for the balancer will receive its input from an accelerometer with closed loop control to force the net vibration of the cold finger to approach zero. It will be a resonant system with its piston moving 180 degrees out of phase from the combined center of mass of the power piston and displacer. The control action will force the balancer piston to assume the inverse of the velocity-displacement profile of the machine.

The selection of capacitive sensing avoids the need to penetrate the cylinder wall but requires a dielectric cylinder. We have selected pyrex glass as the gas barrier with vapor deposited capacitor plates on its outer surface. The construction is shown, again diagramatically, in Figure (8). The precision bore cylinder is filamentary wood with fiberglass in an epoxy matrix to provide the pressure containment. The pressurized gas trapped in each end of the cylinder acts as gas springs which, in conjunction with the mass of the piston, forms a mechanically tuned resonator. The electromagnetic and sensor design is such that the entire stator assembly is mechanically separable from the piston-cylinder assembly. There is no physical contact or mechanical friction in the system. Only magnetic and fluid viscous losses will occur.

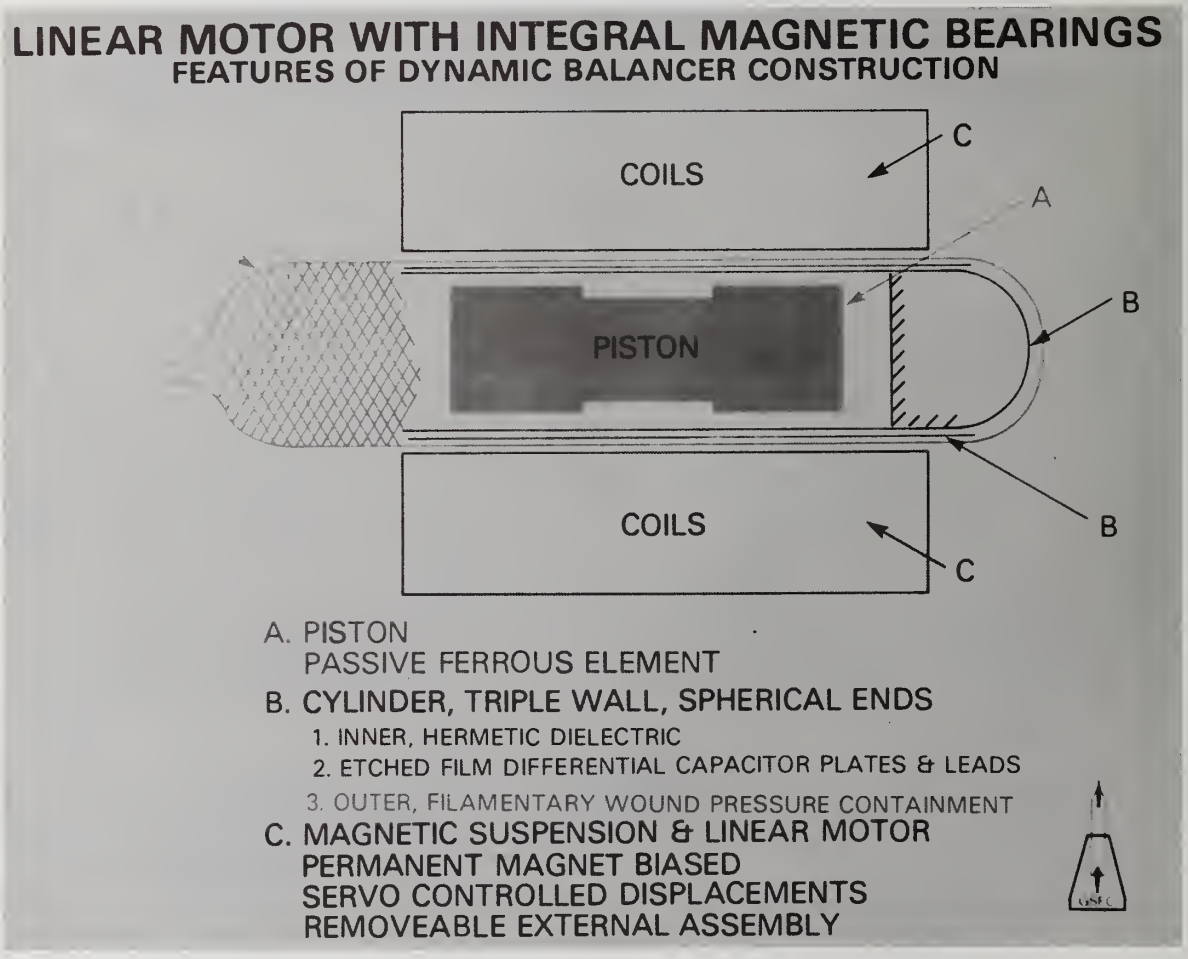

Figure 8. Features of Dynamic Balancer Construction

The entire system for the engineering test unit with associated control electronics is shown in Figure (9). No major changes were necessary as the result of engineering model tests. The design has been scaled up from a 4 cm to a 6 cm diameter bore, all magnetic parts are laminated construction, and a pressure cylinder design following the described approach is underway.

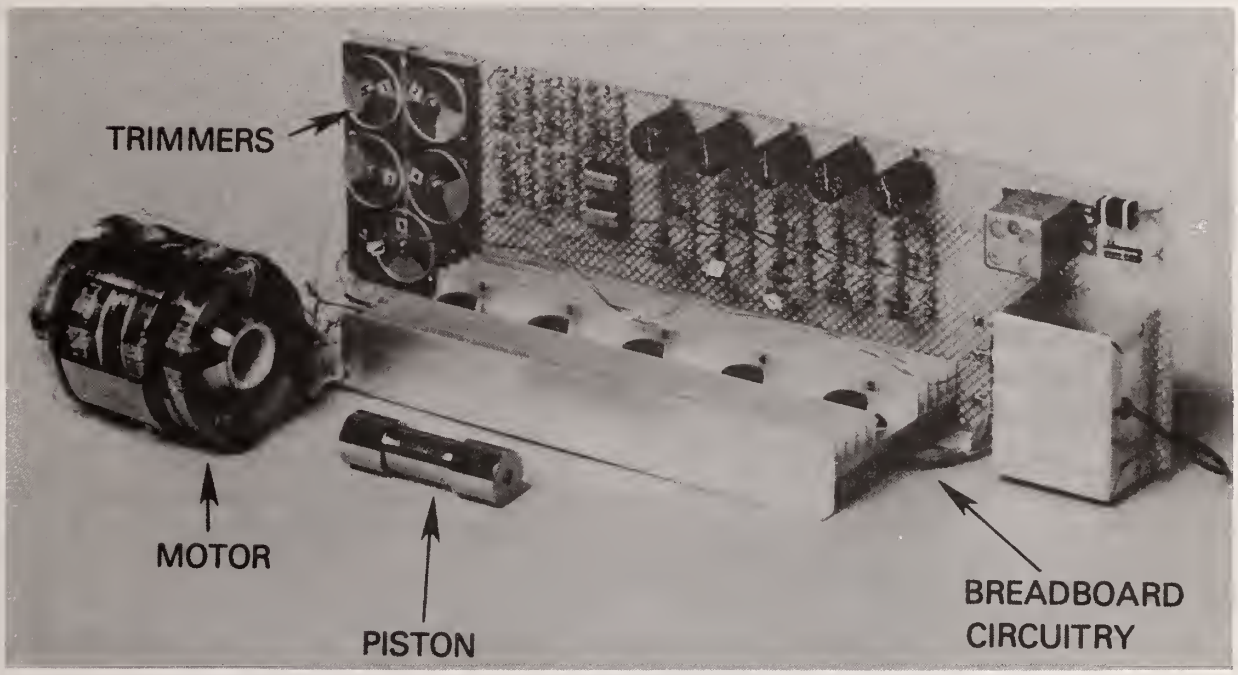

Figure 9. Photograph of Balancer with Breadboard Control Electronics

5. Conclusion

An active dynamic balancer is being developed which is expected to permit the use of reciprocating mechanical coolers of the Stirling cycle type on spacecraft sensors for high resolution imaging. The device has a single moving part and non-contacting magnetic bearings and a novel linear motor/generator. It will provide vibration cancellation with a reliability compatible with multiyear lifetime requirements of upcoming cryogenic cooling systems. In addition, an effort is being made to demonstrate advanced linear motor concepts which are applicable to future designs. The integrated magnetic bearings are also a first and represent a potential weight savings and complexity reduction. Non-contacting sensing techniques particularly well suited to the large area, close clearance, requirements of the suspension and gas springs are being tested.

6. References

[1] Studer, P., "Magnetic Bearings for Spacecraft" GSFC X-721-72-56, Jan. 1972.

[2] Henrikson, et al., "Magnetically Suspended Momentum Wheels" AIAA Aerospace Sciences Conference, 1974.

[3] U.S. Patent No. 3,775,687.

[4] Gasser, M., Sherman, A., and Beale, W., "Developments Toward Achievement of a 3-5 Year Lifetime Stirling Cycle Refrigerator for Space Applications."

DESIGN CONSIDERATIONS FOR MICROMINIATURE REFRIGERATORS USING LAMINAR FLOW HEAT EXCHANGERS

W. A. Little

Physics Department, Stanford University
Stanford, CA 94305

Conventional counter flow heat exchangers are designed to operate with the fluid streams in turbulent flow. The resultant mixing of the fluid allows heat to be transferred from the walls of the exchanger to the body of the fluid. If, however, the dimensions of the exchanger are sufficiently small, enough heat may be transferred by conduction alone that operation in the laminar flow regime is possible. We discuss the design parameters of a microminiature Joule-Thomson cryogenic refrigerator operating in this regime. Such operation offers the advantages of simplicity of design and low noise. The latter is of particular advantage for the cooling of cryogenic sensors.

Key words: Microminiature refrigerators; laminar flow heat exchanger; Joule-Thomson refrigerators.

We have previously discussed the problem of scaling miniature cryocoolers to microminiature size [1]. As discussed by Daunt [2], the pressure gradient in a heat exchanger is related to the mass flow $\dot{m}$ of the fluid, and the diameter d of the tubing through which it flows, by the expression

$$\frac{dp}{d\ell} = 0.10 \frac{16 \dot{m}^2}{\pi^2 \rho d^5 Re^{0.2}} , \qquad (1)$$

where the Re is Reynolds number ($Re = \frac{4\dot{m}}{\pi d \xi}$) and ρ is the density and ξ the viscosity of the fluid. We had shown previously that for a Joule-Thomson (J-T) refrigerator with the heat exchangers operating over the same temperature and pressure regime the diameter of the exchanger tubing should be scaled so that $d \approx \dot{m}^{0.5}$. Where $\dot{m}$ is proportional, of course, to the refrigeration capacity of the device. Reynolds number for the fluid flow in each part of the exchanger is then proportional to $\dot{m}^{0.5}$ too. Thus, as one scales the device to smaller and smaller size, eventually one comes to the point where Reynolds number is too low for turbulent flow of the fluid to occur. For this reason we have considered the possiblity of designing a heat exchanger for operation under laminar flow conditions.

It should be noted that turbulent flow is normally considered essential for the operation of a heat exchanger for the resultant mixing of the fluid allows heat to be transferred from the walls of the exchanger to the body of the fluid. If, however, the dimensions of the exchanger are made sufficiently small, this mixing no longer is so important and sufficient heat may be transferred to the fluid by conduction alone. Laminar flow operation is then possible without loss of efficiency. In this paper we consider the conditions under which such operation can be achieved.

In the truly laminar flow regime, one can calculate the velocity flow profile of the fluid directly from the definition of viscosity. For a counter flow exchanger, such as that illustrated in Figure 1, the flow follows the contour illustrated in Figure 2.

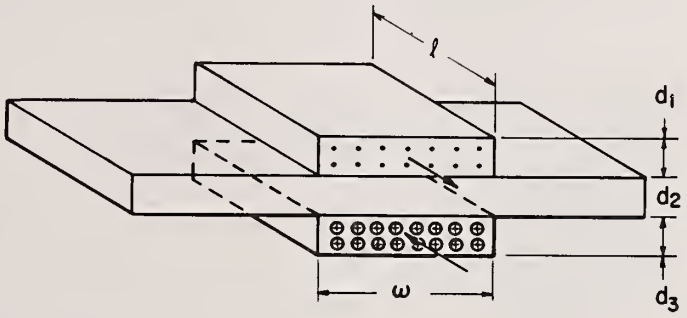

Figure 1. Illustration of counter flow heat exchanger

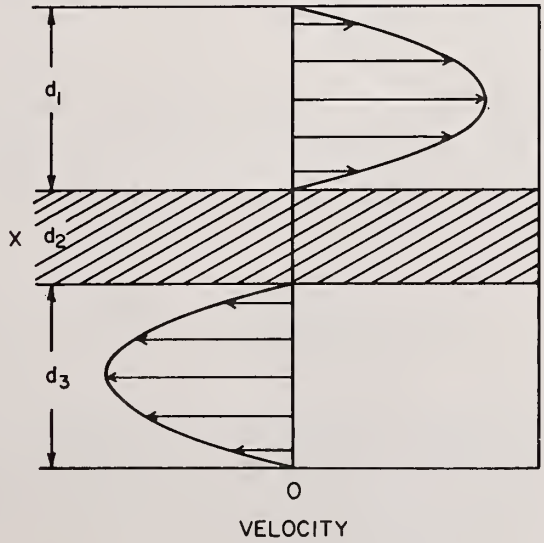

Figure 2. Velocity profile in counter flow exchanger

As the aspect ratio ω/d for the gas channel becomes larger, the edge effects from the finite width of the channel becomes unimportant and the velocity contour becomes almost independent of position. Integrating the volume flow through each channel then gives a mass flow

$$\dot{m} = \left(\frac{\rho}{12\xi}\right) \omega d_1^3 \left(\frac{dp}{d\ell}\right) \quad . \tag{2}$$

Again from first principles one can calculate the temperature profile knowing the thermal conductivity of the two fluids and that of the wall separating the two streams. For the flow profile of Figure 2 one obtains a temperature profile shown in Figure 3.

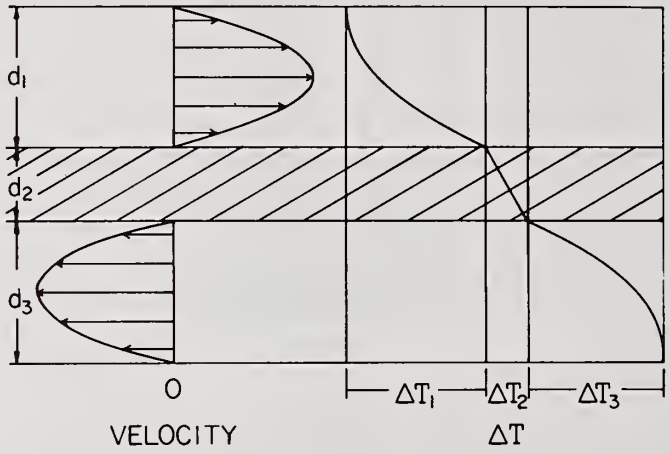

Figure 3. Temperature profile ΔT across a counter-current heat exchanger for the flow profile on the left

Assuming that no heat enters the fluids except through this wall, and that the specific heat per unit mass of each of the two streams is the same; as is the thermal conductivity; and, $d_1 = d_2$, then one can calculate the total temperature drop ΔT from one side of the exchanger to the other. One obtains

$$\Delta T = \dot{m} \left(\frac{C_p}{\kappa_1}\right) \left(\frac{d_1}{\omega\ell}\right) \left(1 + \frac{d_2\kappa_1}{d_1\kappa_2}\right) \left(T_1 - T_2\right) \quad . \tag{3}$$

Where κ_1 is the thermal conductivity of the fluid, κ_2 that of the wall, C_p the specific heat of the fluid, and T_1 and T_2 the temperatures of the hot and cold ends. This expression has a very simple interpretation. Let us rewrite it as

$$\dot{m}\, C_p\, (T_1 - T_2) = \kappa_1 \left\{ \frac{\omega \ell}{d_1 \left(1 + \frac{d_2 \kappa_1}{d_1 \kappa_2}\right)} \right\} \Delta T \quad . \qquad (4)$$

The left hand side represents the heat carried down the exchanger by the movement of the fluid while the right hand side represents the heat conducted across the exchanger perpendicular to this flow. For exchangers of different geometry, the only difference in this expression will be some numerical factors in the denominator of (4).

It is customary to define the efficiency η of a heat exchanger through the expression

$$\eta = 1 - \frac{\Delta T}{T_1 - T_2} \quad . \qquad (5)$$

Where the high and low temperatures and ΔT are as defined as in Figure 4 and expression (3).

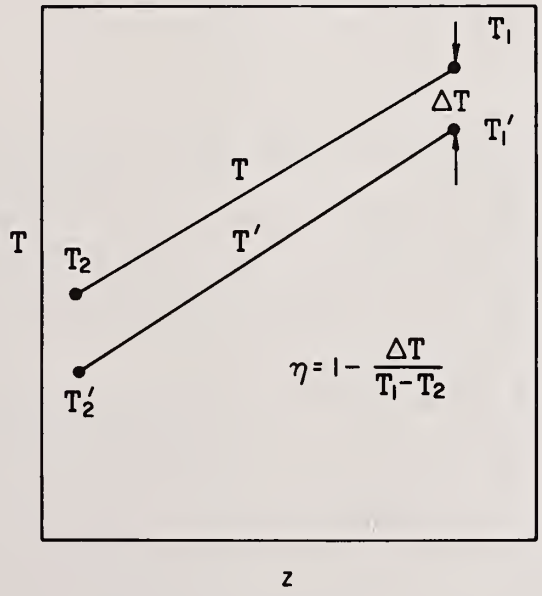

Figure 4. Temperatures in the input (T) and return (T') channels of a counter flow exchanger as a function of distance z along the exchanger

Using (5) in (3) one obtains the result

$$\eta = 1 - \dot{m}\left(\frac{C_p}{\kappa_1}\right)\left(\frac{d_1}{\omega \ell}\right)\left(1 + \frac{d_2\kappa_1}{d_1\kappa_2}\right) \quad . \tag{6}$$

If we assume that the density of the gas is proportional to the pressure so $\rho = \rho_0(p/p_0)$ then (2) can be integrated over the length of the exchanger to give

$$\dot{m} = \left(\frac{\rho_0}{24 p_0 \xi}\right)\frac{\omega d_1^{\,3}}{\ell}\left(p_1^{\,2} - p_2^{\,2}\right) \quad . \tag{7}$$

SCALING CONSIDERATIONS

We consider now the effects of scaling such a laminar flow refrigerator. We assume the ratio d_2/d_1, and the thermal conductivities κ_1 and κ_2 are kept constant. If we eliminate $\dot{m}/\omega$ from (6) and (7) we find that

$$\eta = 1 - \left(\frac{\rho_0 C_p}{24 p_0 \xi\, \kappa_1}\right)\frac{d_1^{\,4}}{\ell^2}\left(1 + \frac{d_2\kappa_1}{d_1\kappa_2}\right)\left(p_1^{\,2} - p_2^{\,2}\right) \quad . \tag{8}$$

So for refrigerators operating over the same pressure regime and having the same efficiency ℓ *should be made proportional to* d^2. Note that this expression is independent of ω the width of the channels so that if we fix p_1, p_2, ℓ and η then we obtain d_1 from (8). Using this value in (7) we can obtain ω for a given mass flow. Different refrigeration capacities can be obtained by varying the width of the channel with no change of the efficiency.

Consider the following example of a 25 mW J-T refrigerator operating with nitrogen gas at a boiler pressure of 3 atmospheres (87K) and an inlet pressure of 120 atmospheres at 300K. If one consults a T-S chart for nitrogen, one finds that for a heat exchanger efficiency of 0.95 a mass flow of about 2.5 mg/sec would be required. Let ℓ = 5 cm for both the high and low pressure channels and assume $d_2\kappa_1/d_1\kappa_2 \ll 1$ (a reasonable assumption in certain configurations) then we find from (8) that d_1 = 35 microns and from (7) the width of the channel ω = 1.1 mm. The pressure drop in the high pressure channel will also be given by (7) and in this case would be about 0.03 atmospheres. A capillary would then be required to drop the pressure from 120 atm to 3 atm. Again using (7) we find that this could be accomplished with a capillary 5 cm long, 110 microns wide, and 6 microns deep. For the flow through the capillary where a large pressure drop is required turbulent flow will persist for refrigerator designs even of very small dimensions. For such cases, the dimensions should be calculated using the turbulent flow expression (1) rather than (2).

This simple analysis shows that microminiature heat exchangers operating in the laminar flow regime can have efficiencies comparable to their larger macroscopic cousins operating under turbulent conditions. One should also note that it is only the area $\omega\ell$ which determines the efficiency of the exchanger in (6) not ℓ alone. This is in contrast to the case for turbulent flow where the requirement of a large Reynolds number and hence a large flow velocity makes it necessary for the exchanger to be long and narrow. For laminar flow, slow flow of the fluid over a broad surface can be used without loss of efficiency. This simplifies the design of miniature laminar flow exchangers and reduces the dimensional constraints in their fabrication. In addition, the absence of turbulence in the exchanger should reduce mechanical noise in the device. The microfabrication techniques described in the accompanying paper by Hollman and Little [3] together with a laminar flow design should make it possible to build efficient J-T refrigerators an order of magnitude smaller than those described hitherto.

Support for this work was provided by the Office of Naval Research Contract N00014-78-C-0514.

REFERENCES

[1] Little, W. A., "Scaling of Miniature Cryocoolers to Microminiature Size" Proc. NBS Cryocooler Conf.
Ed.J. E. Zimmerman and T. M. Flynn, Special Publication 508 (April 1978)

[2] Daunt, J. G., Encyclopedia of Physics, Ed.S. Flügge, Vol XIV, Low Temperature Physics I, Springer Verlag, Berlin (1956).

[3] Hollman, R., and Little W. A., "Progress in the Development of Microminiature Refrigerators using Photolithographic Fabrication Techniques", this issue.

PROGRESS IN THE DEVELOPMENT OF MICROMINIATURE REFRIGERATORS USING PHOTOLITHOGRAPHIC FABRICATION TECHNIQUES

R. Hollman and W. A. Little

Physics Department, Stanford University
Stanford, CA 94305

We report on progress in the development of fabrication techniques for the construction of microminiature cryogenic Joule-Thomson refrigerators using photolithographic means. A new technique for the fabrication of the devices from glass will be described. Consideration has been given to the design of refrigerators operating in this 50 - 200 mWatt region at 77K and 20 mWatt below 20K. Recent results on their operation will be reported.

Key words: Cryogenic; Joule-Thomson; photolithographic fabrication; microminiature devices; refrigerators.

In 1977 Little [1] discussed the scaling laws involved in scaling miniature cryocoolers to microminiature size. It was suggested further that the fabrication of microminiature devices might be accomplished using photolithography. Preliminary work on the development of such a technique for the fabrication of a Joule-Thomson (J-T) refrigerator on a silicon wafer was reported at a conference in Charlottesville in 1978 [2]. We wish to report here the development of a class of J-T liquefiers designed to operate at liquid nitrogen or hydrogen temperatures with a capacity of the order of 100 mW. These have been fabricated using photolithography on glass. Single stage devices have been operated successfully below the critical point of nitrogen with a refrigeration capacity of 100 mW at 122K. Typical channel dimensions are of the order of 100 microns, and the flow rate about 30 ml/sec (STP) of nitrogen at an inlet pressure of 1600 lbs/in^2. The theory of turbulent flow heat exchangers as treated by Daunt [3] was found to be applicable on this scale and our results at these small flow rates confirm the belief that efficient heat exchangers can be built in a very small space. The principal problems in the construction of these devices are now understood. We expect these one stage and two or three stage refrigerators of this type will be useful in cooling very small material samples, or instruments in which heat production is minimal.

A J-T refrigerator consists of three sections: a high pressure inlet channel, a low pressure outlet channel which together form the heat exchanger; and, a narrow capillary connecting the two to confine the pressure drop to the cold end (Fig. 1).

(a) (b) (c)

Figure 1. Detail of microminiature J-T refrigerator showing
(a) inlet and outlet ports
(b) heat exchanger
(c) capillary expansion channel

The present devices are constructed by etching grooves in a glass surface, then sealing them with a glass cover plate.† Earlier work [2] used methods described by Terry [4] to etch channels in silicon sealed with pyrex. These silicon devices operated successfully with carbon dioxide or ethylene as the refrigerant. However, attempts to operate them to LN_2 temperatures failed because the high thermal conductivity of Si necessitated the design of excessively fragile heat exchangers which could not contain the high pressures required for efficient operation with N_2. For these larger temperature differentials, the low thermal conductivity of an amorphous material such as glass is necessary. The geometry of the devices together with the exacting sealing criteria required the development of an etchning technique which would allow deep etching if the grooves with minimal lateral etching or undercutting.

Chemical etching with HF proved unsatisfactory. A new technique for the precise, directive etching of any amorphous or crystalline material was developed.† The surface to be etched is prepared by coating with a thick water solution of gelatin activated with potassium dichromate. It is then dried, exposed through a mask to ultra violet light and developed in hot water. The unexposed gelatin washes out leaving a pattern of unprotected glass. This resist forms an exceedingly tough thin protective coating. The coated glass is then mounted on a rotating holder in a lathe-like device and abraded with 27 micron Al_2O_3 powder entrained in a high velocity gas stream using an S.S. White Airbasive unit with the nozzle scanned across the surface of the glass. Channels of precisely controlled depth in the range of 2 - 100 microns can be etched in this manner.

To complete the fabrication of the refrigerators a cover slide is sealed to the etched plate using a thin film of a UV-curing adhesive. Stainless steel hypodermic tubing epoxied to the glass plate provide inlet and outlet connections (Fig. 2). Details of the etched slide are shown in Figure 3 and Figure 4.

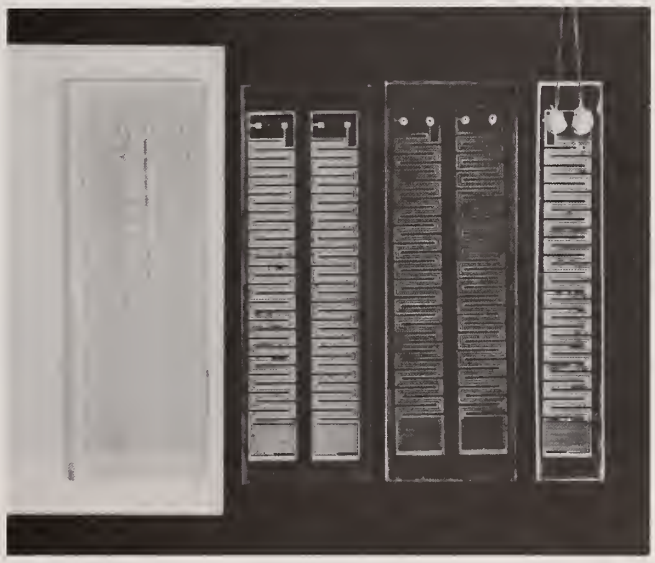

(a) (b) (c) (d)

Figure 2. Steps in fabrication of microminiature refrigerator

(a) coated, exposed and developed glass slide

(b) slide after abrasive etching

(c) slide with cover plate bonded to it and inlet and outlet ports drilled

(d) completed refrigerator with stainless steel gas lines epoxied to inlet and outlet ports

The planar construction together with the need for containing the high pressure requires a cross section of material much greater than that of the channels themselves. For this reason, solid conduction is a significant heat load. This dictates the use of glass for construction, and makes a thin, narrow device preferable.

Bonding the glass proved to be difficult. An adhesive is needed which will hold the pressure used with a layer less than 10 microns thick. Complete wetting of the surfaces must be obtained without filling the narrowest channels with adhesive.

The purity of the refrigerant gas is critical for these open-cycle devices. The capillary can be blocked by about 1 microgram of condensed impurities. We have used nitrogen of 99.996% purity, and passed this through an activated charcoal trap at ambient temperature. Operation for 1 to 2 hours has been achieved to date. Longer operation will require higher purity gas or a trap built in to the heat exchanger. The limitation on the lowest temperature reached is the back pressure of the gas in the return channels: The present devices were designed to have a rather deep capillary to minimize difficulties with the adhesive during the bonding step. This results in a larger flow and a back pressure at the boiler of the order of 200 lbs/in^2, limiting the low temperature end to 110K or above. A minor change in the design should correct this.

Figure 3. Detail of etched channels of heat exchangers showing high pressure channel between the two low pressure return channels. The high pressure channel is 300 microns wide and the separating walls 150 microns wide.

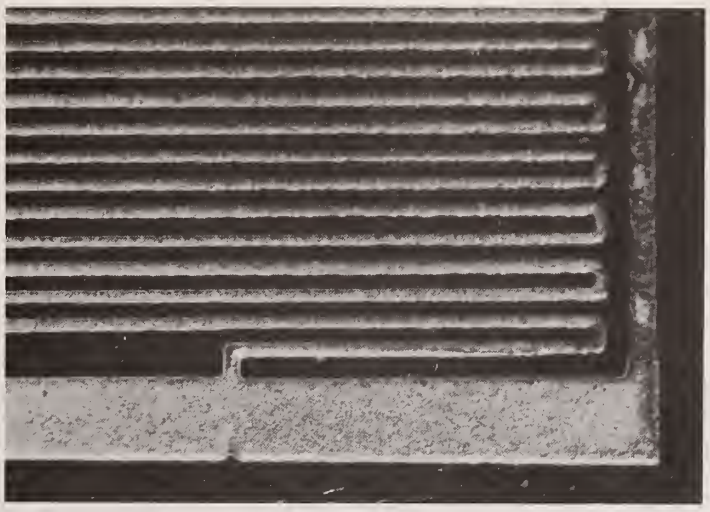

Figure 4. Detail of etched slide showing capillary expansion channel and part of boiler. Capillary is approximately 100 microns wide and 50 microns deep.

The design currently in use measures 75 x 12 x 2 mm and has a 30 cm long heat exchanger. The cooldown time is 8 minutes. Smaller, less massive devices are now being developed using thinner glass substrates which should result in substantially faster cooldown times. A hydrogen liquefier with integrated nitrogen precooler is also being developed for operation to 23K.

The present design is being considered for use in microcalorimetry, optical reflectance spectroscopy, and IR transmission spectroscopy experiments. A sample mount can easily be integrated into the design. For reflectance spectroscopy, the refrigerator and its vacuum shroud are small enough for mounting on a goniometer at room temperature.

This work was supported in part by the Office of Naval Research, Contract N00014-78-C-0514.

REFERENCES

[1] Little, W. A., "Scaling of Miniature Cryocoolers to Microminiature Size" Proc. NBS Cryocooler Conf. Ed J. E. Zimmerman and T. M. Flynn, Special Publication 508 (April, 1978).

[2] Little, W. A., "Design and Construction of Microminiature Cryogenic Refrigerators" in Future Trends in Superconductive Electronics, Ed B. S. Deaver et al, APS Conf. Proc. 44, 421 (1978).

[3] Daunt, J. G., Encyclopedia of Physics, Ed. S. Flügge, Vol XIV, Low Temperature Physics I, Springer Verlag Berlin (1956).

[4] Terry, S. C., Ph.D. thesis Stanford University (1975) (NASA Technical Report 4603-1, 1975).

† Patent Pending.

LOW TEMPERATURE REGENERATORS

Lawrence A. Wade

Lockheed Palo Alto Research Laboratory*
3251 Hanover Street, Palo Alto, California 94304

A study was conducted to examine ways of enhancing the heat capacity of regenerators used in refrigerators for achieving refrigeration below $30^{o}K$. It was found that, due to an increase in the energy of their surface vibrational modes, thin films, thin wires, and ultrafine particles will exhibit a higher specific heat than that which would be normally expected for a bulk sample of the same material.

Based on an idealized refrigerator performance model, it is predicted that a Stirling cycle refrigerator having the third stage of its regenerator replaced with an ultrafine particle (22 Å dia. lead particles) matrix whose void volume is partially filled with mercury, will deliver at a cooling temperature of $10^{o}K$, 2.75 times as much refrigeration as one with a typical third stage regenerator made up of 0.005" dia. lead spheres.

A table showing the expected improvements in refrigerator performance from the use of several ultrafine particle configurations is presented.

Key words: Heat capacity; regenerators; specific heat; refrigeration; cryogenics.

1. Specific heat enhancement

The efficiency of refrigerators for cooling below $20^{o}K$ has been, to date, severely limited by poor regenerator performance. The primary cause of poor regenerator performance at these temperatures is the fall-off of the regenerator matrix's heat capacity.

This paper deals with how the heat capacity of the regenerator might be improved.

The model typically used to describe a material's specific heat at constant volume is:

*Author's present affiliation. This paper presents work partially done while with Scitech. Corp. It was supported by AFWAL Flight Dynamics Laboratory, Wright-Patterson AF Base, Ohio, under Contract F33615-78-C-3425. Also presented is work done at Lockheed Palo Alto Research Laboratory under IR & D funding.

$$C_v = \beta T^3 + \gamma T \quad . \tag{1}$$

This model is based on the assumption that the material is an elastic continuum. In the case of extremely large surface to volume ratios this assumption is not accurate. The number of lattice sites and the number of possible vibration modes were significantly undercounted. E. W. Montroll discerned this and derived a set of frequency distribution functions taking this into account. Using the same approach and assumptions as Debye, with the exception already noted, he derived a new specific heat model.

$$C_v = \beta T^3 + \alpha T^2 + \gamma(1+\varepsilon)T \quad , \tag{2}$$

where

$$\alpha \propto \frac{S' \rho^{2/3} M^{1/3}}{\theta_D^2} \quad ,$$

and

$$\varepsilon = \left(\frac{9\pi}{N_o}\right)^{1/3} \frac{S'}{24} \left(\frac{M}{n^*}\right)^{1/3} \rho^{2/3} \quad ,$$

where S' is the specific surface area, ρ is density, M is atomic weight, θ_D is the Debye temperature, N_o is Avogradros number, and n* is the average number of conduction electrons per lattice site. The surface contribution would be expected to become significant only at very low temperature and for large surface to volume ratios. The details of this derivation are beyond the scope of this paper, but they may be found in Reference [1].

A series of measurements of the specific heat of ultrafine particles have been made over the years. They have been performed on metals such as palladium and vanadium, as well as dielectrics, such as magnesium oxide. They indicate that Montroll underestimated the surface contribution by a factor of between 4 and 6 (Ref. [1]).

Modifying the corrections made by Montroll to take the experimental results into account, we find

$$C_v = \beta T^3 + 4\alpha T^2 + \gamma(1+4\varepsilon)T \quad . \tag{3}$$

Applying equation (3) to lead and mercury, it is evident that the surface effect is indeed quite significant (see figures 1 and 2).

It was assumed in this study that the assumption from which equations (1) - (3) are derived (that $T \ll \theta_D$) was accurate up until $T = \theta_D/8$. Thereafter it was assumed that the surface enhancement effect would decrease to 0 at $\theta_D/3$. No measurement of ultrafine particle specific heat has been attempted yet in the range where the assumption $T \ll \theta_D$ is not reasonably valid.

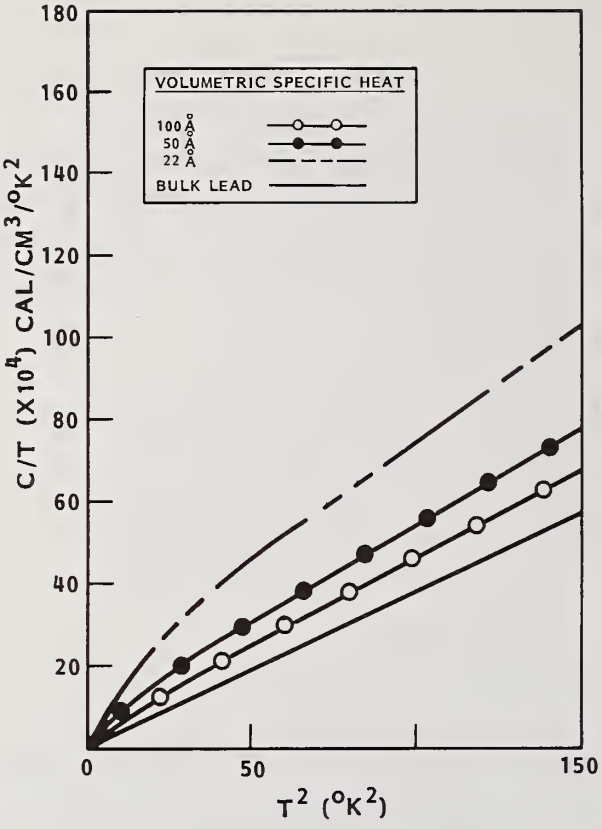

Figure 1. Lead volumetric specific heat.

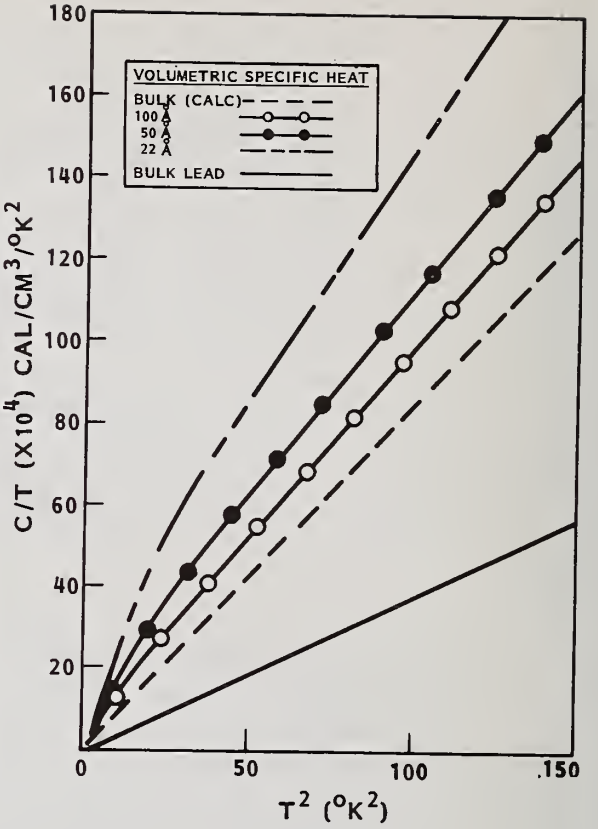

Figure 2. Mercury volumetric specific heat

There are a number of different lattice dynamics models which have been developed since the work by Montroll. However, to date, none of them appear to be superior to the simple model of eq (2) in predictive value. For this reason, the Montroll model was modified to fit the existing experimental data (eq (3)).

An experimental program examining the specific heat of ultrafine particles up to 100°K could give some insight into the physics of specific heat which would be valuable to future workers in this field. A program of this type would allow an empirical modification to be made on eq (2) which would improve on the accuracy of the predictions made by eq (3). In addition, the assumption made as to the degradation of the surface contribution, as a function of temperature, could be eliminated and instead, an empirically based model used to predict refrigerator performance.

2. Utilization of ultrafine particles

There are two candidate methods for the utilization of ultrafine particles, both of which are derived from the powdered metallurgy industry. The first method is derived from techniques used during the formation of sintered parts.

2.1 Green compacts

The first stage of preparation of sintered parts involves pressing metal powder into "green compact". At this stage the metal will hold together but the surface welding between particles is minimal. The extent to which the surface welding occurs is related to the pressure exerted during compaction. The second stage involves heating the green compact to just under the materials melting point. At this temperature heavy surface welding takes place, "sintering" the powder together, and thereby increasing its mechanical strength. For this application, heavy surface welding would be undesirable as it would destroy the discreteness of the particles. An optimum pressure must be determined which will provide maximum strength and density of the element without causing an excessive amount of surface welding.

Once formed into a green compact, gas flow passages will need to be fabricated in order to minimize the pressure drop through the regenerator. The end result would approximate a conventional screen. If the gas flow passages are aligned, pressure drop losses could be kept to a minimum.

It is also expected that the helium gas used as the working fluid will contribute to the regenerators heat capacity. In the model used when predicting the performance of a refrigerator with an ultrafine particle regenerator, the helium gas was at a base cycle pressure of 40 atm. It would seem reasonable that some of the helium gas would be adsorbed and absorbed, and would thereby contribute to the regenerator's heat capacity. In the case of 22Å dia. particles this effect is expected to be maximized because the particles are only about 5 lattice sites across and have a large specific surface area (200 m^2/g).

Absorption refers to the diffusion of the gas through the host metal's lattice structure, thereby forming a solution. Gas which has been absorbed into the lattice can be considered to represent, from the standpoint of the gas specific heat, a solid. Unfortunately, it is found that helium will not diffuse through a metal lattice structure (Ref. [2]). Therefore, there will be no contribution to the regenerator matrix's heat capacity from the absorption of helium gas.

Adsorption is caused by an attractive force which is exerted in a direction normal to the surface by the atoms at the surface of a solid. The attractive force is a result of Van der Waals forces which arise from dipole interactions between the solid and the gas.

This is referred to as physisorption, and is the only kind of adsorption which can occur between an inert gas and a metal. It is therefore found that at a gas/solid interface the concentration of gas exceeds that of the gas not in the solid's immediate vicinity. The excess gas at the surface is referred to as having been adsorbed. At the warm end of the regenerator ($35^{o}K$), it is reasonable to expect that only a few percent of a monolayer of gas will be adsorbed. At the cold end ($10^{o}K$), about one monolayer will be adsorbed (Ref. [3], [4]). In terms of the specific heat contribution from the adsorbed gas, it is best to consider it to be a liquid.

A further contribution to the regenerators heat capacity comes from the helium trapped in the pore structure of the green compact which is not in the gas flow stream.

Green compacts do have the disadvantage of low mechanical strength. It is uncertain what the long term effect of gas cycling would be on a green compact. As it is not presently possible to contain particles smaller than 200 Å, if any particle should break off the compact some migration would result. This is undesirable, as it is conceivable that seal and bearing deterioration could result.

2.2 Mercury impregnated green compacts

The second method of utilization also involves the fabrication of a green compact; after which mercury is pressed into the pore structure. A significant portion of the mercury (greater than 50% if the process is repeated) will be retained in the green compact. This results in the matrix having a significantly higher heat capacity. Mercury has a higher low temperature specific heat than lead, a higher density, and a lower Debye temperature. This results in a large surface contribution to the specific heat. This process is referred to as mercury porosimetry.

This approach has several advantages. Pressed into the pore structure, the mercury will have a high surface to volume ratio, and it is hoped will thereby evidence a surface enhancement of its specific heat. The thermal conduction of the compact is also expected to be enhanced. This will result in a more efficient heat transfer between the regenerator and the refrigerant gas. The contribution to the regenerator's specific heat by the mercury is the most important advantage. Because of the properties already stated, mercury would be the preferred regenerator material if it weren't a liquid at room temperature; but, by containing the mercury within the ultrafine particle pore structure, this difficulty is overcome.

It is expected that some amalgamation will occur between the mercury and the host metal, which will result in a much stronger structure. This results in the individual particles being more tightly bound to the compact structure and will probably solve the potential problem of particle migration. It is unknown whether a sufficient boundary will

exist after amalgamation to form a wave reflection, or scrambling boundary, for the low frequency acoustic vibrations, and therefore, whether the full Montroll effect will be realized.

3. Anomaly materials

An alternative to using ultrafine particles would be to find a material with a very high bulk specific heat. The best materials which has so far been found is GdRh. It evidences a very high heat capacity compared with lead below 20K. There would appear to be at this time no reason why GdRh could not be formed into .005" dia. spheres or into 400 mesh screen.

Because GdRh has a relatively high Debye temperature; in calculating the specific heat of GdRh from equation (3) it is found that the surface contribution is only about 3% of its total specific heat. Therefore, in this report, it is examined as having been fabricated into .005" dia. spheres.

GdRh is exceptional in that it evidences a broad band specific heat anomaly extending from 20^{o}K to below 2^{o}K (Ref. [5]). Most materials which evidence an enhanced specific heat do so over a narrow range of temperatures; or typically only a few degrees. Once the temperature profiles of a regenerator are better understood, another approach might be to utilize a number of materials which evidence this sort of enhancement (called a lamda transition-normally caused by a phase transition) in a segmented approach to regenerator design. Examples of this type of material are $DyRh_xB_y$ and $(ErHo)Rh_xB_y$.

4. Regenerator analysis

The refrigerator performance model is based on an idealized 3-stage Stirling cycle design. The refrigerator is assumed to have a base cycle pressure of 40 atm and to operate at 600 rpm. The third stage is designed to provide .3 watts of net refrigeration at 10^{o}K with a gross output of 2.785 watts utilizing .005" dia. lead spheres as the regenerator matrix. This will require a 167 design NTU value (λ) for the regenerator, and a refrigerant gas mass flow rate of .8077 g/sec. The NTU value is defined as

$$\lambda = \frac{A_T U_{AV}}{C_g} \quad ,$$

where A_T is the heat transfer area, U_{AV} is the overall coefficient of heat transfer and $C_g = \dot{m}c_p$ is the gas flow stream capacity rate. The refrigerator performance model is described in detail in Ref. [1]. The regenerator efficiency was determined using a computer program based on work by Lambertson (Ref. [6]). The program uses the finite difference method to calculate the regenerator's temperature distribution and efficiency. It is assumed that there is no outgassing of the helium contained in the regenerator's pores due to pressure fluctuations.

The results described are functions of regenerator heat capacity only. All else, including pressure drop (7 psi assumed), is held constant for all the cases.

The cases described utilize the .005" dia. lead spheres regenerator matrix as the baseline. Case 2 utilizes .005" dia. GdRh spheres in the last third of the regenerator, the first two-thirds (warm end) being made up of lead spheres. Case 3 deals with 22 Å lead particles in a green compact without gas contributions taken into account. Case 4 is the same as Case 3 except that gas contributions to the regenerator's heat capacity are taken into account as described in section 2.1. Case 5 is a mercury impregnated 22 Å lead particle regenerator without amalgamation. Case 6 is the same as Case 5 except that it is assumed that 75% of the surface specific heat contribution is lost to amalgamation.

The data shown is the percent of required refrigeration delivered where the required refrigeration is 0.3 watts at $10^{o}K$, the design NTU value (λ), the effective NTU value (λ_o), where

$$\lambda_o = \frac{\varepsilon}{1-\varepsilon}$$

and the regenerator efficiency (ε). Note that λ_o and ε are the values for the third stage of the regenerator, not for the entire regenerator.

From the results presented in Table 1 it can be concluded that:

(1) GdRh substituted for lead in the cold end of a regenerator gives a significant improvement in refrigeration over a lead sphere regenerator.

(2) Although a significant portion of the 22 Å green compact regenerators heat capacity is contributed by gas adsorption and gas in the interstitial pores; lead ultrafines, even without the gas contributions, have a high enough specific heat to give significant improvements in regenerator efficiency over conventional regenerators. It can also be seen that if lead proved to be unsuitable for green compact fabrication, a material with a lower specific heat might be utilized in the ultrafine particle configurations, and by taking advantage of the gas contributions, still significantly improve regenerator efficiency.

(3) That lead ultrafine particle green compacts which are impregnated with mercury offer the greatest potential gains in refrigeration.

(4) Although amalgamation might reduce the surface contribution to the regenerator's heat capacity, the mercury bulk specific heat is large enough to provide significant improvements in refrigerator performance. It is apparent that maximizing the quantity of mercury contained within the small particle pore structure will result in optimum regenerator efficiency.

TABLE 1. A comparison of different regenerator configurations

Case No.	Description	% of Required Refrigeration Delivered	λ	λ_o	ε
1	.005" dia. lead spheres	100%	167	54.6	.9820
2	GdRh spheres + lead spheres	193%	167	74.2	.9867
3	22A lead green compact	245%	167	92.5	.9893
4	Case 3 + gas effects	253%	167	96.1	.9897
5	Mercury impregnated 22Å lead green compact	275%	167	107.7	.9908
6	Case 5 + amalgamation base	271%	167	105.4	.9906

5. Conclusions

An enhancement of materials specific heat can be accomplished by the use of ultrafine particles of the same material. The utilization of ultrafine particles presents a number of difficult problems; however, the improvement in refrigerator performance appears to be significant enough to merit experimental research to determine the mechanical properties of green compacts in different configurations and to make an accurate determination of their heat capacity over a wide range of temperatures. This will allow more accurate regenerator efficiency predictions to be made and the feasibility of utilization analyzed. Fabrication of GdRh into .005" dia. spheres would also seem merited as it presents a relatively simple solution to immediate refrigerator needs.

Part of this work was sponsored by Flight Dynamics Laboratory, A.F. Wright Aeronautical Laboratories, Wright-Patterson Air Force Base, Ohio, under contract F33615-78-C-3425, Project 2402, Task 240204, "Aerospace Vehicle Environmental Control." Mr. Ronald White was the Project Engineer for AFWAL/FIEE. This work was conducted at Scitech Corporation, Santa Ana, Ca. The project manager was Mr. Henry Yoshimoto and the principal investigator was Mr. P. J. Walsh.

The extensions on this work were carried out at Lockheed Palo Alto Research Laboratory, Palo Alto, Ca. and sponsored through Internal Research funds.

I would especially like to thank Mr. Jerry Walsh for the help and guidance he gave me throughout this entire project.

6. References

[1] P. J. Walsh, Low Temperature Regenerator Study, Interim Report, Air Force Flight Dynamics Laboratory, Wright-Patterson Air Force Base, Ohio, 45433, AFFDL-TR-79-3099, Aug. 1979, AO 80892.

[2] R. M. Barrer, Diffusion in and Through Solids, Cambridge University Press, 1973, Chapter 3-4.

[3] R. C. Tompkins, Chemisorption of Gases on Metals, Academic Press, 1978, Chapters 1 and 3.

[4] J. H. de Boer, The Dynamical Character of Adsorption, Oxford, 1953, Chapters 1-4.

[5] K. H. J. Buschow, J. F. Olijoek, and A. R. Miedema, "Extremely Large Heat Capacities between 4 and 10K," Cryogenics 15, 261 (1975).

[6] T. J. Lambertson, "Performance Factors of a Periodic-Flow Heat Exchanger," Trans. ASME 80, 586 (1958).

MEASUREMENT OF THERMAL PROPERTIES OF CRYOCOOLER MATERIALS†

J. E. Zimmerman, D. B. Sullivan, R. L. Kautz, and R. D. Hobbs††

National Bureau of Standards
Electromagnetic Technology Division
Boulder, CO 80303

Materials used in several low-power cryocoolers are characterized by very low thermal conductivities and moderate to large heat capacities at low temperature. Consequently, thermal equilibrium times are inordinately long for measurements of thermal properties to be made by the usual quasi-steady-state methods. We have developed a method of measurement in which the thermal conductivity and the specific heat are derived from observations of the time-dependent temperatures at two or more points on a cylindrical sample in response to a step function of heat applied to one end of the sample. Some preliminary results have been obtained on G-10 epoxy laminated tubing. These transient measurements give results in much less time than the steady-state method, and have the additional advantage of being adaptable, with fair accuracy, to the cryocooler structure itself, or to a separate structure geometrically similar to the cryocooler.

Key words: Composites; cryocoolers; plastics; refrigeration; regenerators; specific heat; thermal conductivity.

I. Introduction

Measurement of thermal properties of plastic and composite materials used in the construction of several low-power-cryocoolers requires long times if done by conventional methods. For example, a sample of nylon whose longest dimension is 5 cm would require something like two hours to reach thermal equilibrium after an input of heat at one end. This estimate is based on a thermal conductivity $K \sim 0.5$ mW/cm K and a specific heat $c_p \sim 25$ mJ/cm^3 K at 10 K. Thermal equilibrium times will of course be proportionately greater for special composite materials with large heat capacities. We have therefore developed a method of measurement in which we apply a step function in heat flow to one end of a cylindrical sample and observe the propagation of the transient in temperature as the heat diffuses along the sample. Thus, thermal properties of the sample material are derived from measurements made during the initial development of the transient, rather than after the transient has died out as in conventional equilibrium or steady-state ac methods[1]. This gives an order of magnitude reduction in time required for the measurements, not to mention the fact that both the thermal conductivity and the specific heat are derived from the same set of measurements. In addition, the method can be used for rough measurements on the cryocooler structure itself, the geometry being appropriate.

---

†Contribution of the U. S. Government, not subject to copyright. Work supported by the Office of Naval Research.
††Present address: Physics Department, Indiana State University, Terre Haute, Indiana.

Transient measurements of thermal properties have been made previously on cylindrical samples by a heat pulse method. Our reasons for using a step function rather than a pulse was that an ideal heat pulse momentarily raises the end of the sample to a high temperature, thereby enhancing the possibility of heat loss by extraneous mechanisms such as radiation, and also complicating the analysis through the temperature dependence of the thermal conductivity and specific heat. The magnitude of the step function can be adjusted to give a slow, steady, and relatively small, increase in temperature of the end of the sample.

II. Analysis of the Method

The ideal geometry is a uniform semi-infinite bar with a heater on the free end, $x = 0$, and thermometers to measure temperatures T_1 and T_2 at two points x_1 and x_2 (Fig. 1). The simplest initial condition is to let the bar come to thermal equilibrium at a temperature T_0, and then at time $t = 0$, turn on the heater at a power level P. The one-dimensional diffusion equation for this situation is

$$\frac{\partial^2 T}{\partial x^2} = \frac{C}{k} \frac{\partial T}{\partial t} \quad . \tag{1}$$

where k and C are respectively the thermal conductivity and specific heat per unit volume of the material. The solution for the stated initial condition is:

$$T(t,x) = T_o + \frac{2P}{A\sqrt{\pi kC}} \sqrt{t}\, e^{-Cx^2/(4kt)} - \frac{P}{kA} x \operatorname{erfc}\left[\left(\frac{Cx^2}{4kt}\right)^{1/2}\right] , \tag{2}$$

where erfc means the complementary error function, and A is the cross-sectional area. This solution is plotted as a function of x and of t in Fig. 2.

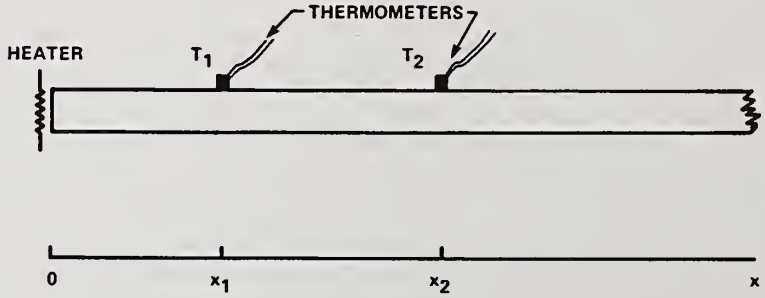

Fig. 1. Experimental arrangement for thermal properties measurement. The heater is turned on abruptly at $t = 0$ (step function) and the resultant temperature variation (sensed by the two thermometers) provides the means for determining the thermal conductivity and specific heat. The right hand end is connected to a heat sink, the temperature of which is controlled to set the equilibrium value of the temperature at T_0. The sample is suspended in a vacuum and surrounded by a liquid helium cooled shroud to minimize heat leaks to it. The leads from the carbon resistance thermometers are heat sunk to this shroud for similar reasons.

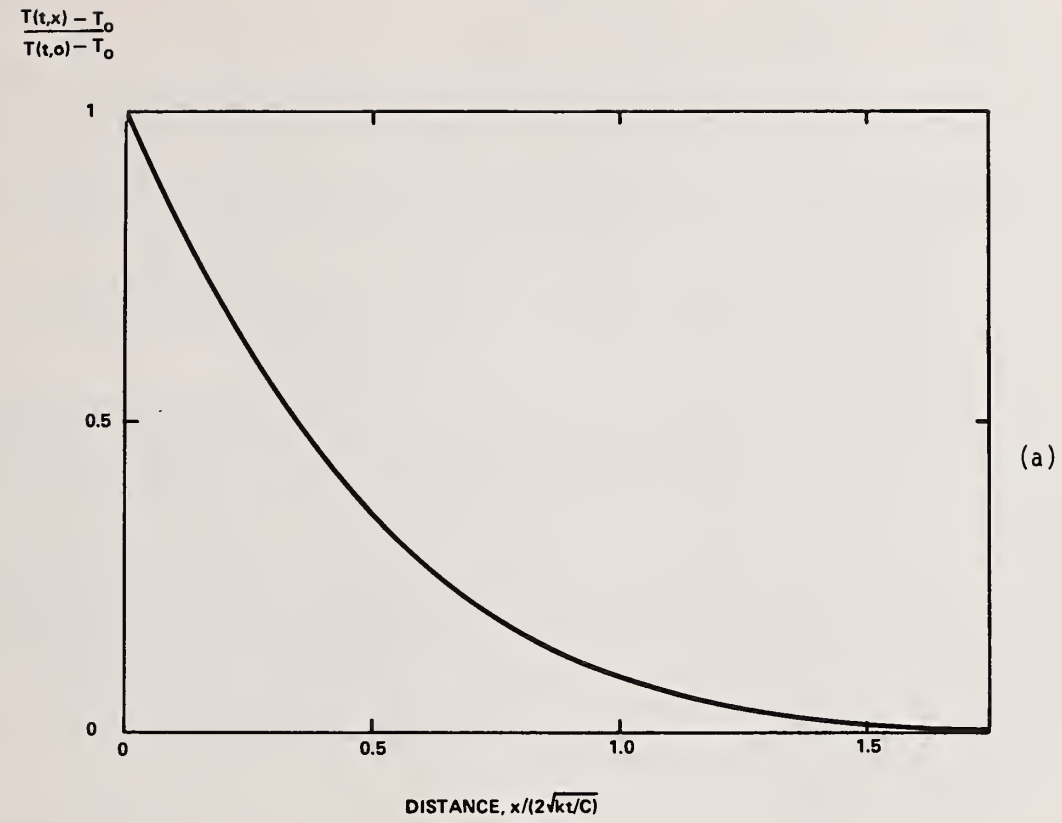

(a)

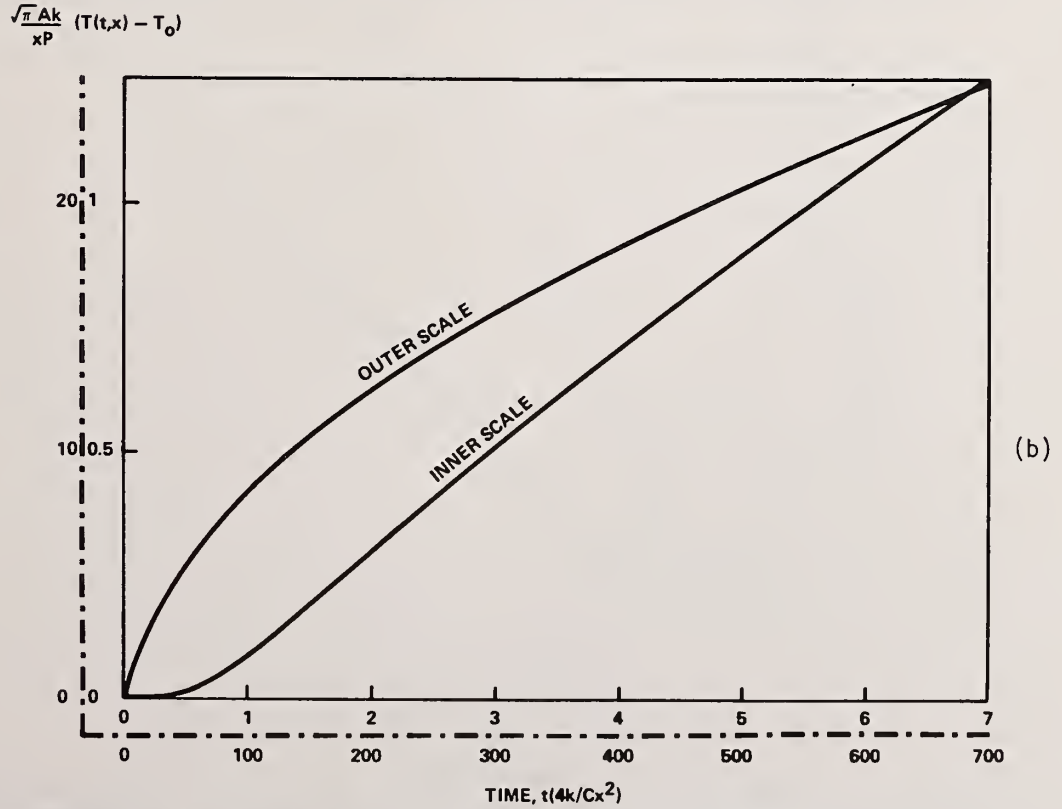

(b)

Fig. 2. Spatial (a) and temporal (b) solutions of diffusion equation.

Our method of measurement is to record the temperatures, T_1 and T_2, as a function of time. This gives a pair of curves of the shape of Fig. 2b, but with different time scales since T_1 changes more rapidly after the power is turned on than T_2, and of course T_2 is always less than T_1. From these curves we can read off a pair of numbers T_1 and T_2 for a particular time t'. For that particular time we then have both coordinates (T_1, x_1) and (T_2, x_2) for two points on the curve of Fig. 2a, which establishes the horizontal and vertical scales of that curve. This process involves use of the ratios x_1/x_2 and T_1/T_2 and an interactive procedure (using a computer) which locates the two unique points having the correct values of these ratios. The ratio, k/C, is obtained directly from the horizontal scale factor and the product kC can be derived at x = 0 from the vertical scale factor and equation (2). The combination of this ratio and product yield the values of k and C.

It is only essential, of course, to measure T_1 and T_2 at some convenient time t. However, measuring T_1 and T_2 as a function of time provides a high degree of redundancy which is useful in checking for errors and inconsistencies in the method.

Since k and C are usually temperature dependent at low temperatures, it is important to choose a power level and time scale such that T_1 and T_2 do not rise very much above the initial value T_0. Otherwise, the temperature dependence of k and C must be considered in equation (2), making the analysis difficult if not impossible. The use of small temperature intervals is standard practice in specific heat and thermal conductivity measurements.

Since the bar is not semi-infinite, the measurement time t' should be chosen small enough that no appreciable amount of heat reaches the far end of the bar, otherwise the spatial and temporal profiles given in Fig. 2 will no longer be accurate. Since the spatial profile, Fig. 2a, approaches zero very quickly at large x, it seems satisfactory to choose x_2 (the position at which T_2 is measured) at about the middle of the real bar, and then choose t' such that the rise in T_2 is no more than about 25% of the rise in T_1. It is assumed that the position x_1 should be near the free end of the bar. Any deviation of the temporal profile from the curve of Fig. 2b might indicate that one or more of these conditions has been violated.

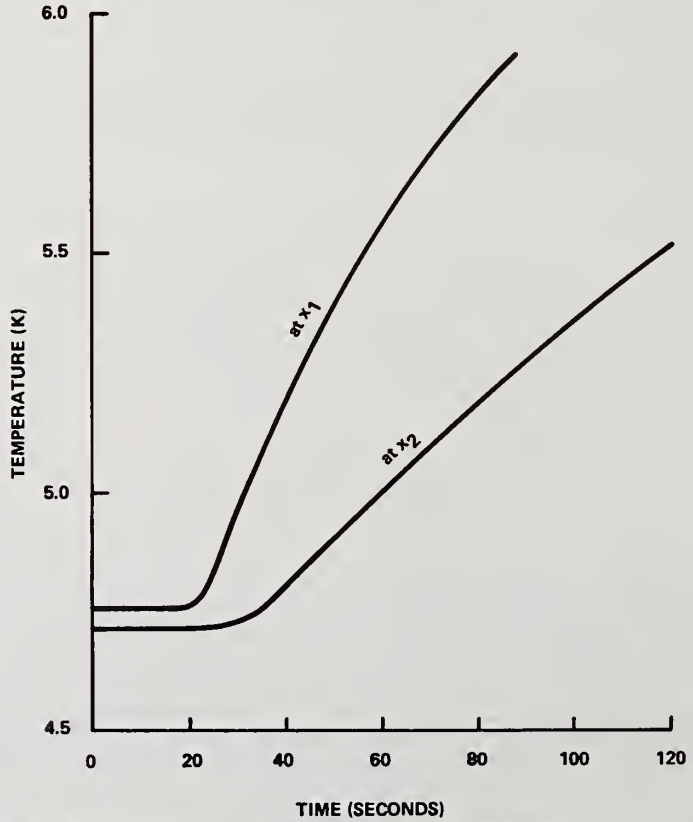

Fig. 3. Temperature as a function of time for two thermometers on a G-10 epoxy fiberglass rod. The thermometers were 1.2 cm and 4 cm from the heater. The rod had a cross-sectional area of 0.895 cm^2.

III. Results

Figure 3 shows the temperature at 2 thermometers on a G-10 epoxy-fiberglass rod as a function of time after a step function was applied to the heater. The rod area was .895 cm^2 and the thermometers were located 1.2 cm and 4.0 cm from the heater.

We found that the consistency of the results was poor if we selected a time t for which the temperature change at the second thermometer was small. This is presumably related to problems of resolution in the temperature at this point. We also found that the results varied considerably if the heat wave was allowed to reach the heat sink (the temperature controlled end of the bar) before the temperature points were taken. This clearly relates to a breakdown in the assumption that the rod was semi-infinite.

For the data of Fig. 3, reasonable consistency in results was achieved over the time interval of 40 to 75 seconds. While the temperature differences are a bit larger than desired, we used the method described in the previous section to determine the thermal conductivity and specific heat of this material at 5 K. The thermal conductivity was found to be 1.1 mW/cm-K and the specific heat was 4.7 mJ/cm^3-K.

These numbers fall within the range of values given by other investigators. Additional work must be done to arrive at a quantitative criterion for selection of valid data regions. The measurement scheme is to be automated so as to provide for rapid acquisition of information over a modest temperature range for a variety of materials. One should note that this technique has been devised to deal with rapid evaluation of a wide range of materials. An accuracy of 10-20% should suffice for such a study and this method seems well suited to the task.

IV. References

[1]. G. C. Danielson and P. H. Sidles, Thermal Diffusivity and Other Non-Steady-State Methods, in Thermal Conductivity, edited by R. P. Type, 149-200 (Academic Press, New York,NY, 1969).

GAS HEAT SWITCHES

Emanuel Tward

Jet Propulsion Laboratory
4800 Oak Grove Drive
Pasadena, California 91103

Thermally operated gas heat switches for use in refrigeration systems operating in the temperature range 4K to 300K have been designed and constructed. The switches are operated by a miniature adsorption pump which when heated supplies gas to the switch, turning it on, and when cooled removes gas from the switch, turning it off. The switches have been operated at 4K, 77K, and 300K with He or H_2 gas adsorbed on either charcoal or zeolite 13X. Switching times as low as a second and switching ratios of 80 have been achieved in miniature devices whose total mass is 8 grams.

Key words: Cryogenics; gas adsorption; heat switch; refrigerators.

1. Introduction

In order to cool sensors in spacecraft, refrigeration systems covering a broad range of temperatures from less than 1K to ambient and having service lifetimes of up to 10 years are being designed and built.

Some of these systems require thermal switches both for switching the load to the refrigerator and as an essential component of the refrigerators themselves. Since the primary goal being addressed is one of lifetime and reliability with the potential for miniaturization, it was decided to develop a gas heat switch. Since the switching function is accomplished by changing the gas pressure between two surfaces, a gas supply and a pump are required. Both of these functions are provided by an adsorption pump connected to the switch. This switch, together with its adsorption pump operator, form a permanently sealed system with no moving parts. This permanent sealing, together with the absence of mechanical motion, should provide the reliability and long lifetime which are required.

2. Principle of Operation

The thermal conductance between two parallel surfaces of area A at temperatures T_1 and T_2 separated by a distance d depends on the gas pressure between the surfaces (1,2). At "high" pressures where the mean free path $L_p \ll d$ (classical conduction region) the thermal conductivity of the gas is essentially independent of pressure and varies almost linearly with temperature (3) as shown in Figure 1. At "low" pressures where $L_p \gg d$ the thermal conductivity of the gas is given by (1)

$$K = \alpha \left[\frac{\gamma + 1}{\gamma - 1}\right] \left[\frac{R}{8\pi}\right]^{\frac{1}{2}} \left[\frac{P}{M T}\right]^{\frac{1}{2}}$$

where α is an accommodation coefficient for the surfaces, $\gamma = Cp/Cv$ is the ratio of specific heats for the gas, R is the gas constant, P is the pressure, M is the molecular weight of the gas, and T is the temperature. It is therefore apparent that at some fixed operating temperature T the thermal conductance between two surfaces may be varied from some high fixed value in the classical regime to some lower value which is pressure dependant. In a real switch, however, the minimum conductance is determined by other thermal conductances which are operating in parallel to the conductance through the gas. These conductances arise due to the heat transfer by radiation between the two surfaces (usually negligible in our applications) and due to the heat transfer by conductance through the supporting structure holding the two surfaces apart. A schematic of a design for a real heat switch is shown in Figure 2. Two high conductivity plates (e.g. copper) of area A are separated by a small gap d and held apart by a low conductivity support (e.g. thin wall stainless steel tube). The gas gap is connected via a stainless steel capillary to a small adsorption pump. The thermal conductance between the two plates at the different temperatures T_1 and T_2 can be modeled as in Figure 3 (a), where the plates 1 and 2 have thermal resistances R_1 and R_2, respectively, the isolation support has a thermal resistance R_s, the radiation resistance is R_r, and the thermal resistance due to changing the gas pressure p is R(p). In practice for the devices which we have made R_1, $R_2 \ll R_s$ and $R_r \gg R(p)$, R_s and therefore the equivalent circuit is adequately described in Figure 3 (b). Therefore, if the gas pressure p is changed from some value p_{high} to some value p_{low} where $R(p_{low}) \gg R_s$, the switch ratio is given as

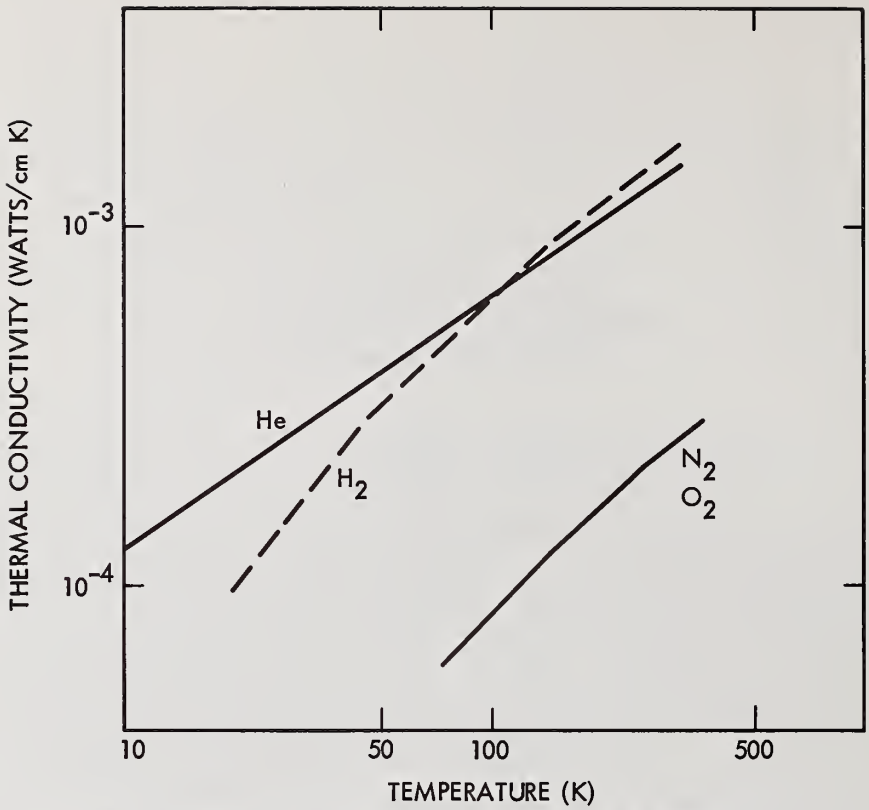

Figure 1. Thermal conductivity of gases as a function of temperature in the classical conduction regime[3].

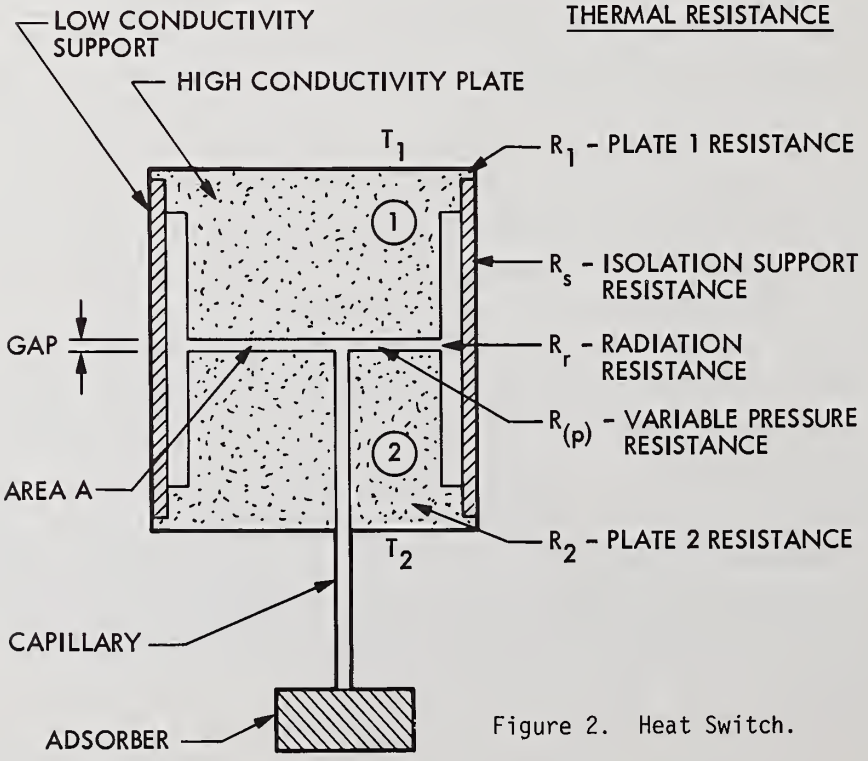

Figure 2. Heat Switch.

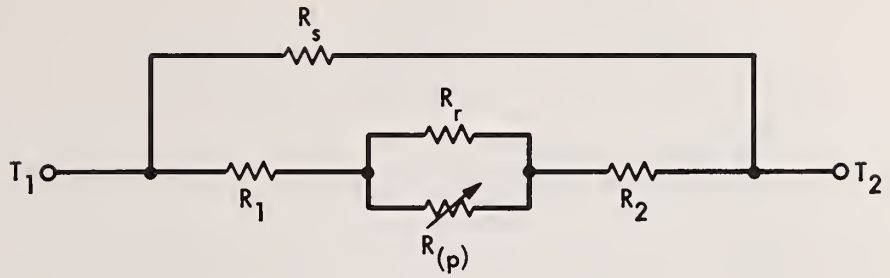

(a)

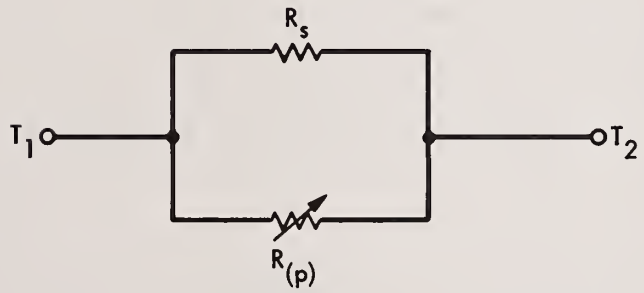

(b)

Figure 3. (a) Model of Heat Switch resistances.
(b) Simplified Heat Switch model.

$$\frac{R_{off}}{R_{on}} = \frac{R_s}{R\left[p_{high}\right]}$$

3. Adsorption Pump

The adsorption pump acts as a source and sink for the gas. It is operated by heating and cooling the adsorber which causes gas to be either released or readsorbed respectively (4,5). A number of materials can be used as adsorbers. In a heat switch where the thermal conductivity of the gas is important, the most appropriate gases for use are He and H_2 (Figure 1). These gases may be adsorbed onto charcoal or zeolite for example, or in the case of H_2 on to metal hydrides. An important feature of these adsorbers is that the adsorbers have extremely large effective surface areas per unit volume ($\sim$500 m^2/gm) and hence can store liquid densities of the gas at low pressures. Storage capacities of 200 cm^3 STP/gm adsorber are possible. If the temperature is raised, gas is released and the pressure builds up. Since a large amount of gas is stored on the adsorber and the pressure range of operation is usually in the millitorr to few torr range, therefore orders of magnitude pressure changes are possible with small temperature changes and with small amounts of adsorber. The principle of operation of the switch operator (adsorption chamber) is shown in Figure 4.

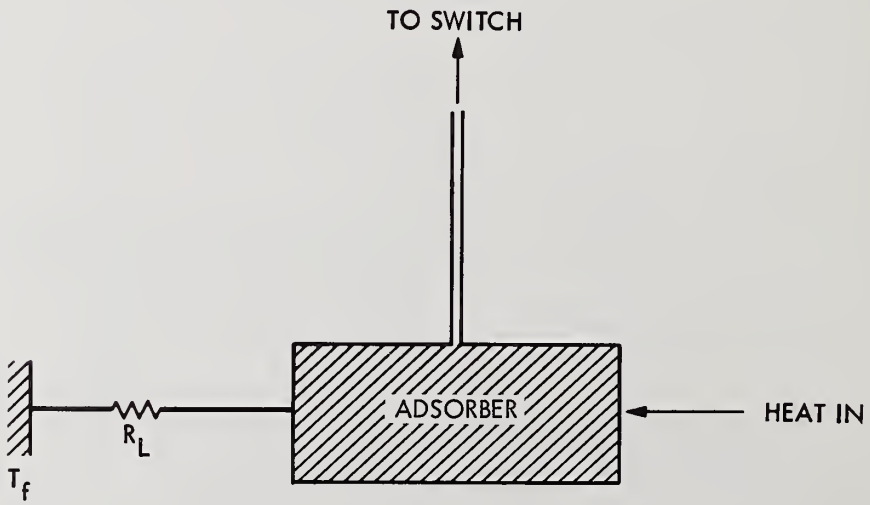

Figure 4. Heat Switch Operator. The adsorption pump is heated to turn the switch on and cooled to turn the switch off.

When the heater is off, the adsorber is held at the temperature T_f. At that temperature, the bulk of the gas is adsorbed and the pressure has been adjusted to be p_{low}, sufficiently small that the conductance between the plates is determined by the isolation support in the switch. When the adsorber is heated by the heater the pressure rises to a value p_{high} where the mean free path $L_p \ll d$ (the gap). For example, using He in a switch operating at 4K, $L_p \left[a \frac{1}{p}\right]$ is 10^{-3}mm at 1 torr. Therefore, for a gap larger than, say 10^{-2}mm, a pressure of 1 torr is large enough for p_{high}.

The quantity of adsorber and the power required to operate the switch are a function of the temperature T_f at which the switch is operated. This results from the strong dependance of the adsorption capacity of the materials on temperature. If T_f is near the boiling point of the operating gas, then very small quantities of the adsorbers such as charcoal and zeolite are required because of the large storage capacities of the adsorbers. For example, one of the switches which we have made has a gas volume of approximately $10^{-1}cm^3$. At 4.2K zeolite 13X adsorbs ~150 cm^3STP/gm at 10^{-3} torr (6). To produce 1 torr in this volume requires only $10^{-4}cm^3$STP of gas or 10^{-4} of the gas stored on 10^{-2} grams of zeolite.

The power required to operate the switch is also a function of the switching time required. For rapid turn off time the thermal resistance of the thermal link must be reduced, thus causing an increased heat load at the temperature T_f and increased power requirement to turn the switch on.

4. Measurements

Measurements were made in a miniature heat switch similar to that shown in Figure 2. The switch is ½" diameter x .200" long and contains a gap of .001". The isolation support is a stainless steel tube ½" diameter x .001" wall. The plates are made of copper. Total mass of the switch is 8 grams.

Figure 5 shows the response of the switch to the alternate heating and cooling of the charcoal pump containing a few mgms of charcoal. The data was taken with one side of the switch (T_1) fixed at 4.2K. 6.5 mW is applied continuously to the lower plate of the switch carrying the increased temperature T_2 recorded in Figure 5. In this example, R_L is relatively small so that the switch off time can be made fast. The He working gas is adsorbed on the activated

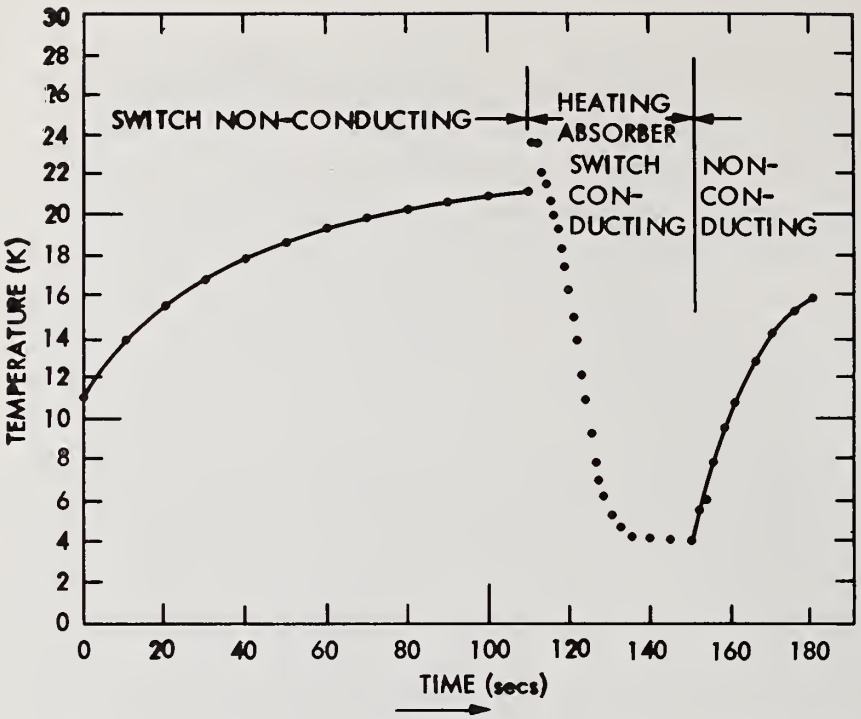

Figure 5. Response of Heat Switch to operation of adsorption pump.

charcoal at T_f=4.2K. At t=0 seconds the 6.5 mW is being applied to the bottom of the heat switch while the switch is non-conducting. At t=110 seconds the charcoal pump is heated. Within 1 second the switch is conducting. At t=150 seconds the charcoal pump heater is turned off. Within 1 second the bottom of the heat switch begins warming indicating that the switch has turned off. The switch ratios for this switch were also measured at 77K. With He as the working gas, this switch has a resistance while on R_{on}=16 K/W. R_{off}=1160K/W giving a switch ratio of 72.5. With H_2 as the working gas, R_{on}=15K/W giving a switch ratio of 77.

The research described in this paper was carried out at the Jet Propulsion Laboratory, California Institute of Technology, under NASA Contract NAS7-100.

5. References

[1] R.R. Conte, Éléments de Cryogènie, pp.17-24, Masson et Cie, Paris (1970).

[2] R.J. Corrucinni, Vacuum, Vol. VII & VIII, 19 (1959).

[3] G.K. White, Experimental Techniques in Low Temperature Physics, p. 82, Oxford U. Press, Oxford (1968).

[4] R.R. Conte, Éléments de Cryogènie, p. 68, Masson et Cie, Paris (1970).

[5] A.C. Rose-Innes and J.J. Rowland, Journal of Physics E: Scientific Instruments, 5, 939 (1972).

[6] J.G. Daunt and C.F. Rosen, Journal Low Temp. Phys., 3, 89 (1970).

OPERATION OF A PRACTICAL SQUID GRADIOMETER IN A LOW-POWER STIRLING CRYOCOOLER†

D. B. Sullivan, J. E. Zimmerman, and J. T. Ives††
National Bureau of Standards
Electromagnetic Technology Division
Boulder, CO 80303

A commercial Nb point-contact SQUID has been used in the construction of a simple magnetic gradiometer system supported by a split Stirling refrigerator. The magnetic interference generated by the cryocooler was sufficiently small to permit the acquisition (for demonstration purposes) of a reasonable magnetocardiogram. Preliminary investigation of the source of the residual refrigerator interference indicates that cyclic temperature variation is the largest single factor influencing the gradiometer output. A simple electronic temperature controller has been added to a different cryocooler to study temperature stabilization. Better than 1 mK stability has been achieved at 8.5 K.

Key words: Cryocoolers; low temperature; magnetic gradiometer, refrigeration; SQUID; Stirling cycle; superconductivity.

1. Introduction

The economic viability of superconducting instrumentation would be greatly enhanced if properly matched cryocoolers were readily available to support their operation. By properly matched we mean: 1. cost comparable to or less than the supported instrument, 2. cooling capacity not significantly greater than that required (often only a few milliwatts), 3. package size comparable to or not much larger than that of the device in a liquid-helium cryostat, and 4. vibration and magnetic interference levels which do not appreciably affect the instrument operation. This last requirement is especially critical for SQUID magnetometers and magnetic gradiometers which are designed to sense environmental magnetic fields or gradients (e.g., geophysical fields or biological fields). The SQUID magnetometer has a sensitivity of the order of 10^{-10} times the earth's magnetic field and thus extremely small angular vibrations translate directly into interference if the device is operated in such a field. In this paper we discuss this and other potential interference sources and describe a SQUID gradiometer supported by a low-power cryocooler [1,2]. As a demonstration of the level of interference for this system, a magnetocardiogram was recorded.

2. Cryocooler

The cryocooler used in this work has been recently described by Zimmerman [2]. Figure 1, taken from this reference, shows the details of construction of the cold end of this split Stirling refrigerator. The refrigerator operating at 1 Hz has achieved a temperature of 7K with no heat load (an aluminum rod occupied the 'cold space for device' shown in Figure 1). The compressor displacement is 90 cm^3 and optimum operating helium pressure is just over 2 atmospheres (gauge pressure). The displacer stroke is 0.7 cm.

† Contribution of the U. S. Government, not subject to copyright. Work supported by the Navy Coastal Systems Laboratory.
†† Present address: Engineering Department, University of Utah, Salt Lake City, Utah.

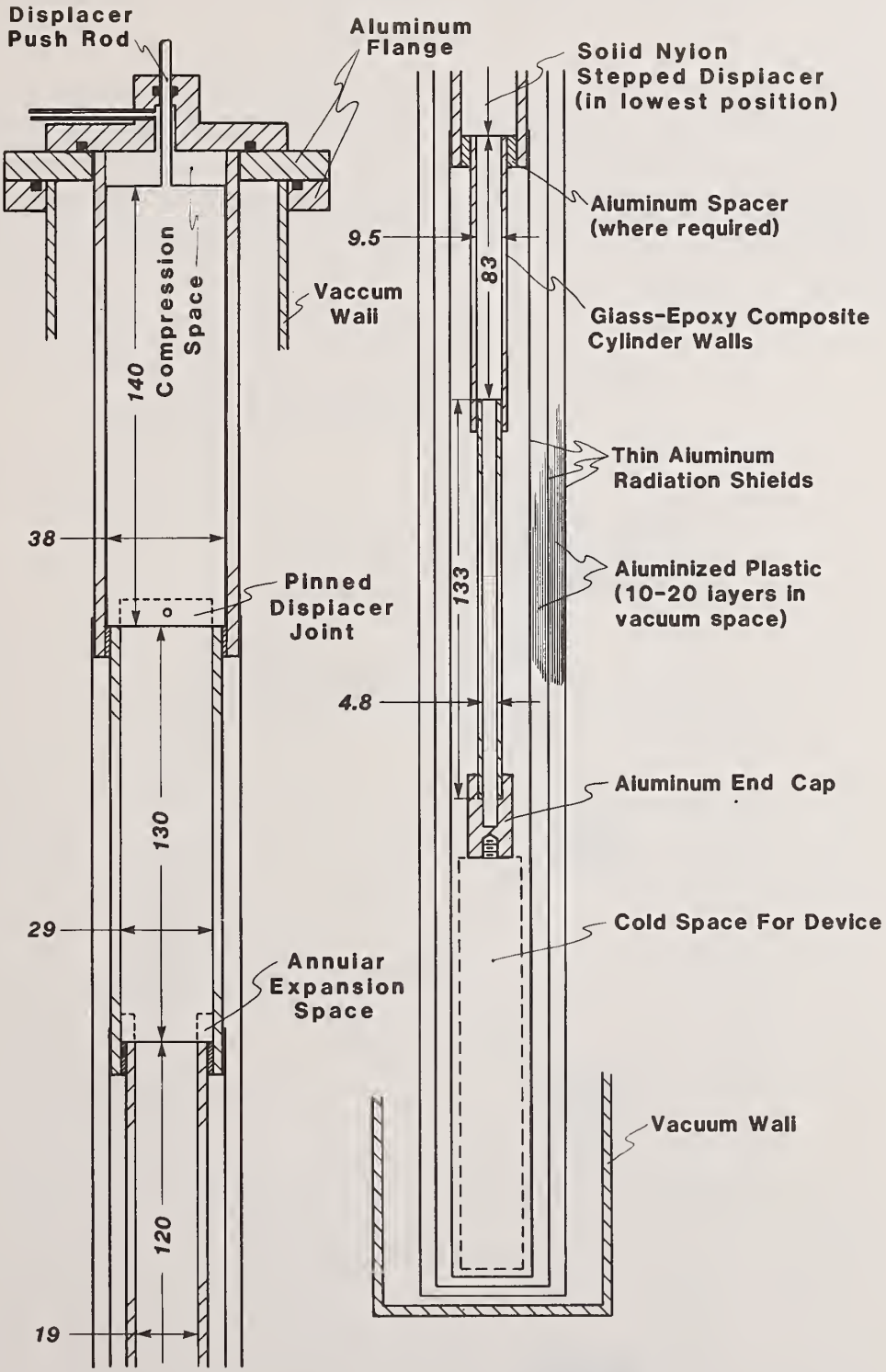

Fig. 1. Details of 5-stage, split Stirling cryocooler. Dimensions are in millimeters. Figure taken from reference [2].

The selection of many of the design features for the cryocooler was influenced by interference considerations. These design features are described in section 4 below under the appropriate potential interference sources.

3. SQUID Gradiometer

The gradiometer and its principal dimensions are shown schematically in Figure 2. The diameter of the gradiometer was selected such that none of the shields of its support refrigerator (Figure 1) would need modification. This was done to keep the system as simple as possible, but the resulting gradiometer was not particularly sensitive with the limited diameter and baseline. The commercial toroidal SQUID is centered within a niobium tube between the end coils. This tube is moved vertically to achieve axial balance. Small superconducting tabs were attached to the tube (in pairs, one at each end) to achieve transverse balance.

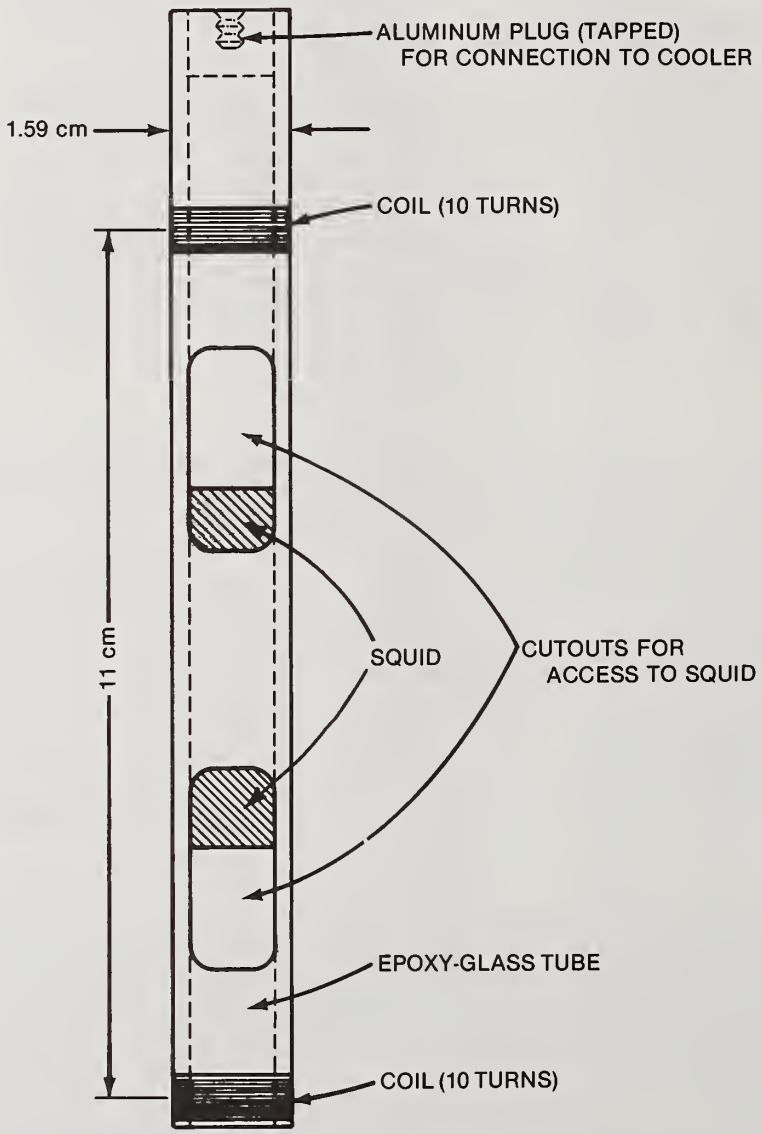

Fig. 2. SQUID gradiometer. The SQUID is inside a niobium cylinder.

The system was balanced to approximately 1×10^{-4} both axially and in the transverse direction while operated in liquid helium. The sensitivity was found to be $\sim 10^{-9}$ T/m per flux quantum with a noise level of $\sim 10^{-11}$ T/m in a 40 Hz bandwidth. For thermal anchoring, four strips of aluminum foil (4 mm wide by 0.3 mm thick) were tied along the entire length of the gradiometer with the ends also tied to the aluminum cold end of the refrigerator. The SQUID was also independently anchored (thermally) to the cold end. The gradiometer coils (10 turns each) were connected in parallel to the SQUID rather than the usual series connection. This was done so that more turns could be used on each coil and still have the combined inductance match that of the SQUID coil.

For the interference tests the gradiometer was operated partly within an aluminum shielded room [3], as shown in Figure 3. The shielded room provides some isolation between compressor and displacer since its cutoff frequency is 1/3 Hz. The cylinder with displacer was mounted rigidly to the roof of the room to avoid any rocking motion induced by the rotation of the displacer drive shaft (see Fig. 3). This rigid mounting led to additional microphonic noise in the 3 to 10 Hz range. Vibrations in this frequency range were generated by some heavy refrigeration equipment in the building.

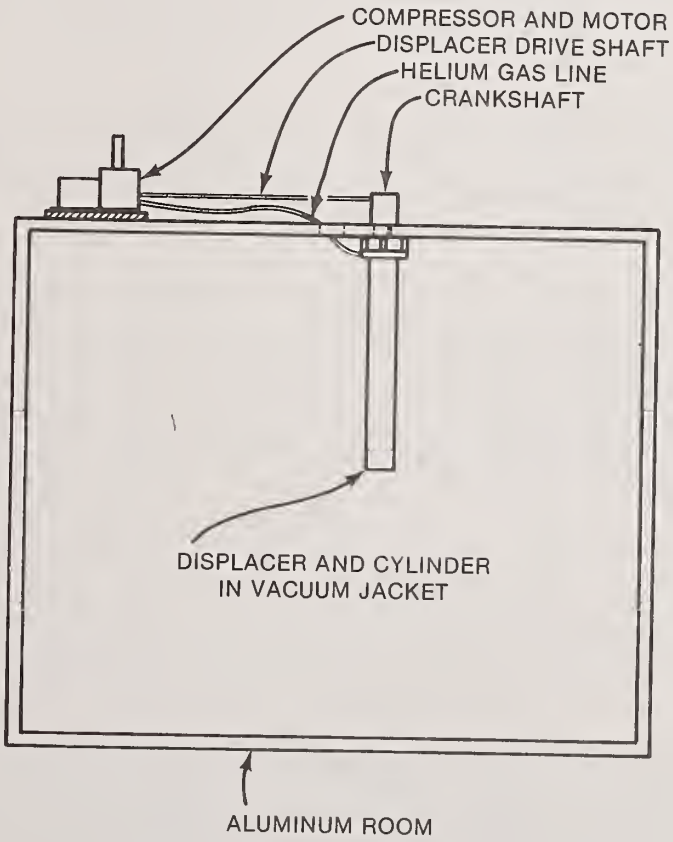

Fig. 3. Mounting of the cryocooler in an aluminum shielded room.

4. Potential Sources of Interference

In previous papers we emphasized the refrigeration aspects of the cryocooler while alluding to certain characteristics which would minimize the magnetic signature of the device. In this section we expand upon the design features relating to magnetic interference.

4.1. Motional Interference

The use of low speed (in the neighborhood of one Hz) and the low power requirement result in low vibrational noise, because of the low static and dynamic forces involved. With the plastic regenerator materials, this low-speed is, in fact, essential since much higher speed operation reduces the thermal penetration depth and thus results in regenerator inefficiency, particularly in the bottom stage.

The displacer requires very little power for operation, so the mechanical components which produce the displacer motion can be very smooth in operation. The compressor and motor are coupled to the cold portion of the cooler through a drive shaft and a tube through which the helium gas is transported between compressor and displacer sections. It is essential that vibration transmission through these two connections be minimized. To this end we use rather light weight and flexible materials (thin-wall brass for the drive shaft and small diameter copper tube for the helium gas) for these components. By separating the compressor and displacer one meter from one another we find little vibration transmission from compressor to displacer. Additional flexibility and versatility might be achieved through use of a simple hydraulic system to transmit the mechanical motion from the motor-compressor to the displacer.

The one component of motion which still remains as a potential problem is that of pressure flexing of the displacer cylinder. It is unlikely that this cylinder is perfectly uniform around its circumference and the cyclic pressure variations could therefore result in some cyclic transverse motion of the cold end. This problem would be reduced by operation at the lowest possible pressure.

An earlier paper [1] described the results of operation of a simple SQUID magnetometer in a four-stage cooler. The peak-to-peak signature at the cooler frequency of 1.5 Hz was 0.5 nT (SQUID operated in the earth's field). This corresponds to a motion of 10^{-5} radian if this is the only interference source, emphasizing the extreme stability required by this type of instrument. This field oscillation was dependent upon the orientation of the SQUID in the horizontal plane, so we concluded that at least part of that signature was due to flexing of the displacer cylinder presumably induced by the pressure oscillations. There was no direct evidence for other interference mechanisms, but they could easily have been present as well.

For magnetic gradiometers, motional interference is often not as severe. If the earth's field is uniform in the vicinity of the device (the usual case), the motional signature is reduced by the degree of balance of the gradiometer. That is, it is the remnant magnetometer response which picks up the field motion. In this particular case the gradiometer is balanced to a part in 10^4 so motional inteference is reduced by the same factor.

4.2 Compressor Interference

It is necessary to minimize direct magnetic interference by the compressor at the cold end. Two precautions are taken. First, the compressor is designed with a minimum of ferromagnetic components. Materials utilized included brass, aluminum, stainless steel, and nylon. We have used bronze and nylon bushings rather than ball and roller bearings which are commonly ferromagnetic. The piston is nylon in a stainless tube. The motor and gearbox selected for the machine has cast aluminum housing components and appears to have only a modest magnetic signature (this motor was once operated within 15 cm of the gradiometer with no severe interference). The second precaution involves modest separation (1/2 to 1 meter) of the motor-compressor and the displacer sections of the refrigerator. It is conceivable that some sort of shielding could be added to the motor and compressor to further reduce their magnetic signature, but this does not yet appear to be a major interference source.

4.3. Magnetism of Cold End Materials

Plastics were chosen for the critical cold parts of the refrigerator because they are nominally nonmagnetic. However, at the sensitivity level of the SQUID, the magnetic properties of virtually all materials are not negligible. Small remanent moments and magnetic susceptibilities often result in readily measured effects. The materials concerns fall into two categories, magnetic interference from moving components and slow drifts which arise from temperature dependent magnetic effects in materials which are fixed relative to the SQUID.

In the first instance two phenomena are important. The presence of a remanent magnetic moment in the displacer leads to an obvious magnetic signature. In general, remanent magnetism in such materials is associated with traces of ferromagnetic substances either introduced into the bulk of the material during manufacture, or quite commonly, by machine work during shaping of the component. The latter contamination can be reduced sharply by careful cleaning procedures. Remaining permanent moments can be reduced by demagnetizing procedures. Even without remanent magnetism, moving components can generate a magnetic signature since the ambient field (often the earth's field) induces a moment in anything with a non-zero magnetic susceptibility.

It is difficult to be quantitative in the case of remanence, but we can estimate the size of the induced moment at the bottom end of the nylon displacer. Assuming for the moment that the lowest part of the displacer produces the strongest effect, we suggest that the displaced volume in the bottom stage is the relevant volume of nylon to consider. That is, we assume that the effect of cyclic axial motion of a semi-infinite rod in a magnetic field is the same as the cyclic appearance of a volume of the rod equal to the cross sectional area times the stroke. Thus for the 5-stage cooler of Figure 3, we have a volume of $0.7 \times \pi \times (2.4)^2$ cm^3. For nylon with a susceptibility of 10^{-5} in a field of 5×10^{-4} T this yields a cyclic induced moment of $\sim 5 \times 10^{-14}$ Am^2. This translates to an interference gradient field of approximately 10^{-14} T/m. (The spacing between the end of the displacer and the top coil of the gradiometer is $\sim$ 3 cm). This is well below any interference level which might be achieved in the near future.

The magnetic susceptibility of many materials can be a rather strong function of temperature leading to long term drift in the induced magnetic moment. The refrigerator components most likely to experience such temperature drift are the radiation shields and mylar superinsulation. Drifts of many degrees C in temperature are likely since radiation heat transfer is very small and the time constant for temperature equilibrium might then be extremely long. Lacking specific knowledge of either the magnitude of such temperature variation or the temperature dependence of the relevant material susceptibilities, it is not practical to dwell on this question. Needless to say, the appearance of drift might eventually lead us to attemp to clarify this situation.

4.4. Temperature Variation

Besides this last effect (induced magnetism which drifts with temperature), there is a more direct influence which temperature change can have on a SQUID. If the critical current of the SQUID is a function of temperature, then temperature change will have an effect on the operating point of the SQUID. In principle this should not change the output of a SQUID operated in a phase-locked loop, but measurements indicate that this is not the case. This relation between SQUID output and operating point (rf level or critical current) is probably a second order effect related to some asymmetry in the interference pattern. It's presence means that temperature changes (either drift or oscillatory changes) can affect the SQUID output directly. The cures for this problem are twofold. First eliminate the temperature variations and second, eliminate (or reduce) the temperature dependence of the SQUID's critical current. Probably both solutions should be considered.

5. Interference Measurement

The gradiometer sensed an interference signal at 1 Hz (compressor frequency) with an amplitude of $\sim 6 \times 10^{-11}$ T/m. We conducted several experiments to isolate the source of the noise. First, we placed a high permeability shield around the SQUID and found no

observable change in the amplitude of the signature. This immediately eliminates compressor-generated magnetic signals as the predominant interference source. Furthermore, this shield attenuated the earth's field by at least a factor of 100. The lack of any change in interference with this shielding suggests that both gradiometer motional noise and induced moments (non-zero susceptibility) are also unimportant at this level. Finally, we noted rapid drift when the cooler was turned off momentarily. During such shutdown the SQUID remained fully in operation. This suggests a strong dependence of SQUID output on temperature as discussed above. From direct measurements we find that the temperature of the bottom end varies by at least several mK at the refrigerator frequency and previous measurements on the SQUID indicated a strong dependence of critical current on temperature. Thus we conclude that the primary source of the apparent magnetic signature at this level is temperature fluctuations at the SQUID. This is also consistent with the observation that the signal amplitude is somewhat dependent on temperature since the slope of the I_c vs. T curve is a function of T and some dependence is thus expected.

We also noted that the very low frequency noise (less than 1 Hz) was small. After achieving temperature equilibrium we noted a rather stable signal (less than 2 x 10^{-11} T/m variation over a period of three minutes). This could probably be improved through temperature regulation which will be discussed in the next section.

6. Interference and Drift Reduction

We used a very simple expedient to cancel most (90%) of the 1 Hz signature. This was to attach a small magnet to the shaft of the compressor so as to generate a field which just canceled the observed signature. The proper way to deal with this sort of interference reduction is to use a commutative filter with a reference derived from the compressor shaft. The advantage of such a filter is that it can also handle harmonics of the fundamental interference which are clearly present. Nonetheless, the simple cancellation of most of the interference allowed the following measurement.

As a demonstration of the system we recorded two magnetocardiograms (see Figure 4). The first was taken with the gradiometer in a simple cryostat and the second with the gradiometer supported by the 5-stage cooler. Bandwidth for the measurements was 2 to 40 Hz (to further reduce the one Hz signature). The added noise in the 3 to 10 Hz range is probably a result of the rigid mounting to the shielded room (see Section 3).

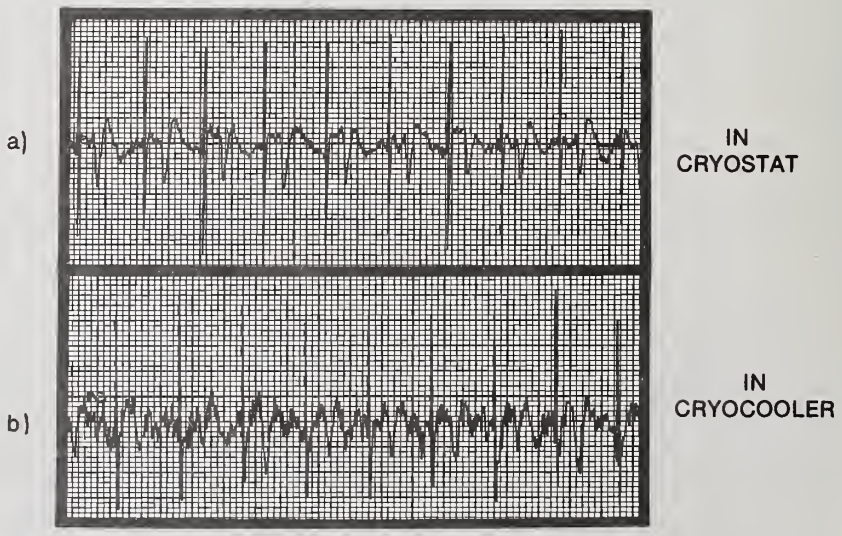

Fig. 4. Magnetocardiograms taken with gradiometer in a simple cryostat (a) and in the 5-stage cryocooler (b).

This result provides a fairly clear indication that mechanical refrigerators can be compatible with SQUID instruments, although there is room for much improvment. Obviously, the problem of temperature fluctuation and drift must be addressed first. (The reduction of SQUID temperature sensitivity will also help, but we assume that complete elimination of such temperature sensitivity is very difficult).

We have experimented with two means for stabilizing the temperature of the cryocooler. These experiments have been carried out with a 4-stage Stirling cryocooler, the bottom end of which is shown in Figure 5. The carbon-resistance thermometer and the heater were used as sensor and control elements in a simple electronic temperature regulator (servo system). This system was quite effective in eliminating drift. Over a period of two hours, the temperature change was no more than a fraction of a mK with the temperature at 8.5 K. Because of the rather slow thermal response, the simple regulation circuit did not significantly reduce the 2 mK oscillation (at 1 Hz) which was observed without the regulator. Further improvement of this regulation is clearly needed. One should note that alternating current at a frequency above the SQUID sense band can be used for both the heater and thermometer to eliminate any possible interaction between the SQUID and a direct current in these elements.

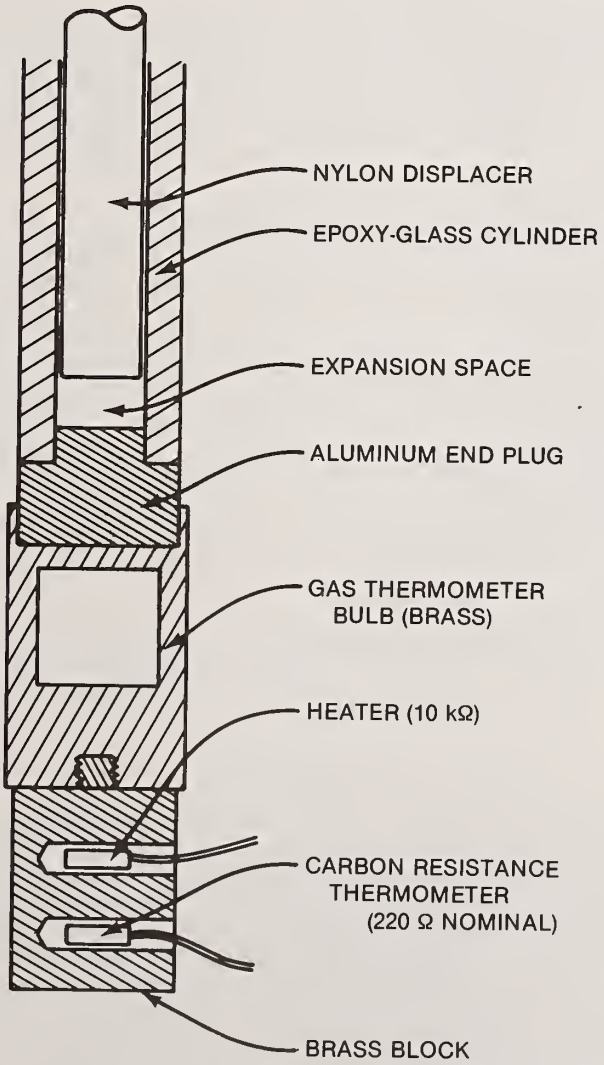

Fig. 5. Details of the bottom end of the 4-stage cryocooler with thermometer and heater for electronic temperature control. The helium gas bulb permits control of the thermal mass of this bottom stage.

The helium gas bulb shown in Figure 5 provides a simple means for changing the heat capacity of the cold end of the refrigerator. Even though the volume of this bulb is only 1 cm^3, the total heat capacity of the bottom stage could be increased by a factor of 10 by pressurizing it with helium gas to only 4 or 5 standard atmospheres. This results in a ten-fold reduction in the oscillatory temperature variation and significantly reduces drift even without the electronic temperature regulator.

7. Summary

In summary then, a SQUID gradiometer supported by a split Stirling cryocooler has been shown to operate at an interference level sufficient to obtain a magnetocardiogram of modest clarity. Temperature fluctuations produce the primary interference signature and methods for temperature stabilization have been studied. We expect that with each improvement which reduces magnetic interference, we will identify other interference sources which affect the system at a lower level. The most logical approach is to proceed to deal with these as they are uncovered.

8. References

[1] J. E. Zimmerman and R. Radebaugh in "Applications of Closed-Cycle Cryocoolers to Small Superconducting Devices," NBS Special Publication SP-508, J. E. Zimmerman and T. M. Flynn, eds.), Superintendent of Documents, U. S. Government Printing Office, Washington, D. C. 20234 (1978). (Also available from the authors), p. 59.

[2] J. E. Zimmerman in "IC-SQUID (Conference)" Berlin, West Germany, May 1980 (to be published).

[3] J. E. Zimmerman, J. Appl. Phys. 48, 702 (1977).

CURRENT STATUS OF HIGH TEMPERATURE JOSEPHSON DEVICE TECHNOLOGY

M. Nisenoff

Code 6854, Naval Research Laboratory, Washington, D.C. 20375

The fabrication of Josephson devices from refractory thin films with high superconducting transition temperatures (T_c) should yield devices which are rugged and reliable, and capable of withstanding repeated thermal cyclings between room and cryogenic operating temperatures. If the onset of Josephson response could be raised to above 15K, the devices could be operated near 10K at a reduced temperature of 0.6 where the temperature dependences of the relevant superconducting parameters are relatively weak. This temperature region is readily accessible using compact, energy-efficient closed cycle refrigeration systems.

A review of recent progress in the fabrication of various types of refractory high temperature Josephson devices is presented. Certain configurations require dimensional resolutions approaching 0.1 micrometer or less for successful operations. In other structures, there are problem areas in the growth of suitable thin films of the superconducting materials of interest and of suitable barrier layers and controlling the properties of the interfacial regions between these layers and the superconducting electrodes. Current progress and accomplishments are summarized and critical areas for future R&D are identified. Based on recent progress, the prospects for preparing all-refractory Josephson devices with onset temperatures exceeding 15K appears very promising.

Key words: Superconducting devices; Josephson effects; proximity effect devices; tunnel devices; weak links; closed cycle refrigeration systems.

1. Introduction

The use of superconductive sensors and circuits as well as cooled circuits employing conventional technologies is slowly gaining acceptance. The recent development of small, reliable and energy efficient cryogenic refrigeration systems operating in the 10-30K region has satisfied the requirements for such electronic circuits as IR detectors and for cryogenic vacuum pumps ("cryopumps"). Such cryocoolers are not particularly suited for superconductive applications as the current generation of superconductive electronic devices are fabricated using niobium (T_c~9.2K) or lead and lead alloys (T_c~7.2K) and an environment in the vicinity of 4.2K must be provided. These low temperatures require the use of an additional low temperature stage for the cryocooler such as a Joule-Thomson stage or a wet expansion engine. These approaches introduce additional complexity, weight, cost

and an associated reduction in reliability and convenience of use. Nevertheless, a number of industrial and government laboratories have undertaken programs to develop small, energy-efficient cryocoolers whose characteristics are designed to optimally match the requirements of present generation superconductive sensors and circuits.

An alternative approach to the problem of integrating superconductive electronic systems and presently available cryocoolers is the development of high operating temperature superconductive device technology. If techniques can be perfected for the fabrication of superconductive devices and circuits using materials with superconductive transition temperatures in excess of 16K, operation in the vicinity of 10K would be practical without imposing severe restrictions on temperature stability and present day cryogenic technology might be adequate. In this paper, the current status of high temperature superconductive device technology will be reviewed, existing problem areas identified, and recommendations made for possible research and development.

2. Background

A partial list of practical superconductors is given in Table 1 (Devices using superconductors with T_c below 4.2K are not deemed "practical"). The present generation of superconductive devices use niobium or lead alloy technologies and are usually operated in an environment provided by a liquid helium bath. Thus, these devices are operating at reduced temperatures between 0.5 and 0.6 (see Table 2). At such reduced temperatures, the temperature dependence of material parameters (e.g., superconducting energy gap, critical current, penetration depth, etc.) are relatively weak compared to the behavior close to T_c. If operation at reduced temperatures of 0.6 or lower is acceptable, operation in the vicinity of 10K would be acceptable for devices and circuits fabricated using materials with T_c in excess of 16K (see Table II). Thus, we will adopt the definition that high temperature superconductive devices are those that can be operated at temperatures in the vicinity of 10K, at a reduced temperature of 0.6 or less.

The advantages that can be gained by the use of cryocoolers operating near 10K relative to those that operate in the vicinity of 4.2K is illustrated in Fig. 1. For convenience of comparison, each set of data has been normalized at 10K. The solid line is the "inverse" Carnot efficiency, that is, the number of watts of power at room temperature required to produce one watt of refrigeration at the indicated operating temperature. The data points in Fig. 1 are for characteristics (thermal efficiency, weight, volume and cost) of crycoolers providing one to several watts of cooling at the indicated temperature [1], [2]. It is not too meaningful to draw lines through a given series of data points as it would be too difficult to correct the data for the wide variation in all the other parameters of the systems. Thus, a shaded region is shown to indicate the trend in these parameters as a function of operating temperatures. It can be seen that although 4K operation is theoretically only 2½ times more difficult to achieve, for practical systems, a factor of about 10 increase is observed in the parameters such as efficiency, size, weight and cost. Hence the cryogenic support portions of an integrated superconductive electronic system can be simplified significantly if 10K operation is feasible compared to 4K operation.

Table 1. Properties of Superconducting Materials of Possible Technological Importance

Material	T_c (K)	$\xi(0)$ (Å)	Mechanical Properties	Substrate Temperature
Lead/Lead Alloys	7.2	800	Soft	~RT
Niobium	9.2	400	Hard	RT→400°C
Mo-Re	15	50	Hard	LN_2→RT
NbN	16	50	Hard	$\lesssim$300°C
NbCN	18	40	Hard	~500°C
V_3Si	17.3	30	Hard	~800°C
Nb_3Sn	18.3	30	Hard	~800°C
Nb_3Ge	23	30	Hard	~900°C

Table 2. Operating Temperature for Superconducting Devices

	Lead and Lead Alloys	Niobium	NbN	Nb_3Ge
Transition Temperature	7.2 K	9.2K	16K	23K
Usual Operating Temperature	4.2K	4.2K	-	-
Reduced Temperature	0.58	0.48	$\lesssim$0.6	$\lesssim$0.6
Projected Operating Temperature	-	-	$\lesssim$9.6K	$\lesssim$13.8

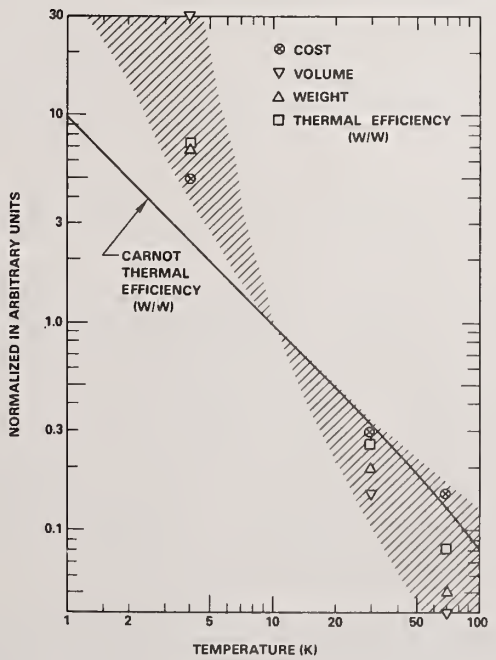

Fig. 1. Variation of selected parameters of closed cycle cryogenic refrigeration systems as a function of operating temperature. The solid line is the inverse Carnot efficiency as function of operating temperature. Each set of data has been normalized to unity at 10K (see text).

In the remaining portion of this paper we will describe recent progress in high temperature Josephson device technology and speculate on the prospects for its eventual realization. Although there are a large number of Josephson configurations, we will limit this review to thin film materials (as contrasted with bulk materials) and to tunnel devices, proximity effect devices, and "weak link" constrictions.

3. High T_c Materials

There is a large volume of literature on the preparation of thin superconducting films with transition temperatures in excess of 15K [3], [4]. However, for the preparation of a given type of device there may be special requirements on certain fabrication parameters such as substrate temperature, film thickness, crystalline grain size, nature and degree of granularity or "inhomogeneity," etc., which may warrant additional activity in material research. Some of these aspects of thin film preparation will be identified in the following sections dealing with specific Josephson device configurations.

4. Proximity Effect Devices

A proximity effect Josephson device can be fabricated by locally suppressing the T_c of the host film. The initial demonstration of this concept was by Notarys and Mercereau [5] who used a very narrow strip of normal material across a film either as an overlay or an underlay to reduce the T_c by the proximity effect between a normal metal and a superconductor. Proximity devices have also been fabricated by reducing the thickness of the best film over a local region by anodization [5], radiation damage [6], ion implantation [7], [8], etc. Josephson proximity effect behavior can be observed whenever the length of the region of suppressed T_c (that is, the dimension along the direction of current flow) is comparable to a characteristic length which is a function of the normal state parameters. When the temperature is maintained below the T_c of the contacts (or "banks") but above the T_c' of the localized region, there will be a critical current with a temperature dependence that will depend exponentially on the ratio of the characteristic length relative to the physical length of the bridge and on the difference in temperature between the operating temperature and some characteristic temperature which will be close to the suppressed T_c' of the region. Josephson effects, both dc and ac, can be observed in this regime which typically spans a temperature interval of 0.2 to 0.5K.

Proximity effect devices have been fabricated from high T_c superconducting films using many of the techniques described above. The highest temperature of operation is about 17K reported by Palmer, Notarys and Mercereau [9] for Nb_3Sn films in which the T_c of a 1-2 μm long region had been suppressed by about 0.5K from the original T_c~17.5K by selective anodization. DC SQUIDS made in this fashion showed clear modulation patterns with good signal-to-noise ratios although no minimum detectable field change was reported. The devices operated over a temperature range of a few tenths of a degree and were reliable, did not degrade under repeated thermal cycling, etc., and exhibited the other desirable characteristics expected for devices fabricated from refractory materials.

The proximity effect behavior can be easily observed provided that the characteristic length associated with the proximity region can be obtained with the resolution available from existing fabrication techniques. The primary disadvantage is that the critical current varies exponentially with temperature and that the temperature range of operation in the proximity mode is quite narrow requiring precise control and regulation of the cryogenic environment.

5. Tunnel Device

The "classical" Josephson device configuration is the oxide tunnel device. This configuration has been extensively studied theoretically and extremely good agreement has been obtained between theory and observed behavior of carefully prepared devices. However, there are serious problems associated with the fabrication of refractory high T_c tunnel devices. First, it is difficult to grow native oxides with controllable and reproducible characteristics on refractory metals, and especially on alloy and compounds of these metals [4]. Secondly, almost all of the high T_c alloys and compounds require elevated substrate temperatures (300°C and above) for proper film growth. During the deposition of the top electrode, such elevated temperatures may degrade the properties of the base electrode and may destroy the very thin (~20Å) oxide barrier region.

Techniques have been developed for reliably growing oxide barriers on the soft superconductors which have very reproducible thicknesses and exhibit very small values of excess current below the energy gap voltage in the I-V tunneling curve [10]. When these techniques have been applied to niobium and other high T_c materials, noticeably poorer quality tunnel junctions have been obtained [11], [12]. This is partially due to the fact that niobium and vanadium, the other refractory material commonly used for high T_c alloy preparation, have a great affinity for oxygen and hence the surface of the base electrode must be thoroughly cleaned by some technique such as sputter etching or glow discharge before the oxide growth is initiated [13]. These cleaning procedures may mechanically damage a shallow region just below the surface, thus degrading the superconductivity at the surface of the base electrode. Since the coherence length of these high T_c materials is less than 100Å (see Table 1), even a very thin surface layer of damage will be evident in the properties of the resultant tunnel device (In the case of the soft, low T_c materials, such as lead and lead alloys, a thin region of damage at the surface of the base electrode does not noticeably affect device operation as the coherence length in these materials is of the order of 1,000Å or greater). Furthermore, in the case of niobium, there are a number of natural oxides, sub-oxides etc., some of which are insulators and some conductors and even superconductors (bulk NbO has T_c~1.5K) [13]. Hence depending on the details of the growth process, the oxide layer grown on niobium and niobium alloys will have varying electrical characteristics.

In the case of the elemental superconductor, niobium, the group at IBM has developed techniques for sputter cleaning the surface of the niobium base electrode, growing an oxide barrier by the Greiner technique and then sputter treating the surface of the oxide layer to minimize the possibility of interaction between surface atoms of the oxide layer and the impinging niobium atoms that form the counter electrode [13]. With these techniques IBM has succeeded in producing fairly good Nb-Nb_2O_5-Nb tunnel junctions as gauged by the low value of the excess current just below the voltage corresponding to the energy gap. However, the characteristics of these devices are still not as good as those obtained for lead alloys devices or for Nb-Nb_2O_5-Pb alloy devices.

In the case of high T_c alloy systems, standard oxidation techniques do not work. When they have been used, the quality of the device characteristics are quite poor (see upper trace in Fig. 2) [14]. Noticeably improved tunneling characteristics have been obtained if the high T_c base electrode is first coated with a thin layer (~20Å) of some material which readily oxidizes such as aluminum or silicon and this artifical layer is then allowed to oxidize [14], [15], [16], [17], [18], [19]. The improvement in the tunneling characteristics of devices with artificial oxide barriers as compared to devices with native oxide barriers is obvious by comparison of the several traces in Fig. 2. The concept of using artificial oxide bar-

riers for refractory Josephson devices was apparently first used by Laibowitz and Mayadas [15] for niobium devices and has subsequently been adapted by other groups interested in tunneling into high T_c materials. Using these artificial oxide barriers and soft low T_c lead or lead alloy counter electrodes, tunneling characteristics of reasonable quality have been obtained. The detailed mechanism of formation of these artificial barriers is not fully understood [20] as a 20Å thick film is obviously not continuous and therefore the nature of the resulting oxide barrier probably is not continuous and "pinhole free." However, once the optimum thickness for the oxidized aluminum or silicon layer has been determined, good quality tunnel junctions with reproducible and controllable thicknesses can be obtained.

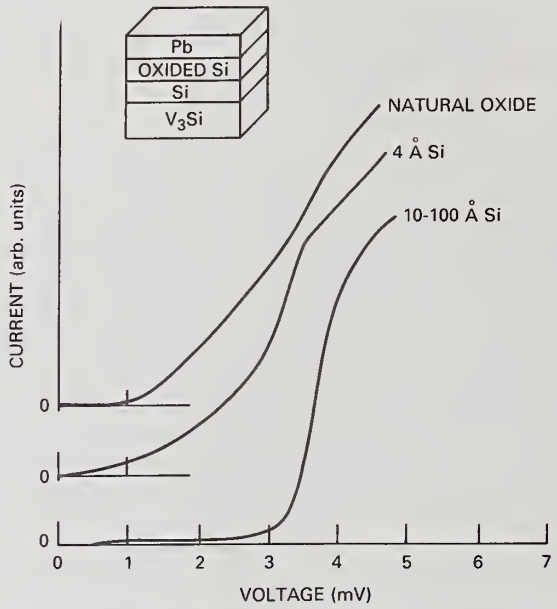

Fig. 2. Tunneling characteristics of V_3Si-Pb junctions for several types of tunneling barriers, natural as well as oxidized silicon layers (see Ref. 14)

Good quality tunneling characteristics have been obtained using artificial oxide barriers on high T_c base electrodes where the counter electrode has been a soft material (such as lead or lead alloys), which can be deposited at or below room temperature [14], [17], [18], [19]. The tunneling characteristics are noticeably poorer if high T_c materials are used for the counter electrode. Good high T_c behavior can only be obtained for the potentially high T_c materials, if they are deposited at elevated temperatures - at least 300C and, in certain cases, at temperatures as high as 1000C. These elevated temperatures can have disastrous effects on the properties of the base electrode and the oxide barrier region that has been grown on the base electrode. It is well known that oxygen can diffuse readily through niobium and niobium alloys at relatively low temperatures. Diffusion of oxygen can either suppress or destroy superconductivity in the layer into which the oxygen has diffused. If superconductivity is suppressed at the surface of the electrode, the desired abrupt transition between uniform superconducting and insulating regions will be smeared out and the quality of the tunneling characteristic will be degraded, and excess current will be observed below the energy gap voltage. Hence, the deposition of the high T_c counter electrode for an all-refractory superconducting tunnel device presents a formidable problem.

An attempt to fabricate an all high T_c Josephson device has been reported recently by Tarutani et al. [21], who used Mo-Re as the counter electrode material. The system of Mo-Re, which in the bulk can have a T_c as high as 12.2K, can be deposited at temperatures near or below room temperature and, if the deposition conditions are suitable, the compound Mo_3Re_2 will be formed with a T_c as high as 11.2K. They report on the preparation of tunnel devices with V_3Si as the base electrode (T_c~16.4K when deposited at 900°C), an artificial oxidized silicon barrier (native oxide barriers did not exhibit tunneling) and Mo-Re counterelectrodes. Films of Mo-Re deposited at ambient temperatures did not exhibit superconductivity as interdiffusion of atoms between the Mo-Re, as it was being deposited, and the remainder of the structure probably occurred as the temperature of the device was raised to about 130C during the Mo-Re deposition. When the deposition was made at LN_2 temperatures, the device probably remained below 100K and Mo_3Re_2 was formed which, even after being warmed to room temperature, exhibited superconductivity with a broad transition extending from 10.5K down to 8.3K. The article did not contain details about the tunneling characteristics of the devices nor did it indicate the highest temperature at which Josephson effects could be detected.

Another likely candidate for the counter electrode in an all refractory tunnel device is NbN. This material is normally deposited at temperatures in the range of 300-500C and transition temperatures of the order of 15K are obtained for films of thickness of 1000 Å or greater. If the device is reactively sputtered at ambient temperature, T_c is reduced to the vicinity of 10-12K. An attempt to fabricate an all NbN tunnel junction has been reported by Shinoki et al. [22], who used an artificial layer of oxidized silicon to form the tunneling barrier. The base electrode was deposited at 500C and exhibited T_c of about 15K. In order to minimize degradation of the base electrode and the oxidized silicon barrier region, the NbN counter electrode was deposited at near ambient temperatures. The tunneling characteristics at 4.2K show a distinct energy gap at 4mv which suggests that the energy gap for the upper film is below 10K. Although no specific value is quoted, the excess current below the gap appears to be large and the device as reported was not suitable for switching application.

6. Semiconductor Barrier Devices

Another Josephson tunneling configuration employs a semiconductor barrier several hundred angstroms thick instead of the oxide barrier which is normally tens of angstroms thick. The Naval Research Laboratory has a joint effort with Sperry Research Center to fabricate all refractory superconducting tunnel devices with CVD deposited polysilicon barrier [23], [24]. The base NbN electrode is reactively sputter-deposited at a substrate temperature of about 500C which results in a T_c of about 15K. A several hundred angstrom thick silicon layer is grown by CVD on the base electrode which is held at a temperature of 300-500C and a counter electrode of NbN is then reactively sputtered at (nominally) ambient temperatures. After fabrication, the base electrode has a T_c~13.5K while the T_c of the counter electrode is found to be about 12K. Josephson currents were observed at temperatures slightly below 10K. Unfortunately, the preliminary results were such that it could not be unequivocally established whether the supercurrent was due to tunneling through the silicon barrier or along shorts across the barrier region. At the time of the preparation of this communication, Sperry had improved their techniques for depositing silicon layers on NbN and new all refractory, semiconductor barrier devices will be fabricated in the near future.

7. Weak Link/Constriction Devices

Another class of device configuration which can exhibit Josephson effects is a structure which contains a very severe reduction in width over a very short distance - the so-called "weak link". The theoretical constraint for the observation of Josephson effect is that length (and width) of the constriction must be comparable to or smaller than three times the superconducting coherence length of the material [25]. In the case of the mechanically soft, low T_c materials, such as tin and aluminum, coherence lengths are of the order of thousands of angstroms and ideal weak links have been fabricated by conventional optical lithographic techniques or scribing with sharp diamond points. However, the coherence length of materials tends to decrease with increasing transition temperature and materials such as niobium and the high T_c materials have coherence lengths so small that conventional techniques cannot be used to fabricate constrictions that are small enough to satisfy the conditions for obtaining ideal Josephson behavior.

In the case of niobium, which has a coherence length of the order of 400Å, recently developed "contamination resist" techniques have been used to fabricate constrictions with widths of the order of 500Å and lengths about 1200Å which have shown ideal Josephson behavior both in their response to incident microwave radiation [26] and when used to fabricate SQUID magnetometers [27]. The techniques for fabricating these so-called "nanobridges" (so named as they are smaller than "microbridges") cannot be employed to fabricate Josephson weak levels in the refractroy alloy materials, especially those that have transition temperatures in excess of 10K. These materials have coherence lengths of the order of 50Å or less (see Table I), a dimension not reachable with any current device fabrication technique.

There are a number of references where the authors have reported phenomena at temperatures approaching 17K which they have attributed to the Josephson effect. Golavashkin et al. [28], [29], has reported on a Nb_3Sn device in which they mechanically scribed two constrictions 1-5 μm wide and 1-2 μm long to produce what is supposedly a DC SQUID. The device was sensitive to changes in the applied magnetic field in a manner resembling a DC SQUID although the response behavior was poor compared to that observed for DC SQUIDs fabricated from low T_c materials. The poor quality of the response might be due to operation by some type of synchronized "flux flow" which one would expect to observe for the case of apparent bridge dimensions at least 100 times larger than the coherence length of Nb_3Sn. Another possible explanation for this type of response (from a device with constrictions with these dimensions) is that there are flaws (such as cracks or grain boundaries) within the constricted region such that the dimensions at some point are very small compared to the apparent dimensions. Another possibility is that the region of the film where that constriction was produced was not uniform and that the operation of the device is attributable to granular or inhomogeneous superconductivity (see below). Until the true nature of the constriction can be established, reservations must be exercised before attributing the observed behavior to true Josephson effect.

The same reservations should be made in considering the recent report by Lee and Falco [30] on the observation at temperatures near 17K of RF induced microwave steps in the I-V characteristics of constrictions made in Nb_3Sn films. A constriction with dimensions of the order of micrometers was sculptured into the film and then the transition temperature of the constriction was adjusted downward by applying across the constriction voltage pulses with microsecond duration. By a mechanism as yet not understood, this technique permitted a systematic and controlled depression of the T_c of the constriction. Using a device in which the T_c had been depressed to about 17K from an original value of about 18K, they observed RF induced steps in the device I-V curve at voltages corresponding to the integer har-

monics of the Josephson frequency: no subharmonic or non-integer harmonic steps were obtained. This type of response is expected for ideal Josephson behavior while synchronized flux flow, which would be expected for a constriction in Nb_3Sn with these dimensions, would also have exhibited subharmonic or non-integer harmonic steps. The modification of the film that occurred during the "pulse" treatment is not understood: small fractures may be created or, possibly, local heating may expedite the diffusion of oxygen along grain boundaries thus creating a region within the constriction which exhibits inhomogeneous superconductivity. (In the latter case, as will be discussed below, the coherence length does not impose a severe constraint on the dimensions of an inhomogeneous weak link.) Notwithstanding the lack of knowledge about the details of the physical and electrical nature of the constriction after the pulse treatment, the preliminary results appear quite convincing that true Josephson effects have been observed in refractory high T_c materials at temperatures as high as 17K. Furthermore, this fabrication technique should be suitable for producing Josephson devices in other refractory materials. This technique, which was first employed in producing superconducting weak link constrictions in niobium films by Duret et al. [31], might be considered to be the thin film equivalent of the bulk mechanical point contact configuration. In both cases, the device is adjusted while observing the superconducting or electrical properties, the thin film version by repeated pulsing while the bulk contact by very careful adjustment of the tension on the point. (Unfortunately the thin film version is not reversible while the point contact is.) The pulsing technique may permit extensive investigations of Josephson effects in high T_c films, much the same way that the point contact was an extremely valuable tool in studying bulk materials. Although this technique may prove to be very useful in making single Josephson devices, it is doubtful that it can be employed to fabricate complex circuits and/or arrays of Josephson devices.

8. Granular Weak Links

As pointed out in the previous section, theory predicts that ideal Josephson behavior should be observed in weak link constrictions only if their dimensions are of the order of or less than three times the coherence length of the material [25]. For refractory alloy materials, coherence lengths are of the order of 100 A or less and thus the observation of Josephson behavior requires constrictions with dimensions of the order of 300 A or less, a value that cannot be achieved by conventional electron beam lithography and is at the limit of what may be achieved with "contamination resist" lithography developed by IBM.

However, the group at NRL has shown that weak link constrictions in refractory alloy films can exhibit Josephson effects with micrometer sized dimensions if the weak link region is sufficiently thin to exhibit granular or inhomogeneous superconducting behavior [32]. When a film of, for example, niobium or niobium nitride of thickness of 1000A is thinned down by anodization or ion milling, the transition temperature begins to decrease (see Fig. 3). The variation of the transition temperature with film thickness obeys the following relation

$$T_c(d) = T_c(\infty) \exp[- d_o/d]$$

For both niobium and niobium nitride, the constant d_o was found to be about 10Å. The significance of this parameter is that T_c of the film appears to be reduced by the proximity effect with non-superconducting layers of 5Å on each surface of the film.

As the film thickness is reduced, a critical value is reached, about 100Å for niobium nitride and about 50Å for niobium films, below which there

is a noticeable decrease in the critical current density of several orders of magnitude (see Fig. 3). The same reduced value of critical current density values is observed for thinner films. However, the T_c varies smoothly through this critical thickness value and obeys the above relation for all values of film thickness.

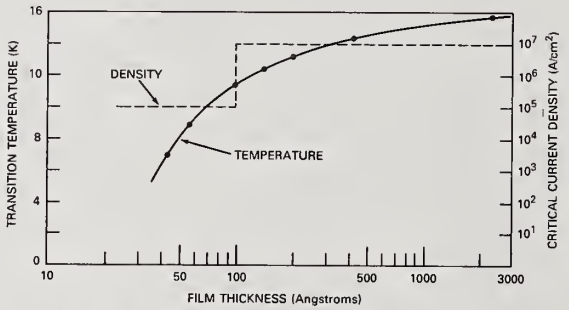

Fig. 3. Variation of the superconducting transition tempeature and critical current density of niobium nitride films as a function of film thickness

The decrease in critical current density is believed to be due to a transition from bulk conduction for the thicker films to a granular or hopping conduction for films with thicknesses less than the critical value. As the film is deposited, it initially grows as isolated islands of materials which develop to sizes of the order of 100A. As the second layer of grains begin to grow, they touch and "bulk-like" conduction occurs. Conversely, when a thick film is thinned until the thickness of the region becomes comparable to the grain size, the conduction changes from bulk-like to tunneling between the isolated grains. The proposed nature of the conduction mechanism for thin films is supported by the observation that many of these films exhibit a negative coefficient of resistance for temperatures above T_c which can be attributed to hopping conduction between isolated grains. Similar behavior has been observed in granular aluminum and tin films which were deposited in an oxygen partial pressure which aided in the formation of isolated grains coated with oxide layers.

SQUIDs have been fabricated using granular regions with dimensions of the order of one micrometer in length which exhibited good Josephson behavior [33], [34]. (Granular regions with lengths greater than several micrometers exhibited rather poor or smeared out Josephson responses.) Depending on the degree of granularity of the weak link region, the width of the localized region can be varied from submicrometer for films which were marginally granular to widths greater than 40 micrometers for weak links which were clearly granular in nature. For niobium nitride SQUIDs with weak links that were clearly in the granular regime, Josephson behavior could be followed from T_c, which for some devices was as high as 10K, down to about 1.2K, the lowest temperature that could be reached (see Fig. 4). Ideal Josephson behavior was obtained for critical currents greater than ϕ_o/L (the condition for hysteretic behavior required by the Kurkijarvi theory) but less than about 6 ϕ_o/L [34], [35]. The degradation of response for large values of critical current is not understood but is being investigated. Several of these devices have been examined at microwave frequencies (about 10 GHz) and exhibited Josephson behavior with extremely good signal-to-noise ratios, over a corresponding wide temperature range from just below T_c down to about 1.2K [34].

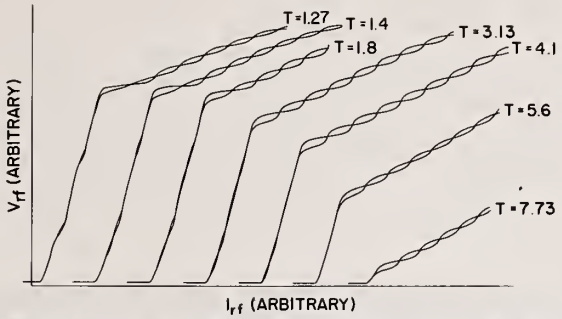

Fig. 4. I-V characteristics of NbN RF SQUID containing a granular weak link measured at 20 MHz as a function of temperature. The onset temperature for observing Josephson behavior was 10K while 1.27K was the lowest temperature that could be achieved in the particular apparatus (see Refs. 34 and 35)

If the weak link region has been thinned down so that it is just marginally granular in nature, Josephson behavior can be observed at much higher temperatures but over a restricted temperature region. For example, the data in Fig. 5 is the response of a NbN SQUID containing a marginally granular weak link which exhibits an onset of SQUID behavior at near 14K. The response can be followed down to about 13K before the critical current becomes too large. As described in the previous paragraph, ideal magnetic flux noise, characteristic of the temperature, is observed for critical currents greater than 1 ϕ_o/L but less than about 6 ϕ_o/L, corresponding to a one degree temperature range of operation. The quality of the response and the temperature range over which it is observed is superior to the previously reported response for any RF-biased SQUID fabricated from refractory alloy materials.

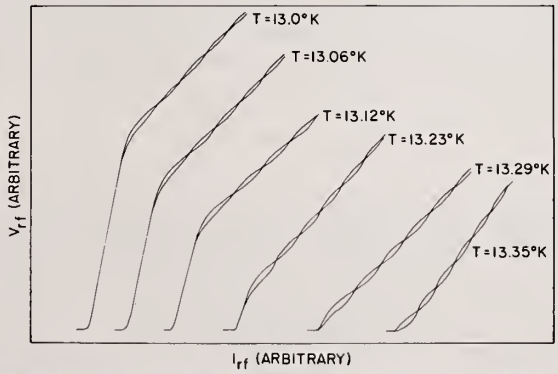

Fig. 5. I-C characteristics for a NbN RF SQUID containing a weak link constriction that is marginally granular in nature (see Refs. 34 and 35)

The physics behind the observed operation of these granular weak link constriction devices is not understood [32], [35]. The grain size in these films is about 100Å and thus in a 1 micrometer by 1 micrometer region, there are more than 10^4 grains. However, a granular region of this dimension built into an RF biased SQUID behaves as if it were a single ideal Josephson device--the 10^4 grains are strongly coupled together and appear to be characterized by a single quantum mechanical phase difference common to the entire array of grains.

Thus far, granular behavior has been observed in two refractory thin film systems - niobium and niobium nitride. If similar type of behavior can be observed in higher T_c material systems, it may be feasible to fabricate weak link structures with micrometer dimensions which may show onsets of SQUID behavior at temperature near 15K and thus, could be operated near 10K (that is, at a reduced temperature of 0.6) where the temperature coefficients of the various superconducting parameters are weak. At these operating temperatures, the cryogenic environment could be provided by small, compact, energy-efficient cryogenic refrigeration systems.

9. Conclusions

Materials. There are a fairly large number of superconducting materials that are potentially suitable for the fabrication of high temperature devices and circuits. Many of these materials have been prepared in thick film form (thicknesses greater than 1 micrometer) with the purpose of exploring their use in high power superconducting applications. However, there has been only limited work on preparing thin refractory films (thicknesses of the order of or less than 1,000A) in a form that would be suitable for fabricating Josephson devices and superconducting electronic circuits. Additional effort will be required to develop procedures for preparing fine grain structures, that adhere well to substrate materials and that can be prepared with desired properties under fabrication conditions that are compatible with multi-layered device processing.

Device Processing. In the fabrication of tunnel junctions using all refractory high temperature superconducting electrodes, the major problem areas are the barrier region, either the natural oxide or artificial barriers, suitable masking, and the deposition of the refractory counter electrode without degrading the base electrode or the barrier region (see Table 3). The fabrication of weak link constrictions in refractory materials that can exhibit ideal Josephson behavior requires device geometry resolutions in the 300Å regime, which is beyond the capabilities of presently available device processing technology. Granular weak links have been fabricated with micrometer dimensions with operating temperatures as high as 14K. Additional materials research would be required for the fabrication of granular systems which have transition temperatures at values in excess of 15K so that devices made from these materials can be operated at 10K at a reduced temperature of 0.6.

Table 3. Problem Areas for Fabricating High Temperature Josephson Devices ($T_{OP} \gtrsim 10K$)

Type of Structure	Highest Reported Operation	Problem Area
Tunnel Junction	-	Barrier layer growth Defining masks Counter electrode
Proximity Effect Device	17K	Limited temperature range Exponential I_c dependence
Weak Link/Constriction	?	Small dimensions ($\lesssim$100Å)
Granular/Inhomogeneous Weak Link	~13K	Preparation of granular specimens of high T_c materials

Prospects for Future Progress. Despite the limited amount of research activity directed at the fabrication of all refractory high operating temperature Josephson devices and circuits, the prospects are quite good that these materials will be used in the near future in Josephson technology. The primary obstacles to their use are materials problems such as producing controlled barrier layers and suitable counter electrodes in the case of tunnel junctions, and producing high T_c materials which exhibit granular behavior in the case of weak links. These are quite serious obstacles, especially given the refractory nature of the materials and the affinity of these materials for such undesirable impurities as oxygen. However, the modest efforts to date at IBM, NRL and in Japan have yielded quite encouraging results.

All refractory devices would be extremely rugged and reliable and would withstand repeated thermal cyclings to cryogenic operating temperatures. These properties are not characteristic of the presently used lead alloy Josephson device technology but are essential if Josephson technology is to become a viable one, either on a commercial basis or for military applications. In addition, these refractory materials often have superconducting transition temperatures in excess of 15K which makes possible their operation near 10K(at a reduced temperature of 0.6). This would permit the use of fairly compact, highly reliable closed cycle refrigeration systems for deployment with Josephson sensor systems and, possibly small Josephson circuits and systems. It would appear that large scale digital processing systems would continue to be operated at liquid helium temperatures as the liquid is probably essential for adequate cooling of the very complex packaging associated with such systems.

The ruggedness and reliability of Josephson devices and circuits fabricated from refractory materials provide the impetus that will motivate the developing of this technology. Current activities are limited but should expand in the near future so that one may confidently expect to see all-refractory Josephson devices within the next five years and fairly complex integrated circuit structures fabricated with refractory metallization within the next ten years. The advent of such circuit technology is crucial to the development of a viable superconducting electronic technology and their development will be pursued despite the serious materials problems that must be overcome.

10. References

[1] Strobridge, T.R., "Cryogenic Refrigerators - An Updated Survey," NBS Technical Note 655, June 1973 (U.S. Government Printing Office, Washington, D.C. 20402, catalogue number C13.46:655), unpublished.

[2] Daunt, J. G., and Goree, W. S., "Miniature Cryogenic Refrigerators," Stanford Research Institute Report (ONR Contract N00014-67-C-0193), unpublished.

[3] Beasley, M. R., "Improved Materials for Superconducting Electronics," Future Trends in Superconductive Electronics, ed. B.S. Deaver, Jr., C.M. Falco, J.H. Harris and S.A. Wolf (American Institute of Physics, New York, 1978), pp. 389.

[4] Beasley, M. R., "Progress Report on High T_c Superconducting Devices," Applications of Closed-Cycle Cryocoolers to Small Superconducting Devices; NBS Special Publication 508 (U.S. Government Printing Office, Washington, D.C. 20434, Stock No. 003-003-0910-1, 1978), p. 167.

[5] Notarys, H. A. and Mercereau, J. E., "Proximity Effect Bridges and Superconducting Microcircuitry," J. Appl. Phys. 44, 1021 (1973).

[6] Wu, C. T. and Falco, C. M., "High Temperature Nb_3Sn Thin-film SQUID's," Appl. Phys. Lett., 30, 609 (1977).

[7] Gu, J., Cha, W., Gamo, K. and Namba, S., "Properties of Niobium Superconducting Bridges Prepared by Electron Beam Lithography and Ion Implantation," J. Appl. Phys., 50, 6437 (1979).

[8] Kraichman, R. K., Hutchby, J. A., Burgess, J. W., McNamara, R. P. and Notarys, H. A., "Comparative Studies of Ion-Implant Josephson-Effect Structures," IEEE Trans. Magnetics, MAG-13, 731 (1977).

[9] Palmer, D. W., Notarys, H. A. and Mercereau, J. E.,"Quantum Interference in High Transition Temperature Thin Film Materials," Appl. Phys. Lett. 25, 527 (1974).

[10] Greiner, J. H.,"Josephson Tunneling Barriers by R-F Sputter Etching in an Oxygen Plasma," J. Appl. Phys. 42, 5151 (1971).

[11] Laibowitz, R. B. and Cuomo, J. J., "Tunneling Sandwich Structures Using Single Crystal Niobium Films," J. Appl. Phys. 41, 2748 (1970).

[12] Broom, R. F., Jaggi, R., Laibowitz, R. B., Mohr, Th. O. and Walter, W., "Thin Film Josephson Tunnel Junctions with Niobium Electrodes," Proceedings of 14th International Conference on Low Tempeature Physics; Otaniemi, Finland; August 1975 (North Holland Publishing Co., Amsterdam); Vol 4, p. 172.

[13] Broom, R. F., Laibowitz, R. B., Mohr, Th. O. and Walter, W., "Fabrication and Properties of Niobium Josephson Tunnel Junction," IBM J. Res. Develop. 24, 212 (1980).

[14] Moore, D. F., Zubeck, R. B., Rowell, J. M. and Beasley, M. R., "Energy Gap of A-15 Superconductors Nb_3Sn, V_3Si and Nb_3Ge measured by Tunneling," Phys. Rev. B20, 2721 (1979).

[15] Laibowitz, R. B. and Mayadas, A. F., "Josephson Junctions with Nb/Al Composite Electrodes," Appl. Phys. Lett. 20, 254 (1972).

[16] Laibowitz, R. B., Tsuei, C. C., Chaudhari, P., Raider, S.I., Drake, R. and Viggiano, J. M., "Proximity Effect Tunnel Junctions with Barriers Formed from Amorphous Alloys," Jour. de Phys. 39, C6-1340 (1978).

[17] Yeh, J. T. C. and Tsuei, C. C., "Tunneling Studies on Thin Film Nb-Al Alloys," IEEE Trans. on Magnetics, MAG-15, 591 (1979).

[18] Buitrago, R. H., Goldman, A. M., Toth, L. E. and Cantor, R. "Preparation of Nb_3Ge Superconducting Tunneling Junctions," IEEE Trans. on Magnetics, MAG-15, 589 (1979).

[19] Howard, R. E., Rudman, D. A. and Beasley, M. R., "Josephson Properties of Nb_3Sn/Pb tunnel Junctions," Appl. Phys. Lett. 33, 671 (1978).

[20] Rudman, D. A. and Beasley, M. R., "Oxidized Amorphous-Silicon Superconducting Tunnel Junction Barriers," Appl. Phys. Lett. 36, 1010 (1980).

[21] Tarutani, Y., Yamada, K. and Kawabe, U., "Superconducting Tunneling Junctions with V_3Si-SiO_2-Mo_3Re_2," Appl. Phys. Lett. 37, 239 (1980).

[22] Shinoki, F., Takada, S., Kosada, S. and Hayakawa, H., "Fabrication of High Quality NbN/Pb Josephson Junctions," Jap. Jour. Appl. Phys. 19, Suppl. 1, 591 (1980).

[23] Kroger, H., Potter, C. N. and Jillie, D. W. "Niobium Josephson Junctions with Doped Amorphous Silicon Barriers," IEEE Trans. on Magnetics, MAG-15, 488 (1979).

[24] Kroger, H. "Josephson Devices Coupled by Semiconductor Links," IEEE Trans. Electron Devices ED-27, 2016 (1980).

[25] See for example, Likharev, K. K., "Superconducting Weak Links," Rev. Mod. Phys. 51, 101 (1979).

[26] Laibowitz, R. B., Broers, A. N., Yeh, J. T. C. and Viggiano, J. M., "Josephson Effect in Nb Nanobridges," Appl. Phys. Lett. 35, 891 (1979).

[27] Voss, R. F., Laibowitz, R.B. and Broers, A.N., "Niobium Nanobridge dc SQUID," Appl. Phys. Lett. 37, 656 (1980).

[28] Golovashkin, A.I., Levchenko, I.S., Lykov, A.N. and Makhashvili, L.I., "Quantum Interference on Nb_3Sn Thin Film Contacts at Hydrogen Temperatures," JETP Lett. 24, 521 (1976).

[29] Golovashkin, A. I., Levchenko, I. S. and Lykov, A. N., "Quantum Interference at Nb and Nb_3Sn Superconducting Microbridges," Soviet Physics Solid State 18, 2121 (1977).

[30] Lee, T. W. and Falco, C. M., "Josephson Effects in Nb_3Sn Microbridges," Applied Superconductivity Conference, Santa Fe, N.M., October 1980; IEEE Trans. on Magnetics, Spring 1981, to be published.

[31] Duret, D., Bernard, P. and Zenatti, D., "A UHF Superconducting Magnetometer Utilizing a New Thin Film Sensor," Rev. Sci. Instr. 46, 475 (1975).

[32] Claassen, J. H., Cukauskas, E. J. and Nisenoff, M., "Granular Weak Link Josephson Devices," Inhomogeneous Superconductors-1979, ed. Gubser, D. U., Francavilla, T. L., Leibowitz, J. R. and Wolf, S. A. (American Institute of Physics, New York, 1980), p. 169.

[33] Rachford, F. J. and Cukauskas, E. J., "High T_c Refractory Thin-Film Microwave SQUIDs," Appl. Phys. Lett. 35, 891 (1979).

[34] Cukauskas, E. J. and Nisenoff, M., "Intrinsic Noise Characteristics of NbN SQUIDs," J. Appl. Phys. 52 (Feb 1981), accepted for publication.

[35] Cukauskas, E. J. and Nisenoff, M., "Noise Properties of Thin Film Granular Weak Link SQUIDs," Applied Superconductivity Conference, Santa Fe, N.M., October 1980; IEEE Trans. on Magnetics MAG-17, Spring 1981, to be published.

[36] Claassen, J. H., "Josephson Behavior in Granular NbN Weak Links," Appl. Phys. Lett. 36, 771 (1980).

ATTENDANCE LIST

Conference on Refrigeration for Cryogenic Sensors and Electronic Systems
October 6 & 7, 1980

Robert A. Ackermann
Project Manager, Stirling Engine Sys. Div.
Mechanical Technology Incorporated
968 Albany-Shaker Road
Latham, NY 02110

Fernand D. Bedard
Lab for Physical Sciences
4928 College Avenue
College Park, MD 20740

W. G. Baechler
Leybold-Heraeus
Bonner Str. 504
5000 Cologne
West Germany

Mel Bello
The Aerospace Corporation
Bldg. D5 - P. O. Box 92957
Los Angeles, CA 90009

Abe Bakst
27764 Edgeton Road
Los Altos Hills, CA 94022

G. M. Benson
ERG, Inc.
Lowell and 57th Street
Oakland, CA 94608

Mike Balister
National Radio Astronomy Observatory
P. O. Box 2
Green Bank, WV 24944

B. W. Birmingham
National Bureau of Standards
325 S. Broadway
Boulder, CO 80303

C. Barbe
L'Air Liquide
Centre de Recherche
Claude-Delorme
75321 Paris
Cedex 07
France

R. D. Blaugher
Manager, Cryogenic Technology
Westinghouse Electric Corp.
1310 Beulah Road
Pittsburgh, PA 15235

John Barclay
Group P-10
M. S. 764
Los Alamos Scientific Lab.
Los Alamos, NM 87545

Richard G. Brandt
Office of Naval Research
1030 E. Green Street
Pasadena, CA 91106

Carlisle Barnes
Lockheed Aerospace
P. O. Box 4346
Foster City, CA 94404

R. W. Breckenridge
A. D. Little, Inc.
Acorn Park
Cambridge, MA 02140

ATTENDANCE LIST, continued

Howard Brown
P. O. Box 2
National Radio Astronomy Observatory
Green Bank, WV 24944

Eldon Byrd
Naval Surface Weapons Center
White Oak Laboratory
Mail Code R-34
Silver Spring, MD 20910

Pasquale Carelli
Consiglio Nazionale Delle Ricerche
Laboratorio Di Elettronics
Dello Stato Solido
Romano 42
Rome
Italy

Charles Class
Martin Marietta Aerospace
Denver Division P. O. Box 179
M. S. 30484
Denver, CO 80201

William Colyer
Energy Systems Corp.
169 Los Cordovak Rt.
Taos, NM 87571

Larry Daddario
P. O. Box 2
National Radio Astronomy Observatory
Green Bank, WV 24944

David E. Daney
NBS - Thermophysical
Properties Division
Boulder, CO 80303

A. Daniels
345 Scarborough Rd.
Philips Lab.
Briarcliff Manor, NY 10510

V. J. deWaal
Laboratorium voor
Technische Naturhunde
University of Delft
Delft
The Netherlands

Denis Duret
L.E.T.I.
Commissariat a l'Energie Atomique
85X 38041
Grenoble, Cedex
France

Nicholas Eber
Dept 6/65
Sulzer Brothers Limited
CH-8401 Winterhur
Switzerland

Edgar A. Edelsack
Dept. of the Navy
Code 427
Office of Naval Research
800 N. Qunicy St. Room 332
Arlington, VA 22217

Alain Faure
L'Air Liquide-Etablissement de Sassenage
Dept. de Construction et de Vente Mecanique
B.P.15
38360 Sassenage
France

A. A. Fife
CTF Systems
#15 1750 McLean Ave.
Port Coquitlam B.C.
Canada V3C1MG

Ephraim B. Flint
IBM - Thomas J. Watson
Research Center
P. O. Box 218
Yorktown Heights, NY 10598

Robert W. Guernsey, Jr.
IBM - Watson Res. Center
P. O. Box 218
Yorktown Heights, NY 10598

M. X. Francois
Laboratoire de Thermodynamique des Fluides
Campus Universitaire Bat 502 Ter
91405 Orsay
Cedex
France

J. Bindslev Hansen
Physics Lab. - Univ. of Copenhagen
Universitetsparken 5
DK-2100
Copenhagen
Denmark

Max G. Gasser
NASA Goddard SFC
Code 713
Greenbelt, MD 20771

Robert G. Hansen
R. G. Hansen & Associates
1324 State Street
Santa Barbara, CA 93101

Peter E. Gifford
President, Cryomech, Inc.
314 Ainsley Drive
Syracuse, NY 13210

W. H. Hartwig
Dept. of Electrical Engineering
P. O. Box 7728
University of Texas at Austin
Austin, TX 78712

Dave Giguere
Hughes Aircraft Company
EED Bldg. 240
3100 Lomitom Blvd.
Torrance, CA 90509

William Haskin
Adv. Cryogenic Systems Group
Environmental Control Branch
Dept. of the Air Force
Wright-Patterson Air Force Base, OH 45433

Mike Goldowsky
Philips Lab.
345 Scarborough Road
Briarcliff Manor, NY 10510

C. Heiden
Institut fur Angewandte
University of Giessen
Heinrich-Buff-Ring 16
D-6300 GieBen
W. Germany

Geoffrey Green
DTNSRDC (Annapolis Lab.)
Code 2712
Annapolis, MD 21402

Thomas E. Hoffman
Arthur D. Little, Inc.
Acorn Park
Cambridge, MA 02140

R. Hollman
Physics Department
Stanford University
Stanford, CA 94305

Stuart Horn
U. S. Army Night Vision Lab.
NV & E.O. Lab.
Ft. Belvoir, VA 22060

Yoshihiro Ishizaki
University of Tokyo
Tokyo, Japan

Lyle M. Ishol
Code 792
Naval Coastal Systems Center
Panama City, FL 32407

A. L. Johnson
Aerospace Corp.
D-5 P. O. Box 92957
Los Angeles, CA 90009

Dean L. Johnson
Jet Propulsion Laboratory
M. S. 238-737
4800 Oak Grove Drive
Pasadena, CA 91106

Yasuharu Kamioka
University of California
7671 Boelter Hall
Los Angeles, CA 90024

Kenjiro Kasai
Kasado Research Dept.
Hitachi Ltd.
794 Kudamatsu-City
Yamaguchi-Ken 744
Japan

Dale Kennedy
AFWAL/FIEE
Wright-Patterson AFB
Ohio 45433

Peter J. Kerney
CTI Cryogenics
Kelvin Park
Waltham, MA 02254

T. Kondo
Engineering Research Institute
Faculty of Engineering
University of Tokyo
Bunkyo-Ku, Tokyo
Japan

Tadashi Kondoh
Manager, 2nd Technical Lab.
Aisin Seiki Co., Ltd.
1-Asahi-Machi, 2-Chome
Kariya City, Aichi Pref.
448
Japan

Herbert Korf
AGE-Telefunken
Theresienstr.2
D-7100 Heilbronn
W. Germany

Tomoo Kurumada
Osaka Oxygen Industries, Ltd.
Utajima, Nishiyodogawa-Ku
Osaka
Japan

Kurt Kwasnitza
ETH - Zurich
Institute of Solid State Physics
Zurich
Switzerland

Del Linenberger
NBS-Thermophysical
Properties Division
Boulder, CO 80303

Rudy Latasa
National Radio Astronomy Observatory
P. O. Box 2
Green Bank, WV 24944

William A. Little
Physics Department
Stanford University
Stanford, CA 94305

William Lawless
Lake Shore Cryotronics
64 E. Walnut Street
Westerville, OH 43081

Ralph C. Longsworth
Air Products & Chemicals, Inc.
Advanced Products Department
Box 2802
Allentown, PA 18105

Otto Ledford
Aerospace Corp.
Box 92957
Los Angeles, CA 90009

J. C. Lottin
Commissariat Al'Energie Atomique
C.E.N. Saclay-Orme des Merisiers, Stipe
Postale No. 2, 91-Gif-Sur-Yvette
France

Daniel Lehrfeld
Magnavox
34 Greenwood Drive
New City, NY 10956

K. Lueders
Freie Univ. Berlin
Fach Physik (FB 20)
Institut fur Atom & Feskorperphysik
Koenigin-Luise-Str. 28/30
1000 Berlin 33
W. Germany

Robert Lepobsky
CTI, Cryogenics
266 Second Ave.
Waltham, MA 02154

John T. Lynch
MIT - Lincoln Labs.
Room 329-Box 73
Lexington, MA 02173

James Lester
Ball Aerospace
Box 1062
Boulder, CO 80306

Thomas J. Marusak
Mechanical Technology Incorporated
968 Albany-Shaker Road
Latham, NY 02110

Yoichi Matsubara
Atomic Energy Research Institute
Nihon University
Kanda-Surugadai Chiyoda Ku
Tokyo
Japan 101

George Patton
DTNSRDC (Annapolis Lab.)
Code 2712
Annapolis, MD 21402

Ken Myrtle
Dept. of Physics
Simon Fraser University
Burnaby B. C. V5A156
Canada

Dusan Petrac
Jet Propulsion Lab, CIT
4800 Oak Grove Drive, 183/401
Pasadena, CA 91103

Lawrence G. Nelsen
Rockwell International
10202 Flintndge
Villa Park, CA 92667

Warren Pierce
Lake Shore Cryotronics
64 E. Walnut Street
Westerville, OH 43081

M. Nisenoff
Naval Research Laboratory
Code 6854
Washington, D. C. 20375

H. Quack
Sulzer Brothers Limited
CH-8401 Winterthur
Switzerland

J. J. Orth
Hughes Aircraft Company
Culver City, CA 90230

Ray Radebaugh
NBS - Thermophysical
Properties Division
Boulder, CO 80303

Isao Oshima
Osaka Oxygen Industries, Ltd.
Utajima, Nishiyodogawa-Ku
Osaka
Japan

Richard M. Rall
Hughes Aircraft Company
EED-Bldg.240/113
3100 W. Lomita Blvd.
Torrance, CA 90509

J. A. Pals
Philips Research Lab.
Eindhoven
Nederland

Piter Roos
Magnavox
46 Industrial Ave.
Mahwah, NJ 07430

Pierre M. Roubeau
Commissariat A l'Energie Atomique
C. E. N. Saclay -Orme des Merisiers, Boite
Postale No. 2, 91-Gif-Sur-Yvette
France

S.C. Russo
Bldg. 12/V137
Hughes Aircraft Company
Culver City, CA 90230

Ronald E. Sager
S.H.E. Corporation
4174 Sorrento Valley Blvd.
San Diego, CA 92121

Raymond Sarwinski
S.H.E. Corporation
4174 Sorrento VAlley Blvd.
San Diego, CA 92121

E. Saur
Institut fur Angewandte Physik
der Universitat Giessen
Heinrich Buff-Ring 16
6300 GieBen
West Germany

Aron Sereny
Philips Lab.
345 Scarborough Rd.
Briarcliff Manor, NY 10510

G. W. Shepherd
Magnavox
46 Industrial Ave.
Mahwah, NJ 07430

Allan Sherman
NASA Goddard Space Flight Center
Code 713
Greenbelt, MD 20771

Arnold H. Silver
Aerospace Corp.
Box 92957
Los Angeles, CA 90009

J. F. Skinner
Hughes Aircraft Company
Bldg. 5 M.S. B151
Culver City, CA 90230

Hans A. Steinherz
CTI Cryogenics
Kelvin Park
Waltham, MA 02254

William Steyert
Los Alamos Scientific Lab.
Mail Stop 764 - P. O. Box 1663
Los Alamos, NM 87545

Philip Studer
NASA Goddard SFC
Code 716
Greenbelt, MD 20771

Donald B. Sullivan
Division 724.03 - Room 2137
National Bureau of Standards
325 Broadway
Boulder, CO 80303

Jean-Jacques Thibault
L'Air Liquide, Centre d'Etudes Cryogeniques
Claude-Delorme, Boite Postale No. 15
38360 Sassenge
FRANCE

K. D. Timmerhaus
Engineering Center AD1-25
University of Colorado
M. S. 423
Boulder, CO 80309

Bryan C. Troutman
IBM 2L50
18100 Frederick Pike
Gaithersburg, MD 20760

E. Tward
Jet Propulsion Laboratory
M. S. 183-901
4800 Oak Grove Drive
Pasadena, CA 91103

A. R. Urbach
Ball Aerospace Corp.
Box 1062
Boulder, CO 80306

Eugene Urban
Es. 63, NASA
Marshall Space Flight Center
Huntsville, AL 35812

R. J. Vincent
ERG, Inc.
Lowell and 57th Street
Oakland, CA 94608

Lawrence A. Wade
Lockheed Research Lab.
3251 Hanover Street
Bldg. 205 - Dept. 52-32
Palo Alto, CA 94304

G. Walker
Dept. of Mechanical Engineering
2920 24 Ave. N.W.
University of Calgary
Calgary, Alberta
CANADA

Sander Weinreb
National Radio Astronomy Observatory
P. O. Box 2
Green Bank, WV 24944

Nancy K. Welker
Lab for Physical Sciences
4928 College Avenue
College Park, MD 20740

R. White
Adv. Cryogenic Systems Group
Environmental Control Branch
Dept. of the Air Force
Wright-Patterson AFB
Ohio 45433

Calvin Winter
Simon Fraser Univ.
Dept. of Physics
Burnaby B. C. V5A156
Canada

James E. Zimmerman
Division 724.03 - Room 2137
National Bureau of Stds.
325 Broadway
Boulder, CO 80303

☆ U.S. GOVERNMENT PRINTING OFFICE : 1981 O - 344-816 : QL 3

NBS-114A (REV. 2-8C)

U.S. DEPT. OF COMM. BIBLIOGRAPHIC DATA SHEET (See instructions)	1. PUBLICATION OR REPORT NO. NBS SP 607	2. Performing Organ. Report No.	3. Publication Date May 1981

4. TITLE AND SUBTITLE

Refrigeration for Cryogenic Sensors and Electronic Systems
Proceedings of a Conference held at the National Bureau of Standards, Boulder, CO, October 6-7, 1980

5. AUTHOR(S)

J. E. Zimmerman, D. B. Sullivan, and S. E. McCarthy, Editors

6. PERFORMING ORGANIZATION (If joint or other than NBS, see instructions)

NATIONAL BUREAU OF STANDARDS
DEPARTMENT OF COMMERCE
WASHINGTON, D.C. 20234

7. Contract/Grant No. 7240187

8. Type of Report & Period Covered Final

9. SPONSORING ORGANIZATION NAME AND COMPLETE ADDRESS (Street, City, State, ZIP)

International Institute of Refrigeration - Commission A 1/2
Office of Naval Research - Naval Research Laboratory
Cryogenic Engineering Conference
National Bureau of Standards

10. SUPPLEMENTARY NOTES

Library of Congress Catalog Card Number: 81-600038

☐ Document describes a computer program; SF-185, FIPS Software Summary, is attached.

11. ABSTRACT (A 200-word or less factual summary of most significant information. If document includes a significant bibliography or literature survey, mention it here)

This document contains the proceedings of a meeting of refrigeration specialists held at the National Bureau of Standards, Boulder, CO, on October 6 and 7, 1980. Participation included representatives of industry, government, and academia. The purpose of the meeting was to discuss progress in the development of refrigeration systems which have been specialized for use with cryogenic sensors and electronic systems. The meeting focused primarily on the temperature range below 20 K and cooling capacity below 10 W. The meeting was jointly sponsored by the International Institute of Refrigeration-Commission A 1/2, the Office of Naval Research, the Naval Research Laboratory, the Cryogenic Engineering Conference, and the National Bureau of Standards.

12. KEY WORDS (Six to twelve entries; alphabetical order; capitalize only proper names; and separate key words by semicolons)

Cryocoolers; cryogenic sensors; helium; refrigeration; superconducting devices.

13. AVAILABILITY

☒ Unlimited

☐ For Official Distribution. Do Not Release to NTIS

☒ Order From Superintendent of Documents, U.S. Government Printing Office, Washington, D.C. 20402.

☐ Order From National Technical Information Service (NTIS), Springfield, VA. 22161

14. NO. OF PRINTED PAGES 223

15. Price $6.50

USCOMM-DC 6043-P80

NBS TECHNICAL PUBLICATIONS

PERIODICALS

JOURNAL OF RESEARCH—The Journal of Research of the National Bureau of Standards reports NBS research and development in those disciplines of the physical and engineering sciences in which the Bureau is active. These include physics, chemistry, engineering, mathematics, and computer sciences. Papers cover a broad range of subjects, with major emphasis on measurement methodology and the basic technology underlying standardization. Also included from time to time are survey articles on topics closely related to the Bureau's technical and scientific programs. As a special service to subscribers each issue contains complete citations to all recent Bureau publications in both NBS and non-NBS media. Issued six times a year. Annual subscription: domestic $13; foreign $16.25. Single copy, $3 domestic; $3.75 foreign.

NOTE: The Journal was formerly published in two sections: Section A "Physics and Chemistry" and Section B "Mathematical Sciences."

DIMENSIONS/NBS—This monthly magazine is published to inform scientists, engineers, business and industry leaders, teachers, students, and consumers of the latest advances in science and technology, with primary emphasis on work at NBS. The magazine highlights and reviews such issues as energy research, fire protection, building technology, metric conversion, pollution abatement, health and safety, and consumer product performance. In addition, it reports the results of Bureau programs in measurement standards and techniques, properties of matter and materials, engineering standards and services, instrumentation, and automatic data processing. Annual subscription: domestic $11; foreign $13.75.

NONPERIODICALS

Monographs—Major contributions to the technical literature on various subjects related to the Bureau's scientific and technical activities.

Handbooks—Recommended codes of engineering and industrial practice (including safety codes) developed in cooperation with interested industries, professional organizations, and regulatory bodies.

Special Publications—Include proceedings of conferences sponsored by NBS, NBS annual reports, and other special publications appropriate to this grouping such as wall charts, pocket cards, and bibliographies.

Applied Mathematics Series—Mathematical tables, manuals, and studies of special interest to physicists, engineers, chemists, biologists, mathematicians, computer programmers, and others engaged in scientific and technical work.

National Standard Reference Data Series—Provides quantitative data on the physical and chemical properties of materials, compiled from the world's literature and critically evaluated. Developed under a worldwide program coordinated by NBS under the authority of the National Standard Data Act (Public Law 90-396).

NOTE: The principal publication outlet for the foregoing data is the Journal of Physical and Chemical Reference Data (JPCRD) published quarterly for NBS by the American Chemical Society (ACS) and the American Institute of Physics (AIP). Subscriptions, reprints, and supplements available from ACS, 1155 Sixteenth St., NW, Washington, DC 20056.

Building Science Series—Disseminates technical information developed at the Bureau on building materials, components, systems, and whole structures. The series presents research results, test methods, and performance criteria related to the structural and environmental functions and the durability and safety characteristics of building elements and systems.

Technical Notes—Studies or reports which are complete in themselves but restrictive in their treatment of a subject. Analogous to monographs but not so comprehensive in scope or definitive in treatment of the subject area. Often serve as a vehicle for final reports of work performed at NBS under the sponsorship of other government agencies.

Voluntary Product Standards—Developed under procedures published by the Department of Commerce in Part 10, Title 15, of the Code of Federal Regulations. The standards establish nationally recognized requirements for products, and provide all concerned interests with a basis for common understanding of the characteristics of the products. NBS administers this program as a supplement to the activities of the private sector standardizing organizations.

Consumer Information Series—Practical information, based on NBS research and experience, covering areas of interest to the consumer. Easily understandable language and illustrations provide useful background knowledge for shopping in today's technological marketplace.

Order the **above** *NBS publications from: Superintendent of Documents, Government Printing Office, Washington, DC 20402.*

Order the **following** *NBS publications—FIPS and NBSIR's—from the National Technical Information Services, Springfield, VA 22161.*

Federal Information Processing Standards Publications (FIPS PUB)—Publications in this series collectively constitute the Federal Information Processing Standards Register. The Register serves as the official source of information in the Federal Government regarding standards issued by NBS pursuant to the Federal Property and Administrative Services Act of 1949 as amended, Public Law 89-306 (79 Stat. 1127), and as implemented by Executive Order 11717 (38 FR 12315, dated May 11, 1973) and Part 6 of Title 15 CFR (Code of Federal Regulations).

NBS Interagency Reports (NBSIR)—A special series of interim or final reports on work performed by NBS for outside sponsors (both government and non-government). In general, initial distribution is handled by the sponsor; public distribution is by the National Technical Information Services, Springfield, VA 22161, in paper copy or microfiche form.

U.S. DEPARTMENT OF COMMERCE
National Bureau of Standards
Washington, D.C. 20234

OFFICIAL BUSINESS

Penalty for Private Use, $300

POSTAGE AND FEES PAID
U.S. DEPARTMENT OF COMMERCE
COM-215

SPECIAL FOURTH-CLASS RATE
BOOK